

# Chain stoppers in reversible supramolecular polymer solutions

*Promotor:*

prof. dr. M.A. Cohen Stuart  
hoogleraar Fysische chemie met bijzondere aandacht voor de kolloïdchemie  
Wageningen Universiteit

*Copromotor:*

dr. ir. N.A.M. Besseling  
universitair docent bij het laboratorium voor Fysische chemie en kolloïdkunde  
Wageningen Universiteit

*Promotiecommissie:*

|                              |   |
|------------------------------|---|
| prof. dr. L. Bouteiller      | (Université Pierre et Marie Curie, Paris) |
| prof. dr. A.P. Philipse      | (Universiteit Utrecht)                    |
| prof. dr. W.H. van Riemsdijk | (Wageningen Universiteit)                 |
| prof. dr. R.P. Sijbesma      | (Technische Universiteit Eindhoven)       |

Dit onderzoek is uitgevoerd binnen de onderzoeksschool PTN

# Chain stoppers in reversible supramolecular polymer solutions

Wout Knoben

Proefschrift

ter verkrijging van de graad van doctor  
op gezag van de rector magnificus  
van Wageningen Universiteit,  
prof. dr. M.J. Kropff,  
in het openbaar te verdedigen  
op vrijdag 19 januari 2007  
des namiddags te half twee in de Aula

ISBN 90-8504-574-6

*In science, one tries to tell people, in such a way as to be understood by everyone, something that no one ever knew before. In poetry, it's the exact opposite.*

**Paul Dirac** <sup>1</sup>

*Everything should be made as simple as possible, but not simpler.*

**Albert Einstein** <sup>2</sup>

---

<sup>1</sup>Paul Dirac (1902-1984) was awarded the 1933 Nobel prize in physics. He also 'derived' the existence of the purling stitch (averechte steek) in knitting after watching someone using the knit stitch (rechte steek)

<sup>2</sup>Albert Einstein (1879-1955) won the 1921 Nobel prize in physics. In 1926, he was also the co-inventor of a new type of refrigerator.



# Contents

|          |  |           |
|----------|--|-----------|
| <b>1</b> | <b>Introduction</b>  | <b>1</b>  |
| 1.1      | A brief (pre)history of polymer science . . . . .  | 1         |
| 1.2      | (Reversible) supramolecular polymers . . . . .   | 3         |
| 1.3      | Chain architectures . . . . .  | 4         |
| 1.4      | Average degree of polymerisation . . . . .   | 6         |
| 1.4.1    | Effect of chain stoppers . . . . .   | 7         |
| 1.5      | Applications of supramolecular polymers . . . . .  | 8         |
| 1.6      | Outline of this thesis . . . . .   | 9         |
| <b>2</b> | <b>Multiple shear-banding transitions in a supramolecular polymer solution</b>   | <b>15</b> |
| 2.1      | Introduction . . . . .   | 16        |
| 2.2      | Theoretical background . . . . .   | 16        |
| 2.3      | Experimental . . . . .   | 17        |
| 2.4      | Results and discussion . . . . .   | 17        |
| 2.5      | Concluding remarks . . . . .   | 23        |
| <b>3</b> | <b>Rheology of a reversible supramolecular polymer, studied by comparison of the effects of temperature and chain stoppers</b>     | <b>25</b> |
| 3.1      | Introduction . . . . .   | 26        |
| 3.2      | Theoretical background . . . . .   | 28        |
| 3.2.1    | Supramolecular polymers and chain stoppers . . . . .   | 28        |
| 3.2.2    | Linear rheology . . . . .  | 30        |
| 3.3      | Experimental . . . . .   | 32        |
| 3.4      | Results and discussion . . . . .   | 33        |
| 3.4.1    | Linear rheology . . . . .  | 33        |
| 3.4.2    | Flow curves . . . . .  | 39        |
| 3.5      | Concluding remarks . . . . .   | 44        |
| <b>4</b> | <b>Chain stoppers in reversible supramolecular polymer solutions, studied by static and dynamic light scattering and osmometry</b> | <b>49</b> |
| 4.1      | Introduction . . . . .   | 50        |
| 4.2      | Theoretical background . . . . .   | 52        |
| 4.2.1    | Average chain length . . . . .   | 52        |
| 4.2.2    | Static light scattering . . . . .  | 56        |

|          |  |            |
|----------|--|------------|
| 4.2.3    | Dynamic light scattering . . . . .   | 58         |
| 4.3      | Experimental . . . . .   | 60         |
| 4.3.1    | Materials . . . . .  | 60         |
| 4.3.2    | Osmometry . . . . .  | 60         |
| 4.3.3    | Light scattering . . . . .   | 60         |
| 4.4      | Results and discussion . . . . .   | 61         |
| 4.4.1    | Vapor pressure osmometry . . . . .   | 62         |
| 4.4.2    | Static light scattering . . . . .  | 63         |
| 4.4.3    | Effectiveness of chain stoppers . . . . .  | 69         |
| 4.4.4    | Dynamic light scattering . . . . .   | 70         |
| 4.5      | Concluding remarks . . . . .   | 74         |
|          | Appendix: CONTIN spectra . . . . .   | 75         |
| <b>5</b> | <b>Dynamics of reversible supramolecular polymers: independent de-<br/>termination of the dependence of linear viscoelasticity on concentra-<br/>tion and chain length by using chain stoppers</b> | <b>81</b>  |
| 5.1      | Introduction . . . . .   | 82         |
| 5.2      | Theoretical background . . . . .   | 84         |
| 5.2.1    | Chain stoppers . . . . .   | 84         |
| 5.2.2    | Viscoelasticity of supramolecular polymers . . . . .   | 85         |
| 5.2.3    | Probe particle diffusion . . . . .   | 87         |
| 5.3      | Experimental . . . . .   | 90         |
| 5.3.1    | Materials . . . . .  | 90         |
| 5.3.2    | Dynamic light scattering by probe particles . . . . .  | 90         |
| 5.3.3    | Rheometry . . . . .  | 91         |
| 5.4      | Results and discussion . . . . .   | 91         |
| 5.4.1    | Macroscopic viscoelasticity . . . . .  | 92         |
| 5.4.2    | Scaling of the zero-shear viscosity . . . . .  | 93         |
| 5.4.3    | Scaling of the terminal relaxation time . . . . .  | 96         |
| 5.5      | Microscopic versus macroscopic viscoelasticity . . . . .   | 99         |
| 5.6      | Concluding remarks . . . . .   | 103        |
| <b>6</b> | <b>Direct measurement of depletion and hydrodynamic forces in solu-<br/>tions of a reversible supramolecular polymer</b>   | <b>107</b> |
| 6.1      | Introduction . . . . .   | 108        |
| 6.2      | Theoretical background . . . . .   | 110        |
| 6.2.1    | Depletion interaction . . . . .  | 110        |
| 6.2.2    | Concentration dependence of $\delta$ . . . . .   | 111        |
| 6.2.3    | Concentration dependence of $\Pi_{bulk}$ . . . . .   | 112        |
| 6.2.4    | Non-equilibrium forces in Colloidal Probe Atomic Force<br>Microscopy . . . . .   | 113        |
| 6.3      | Experimental . . . . .   | 116        |

|          |   |            |
|----------|---|------------|
| 6.3.1    | Solutions . . . . .   | 116        |
| 6.3.2    | Materials . . . . .   | 117        |
| 6.3.3    | Colloidal probe AFM . . . . .   | 117        |
| 6.3.4    | Phase separation . . . . .  | 119        |
| 6.4      | Results . . . . .   | 119        |
| 6.4.1    | Depletion force measurements . . . . .  | 119        |
| 6.4.2    | Hydrodynamic forces . . . . .   | 124        |
| 6.4.3    | Macroscopic phase separation . . . . .  | 130        |
| 6.4.4    | Discussion . . . . .  | 132        |
| 6.5      | Concluding remarks . . . . .  | 134        |
| <b>7</b> | <b>Long range depletion forces induced by associating small molecules</b>       | <b>139</b> |
| 7.1      | Introduction . . . . .  | 140        |
| 7.2      | Theoretical background . . . . .  | 142        |
| 7.3      | Experimental . . . . .  | 143        |
| 7.4      | Results and discussion . . . . .  | 143        |
| 7.5      | Concluding remarks . . . . .  | 146        |
| <b>8</b> | <b>Functionalisation of silica surfaces with 2,7-diamido-1,8-naphthyridines</b> | <b>149</b> |
| 8.1      | Introduction . . . . .  | 150        |
| 8.2      | Experimental . . . . .  | 153        |
| 8.2.1    | Synthesis . . . . .   | 153        |
| 8.2.2    | Functionalisation and characterisation of SiO <sub>2</sub> surfaces .           | 156        |
| 8.3      | Results and discussion . . . . .  | 157        |
| 8.3.1    | Synthesis . . . . .   | 157        |
| 8.3.2    | Functionalisation of SiO <sub>2</sub> strips . . . . .                          | 161        |
| 8.3.3    | Preliminary results . . . . .   | 165        |
| 8.4      | Concluding remarks . . . . .  | 167        |
|          | <b>Summary</b>  | <b>171</b> |
|          | <b>Samenvatting voor dummies</b>  | <b>177</b> |
|          | <b>Dankwoord</b>  | <b>189</b> |
|          | <b>List of publications</b>   | <b>192</b> |
|          | <b>Levensloop</b>   | <b>193</b> |
|          | <b>Education programme</b>  | <b>194</b> |



# 1

## Introduction

### 1.1 A brief (pre)history of polymer science

Ever since the earliest civilizations, people have used the materials that nature provided to make tools for hunting, warfare, cooking and agriculture, and also for the fabrication of clothing and jewelry. For thousands of years, stone, wood, clay and animal skin and bone were the only available materials. As time passed, people found out how to use other materials such as wool, silk, rubber and cotton. Around 2000 BC (in Europe), bronze replaced stone and after another 1000 years, iron made its appearance. During the centuries that followed, more advanced techniques were developed for harvesting, working and processing these materials, but the materials themselves remained the same for a very long time.

This situation rapidly changed when John Dalton came up with the idea that molecules contained different types of unchangeable *atoms* in 1808 [1]. He postulated that atoms can rearrange to form new molecules, but one atom can never change into another type of atom. This brought an end to the alchemistic belief that gold could be made from other metals, and marks the beginning of modern chemistry. Jöns Berzelius recognized that two compounds with the same types of atoms in the same ratios (isomers) can have different molecular weights, and he called the 'heavy' isomers *polymers* [2]. At that time, people started experimenting with synthetic (organic) chemistry: the deliberate manufacture of a compound, or the alteration of its properties, by chemical reaction. This led to the discovery of several revolutionary new (semi-)synthetic materials, such as vulcanized rubber, which was invented (or, as the story has it, discovered by luck) in 1839 by Charles Goodyear when he experimented with adding sulfur to natural rubber [3]. In the same year, distillation and (unintentional) oxidation of resin from the sweetgum plant yielded styroloxyd, a material now known as polystyrene. In 1856, reaction of cellulose with nitric acid yielded 'celluloid', a polymer which was widely used for photographic film.

The next landmark in chemistry was the notion of the valence of atoms

## 1.1. A brief (pre)history of polymer science

---

and *molecular structure*, published independently by Archibald Couper [4] and Friedrich Kekulé [5] in 1858. They argued that the order in which the atoms of a compound are connected determines its properties. This explained the observation that some materials can have the same atomic composition, but very different properties. Experiments revealed that some materials, like rubber, cotton, starch and proteins had incredibly high molecular masses. Scientists assumed that these 'high polymers' were made of many small molecules, which somehow aggregated into large structures. Solutions of these polymers often displayed glue-like properties, and the aggregates were therefore called *colloids*, from the Greek 'kolla' (κόλλα), meaning 'glue'.

In 1907, Leo Bakeland was the first to make a truly new synthetic polymer. Reaction of phenol and formaldehyde yielded a rigid, light weight material that he called 'Bakelite'. Soon, Bakelite was used to make almost anything, from jewelry to telephone housings. In spite of all the new materials being developed based on the view of polymers as colloidal aggregates, Herman Staudinger [6] did not believe in this theory. He proposed that materials with high molecular weights were made of giant chainlike molecules which he called *macromolecules*, rather than aggregates of small molecules [7]. After publishing his idea in 1920, it took more than a decade before the scientific community accepted Staudinger's macromolecular theory. Convincing evidence came in 1928 from the X-ray diffraction experiments of Kurt Meyer and Herman Mark, which showed that cellulose was made of long chains of cellobiose (a 1-4-glucose dimer) [8]. DuPont scientist Wallace Carothers also believed Staudinger, and he attempted to prove the existence of giant molecules by synthesizing them in the laboratory. He succeeded, and his experiments yielded a large number of synthetic macromolecules, such as polyamides [9], which eventually led to the discovery of *nylon* in 1935, and the first synthetic rubber polychloroprene [10] (sold as *neoprene*). During his investigations, Carothers redefined polymers as molecules, characterized by a recurring structural unit (monomer): "*The structural units -R- are bivalent radicals which, in general, are not capable of independent existence*" [11]. This definition, which implies that monomers are connected by covalent bonds, was generally adopted by polymer scientists, and remained unchanged for 60 years.

Since then, countless new polymers have been synthesized. New polymerisation reactions and processes were discovered, and the range of applications for polymers has grown explosively. Nowadays, synthetic polymers are present everywhere. To name just a few examples, they are in our clothes, cars and computers, we use them to make all kinds of packings, they are an essential component of paints and inks, and they are even in our body as implants or contact lenses.

## 1.2 (Reversible) supramolecular polymers

In the last 20 years, there has been increasing interest in self-assembly: the spontaneous arrangement of molecules into structured, stable, non-covalently joined aggregates [12]. Much inspiration in this field comes from nature, where very complex non-covalent aggregates are found, such as cell membranes and protein filaments. The branch of chemistry involved with this ‘chemistry beyond the molecule’ is called *supramolecular chemistry* [13].

Supramolecular chemistry gained momentum when the 1987 Nobel prize in chemistry was awarded to Donald Cram, Jean-Marie Lehn and Charles Pedersen for “their development and use of molecules with structure-specific interactions of high selectivity”. Of these three laureates, Lehn is generally credited with the synthesis of the first *supramolecular polymers* [14, 15]: self-assembled chains of small molecules, held together by reversible non-covalent interactions [16–19]. It is noteworthy that supramolecular polymers do not comply with Carothers’ definition of a polymer as a (single) macromolecule. In fact, they are rather reminiscent of the 19th century idea of polymers as colloidal aggregates. Nevertheless, supramolecular polymers have a lot in common with their covalent counterparts, and are now accepted as a special type of polymer.

The above definition of a supramolecular polymer does not specify the type of interaction which holds the monomers together, only that it should be non-covalent. However, association of molecules by interactions which lack directionality does not lead to the formation of chains, but to randomly shaped aggregates. In practice, only interactions which display a high specificity and directionality are useful to create supramolecular polymers, see figure 1.1a and b. The two classes which are most intensively studied are (water-soluble) supramolecular polymers based on metal-ligand complexation [20, 21] and supramolecular polymers in apolar solvents based on hydrogen bonding [22–24]. There are also examples of supramolecular polymers based on other type of interactions, such as DNA hybridization [25], host-guest interactions [26, 27] and  $\pi - \pi$ -stacking [28].

Since the bonds between monomers are non-covalent, they are in principle reversible: a bond can break up into two free binding groups, and two free binding groups can form a bond. Thus, the chains can break and recombine, and there is a continuous exchange of bound and free monomers. If breaking and recombination of bonds occurs on experimental time scales, it affects the properties of the supramolecular polymer, especially the dynamics. For these systems, the term *reversible* supramolecular polymers may be used. However, in practice the prefix ‘reversible’ is often omitted, and the general term ‘supramolecular polymer’ is used.

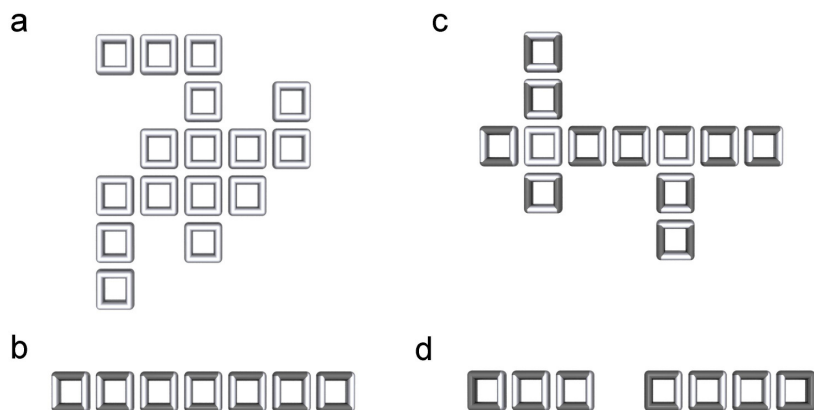


Figure 1.1: Schematic representation of different types of non-covalent aggregates. Monomers are represented by squares, white faces can form bonds, gray faces cannot. a: random aggregate by non-directional interactions; b: linear chain of bifunctional monomers; c: branching by tri- and tetrafunctional monomers; d: monofunctional monomers act as chain stoppers.

### 1.3 Chain architectures

To form a linear chain, the monomers of a supramolecular polymer must be bifunctional: they must contain two binding groups which are capable of binding with another monomer (see figure 1.1b). The presence of monomers with more than two binding groups leads to branching of chains and network formation (figure 1.1c). Monomers with only one binding group can bind to a chain, but prevent it from growing any further (figure 1.1d). These monofunctional monomers are therefore also known as *chain stoppers*. Their presence decreases the average degree of polymerisation. Hereafter, only linear chains and chain stoppers will be considered.

The formation of a supramolecular polymer has many similarities with condensation polymerisation, which also involves the association of bifunctional monomers into polymer chains [29, 30]. During the polymerisation step, the process is reversible, since the liberated condensation product can hydrolyze bonds between monomers. Therefore, many results obtained for condensation polymers can also be applied to supramolecular polymers. For example, for sufficiently high association constants, an exponential chain length distribution is predicted, with a polydispersity index  $M_w/M_n = 2$ . Also the concepts of

chain stoppers and crosslinkers are known from condensation polymerisation.

The simplest type of supramolecular polymer consists of symmetric bifunctional monomers, see figure 1.2a. That is, a monomer contains two self-complementary binding groups (BB-type monomers). These monomers form supramolecular homopolymers without any directionality in the chain. The well-known supramolecular polymers based on the ureido-pyrimidinone (UPy) unit are an example of such a system [22]. Monofunctional chain stoppers can bind to both sides of the chain.

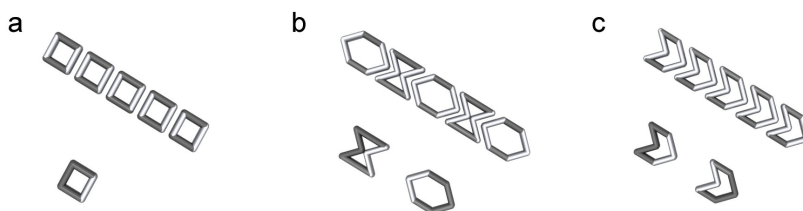


Figure 1.2: Different types of supramolecular chains and chain stoppers. a: non-directional homopolymer of symmetric (BB-type) monomers; b: alternating copolymer of symmetric AA- and DD-type monomers; c: directional homopolymer of AD-type monomers.

Supramolecular alternating block-copolymers can be made by mixing two types of symmetric bifunctional monomers (AA and DD), each bearing two heterocomplementary binding groups. That is, a AA monomer cannot bind to another AA monomer, but only to a DD monomer, see figure 1.2b. Examples are supramolecular polymers based on metal-ligand complexation [21], where the bis-ligand and the metal ion are the AA and DD monomers, respectively. Monofunctional monomers of both types will act as chain stoppers. Also stoichiometry is very important. Long chains are obtained only if both monomers are present exactly in a 1:1 ratio. If there is an excess of either monomer, it will occupy the chain ends and act as a chain stopper, decreasing the average degree of polymerisation.

A third type of supramolecular polymer can be made from asymmetric bifunctional monomers of the acceptor-donor (AD) type, see figure 1.2c. Bisurea EHUT [31, 32] is such an asymmetric monomer, although it may also exist in a symmetric form. Another example are monomers which contain one UPy group and one 2,7-diamido-1,8-naphthyridine (Napy) group [33]. Chains of these monomers are homopolymers, but in contrast to the BB-type monomers, there is directionality in the chains: one end of a chain is always formed by an acceptor group, the other end by a donor group. Monomers with either only

## 1.4. Average degree of polymerisation

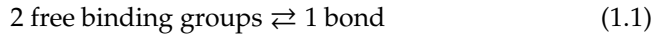
---

an acceptor or only a donor group act as chain stoppers. In contrast to the BB-type monomers, they can only bind to one end of the chain.

Of course, more complicated structures can be designed, for example by using more different binding groups or by combining different association mechanisms in one polymer [34, 35]. However, these exotic examples are not fundamentally different from the examples mentioned above, and will not be treated here.

### 1.4 Average degree of polymerisation

If we consider a system of only bifunctional monomers, and we represent the equilibrium between breaking and formation of bonds as follows:



we can write for the association constant  $K$  of this equilibrium

$$K = \frac{[\text{bonds}]}{[\text{free binding groups}]^2} \quad (1.2)$$

Here, we assume that  $K$  is independent of the length of the chain to which a monomer binds. The association constant is related to the bond strength, which can be expressed as the free energy  $E_b$  needed to cleave a bond [36]:

$$K \sim \exp\left(\frac{E_b}{k_B T}\right) \quad (1.3)$$

This expression shows that  $K$  is a function of temperature, but the bond strength is also determined by other parameters such as pH, salt concentration and solvent polarity.

A chain of  $N$  monomers contains  $N - 1$  bonds and 2 free binding groups at its ends. A solution with a concentration  $c$  of bifunctional monomers and an average degree of polymerisation  $\langle N \rangle$  contains  $c/\langle N \rangle$  chains, so the concentration of bonds in this solution is  $(c/\langle N \rangle)(\langle N \rangle - 1)$ , and the concentration of free end groups equals  $2c/\langle N \rangle$ . Substituting this in equation 1.2 leads to

$$K = \frac{\langle N \rangle (\langle N \rangle - 1)}{4c} \quad (1.4)$$

From this equation, it follows that the average degree of polymerisation  $\langle N \rangle$  is a function of  $c$  and  $K$ :

$$\langle N \rangle = \frac{1 + \sqrt{1 + 16Kc}}{2} \approx 2\sqrt{Kc} \quad (1.5)$$

where the approximate equality applies if the chains are long, or more precisely if  $Kc \gg 1$ .

Thus, the average degree of polymerisation of a supramolecular polymer depends on the overall monomer concentration and the association constant, which is in turn determined by a number of other parameters (equation 1.3).

### 1.4.1 Effect of chain stoppers

We may quantify the effect of chain stoppers by assuming that for every  $n$  chain stoppers added to the solution, one extra chain is created. Let us consider a solution with a concentration  $c$  of bifunctional monomers and an average degree of polymerisation  $\langle N(0) \rangle$  (without any chain stoppers, given by equation 1.5). The concentration of chains is given by  $c/\langle N(0) \rangle$ . To this solution, a concentration  $k$  of chain stoppers is added. As a result, the concentration of chains is increased by  $k/n$ , and the average degree of polymerisation  $\langle N(k) \rangle$  is now given by

$$\langle N(k) \rangle = \frac{c + k}{c/\langle N(0) \rangle + k/n} \quad (1.6)$$

The chain stoppers make up a fraction  $x = k/(c + k)$  of the solutes, so  $k = cx/(1 - x)$ . Substituting this expression in equation 1.6 leads to  $\langle N(x) \rangle$ :

$$\langle N(x) \rangle = \frac{n\langle N(0) \rangle}{n(1 - x) + x\langle N(0) \rangle} \quad (1.7)$$

To obtain long supramolecular chains, the purity of the monomers is of great importance. In particular the presence of chain stoppers, even in small amounts, can have a detrimental effect on the length of the chains. For example, consider a supramolecular polymer with an association constant  $K$  of  $10^7 \text{ M}^{-1}$ . In a solution with a monomer concentration of  $0.01 \text{ M}$ , the average degree of polymerisation is given by equation 1.5:  $\langle N(0) \rangle = 6.3 \cdot 10^2$ . If 1% of the monomers is monofunctional ( $x = 0.01$ ) and we assume that  $n = 1$ , the average degree of polymerisation can be calculated by equation 1.7. This leads to  $\langle N(x) \rangle = 85$ , the average degree of polymerisation is strongly decreased by the chain stoppers. It can be seen from equation 1.7 that above a certain value of  $x$  (depending on  $\langle N(0) \rangle$  and  $x$ ), the first term in the denominator can be neglected, leading to  $\langle N(x) \rangle \approx n/x$ . Thus, at sufficiently high stopper fractions, the average degree of polymerisation is completely determined by the stopper fraction, and independent of  $\langle N(0) \rangle$ .

## 1.5 Applications of supramolecular polymers

A number of recent patents demonstrate that supramolecular polymers are not just an interesting scientific toy, but they can be used in a variety of applications [37]. The reversibility of the bonds gives supramolecular polymers some unique properties compared to their covalent counterparts. For example, supramolecular polymers generally reach thermodynamic equilibrium faster than covalent ones. Breaking and reformation of bonds gives supramolecular polymers an additional mechanism for stress relaxation, which is unavailable to covalent polymers. Supramolecular polymer networks were shown to reach higher crosslink densities than covalent networks as a result of the fast equilibration [38]. This may lead to enhanced material properties.

Supramolecular polymers are often compared to wormlike micelles, which are also long, non-covalent aggregates of small molecules [36]. Like wormlike micelles, supramolecular polymers could be used to (reversibly) alter the rheological properties of liquids [39]. However, the interactions between the monomers in supramolecular polymers are much more specific than in wormlike micelles, which enables a better control over the structure of the chains. For example, cross-linkers or chain stoppers (see section 1.3) can be added to adjust the chain architecture. The viscosity of supramolecular polymers depends strongly on temperature, owing to the temperature dependence of the chain length. This fact may be useful for the fabrication of materials which are easily processable at elevated temperatures (if the chains are short), but display good properties at low temperatures (if the chains are long) [40].

Furthermore, there has been increasing interest in the synthesis of so-called ‘intelligent’ or ‘responsive’ materials, which can react to changes in their environment [41, 42]. Supramolecular polymers hold promise for applications in such materials, because of their ability to adapt their chain length upon application of various stimuli. Basically, any parameter which affects the equilibrium between breaking and formation of bonds (equation 1.1) can be used. Examples include the use of temperature [43], pH [44], ultrasound [45] and light [46]. Systems which respond to multiple stimuli can also be designed [47].

Beside the bulk and solution properties, also the interfacial behavior of supramolecular polymers is expected to be highly dynamic. Supramolecular polymers may for example be used for the regulation of colloidal stability. The range and strength of the interactions between particles often depends on the size of the polymer chains. By changing temperature, monomer concentration or any other parameter which affects  $\langle N \rangle$ , the range of interaction between colloidal particles could easily and reversibly be adjusted. Furthermore, by using asymmetric monomers (AD-type, see section 1.3), directionality can be introduced in supramolecular polymer chains. It is predicted that the

interfacial behavior of end-attached supramolecular chains strongly depends on the symmetry of the monomers [48].

## 1.6 Outline of this thesis

When the first supramolecular polymers appeared, the importance of the purity of the bifunctional monomers was immediately recognized. Small amounts of contaminations can have a detrimental effect on the chains. Especially the presence of monofunctional chain stoppers, even in very small amounts, has to be prevented. If a chain stopper binds to a chain the resulting chain end is non-functional or 'dead': no new monomers can bind to this chain end. By blocking functional chain ends, the addition of chain stoppers leads to a decrease of the average degree of polymerisation.

In fact, chain stoppers were deliberately added to supramolecular polymer solutions to break up the chains and thus to demonstrate the specificity of the bonds between the monomers [22]. A statistical model was developed, which showed the effects of chain stoppers on the chain length (distribution) [49]. The effect of chain stoppers is discussed in a number of experimental papers, but usually in a rather qualitative way. For example, chain stoppers are shown to decrease the average chain length by size exclusion chromatography [50, 51], or by measuring the solution viscosity [52, 53]. In this thesis, the effects of chain stoppers on supramolecular polymer solutions is investigated in more detail. Furthermore, it is demonstrated that chain stoppers are not only an unpleasant contamination in supramolecular polymer solutions, but they can also be used to obtain information which is otherwise inaccessible.

The experimental system under investigation consists of bifunctional monomer EHUT (*2,4-bis(2-ethylhexylureido)toluene*, see figure 1.3) [31]. EHUT forms rigid linear chains of monomers in various apolar organic solvents by the cooperative formation of four hydrogen bonds between two consecutive monomers [32, 54]. A number of chain stoppers for EHUT were synthesized, and of these, *2,4-bis(dibutylureido)toluene* (DBUT, figure 1.3) was found to be the most effective [55]. The first part of this thesis deals with the solution behavior of EHUT/DBUT. In **chapter 2**, the highly complex non-linear rheology of EHUT solutions is investigated. Rheometry and heterodyne light scattering yield evidence for the existence of no less than three shear banding regimes. It is suggested that the rheological behavior is related to a strong coupling between flow-induced alignment and subsequent elongation of chains. This hypothesis is tested in **chapter 3**, in which the effects of the addition of chain stoppers and an increase in temperature are compared. Both decrease the average degree of polymerisation, but the addition of chain stoppers leads to blocked chain ends, which may prevent aligned chains from associating. A

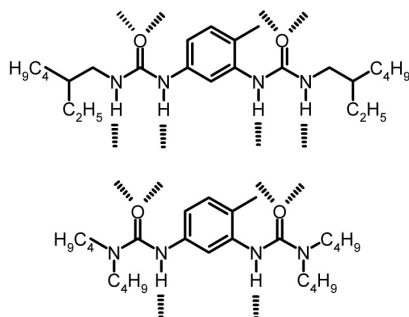


Figure 1.3: Bifunctional monomer EHUT (top) and monofunctional chain stopper DBUT (bottom). Possible hydrogen bonds are represented by dashed lines.

simple model for the effect of chain stoppers on the average degree of polymerisation is presented. This model is consistent with the experimental data.

**Chapter 4** deals with static properties of EHUT/DBUT solutions, studied with light scattering and osmometry. Estimates for the association constant and the persistence length of EHUT chains are obtained. Furthermore, it is shown that DBUT can completely block the concentration dependence of the average degree of polymerisation, and the effectiveness of DBUT as a chain stopper is discussed. In **chapter 5**, the linear rheology is investigated. By using chain stoppers, the separate effects of the overall monomer concentration and the average degree of polymerisation are studied, which is otherwise impossible. The results show that EHUT chains are semiflexible, and both breaking and reptation of chains contribute to stress relaxation.

In the second part of this thesis, the interfacial behavior of supramolecular polymers is studied. The measurement with colloidal probe atomic force microscopy of attractive depletion forces between stearylated silica surfaces immersed in EHUT/DBUT solutions is described. In **chapter 6**, the concentration dependence of the depletion force is investigated. Furthermore, the results indicate that the presence of the depletion layer causes a significant decrease of the hydrodynamic interaction between the probe and the substrate, which greatly facilitates the experiments. In **chapter 7**, it is demonstrated that by varying the amount of chain stoppers, the depletion force can be tuned, an effect which is unique to supramolecular polymers.

**Chapter 8** does not deal with EHUT and DBUT, but with supramolecular polymers based on the UPy and Napy units (see section 1.3. In this chapter, the functionalisation of silica surfaces with a Napy derivative is described.

Fluorescence spectroscopy showed that the functionalised surface is capable of selectively and reversibly binding Upy groups. A more detailed investigation was hampered by degradation of the surface-bound Napys.

## References

- [1] J. Dalton. *A new system of chemical philosophy*, vol. 1. Manchester, 1808.
- [2] J.J. Berzelius. *Jahresber. Fortschr. Phys. Wissensch.*, 12: 63–67, 1833.
- [3] H. Morawetz. *Polymers: the origins and growth of a science*. Dover Publications, New York, 1985.
- [4] A.S. Couper. *Phil. Mag.*, 16: 104–116, 1858.
- [5] A. Kekulé. *Ann. Chem. Pharm.*, 106: 129–159, 1858.
- [6] H. Ringsdorf. *Angew. Chem. Int. Ed.*, 43: 1064–1076, 2004.
- [7] H. Staudinger. *Ber. Dtsch. Chem. Ges.*, 53: 1073–1085, 1920.
- [8] K.H. Meyer and H. Mark. *Ber. Dtsch. Chem. Ges.*, 61: 593–614, 1928.
- [9] W.H. Carothers and G.J. Berchet. *J. Am. Chem. Soc.*, 52: 5289–5291, 1930.
- [10] W.H. Carothers, I. Williams, A.M. Collins, and J.E. Kirby. *J. Am. Chem. Soc.*, 53: 4203–4225, 1931.
- [11] W.H. Carothers. *J. Am. Chem. Soc.*, 51: 2548–2559, 1929.
- [12] G.M. Whitesides, J.P. Mathias, and C.T. Seto. *Science*, 254: 1312–1319, 1991.
- [13] J-M. Lehn. *Supramolecular chemistry: concepts and perspectives*. VCH, Weinheim, 1995.
- [14] J-M. Lehn, M. Mascal, A. Decian, and J. Fischer. *J. Chem. Soc. Chem. Comm.*, (6): 479–481, 1990.
- [15] J-M. Lehn, M. Mascal, A. Decian, and J. Fischer. *J. Chem. Soc. Perkin Trans. 2*, (4): 461–467, 1992.
- [16] N. Zimmerman, J.S. Moore, and S.C. Zimmerman. *Chem. Ind.*, (15): 604–610, 1998.
- [17] J.S. Moore. *Curr. Opin. Colloid Interface Sci.*, 4: 108–116, 1992.
- [18] L. Brunsveld, B.J.B. Folmer, E.W. Meijer, and R.P. Sijbesma. *Chem. Rev.*, 101: 4071–4097, 2001.

## References

---

- [19] A. Ciferri, editor. *Supramolecular polymers*. CRC Press, Boca Raton, 2nd edition, 2005.
- [20] U.S. Schubert and C. Eschbaumer. *Angew. Chem. Int. Ed.*, 41: 2893–2926, 2002.
- [21] T. Vermonden, G. van der Gucht, P. de Waard, A.T.M. Marcelis, N.A.M. Besseling, E.J.R. Sudhölter, G.J. Fleer, and M.A. Cohen Stuart. *Macromolecules*, 36: 7035–7044, 2003.
- [22] R.P. Sijbesma, F.H. Beijer, L. Brunsveld, B.J.B. Folmer, J.H.K.K. Hirschberg, R.F.M. Lange, J.K.L. Lowe, and E.W. Meijer. *Science*, 297: 1601–1604, 1997.
- [23] D.C. Sherrington and K.A. Taskinen. *Chem. Soc. Rev.*, 30: 83–93, 2001.
- [24] R.P. Sijbesma and E.W. Meijer. *Chem. Comm.*, 1: 5–16, 2003.
- [25] E. A. Fogleman, W. C. Yount, J. Xu, and S. L. Craig. *Angew. Chem. Int. Ed.*, 41: 4026–4028, 2002.
- [26] H.W. Gibson, N. Yamguchi, and J.W. Jones. *J. Am. Chem. Soc.*, 125: 3522–3533, 2003.
- [27] A. Harada. *J. Polym. Sci. Part A: Polym. Chem.*, 44: 5113–5119, 2006.
- [28] A. Arnaud, J. Belleney, F. Boue, L. Bouteiller, G. Carrot, and W. Wintgens. *Angew. Chem. Int. Ed.*, 43: 1718–1721, 2004.
- [29] P.J. Flory. *Principles of polymer chemistry*. Cornell University Press, Ithaca, New York, 1964.
- [30] P.J. Flory. *J. Am. Chem. Soc.*, 58:1877–1885, 1936.
- [31] S. Boileau, L. Bouteiller, F. Lauprêtre, and F. Lortie. *New J. Chem.*, 24:845–848, 2000.
- [32] F. Lortie, S. Boileau, L. Bouteiller, C. Chassenieux, B. Demé, G. Ducouret, M. Jalabert, F. Lauprêtre, and P. Terech. *Langmuir*, 18:7218–7222, 2002.
- [33] O.A. Scherman, G.B.W.L. Ligthart, R.P. Sijbesma, and E.W. Meijer. *Angew. Chem. Int. Ed.*, 45:2072–2076, 2006.
- [34] H. Hofmeier, A. El-Ghayoury, A.P.H.J. Schenning, and U.S. Schubert. *Chem. Comm.*, (3):318–319, 2004.
- [35] X-Q. Li, M-X. Jia, X-Z. Wang, X-K. Jiang, Z-T Li, G-J Chen, and Y-H Yu. *Tetrahedron*, 61:9600–9610, 2005.

- 
- [36] M.E. Cates and S.J. Candau. *J. Phys.: Condens. Matter*, 2: 6869–6892, 1990.
- [37] A.W. Bosman, R.P. Sijbesma, and E.W. Meijer. *Mater. Today*, 7: 34–39, 2004.
- [38] R.F.M. Lange, M. van Gurp, and E.W. Meijer. *J. Polym. Sci. Part A: Polym. Chem.*, 37: 3657–3670, 1999.
- [39] J. Yang. *Curr. Opin. Colloid Interface Sci.*, 7: 276–281, 2002.
- [40] B.J.B. Folmer, R.P. Sijbesma, R.M. Versteegen, J.A.J. van der Rijt, and E.W. Meijer. *Adv. Mater.*, 12: 874–878, 2000.
- [41] R. Yerushalmi, A. Scherz, M.E. van der Boom, and H.B. Kraatz. *J. Mater. Chem.*, 15: 4480–4487, 2005.
- [42] N.M. Sangeetha and U. Maitra. *Chem. Soc. Rev.*, 34: 821–836, 2005.
- [43] S. Kiyonaka, K. Sugayisu, S. Shinkai, and I. Hamachi. *J. Am. Chem. Soc.*, 124:10954–10955, 2002.
- [44] S-L. Zhou, S. Matsumoto, H-D. Tian, H. Yamane, A. Ojida, S. Kiyonaka, and I. Hamachi. *Chem. Eur. J.*, 11:1130–1136, 2005.
- [45] J.M.J. Paulusse and R.P. Sijbesma. *Angew. Chem. Int. Ed.*, 45: 2334–2337, 2006.
- [46] T. Suzuki, S. Shinkai, and K. Sada. *Adv. Mater.*, 18:1043–1046, 2006.
- [47] W. Weng, J.B. Beck, A.M. Jamieson, and S.J. Rowan. *J. Am. Chem. Soc.*, 128: 11663–11672, 2006.
- [48] J. van der Gucht, N.A.M Besseling, and M.A. Cohen Stuart. *J. Am. Chem. Soc.*, 124: 6202–6205, 2002.
- [49] P.M. Saville and E.M. Sevick. *Langmuir*, 14:3137–3139, 1998.
- [50] U. Michelsen and C.A. Hunter. *Angew. Chem. Int. Ed.*, 39(4):764–767, 2000.
- [51] K. Ogawa and Y. Kobuke. *Angew. Chem. Int. Ed.*, 39:4070–4073, 2000.
- [52] B.J.B. Folmer, E. Cavini, R.P. Sijbesma, and E.W. Meijer. *Chem. Comm.*, (17):1847–1848, 1998.
- [53] P. Terech and A. Coutin. *J. Phys. Chem. B*, 105:5670–5676, 2001.
- [54] J. van der Gucht, N.A.M. Besseling, W. Knoben, L. Bouteiller, and M.A. Cohen Stuart. *Phys. Rev. E*, 67:051106, 2003.
- [55] F. Lortie, S.B. Boileau, L. Bouteiller, C. Chassenieux, and F. Lauprêtre. *Macromolecules*, 38:5283–5287, 2005.
-



# 2

## Multiple shear-banding transitions in a supramolecular polymer solution

### Abstract

We report on the non-linear rheology of a reversible supramolecular polymer based on hydrogen bonding. Coupling between flow-induced chain alignment and breakage and recombination of bonds between monomers leads to a very unusual flow behavior. Measured velocity profiles indicate three different shear-banding regimes upon increasing shear rate, each with different characteristics. While the first of these regimes has features of a mechanical instability, the second shear banding regime is related to a shear-induced phase separation and the appearance of birefringent textures. The shear-induced phase becomes itself unstable at very high shear rates, giving rise to a third banding regime.

### 2.1 Introduction

Coupling between fluid microstructure and flow yields a rich scala of non-Newtonian behavior in complex fluids. Many complex fluids display flow instabilities or flow-induced phase transitions above a critical shear rate or stress. Solutions of wormlike micelles, for example, undergo a shear-banding instability in which the fluid separates in the gradient direction into coexisting regions (bands) supporting different shear rates (“gradient banding”) [1, 2]. Rod-like colloids, on the other hand, display “vorticity banding”, in which the different shear bands are separated in the vorticity direction [3]. Several other systems, such as attractive emulsions or carbon nanotube suspensions, show an elastic instability that leads to the formation of shear-induced aggregates aligned in the vorticity direction [4, 5].

### 2.2 Theoretical background

Several aspects of these instabilities can be reproduced by phenomenological models, see e.g. [6]. Shear banding in the gradient direction, for example, can be related to a non-monotonic constitutive equation relating the shear stress  $\sigma$  and the shear rate  $\dot{\gamma}$ . When a shear rate is applied in the region where  $\sigma$  decreases with  $\dot{\gamma}$ , an initially homogeneous flow becomes mechanically unstable. In the simplest scenario, the system then separates into a weakly sheared band that flows at  $\dot{\gamma}_1$  and a highly sheared band that flows at  $\dot{\gamma}_2$  [2]. Increasing the overall shear rate within the unstable region leads to an increase of the width of the high-shear band, while the stress remains constant. The microscopic origin of the shear-banding instability varies for different systems. For wormlike micelles two alternative mechanisms for shear banding have been proposed. Cates and coworkers predicted a non-monotonic constitutive equation leading to a shear-banding instability, based on the Doi and Edwards reptation model for polymers [2]. This purely mechanical instability is responsible for shear banding in semidilute solutions of wormlike micelles, far from an equilibrium phase transition [1]. In more concentrated systems, on the other hand, the appearance of a banded flow is related to a first-order phase transition induced by the flow, such as an isotropic to nematic transition [6, 7]. In this case, the two shear bands correspond to two structurally different coexisting phases.

Most experimental studies on shear banding have been performed with solutions of wormlike micelles. These have been successfully described as reversible equilibrium polymers that can break and recombine on experimental timescales [8]. In recent years, various other types of reversible supramolecular polymers have been synthesized, based on more specific reversible interactions, such as metal coordination complexes and hydrogen bonding [9].

The availability of these polymers paves the way for experiments that will lead to a more general understanding of the flow behavior of reversible polymers.

In this Letter, we report for the first time on shear banding in a solution of reversible supramolecular polymers based on hydrogen bonding. The unique feature of this system is that we observe *three* different shear banding regimes upon variation of the shear rate, each with different characteristics. While the banded state at low shear rates has features of a mechanical instability, the second shear banding regime is related to a shear-induced phase transition and the appearance of texture. In this region, we find a very unusual relation between the relative widths of the two shear bands and the overall shear rate: the width of the high-shear band *decreases* when the global shear rate increases. At very high shear rates, the shear-induced phase becomes itself unstable, giving rise to a third banding regime.

## 2.3 Experimental

The system under examination is a solution of bis-urea-substituted toluene (EHUT), a bifunctional monomer that assembles reversibly into long, semi-flexible polymer chains by multiple hydrogen bonds [10]. The persistence length of EHUT polymers was estimated to be at least 100 nm [11], which is an order of magnitude larger than for most wormlike micelles [8]. We study solutions of EHUT in dodecane at concentrations up to 6.4 g/l at 20 °C. No evidence for an isotropic-to-nematic phase transition (at rest) was observed for this concentration range and temperature. Rheological measurements were performed on a Paar Physica MCR 300 rheometer in controlled strain mode using a Couette geometry of 26.66 mm inner diameter and 1.13 mm gap width and a solvent trap to minimize evaporation. It was checked that a different Couette geometry gave only small differences. Spatially resolved velocity profiles were measured in a closed transparent Couette cell (43 mm inner diameter, 2.5 mm gap) using heterodyne dynamic light scattering in combination with a differential Laser Doppler velocimeter [12]. The rheo-optical properties of the sheared solutions were studied by placing a transparent Couette cell (43 mm inner diameter, 2.5 mm gap) between crossed polarizers. Images were taken in the plane defined by the flow and vorticity directions, so that the measured birefringence is an average over the gap.

## 2.4 Results and discussion

Figure 2.1 shows the steady-state shear stress  $\sigma$  as a function of the shear rate  $\dot{\gamma}$  for a 5.9 g/l EHUT solution at 20°C. Several regimes are indicated in this figure. In regime A ( $\dot{\gamma} < \dot{\gamma}_1 \approx 0.01 \text{ s}^{-1}$ ), the stress increases linearly with the

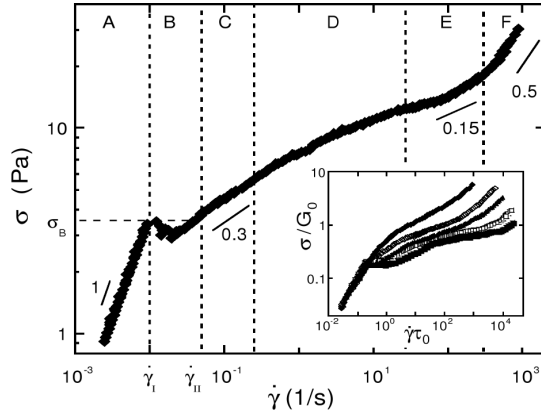


Figure 2.1: Shear stress as a function of shear rate for a 5.9 g/l EHUT solution at 20°C (measured under controlled shear rate). A-F indicate different flow regimes. In regimes B, D, and E, a banded flow is observed. Inset: flow curves for EHUT concentrations of 1.4 (◆), 2.0 (◇), 3.1 (▲), 5.9 (□), and 6.4 (■) g/l;  $\dot{\gamma}$  is normalized by the terminal relaxation time  $\tau_0$  and  $\sigma$  is normalized by the plateau modulus  $G_0$ .

shear rate. The solution behaves as a Maxwell fluid in this regime with a viscosity  $\eta$  of 368 Pa·s, plateau modulus  $G_0$  of 16 Pa and a relaxation time  $\tau_0$  of 23 s as obtained from the transient stress response after start-up of shear flow and from dynamic linear rheology measurements. At  $\dot{\gamma} = \dot{\gamma}_I \approx 0.01 \text{ s}^{-1}$  and  $\sigma = \sigma_B \approx 3.3 \text{ Pa}$ , there is an abrupt change of slope, after which the stress decreases slightly with increasing shear rate. After reaching a minimum, the stress increases again, but with a much lower slope than in the linear regime. Region B is characterized by stress overshoots, very slow transient behavior (it may take hours before a steady state is reached), and metastability. At  $\dot{\gamma} > \dot{\gamma}_{II} \approx 0.06 \text{ s}^{-1}$ , the stress exceeds  $\sigma_B$  and increases with increasing shear rate with a slope of about 0.3 (regime C). In regime D, the slope of the flow curve decreases and reaches a minimum of around 0.08 at  $\dot{\gamma} \approx 30 \text{ s}^{-1}$ . In regime E, the slope increases again and it eventually reaches a value of around 0.5 in regime F. Regimes D and E are again characterized by slow transient behavior. Care was taken to ensure that the points in figure 2.1 really correspond to the steady-state values for the stress. Different shear histories were applied to the solution, which all resulted in the same steady-state value. We also measured a flow curve in controlled stress mode. This gave the same result, except that no points could be measured in regime B: at  $\sigma = \sigma_B$ , the shear rate ‘jumps’ from  $\dot{\gamma}_I$  to  $\dot{\gamma}_{II}$ . As indicated in the inset in Fig. 2.1, flow curves at different

concentrations exhibit qualitatively the same characteristics. The onset of regime B occurs at the same normalized shear rate  $\dot{\gamma}_1\tau_0 = 0.20 \pm 0.03$  and stress  $\sigma_B/G_0 = 0.18 \pm 0.03$  for all concentrations, where  $G_0$  and  $\tau_0$  both increase with increasing concentration [11]. At higher shear rates, the normalized flow curves do not superimpose, and the normalized stress at a certain normalized shear rate decreases with increasing concentration.

Figure 2.2 shows velocity profiles in the gap of the Couette cell measured at different applied overall shear rates. The lowest shear rate for which a velocity profile could be measured was  $0.01 \text{ s}^{-1}$ , just on the boundary of regimes A and B. The velocity profile is linear, as expected for a Newtonian solution. At shear rates between  $0.015$  and  $0.066 \text{ s}^{-1}$  (regime B, Fig. 2.2a), the profiles exhibit a ‘kink’, indicating a banded structure. The kink becomes more pronounced with increasing shear rate. The measured velocity profiles also enable a quantification of wall slip. In regime B, there is a marginal slip at the stationary outer cylinder. At shear rates between  $0.066$  and  $0.25 \text{ s}^{-1}$  (regime C, Fig. 2.2b) the profiles are linear, indicating that the flow is homogeneous. Slip is negligible in this regime. An unambiguous banded state is observed again in regimes D and E, at shear rates between  $0.25$  and  $300 \text{ s}^{-1}$ . In regime D, between  $0.25$  and  $30 \text{ s}^{-1}$ , the velocity profile in both shear bands is approximately linear (Fig. 2.2c), while in regime E, above  $30 \text{ s}^{-1}$ , the high-shear band has a strongly curved profile (Fig. 2.2d). At the highest shear rate applied ( $\dot{\gamma} = 308 \text{ s}^{-1}$ ), the low shear band has disappeared and only one band is left, also with a curved velocity profile (regime F, Fig. 2.2d). The curved velocity profiles in regimes E and F are an indication for strong shear thinning in these regimes [12]. The profile for  $\dot{\gamma} = 308 \text{ s}^{-1}$  can be fitted with a power-law fluid  $\sigma \sim \dot{\gamma}^a$  with an exponent  $a = 0.15$  [13]. The same shear-thinning exponent accounts for the profiles in the high shear band in regime E. A slope of  $0.15$  is also indicated in the flow curve shown in Fig. 2.1. It can be seen in this figure that this exponent is in reasonable agreement with the slope of the measured flow curve in the relevant region (regime E and the beginning of regime F).

Solutions of EHUT thus exhibit *three* different shear banding regimes. The onset of the first shear banding regime (B) occurs at the same normalized shear rate  $\dot{\gamma}_1\tau_0$  and stress  $\sigma_B/G_0$  for different EHUT concentrations (Fig. 2.1, inset), suggesting that the origin of shear banding in this regime is a mechanical instability of the underlying constitutive relation, such as proposed by Spenley and Cates [2]. Indeed, birefringence images show no evidence for a shear-induced phase transition in regime B (Fig. 2.3a): no significant increase of the birefringence could be detected in regimes B and C. The unstable flow behavior is also supported by the jump in the flow curve when measured under controlled stress. The shear-banded flow at higher shear rates, in regimes D and E, on the other hand, is accompanied by the appearance of birefringent textures in the solution (Fig. 2.3b-d). These textures could be seen for the

## 2.4. Results and discussion

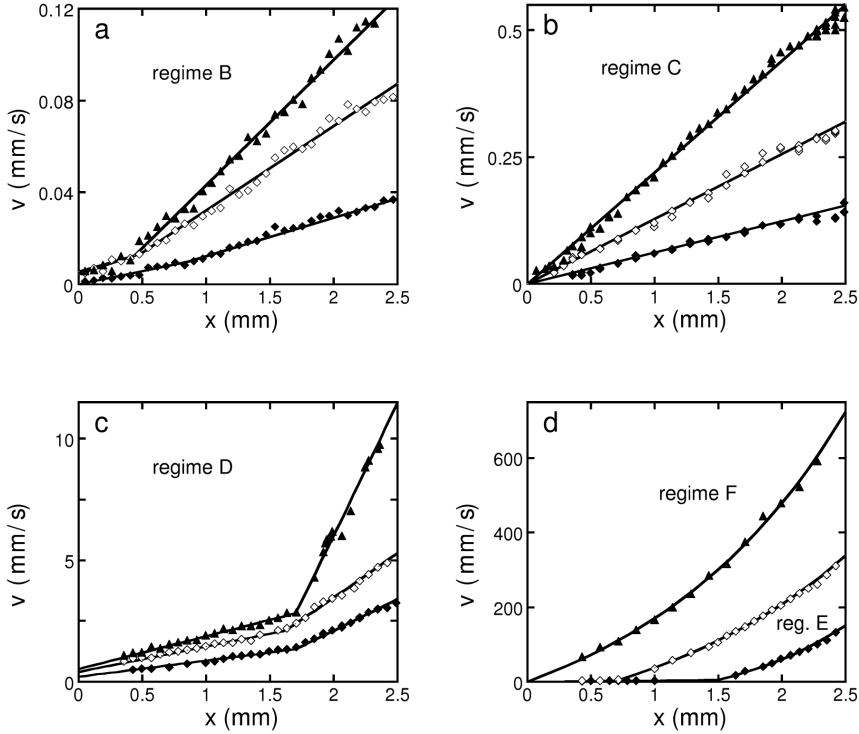


Figure 2.2: Velocity profiles in the Couette cell at different applied shear rates  $\dot{\gamma}$ . (a) Regime B,  $\dot{\gamma} = 0.015$  ( $\blacklozenge$ ),  $\dot{\gamma} = 0.025$  ( $\diamond$ ), and  $\dot{\gamma} = 0.05$  ( $\blacktriangle$ )  $s^{-1}$ . Drawn lines are linear fits for both bands. (b) Regime C,  $\dot{\gamma} = 0.066$  ( $\blacklozenge$ ),  $\dot{\gamma} = 0.14$  ( $\diamond$ ), and  $\dot{\gamma} = 0.23$  ( $\blacktriangle$ )  $s^{-1}$ . Drawn lines corresponds to  $v = \dot{\gamma}x$ . (c) Regime D,  $\dot{\gamma} = 0.59$  ( $\blacklozenge$ ),  $\dot{\gamma} = 1.5$  ( $\diamond$ ), and  $\dot{\gamma} = 4.9$  ( $\blacktriangle$ )  $s^{-1}$ . Lines are linear fits for both bands. (d) Regime E,  $\dot{\gamma} = 64$  ( $\blacklozenge$ ) and  $\dot{\gamma} = 147$  ( $\diamond$ )  $s^{-1}$ , and beginning of regime F,  $\dot{\gamma} = 308$   $s^{-1}$  ( $\blacktriangle$ ). Drawn lines correspond to a linear profile for the low shear band and a power law fluid ( $\sigma \sim \dot{\gamma}^{0.15 \pm 0.02}$ ) for the high shear band. No slip was observed at the moving wall in all cases.

first time at a shear rate of about  $1 s^{-1}$  (i.e. in regime D). They appear a few seconds after start-up of shear flow and remain visible for many hours under steady flow. After cessation of the shear flow, the textures disappear again on the timescale of several seconds. With increasing shear rate, the overall birefringence increases and the textures become finer and at very high shear rates, they seem to disappear (Fig. 2.3d). Without polarized incoming light, no texture could be seen. The textures can be interpreted as domains of a

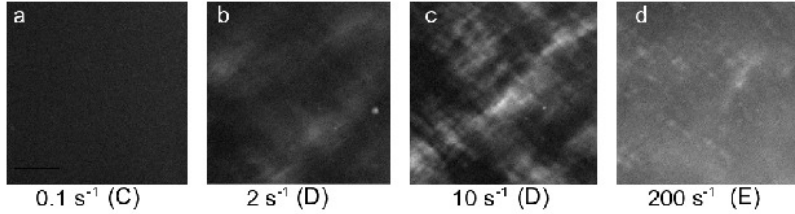


Figure 2.3: Birefringence images taken in the plane defined by the flow and vorticity directions of a 5.9 g/l EHUT solution at 20°C under shear flow for different applied shear rates (as indicated). The flow regime is indicated in brackets. Each image is 1x1 cm.

new phase induced by the shear flow and suggest that, contrary to regime B, the banded structure in regimes D and E is related to a shear-induced phase separation (for example between an isotropic and a nematic phase). Similar domain patterns have been seen in other multi-phase flows where they were attributed to a viscoelastic asymmetry between the two phases [5]. In wormlike micelle solutions, a shear-induced phase transition is observed only for very concentrated micellar solutions, close to an equilibrium phase transition [7]. For EHUT solutions, we did not see evidence for a phase transition at rest for the concentrations used, but, nevertheless, a transition is induced by the flow. This suggests that the flow couples more strongly to chain alignment and growth for EHUT than for wormlike micelles, probably because of the longer persistence length of EHUT polymers [8, 11].

In order to obtain more detailed information about the behavior in the three different shear banding regimes, we extract from the velocity profiles displayed in Fig. 2.2 the average shear rates in both shear bands and the width of the two bands. These are shown in Fig. 2.4 as a function of the overall applied shear rate. Clearly, our observations do not correspond to the simple picture in which a change of the applied shear rate only affects the relative proportion of each layer, while the shear rates in both bands and the value of the stress remain constant [2]. In regime B, we find that both the shear rate in the low-shear band  $\dot{\gamma}_1$  and that in the high-shear band  $\dot{\gamma}_2$  increase with increasing  $\dot{\gamma}$ . Moreover, we do not see a clear stress plateau in the flow curve (Fig. 2.1). These observations may be due to the inherent stress gradient of the Couette cell. Alternatively, the compositions of the two bands could be different and vary when the overall shear rate is varied [6]. The relative width of the high-shear band  $\epsilon_2$  increases with the overall shear rate  $\dot{\gamma}$  in regime B, as expected [2]. It approaches unity as regime C is approached, where the banded structure

## 2.4. Results and discussion

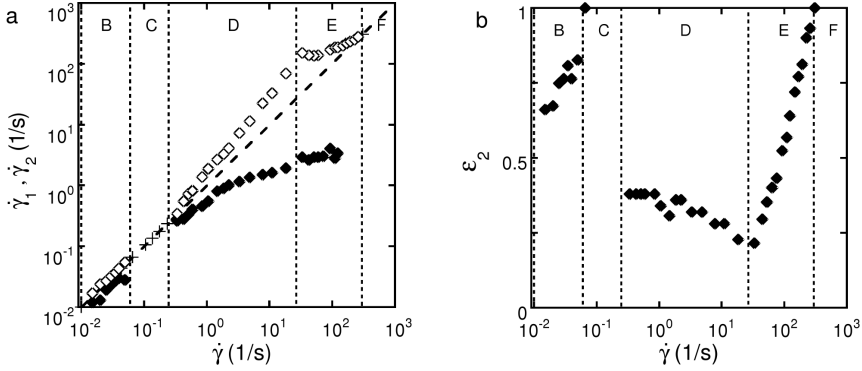


Figure 2.4: (a) Average shear rates  $\dot{\gamma}_1$  in the low shear band ( $\blacklozenge$ ) and  $\dot{\gamma}_2$  in the high shear band ( $\blacklozenge$ ) as a function of the overall shear rate. + indicates shear rates in regime C, where no shear banding is observed. The diagonal dashed line denotes homogeneous flow. (b) Fraction  $\varepsilon_2$  of the gap occupied by the high shear band as a function of the overall shear rate. Note that there is only one band in regimes A, C, and F. Vertical dashed lines in both Figs. indicate different regimes A-F.

disappears. The difference in viscosity between the two bands in regime B is rather small: the ratio  $\dot{\gamma}_2/\dot{\gamma}_1$  varies between 1 and 2. In regime D, where shear banding is related to a phase transition (as seen from birefringence images), the variation of  $\dot{\gamma}_1$ ,  $\dot{\gamma}_2$ , and  $\varepsilon_2$  with  $\dot{\gamma}$  is rather unusual. Upon increasing the shear rate,  $\varepsilon_2$  first remains more or less constant and then *decreases*, while the ratio between the shear rates in both bands ( $\dot{\gamma}_2/\dot{\gamma}_1$ ) increases from 1 to approximately 50. Clearly, such behavior cannot be explained by current theory. It suggests a complex interplay between the structure of the two phases, the concentrations and length distributions in both phases, and the shear flow. In regime E, the behavior is more or less as expected. Upon increasing the overall shear rate, the shear rates in the two bands remain approximately constant, while  $\varepsilon_2$  increases monotonically to unity at the boundary between regimes E and F, where also the textures disappear. The behavior of  $\dot{\gamma}_1$ ,  $\dot{\gamma}_2$ , and  $\varepsilon_2$  upon variation of the overall shear rate changes very abruptly at  $\dot{\gamma} \approx 30 \text{ s}^{-1}$ , between regimes D and E. As noted above, the shapes of the velocity profiles also change here: in regime D the profiles are linear in both bands, while in regime E the high-shear band is strongly curved (Fig. 2.2c,d). These observations suggest that the shear-induced phase that is formed in regime D becomes unstable in regime E, thus giving rise to a third shear banding regime. Whether this instability is a mechanical instability or a phase transition to a new shear-induced phase

or structure is unclear. It would be useful to extend the present rheological study with scattering techniques, microscopy, or birefringence imaging in the vorticity direction to obtain information about the microstructure of the two phases.

## 2.5 Concluding remarks

In summary, we studied the non-linear rheology of a solution of hydrogen-bonded supramolecular equilibrium polymers. Upon variation of the shear rate, these polymers exhibit a very rich and complex behavior with three different shear banding regimes. For the first time, we observe within the same system the two different types of gradient shear banding that have been described: a mechanical instability at low shear rates and a shear-induced phase transition at higher shear rates. The characteristics of the banded flow regimes can not be fully explained by current theories and ask for a detailed microscopic modeling of equilibrium polymers under flow, that takes into account the coupling between flow alignment, reversible breakage and recombination reactions, and concentration gradients in the gap. By comparing with other types of reversible supramolecular polymers and contrasting to wormlike micelles, we may be able to extract the role of specific bonding interactions and chain flexibility in these systems. Alternatively, by adding monofunctional monomers that block chain ends and prevent their recombination [14], one could investigate the role of recombination reactions, while adding trifunctional monomers would give the possibility of bundle or network formation.

## References

- [1] H. Rehage and H. Hoffmann. *Mol. Phys.*, 74:933, 1991.
- [2] N. A. Spenley, M. E. Cates, and T. C. B. McLeish. *Phys. Rev. Lett.*, 71:939, 1993.
- [3] M. P. Lettinga and J. K. G. Dhont. *J. Phys. Condens. Matter*, 16:S3929, 2004.
- [4] A. Montesi, A. Peña, and M. Pasquali. *Phys. Rev. Lett.*, 92:058303, 2004.
- [5] E. K. Hobbie, S. Lin-gibson, H. Wang, J. A. Pathak, and H. Kim. *Phys. Rev. E*, 69:061503, 2004.
- [6] S. M. Fielding and P. D. Olmsted. *Eur. Phys. J. E*, 11:65, 2003.
- [7] J. F. Berret, D. C. Roux, and P. Lindner. *Eur. Phys. J. B*, 5:67, 1998.

## References

---

- [8] M. E. Cates and S. J. Candau. *J. Phys. : Condens. Matter*, 2:6869, 1990.
- [9] L. Brunsveld, B. J. B. Folmer, E. W. Meijer, and R. P. Sijbesma. *Chem. Rev.*, 101:4071, 2001.
- [10] S. Boileau, L. Bouteiller, F. Lauprêtre, and F. Lortie. *New J. Chem.*, 24:845, 2000.
- [11] J. Van der Gucht, N. A. M. Besseling, W. Knoben, L. Bouteiller, and M. A. Cohen Stuart. *Phys. Rev. E*, 67:051106, 2003.
- [12] J.-B. Salmon, A. Colin, and S. Manneville. *Phys. Rev. Lett.*, 90:228303, 2003.
- [13] The velocity profile for a power law fluid with  $\sigma \sim \dot{\gamma}^a$  in a Couette geometry is  $v(r) = \omega_0 r (r^{-2/a} - R_2^{-2/a}) / (R_1^{-2/a} - R_2^{-2/a})$ , with  $\omega_0$  the applied angular velocity,  $R_1$  the radius of the inner cylinder,  $R_2$  that of the outer cylinder, and  $r = R_2 - x$  the distance from the center of the cylinders [12].
- [14] W. Knoben, N. A. M. Besseling, L. Bouteiller, and M. A. Cohen Stuart. *Phys. Chem. Chem. Phys.*, 7:2390, 2005.

# 3

## Rheology of a reversible supramolecular polymer, studied by comparison of the effects of temperature and chain stoppers

### Abstract

The rheology of a reversible supramolecular polymer is studied by comparing the effects of an increase in temperature and the addition of chain stoppers. The dependence of the zero-shear viscosity and the terminal relaxation time on temperature is exponential, and the activation energy for viscous flow can be calculated. Above a critical stopper fraction, power laws describe the stopper dependence of the viscosity and relaxation time. A simple model for the effect of the addition of chain stoppers on the average degree of polymerisation adequately describes the results. A comparison of flow curves at several temperatures and stopper fractions reveals considerable differences between solutions with the same zero-shear viscosity. These are mainly associated with differences in the terminal relaxation time. A mechanism of shear-induced alignment and subsequent elongation of chains is proposed, with which the experimental results are consistent.

## 3.1 Introduction

For ages, scientists have used biological systems as a source of inspiration for the development of new structures and materials. One of the defining processes in biology is the ability to respond to changes in external conditions such as temperature, light, pH or the presence of certain chemicals. Much recent scientific effort is aimed at the incorporation of this responsiveness in synthetic polymeric materials [1–5]. On a fundamental level, this may increase our understanding of complex biological systems. In terms of practical applications, the synthesis of so-called ‘intelligent’ or ‘self-healing’ materials is a promising perspective.

To react adequately and sensitively to a change in conditions, a responsive polymer must be able to quickly and reversibly change its properties. A relatively new class of polymers, with inherently highly dynamic properties are ‘reversible supramolecular’ polymers [6, 7]. In contrast to ‘normal’ polymers, the monomers of a supramolecular polymer are not connected by covalent chemical bonds, but by weaker, reversible interactions such as hydrogen bonds, metal-ligand complexation or  $\pi - \pi$ -interactions. Supramolecular polymers reproduce many of the characteristics associated with the macromolecular nature of covalent polymers. For example, they form viscous solutions or gels at sufficiently high concentrations. But the reversibility of the bonds also leads to important differences between supramolecular and covalent polymers. For example, the equilibrium chain length (distribution) of a supramolecular polymer is not fixed, but it depends on conditions like the overall monomer concentration, temperature and solvent. Furthermore, supramolecular polymers have interesting dynamical properties, owing to the continuous breaking and reformation of bonds. The ability to adapt their chain length makes supramolecular polymers promising candidates for applications in responsive materials [8–11]. Such applications require that the equilibration (caused by the breaking and reformation of bonds) is sufficiently fast, so a change in conditions is translated into a measurable change in the material properties within a practically relevant time. For systems which satisfy both criteria (non-covalent bonds between monomers and sufficiently fast equilibration) the term ‘reversible supramolecular polymers’ is used.

In many respects, supramolecular polymers are similar to the surfactant aggregates known as wormlike micelles [12]. These are also long, thin structures of small molecules, held together by non-covalent interactions. Wormlike micelles also have a temperature- and concentration-dependent length, and a continuous exchange of monomers. They are used in a variety of applications, mainly based on their ability to (reversibly) alter the rheological properties of liquids [13]. Despite the similarities, there are also fundamental differences between wormlike micelles and reversible supramolecular polymers.

For example, wormlike micelles only exist within a certain range of conditions (surfactant and salt concentration, temperature, etc.), whereas supramolecular polymers display polymeric properties in dilute and concentrated solutions as well as in the bulk [14]. Furthermore, the interactions between the monomers in supramolecular polymers are much more specific than in wormlike micelles, which enables a better control over the structure of the chains. For example, cross-linkers or chain stoppers (vide infra) can be added to adjust the chain architecture. Furthermore, directionality can be introduced in supramolecular polymer chains, which is predicted to strongly affect the interfacial behavior of supramolecular polymers [15, 16].

Generally, the monomers of a supramolecular polymer contain two binding groups (bifunctional monomers), enabling them to associate into linear chains [7, 14]. The presence of monomers with three or more binding groups leads to branching and network formation. On the other hand, monomers with only one binding group stop the growth of the chain to which they bind, they form a non-functional or 'dead' chain end. These monofunctional monomers are therefore also called 'chain stoppers', and they decrease the average degree of polymerisation.

Many types of non-covalent interactions can be used to form supramolecular polymers. In aqueous environment, mixing of bis-ligands with chelating metal ions has proven to be a successful approach [17, 18]. Attempts to make water-soluble supramolecular polymers without metal ions include the use of  $\pi - \pi$ -interactions [19], DNA base pairing [20] and several types of host-guest interactions [21, 22]. In apolar organic solvents, (multiple) hydrogen bonds can be used to create supramolecular polymers [23, 24]. An example of a supramolecular polymer, based on the cooperative formation of four hydrogen bonds between consecutive monomers, is bisurea EHUT (2,4-bis-(2-ethylhexylureido)toluene) [25, 26]. This molecule forms long, semiflexible supramolecular chains in several apolar organic solvents, and has a very rich and complex rheological behavior [27]. Previously, it was demonstrated that 2,4-bis(dibutylureido)toluene (DBUT) can be used as a monofunctional chain stopper for EHUT, and the effect of the chain stopper on static properties of EHUT solutions was reported [28, 29]. It was also shown that chain stoppers can be used to investigate separately the effect of monomer concentration and degree of polymerisation on linear rheology, which is normally impossible for supramolecular polymers [30].

In the present paper, two ways of adjusting the average degree of polymerisation of EHUT solutions are compared: (1) increasing temperature and (2) addition of chain stoppers. The fact that chain stoppers form 'dead' chain ends sets them apart from the other parameters which affect the average degree of polymerisation (like temperature). The addition of chain stoppers may therefore affect the solution properties in a different way than an increase in

## 3.2. Theoretical background

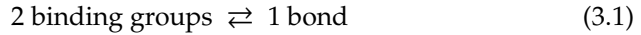
---

temperature. For example, it was recently suggested that there is a strong coupling between the shear-induced alignment of chains and chain growth in EHUT solutions due to their high persistence length [27]. This coupling could be weakened by the presence of ‘dead’ chain ends, which prevent chains from associating to each other. The effect of chain stoppers and temperature on the linear rheology is investigated in section 3.4.1, and flow curves at several temperatures and stopper concentrations are compared in section 3.4.2.

## 3.2 Theoretical background

### 3.2.1 Supramolecular polymers and chain stoppers

The equilibrium between breaking and reformation of bonds in a supramolecular polymer can be written as follows:



This equilibrium is very similar to that used in Flory’s mean-field theory of condensation polymerisation [31, 32]. The latter is also an equilibrium reaction (during the polymerisation step) between bifunctional monomers, as the released condensation product can reversibly hydrolyze bonds between monomers. Flory’s equation for the average degree of polymerisation  $\langle N \rangle$  as a function of the overall concentration  $c$  of bifunctional monomers can thus also be applied here:

$$\langle N \rangle = 2 \sqrt{Kc} \sim \exp\left(\frac{E_b}{2k_B T}\right) \sqrt{c} \quad (3.2)$$

where  $K$  is the association constant of the equilibrium and  $E_b \sim k_B T \ln(4K)$  is the effective bonding free energy (also called the end-cap or scission energy), the net free energy needed to cleave a bond. If the association constant is independent of the length of the chain to which a monomer binds (isodesmic association), the chain length distribution at thermodynamic equilibrium is exponential [29, 32].

If the solution contains a concentration  $c$  of bifunctional monomers and a concentration  $k$  of monofunctional chain stoppers, the stopper fraction  $x$  is defined as  $x = k/(c + k)$ . We assume that for every  $n$  chain stoppers added to the solution, one extra chain is formed. Under this assumption,  $\langle N \rangle$  as a function of  $x$  can be calculated [29]. Since the number of chains increases upon the addition of chain stoppers, the average degree of polymerisation must decrease:

$$\langle N(x) \rangle = \frac{n \langle N(0) \rangle}{n(1 - x) + x \langle N(0) \rangle} \approx \frac{n}{x} \quad (3.3)$$

where  $\langle N(0) \rangle$  is the average degree of polymerisation without any chain stoppers, as given by equation 3.2. Figure 3.1 shows  $\langle N(x) \rangle$  for several values of  $n$ . At very low stopper fractions,  $\langle N \rangle$  is hardly affected by  $x$  and  $\langle N(x) \rangle \approx \langle N(0) \rangle$ .

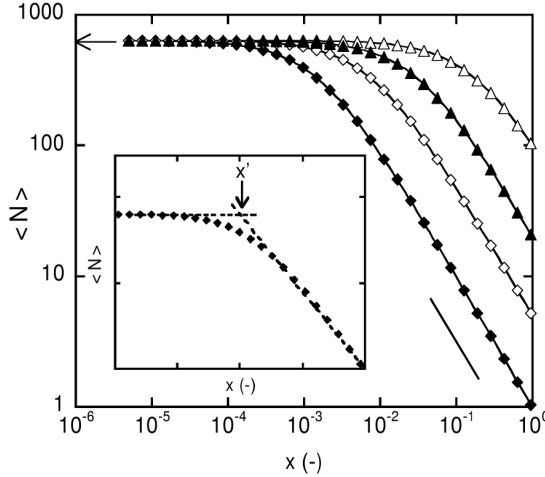


Figure 3.1: Average degree of polymerisation as a function of stopper fraction, calculated with equation 3.3 using  $c = 10^{-2}$  M and  $K = 10^7$  M $^{-1}$  with  $n = 1$  ( $\blacklozenge$ ), 5 ( $\diamond$ ), 20 ( $\blacktriangle$ ) and 100 ( $\triangle$ ). The arrow indicates  $\langle N(0) \rangle$ , the line next to the curves has slope 1 and indicates  $\langle N(x) \rangle \sim 1/x$ . Inset: graphical representation of the determination of the critical stopper fraction  $x'$ , which can be calculated with equation 3.4.

On the other hand, at very high  $x$  (depending on  $\langle N(0) \rangle$  and  $n$ ), the first term in the denominator of equation 3.3 may be neglected, which leads to the approximation  $\langle N(x) \rangle \approx n/x$ . In this regime, virtually all chains are terminated by chain stoppers, and  $\langle N \rangle$  is proportional to  $1/x$  and independent of  $\langle N(0) \rangle$ , and thus of the overall monomer concentration. The intersection of the limiting behavior at low and high  $x$  yields a critical stopper fraction  $x'$  (see also the inset of figure 3.1) above which  $\langle N(x) \rangle$  becomes independent of  $\langle N(0) \rangle$  and is only determined by  $x$  and  $n$ . It can be calculated by equating  $n/x'$  to  $\langle N(0) \rangle$ , leading to

$$x' = \frac{n}{\langle N(0) \rangle} = \frac{n}{2\sqrt{cK}} \quad (3.4)$$

The parameter  $n$  indicates the effectiveness of the chain stopper [29]. If one extra chain is formed for every stopper molecule added ( $n = 1$ ), the stopper has a maximum efficiency. If many stopper molecules are needed to form one

## 3.2. Theoretical background

---

new chain ( $n \gg 1$ ), the stopper is not very effective. The effectiveness of a chain stopper can thus be defined as  $1/n$  and can range from 0 ( $n = \infty$ , no stopper effect) to 1 ( $n = 1$ , perfect stopper).

Equations 3.2 and 3.3 only give the average degree of polymerisation. They contain no information about the distribution of chain lengths. Both with and without chain stoppers, bonds between monomers are continuously broken and formed. Thus, also in the presence of chain stoppers, the chain length distribution is still determined by thermodynamic equilibrium. In other words, the average degree of polymerisation is decreased by the addition of chain stoppers, but the chain length distribution is not quenched and remains exponential. Note that equations 3.2 and 3.3 were derived assuming a homogenous solution in equilibrium. However, different regions in the system may have different average chain lengths, for example in a two-phase system [33]. Also the presence of external fields (such as shear) may affect the average chain length and the chain length distribution [27].

### 3.2.2 Linear rheology

The dynamics of supramolecular polymers are usually considered within the theoretical framework developed by Cates and co-workers for wormlike micelles [12, 34]. This theory is based on the reptation model for entangled covalent polymers [35, 36], to which the kinetics of breaking and reformation of chains are added. In the reptation model, a chain is considered to be trapped in a ‘tube’, consisting of neighbouring chains. Stress relaxation can only occur by curvilinear diffusion of the chain out of its original tube (reptation), which occurs on a characteristic time scale  $\tau_{rep}$ . For monodisperse chains, this leads to a single exponential decay of the stress  $\sigma$ , with relaxation time  $\tau_0 = \tau_{rep}$ . For polydisperse systems, on the other hand, every chain length has its own reptation time, and the stress relaxation becomes strongly non-exponential.

When the reptation model is applied to wormlike micelles or supramolecular polymers, which are by definition polydisperse, it is important how fast a chain breaks and recombines relative to the reptation time. If the characteristic time scale on which a supramolecular chain breaks ( $\tau_{break}$ ) is much shorter than the reptation time, the chains will break and recombine many times before they have reptated out of their original tube. On the time scale of reptation, the chains lose the information about their initial length. The stress relaxation will therefore still be a single exponential, but with a different relaxation time  $\tau_0$ , which contains contributions from  $\tau_{break}$  and  $\tau_{rep}$ , depending on the flexibility of the chains [30, 37]. On the other hand, if  $\tau_{break}$  is much slower than  $\tau_{rep}$ , the chains do (on average) not break during the time they need to reptate out of their tube. In this case, the solution effectively contains a polydisperse mixture of non-breakable chains and the same result as for polydisperse covalent

polymers is obtained.

At time scales much longer than  $\tau_{break}$ , corresponding to low shear rates, supramolecular polymer solutions thus display remarkably simple viscoelasticity, due to the frequent breaking and recombination of chains. The rheology can be described by the Maxwell model, in which a viscoelastic material is characterized by its zero-shear viscosity  $\eta_0$  and its terminal relaxation time  $\tau_0$ . When a shear rate  $\dot{\gamma}$  is applied at  $t = 0$ , the stress increases monotonically to its steady-state value according to

$$\sigma(t) = \eta_0 \dot{\gamma} (1 - e^{-t/\tau_0}) \quad (3.5)$$

On the other hand, if the shear is stopped at  $t = 0$  after the steady-state stress has been reached, the stress decay is given by:

$$\sigma(t) = \eta_0 \dot{\gamma} e^{-t/\tau_0} \quad (3.6)$$

Thus, the zero-shear viscosity and the terminal relaxation time can be obtained from the transient stress response upon start-up or cessation of steady shear if the Maxwell model is obeyed. Within this model, there is a very simple relation between  $\eta_0$ ,  $\tau_0$  and the elastic plateau modulus  $G_0$ :

$$\eta_0 = \tau_0 G_0 \quad (3.7)$$

### Dependence on $\langle N \rangle$

According to Cates' model [12, 34], the zero-shear viscosity and the terminal relaxation time depend on the overall monomer concentration and the average degree of polymerisation according to power laws:

$$\eta_0 \sim \langle N \rangle^\alpha c^\beta \quad (3.8)$$

$$\tau_0 \sim \langle N \rangle^\gamma c^\delta \quad (3.9)$$

The values of the exponents depend on the flexibility of the chains and on the ratio of the breaking and reptation (or for rodlike chains the angular reorientation) time. Limiting values for flexible and rodlike chains in the fast- and slow-breaking limit were previously calculated [30, 37]. Note that without taking special measures, the separate exponents  $\alpha$  to  $\delta$  cannot be measured by measuring  $\eta_0$  and  $\tau_0$  as a function of the overall monomer concentration, since  $\langle N \rangle$  and  $c$  both change if the concentration is varied (equation 3.2). It was previously shown that the separate scaling exponents can be measured by using chain stoppers [30].

### 3.3. Experimental

---

#### Temperature dependence

Viscous flow can be considered as a thermally activated diffusion process. This was originally derived for simple liquids [38], but it is applied much more generally [39, 40]. Like other processes with an activation energy barrier, the temperature-dependence of the viscosity can be described by an Arrhenius-type expression with an activation energy  $E_\eta$ , which contains contributions from the breaking of bonds and the reptation of chains. Moreover, the viscosity is proportional to  $\langle N \rangle^\alpha$  (equation 3.8), and for supramolecular polymers,  $\langle N \rangle$  also depends on temperature, as given by equation 3.2. This leads to an overall temperature dependence for the viscosity, given by

$$\eta_0 \sim \langle N \rangle^\alpha \exp\left(\frac{E_\eta}{k_B T}\right) \sim \exp\left(\frac{\alpha E_b}{k_B T}\right) \exp\left(\frac{E_\eta}{k_B T}\right) = \exp\left(\frac{\alpha E_b + E_\eta}{k_B T}\right) \quad (3.10)$$

The same line of argument can be applied to the terminal relaxation time. The temperature dependence of the viscosity is characterized by an Arrhenius-type equation with activation energy  $E_\tau$ , and the temperature dependence of  $\langle N \rangle$  is included by combining equations 3.2 and 3.9:

$$\tau_0 \sim \langle N \rangle^\gamma \exp\left(\frac{E_\tau}{k_B T}\right) \sim \exp\left(\frac{\gamma E_b}{k_B T}\right) \exp\left(\frac{E_\tau}{k_B T}\right) = \exp\left(\frac{\gamma E_b + E_\tau}{k_B T}\right) \quad (3.11)$$

Since both the viscosity and the relaxation time are determined by the typical breaking and reptation times of a chain and its flexibility, the overall temperature dependence exponents are expected to be equal [41], leading to the expression  $\alpha E_b + E_\eta = \gamma E_b + E_\tau$ .

## 3.3 Experimental

### Solutions

The syntheses of EHUT and DBUT were described elsewhere [25, 28]. Samples were prepared by dissolving EHUT and DBUT in dodecane under stirring for at least one night at  $\pm 50^\circ\text{C}$ . Solutions of 5.0 g/l EHUT were prepared with stopper fractions  $x$  ranging from 0 to 0.10. Experiments were done with solutions containing varying amounts of chain stoppers at a fixed temperature ( $0 \leq x \leq 0.10, T = 20^\circ\text{C}$ ) and with solutions without chain stoppers at varying temperatures ( $20 < T < 70^\circ\text{C}, x = 0$ ).

### Rheology

Rheological measurements were done using a Paar Physica MCR 300 rheometer. This apparatus was used in controlled strain mode. We employed Couette geometries (with rotating inner cylinder) of different gap widths. No significant differences were observed for the different geometries. The temperature

was controlled using a water bath. A solvent trap was used to minimize evaporation.

The steady-state stress was measured as a function of the applied shear rate, which was varied between  $10^{-3}$  and  $10^3$   $s^{-1}$ . These flow curves were recorded from high to low shear rate. Different shear histories were applied to the samples. These all lead to the same result, indicating that it is indeed the steady-state stress which is measured.

Transient stress responses were measured after the sample was left for at least 30 minutes to equilibrate. Shear flow was then started and the stress response was recorded as a function of time. After the steady-state stress had been reached, the shear was stopped and the relaxation of the stress was measured.

## 3.4 Results and discussion

### 3.4.1 Linear rheology

The starting point for our experiments is a 5.0 g/l EHUT solution in dodecane at 20°C without added chain stoppers ( $x = 0$ ). For this solution, the shear stress  $\sigma$  upon application of a steady shear rate of  $0.002$   $s^{-1}$  is shown as a function of time in figures 3.2a and b (top curve). The line is a fit to equation 3.5 with  $\eta_0 = 357$  Pa s and  $\tau_0 = 27$  s. After reaching the steady-state stress (which equals  $\dot{\gamma}\eta_0 = 0.71$  Pa), the shear was stopped instantaneously, and the decay of the shear stress was measured. The result is shown in the insets of figures 3.2a and b (top curve). The line is a fit to equation 3.6 with the same parameters as used for the start-up curve. From these results, it is clear that at this shear rate, the transient rheology is described very well by the Maxwell model. Since  $\eta_0$  and  $\tau_0$  are known,  $G_0$  (the elastic plateau modulus) can easily be calculated with equation 3.7:  $G_0 = 13.2$  Pa.

When the same experiment is done at a higher temperatures (figure 3.2a), there is a strong decrease of the steady-state stress, due to the decreased viscosity of the solution. It can also be seen that the steady-state stress is reached much faster at higher temperatures, which indicates that  $\tau_0$  is also decreased. The stress relaxation curves (shown in the inset) give the same results for  $\eta_0$  and  $\tau_0$ . A decrease in viscosity and relaxation time can also be achieved by adding chain stoppers to the solution (figure 3.2)b. The addition of 0.1% of chain stoppers ( $x = 0.001$ ) already causes a decrease of the viscosity of well over 50%.

Qualitatively, an increase in temperature thus has the same effect as the addition of chain stoppers to the solution. This is not surprising, as in both cases the average degree of polymerisation of the supramolecular chains is decreased (equations 3.2 and 3.3). It is more interesting to focus on quantitative

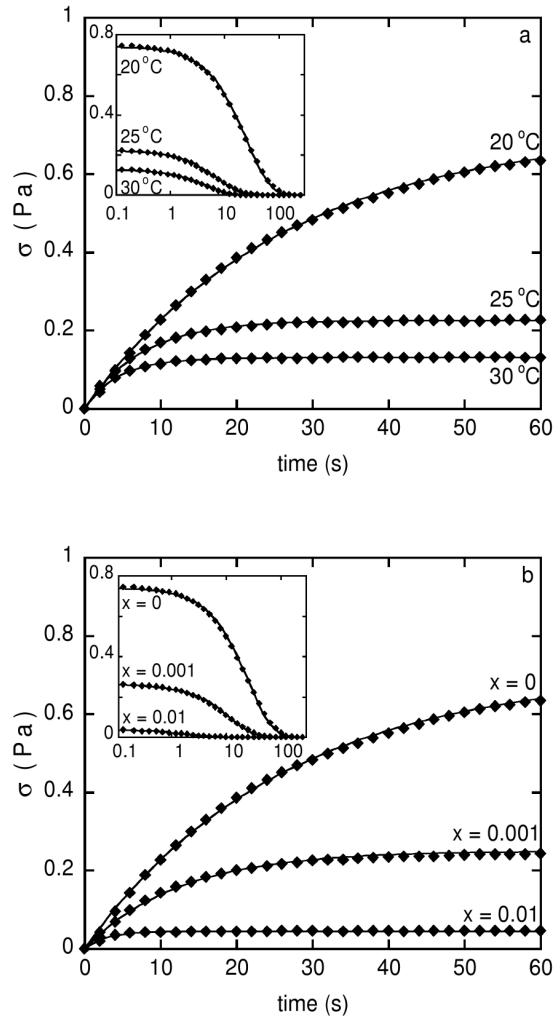


Figure 3.2: Transient stress response of a 5.0 g/l EHUT solution upon start-up (main figures, lines are fits to equation 3.5) or cessation (insets, lines are fits to equation 3.6) of steady shear ( $\dot{\gamma} = 0.002 \text{ s}^{-1}$  for all curves). a: for several temperatures; b: for several stopper fractions.

differences in the dependence of the linear rheological parameters. In section 3.4.1, we describe the effect of temperature on  $\eta_0$  and  $\tau_0$  in more detail, while the effect addition of chain stoppers is investigated in section 3.4.1.

### Effect of temperature

When increasing the temperature from 20 to 70 °C,  $\eta_0$  decreases dramatically over almost four orders of magnitude (as shown by the Arrhenius plot, figure 3.3a). Over this whole range of temperatures, the dependence is described by an exponential, as shown by the fitted line. From the slope of the fit, the activation energy  $\alpha E_b + E_\eta$  can be calculated with equation 3.10. The result is an activation energy for viscous flow of  $2 \cdot 10^{-19}$  J, which is equivalent to approximately 150 kJ/mol or to  $50 k_B T$  at room temperature. Values of the same order of magnitude were found for wormlike micelles and other supramolecular polymers [7, 12, 42]. The temperature-dependence of  $\tau_0$  is shown in figure 3.3b. As can be seen, the terminal relaxation time also decreases exponentially with increasing temperature. The slope of the fitted line is virtually the same as for the viscosity, and the calculated activation energy is therefore also the same (equation 3.11):  $\gamma E_b + E_\tau = 2 \cdot 10^{-19}$  J).

### Effect of chain stoppers

The addition of chain stoppers can also decrease the viscosity by several orders of magnitude, as shown in figure 3.4a. The results obtained from the transient stress response and from the flow curves (see section 3.4.2) are in good agreement. At very low  $x$  ( $< 10^{-3}$ ), the effect on  $\eta_0$  is small. At higher  $x$ , the viscosity starts to decrease significantly and at stopper fractions  $\geq 0.01$ , the viscosity can be described by a power law with a slope of  $-3.0$ . The experimental data over the whole range of  $x$  may be compared to our model describing the effect of chain stoppers by substituting equation 3.3 in equation 3.8. The concentration of bifunctional monomers does not change during our experiments, and neglecting the  $c$ -dependence leads to  $\eta_0 \sim \langle N(x) \rangle^\alpha$ . At high  $x$ , it is expected that  $\langle N(x) \rangle \sim 1/x$ , and thus  $\eta_0 \sim \langle N(x) \rangle^\alpha \sim x^{-\alpha}$ . The value of  $\alpha$  thus follows from the power-law fit to the experimental data at high  $x$ :  $\alpha = 3.0$ . This value is somewhat larger than that obtained previously for EHUT/DBUT solutions in cyclohexane (2.7) [30], but the difference can be explained by the scatter in the experimental data. Equation 3.3 contains two adjustable parameters:  $\langle N(0) \rangle$  and  $n$ .  $\langle N(0) \rangle$  is given by equation 3.2 and contains the known concentration of bifunctional monomers and the association constant  $K$ . By changing  $K$ , the plateau at low  $x$  (denoted by the horizontal dashed line) is shifted vertically, so  $K$  can be used to fit the data at low  $x$  (denoted by the horizontal dashed line in figure 3.4a). The parameter  $n$  indicates the effectiveness of the chain stopper

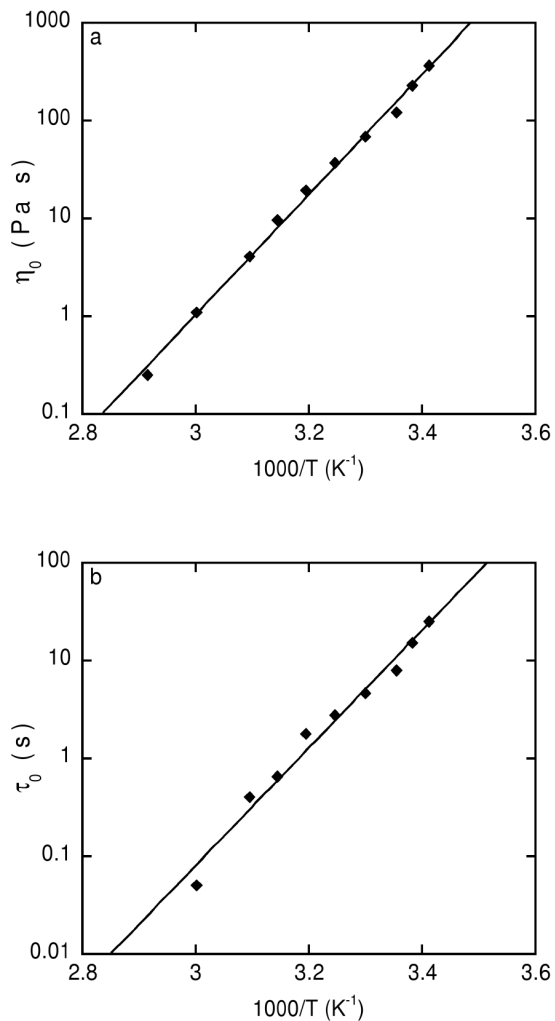


Figure 3.3: Arrhenius plots showing the temperature dependence of the Maxwell parameters of a 5.0 g/l EHUT solution; a: zero-shear viscosity, the line corresponds to  $\eta_0 = 3.78 \cdot 10^{-19} \exp(1.41 \cdot 10^4/T)$ ; b: terminal relaxation time, the line corresponds to  $\tau_0 = 6.93 \cdot 10^{-20} \exp(1.39 \cdot 10^4/T)$ .

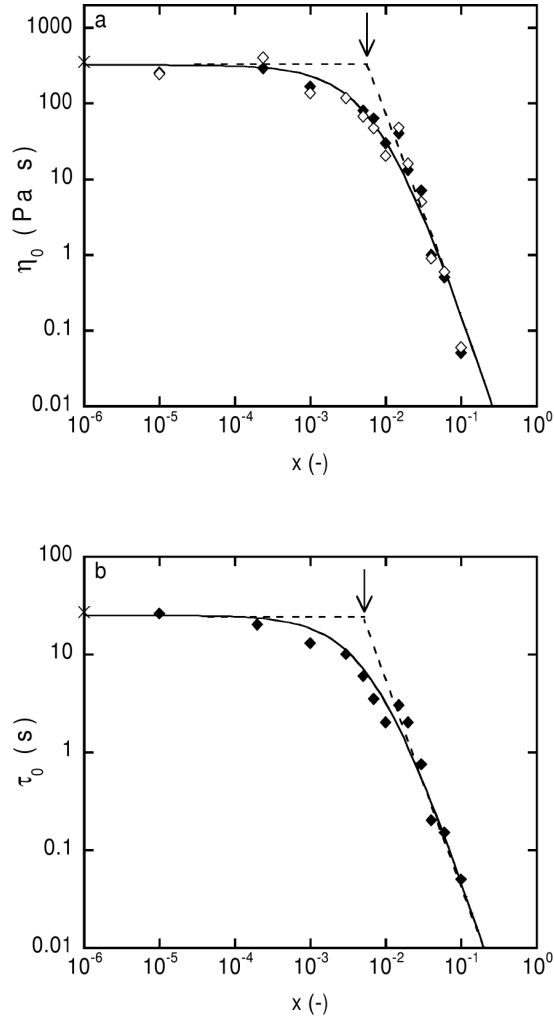


Figure 3.4: Effect of stopper fraction on a 5.0 g/l EHUT solution.  $\times$  denotes  $\eta_0$  and  $\tau_0$  of the solution at 20°C and  $x = 0$ . a: zero-shear viscosity, obtained from transients ( $\blacklozenge$ ) and from the flow curves ( $\diamond$ ). The solid line corresponds to  $\eta_0 = 4 \cdot 10^{-8} \langle N(x) \rangle^{3.0}$ , with  $\langle N \rangle$  calculated with equation 3.3. The arrow denotes the critical stopper fraction  $x'$ . b: terminal relaxation time. The solid line corresponds to  $\tau_0 = 4 \cdot 10^{-7} \langle N(x) \rangle^{2.3}$ .

### 3.4. Results and discussion

---

and can be used to fit the power-law part of the data (denoted by the dashed line at high  $x$  in figure 3.4a). The curve shown in figure 3.4a was calculated using  $K = 8.6 \cdot 10^7 \text{ M}^{-1}$  ( $= 2 \cdot 10^5 \text{ l/g}$ , using that the molar mass of EHUT is 432 g [25]) and  $n = 17$ .

By calculating the intersection of the horizontal plateau at low  $x$  and the power-law dependence at high  $x$ , we obtain the critical stopper fraction  $x'$  (denoted by the arrow in figure 3.4a), above which  $\langle N \rangle$  becomes independent of  $\langle N(0) \rangle$  (and thus of  $c$ ) and inversely proportional to  $x$ . The value obtained from the viscosity data is  $x' = 8 \cdot 10^{-3}$ .

the terminal relaxation time as a function of  $x$  is shown in figure 3.4b. The same analysis as above can be applied to these data, which can be fitted to equation 3.9. The scaling exponent  $\gamma$  is found to be 2.3, which is the same value as obtained for EHUT/DBUT solutions in cyclohexane [30]. The curve shown in the plot was calculated with  $K = 1.3 \cdot 10^8 \text{ M}^{-1}$  ( $= 3 \cdot 10^5 \text{ l/g}$ ) and  $n = 17$ . The critical stopper fraction is calculated as  $x' = 7 \cdot 10^{-3}$ . Both results agree within the experimental error with the result obtained from the viscosity data.

We may compare our values of  $K$  and  $n$  to independent estimates of these parameters. From light scattering and calorimetry experiments, values of  $K$  for EHUT in several solvents were obtained. Values (at room temperature) vary from  $1 \cdot 10^5 \text{ M}^{-1}$  in chloroform [19] to  $4 \cdot 10^9 \text{ M}^{-1}$  in cyclohexane [29], which shows that the association constant is very sensitive to the polarity of the solvent. This is not surprising, as the polarity of the solvent strongly affects the strength of the hydrogen bonds between the monomers. Unfortunately, no data for dodecane are available. Compared to the existing data, an association constant of the order of  $10^8 \text{ M}^{-1}$  in dodecane at 20°C is a reasonable value. The value of  $n$  was estimated from osmometry and light scattering experiments on EHUT/DBUT solutions in cyclohexane [29]. It was found that  $n$  as calculated from osmometry data ( $n = 4$ ) was much lower than the result obtained from light scattering ( $n = 17$ ). This was explained by the fact that with light scattering, only objects above a certain size are measured, whereas osmometry is also sensitive to very short chains. Short chains will also have a small contribution to the solution viscosity, so it is reasonable that the value of  $n$  as obtained from light scattering also shows a good agreement with the experimental viscosity data of figure 3.4a.

It must be noted that equations 3.3, 3.8 and 3.9 contain many adjustable or experimentally obtained parameters (numerical prefactors,  $K$  and  $n$  and the scaling exponents  $\alpha$  and  $\gamma$ ). Nevertheless, the results demonstrate that our simple model describing the dependence of  $\eta_0$  and  $\tau_0$  on the stopper fraction can be used to describe the experimental data using reasonable values of  $K$ ,  $n$ ,  $\alpha$  and  $\gamma$ , consistent with those obtained in previous experiments.

In section 3.4.1, it was found that the overall temperature dependence exponents of  $\eta_0$  and  $\tau_0$  are the same, both lead to an activation energy of

$2 \cdot 10^{-19}$  J. We may substitute the experimentally determined values of  $\alpha$  and  $\gamma$  in equations 3.10 and 3.11:  $3.0E_b + E_\eta = 2.3E_b + E_\tau = 2 \cdot 10^{-19}$ . Without an independent measure of one of the energies, the others cannot be calculated from the present data. The activation energies  $E_\eta$  and  $E_\tau$  and the bonding energy  $E_b$  are often hard to access experimentally, due to the complex interplay between relaxation, breaking and reptation times, chain length and flexibility and temperature on rheological parameters [37, 43].

### 3.4.2 Flow curves

Solutions of supramolecular polymers and wormlike micelles are well-known for their rich non-linear rheological behavior. Among the observed phenomena are flow instabilities, which can lead to phase separation. Such instabilities were first observed and classified by Schmitt *et al.* [44, 45]. EHUT too has a complex non-linear rheology, as can be seen from the flow curves (steady-state shear stress as a function of applied shear rate) in figures 3.5 a and b. The symbol  $\blacklozenge$  denotes a 5.0 g/l EHUT solution at 20°C and  $x = 0$ . In a recent paper, six regimes were identified in the flow curve of EHUT solutions [27]. At very low shear rates, the solution behaves Newtonian: the slope of the curve is unity. All experiments described in section 3.4.1 were done in this Newtonian regime. At  $\dot{\gamma} \approx 0.01 \text{ s}^{-1}$ , there is a sudden change of the slope, and the stress even seems to pass a maximum. In this regime, ‘shear banding’ occurs: the separation of the solution into regions with different shear rates. The presence of shear bands was confirmed by heterodyne light scattering. At higher shear rates, two more shear banding transitions are observed, which are associated with a shear-induced phase transition.

It was suggested [27] that the first shear banding transition (where the maximum in the flow curve occurs) is caused by a strong coupling between the shear flow and the alignment of EHUT chains, owing to their large persistence length [26, 29]. Alignment of chains in the flow direction may facilitate their association into longer chains. The elongated chains would have a stronger tendency to align, and this would provide a positive feedback mechanism which could explain the extreme shear thinning which can eventually lead to shear banding. A possible way to test this hypothesis is by comparing the effect on the flow curve of increasing temperature and the addition of chain stoppers. An increase in temperature decreases the association constant (equation 3.2) and shifts the equilibrium between breaking and formation of bonds (equation 3.1) towards the side of ‘free binding groups’, thus decreasing  $\langle N \rangle$ . Chain stoppers, on the other hand, do not affect  $K$ . They reduce  $\langle N \rangle$  by blocking chain ends, thus preventing the addition of more monomers. Blocked chain ends would interfere with the proposed coupling between chain alignment and growth.

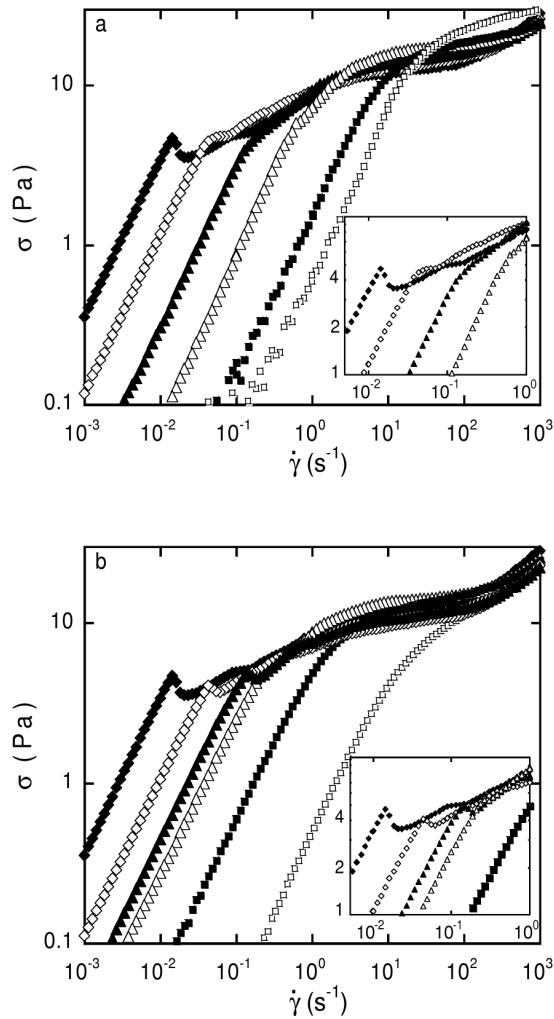


Figure 3.5: a: Flow curves of a 5.0 g/l EHUT solution at 20 ( $\blacklozenge$ ), 30 ( $\diamond$ ), 40 ( $\blacktriangle$ ), 50 ( $\triangle$ ), 60 ( $\blacksquare$ ) and 70 ( $\square$ ) °C. Inset: magnification of the area where the maximum in the flow curve occurs. b: Flow curves of a 5.0 g/l EHUT solution at 20 °C with stopper fractions  $x = 0$  ( $\blacklozenge$ ), 0.005 ( $\diamond$ ), 0.007 ( $\blacktriangle$ ), 0.015 ( $\triangle$ ), 0.030 ( $\blacksquare$ ) and 0.060 ( $\square$ ). Inset: magnification of the area where the maximum in the flow curve occurs.

Flow curves at several temperatures are shown in figure 3.5a. With increasing temperature, the steady-state stress at a given shear rate in the Newtonian regime decreases strongly, which reflects the decreased solution viscosity. Furthermore, the maximum in the flow curve rapidly becomes less pronounced with increasing temperature. At 30°C it is hardly visible anymore, and at higher temperatures, the stress is a monotonously increasing function of the applied shear rate. At shear rates beyond the stress maximum, there is not much difference between the flow curves at different temperatures. Figure 3.5b shows that the dependence of the flow curve on the stopper fraction is similar to that of temperature: the viscosity decreases, the maximum becomes less pronounced and beyond the stress maximum the flow curves are almost independent of the stopper fraction. It is noticeable that the maximum disappears at  $x \approx 0.01$ , close to the critical stopper fraction  $x'$  (section 3.4.1). This observation is consistent with the proposed coupling between shear flow and the alignment and subsequent elongation of chains. Above  $x'$ , most chains are terminated by chain stoppers. This would severely hinder the association and elongation of shear-aligned chains, and thus prevent the flow instability and shear banding to occur.

#### Effect of increased temperature *versus* the addition of chain stoppers

Let us now compare the flow curves of solutions with the same zero-shear viscosity, which is reached by either increasing temperature (at  $x = 0$ ) or by adding chain stoppers (at 20°C). The results for two such pairs of solutions are shown in figure 3.6. The parameters of these solutions are summarized in table 3.1.

Table 3.1: Parameters of solutions  $S_{T1}$  and  $S_{x1}$  of pair 1 ( $\eta_0 \approx 70$  Pa s), and solutions  $S_{T2}$  and  $S_{x2}$  of pair 2 ( $\eta_0 \approx 30$  Pa s). Relaxation times were obtained from the transients at low shear rates, see section 3.4.1. Values of  $G_0$  were calculated from  $\eta_0$  and  $\tau_0$  with equation 3.7.

| <b>solution</b> | <b><math>S_{T1}</math></b> | <b><math>S_{x1}</math></b> | <b><math>S_{T2}</math></b> | <b><math>S_{x2}</math></b> |
|-----------------|----------------------------|----------------------------|----------------------------|----------------------------|
| $T$ (°C)        | 30                         | 20                         | 40                         | 20                         |
| $x$ (-)         | 0                          | 0.005                      | 0                          | 0.015                      |
| $\eta_0$ (Pa s) | 71                         | 67                         | 31                         | 34                         |
| $\tau_0$ (s)    | 4.5                        | 6.0                        | 1.8                        | 3.0                        |
| $G_0$ (Pa)      | 16                         | 11                         | 17                         | 11                         |

Because they have nearly the same zero-shear viscosity, the flow curves of solutions  $S_{T1}$  and  $S_{x1}$  and those of  $S_{T2}$  and  $S_{x2}$  overlap in the Newtonian region.

### 3.4. Results and discussion

---

However, there are marked differences at higher shear rates. The flow curve of  $x_1$  shows a distinct maximum, whereas that of  $S_{T1}$  only has a very weak maximum. The curve of solution  $S_{x2}$  does not have a maximum anymore, but there still is an inflection point. The slope of the flow curve of  $S_{T2}$  also decreases in this range of shear rates, but much less strong. At higher shear rates, the flow curves of  $S_{T1}$  and  $S_{x1}$  and those of  $S_{T2}$  and  $S_{x2}$  are more or less parallel.

Even though solutions belonging to the same pair have nearly the same zero-shear viscosity, their terminal relaxation time may be different. To investigate to what extent the differences between the flow curves are correlated with differences in  $\tau_0$ , the flow curves were plotted in a reduced dimensionless form, where the shear rate is multiplied by the terminal relaxation time and the stress is divided by the plateau modulus. The reduced flow curves are shown in figure 3.6b. Now, the curves belonging to the same pair overlap over the whole range of reduced shear rates, except around the maximum (pair 1) or the inflection point (pair 2). As can be seen from table 3.1, solutions  $S_{T1}$  and  $S_{T2}$  have shorter relaxation times compared to  $S_{x1}$  and  $S_{x2}$ , respectively. As explained in section 3.2,  $\tau_0$  is determined by both the reptation time  $\tau_{rep}$  and the breaking time  $\tau_{break}$  of a chain. It is reasonable to assume that solutions with equal  $\eta_0$  have the same chain length distribution and thus the same reptation time:  $\tau_{rep}(T) = \tau_{rep}(x)$ . The difference in relaxation time must thus be due to a difference in breaking time. Indeed, an increase in temperature enhances the exchange rate of monomers between chains [12], whereas the addition of chain stoppers does not. Thus,  $\tau_{break}(T) < \tau_{break}(x)$ . The foregoing leads to the conclusion that  $\tau_0$  of a solution with a given amount of chain stoppers is longer than the relaxation time of a solution without chain stoppers with the same viscosity, reached by increasing temperature. In other words:  $\tau_0(T) < \tau_0(x)$ , in agreement with the experimental observations.

The reduced flow curves show that most of the difference between the temperature and the stopper curves can be explained by the difference in  $\tau_0$ , except for the area where the maximum in the flow curve occurs. This is also the range of shear rates where the first shear banding transition occurs. This is consistent with the hypothesis that this transition is somehow related to a coupling of chain alignment and growth, leading to a flow instability. At these shear rates, the curves of  $S_{x1}$  and  $S_{x2}$  show more pronounced features (maximum and inflection point) and higher reduced stresses than those of  $S_{T1}$  and  $S_{T2}$ , respectively. However, the present data do not allow detailed conclusions to be drawn about the molecular mechanism behind this flow behavior.

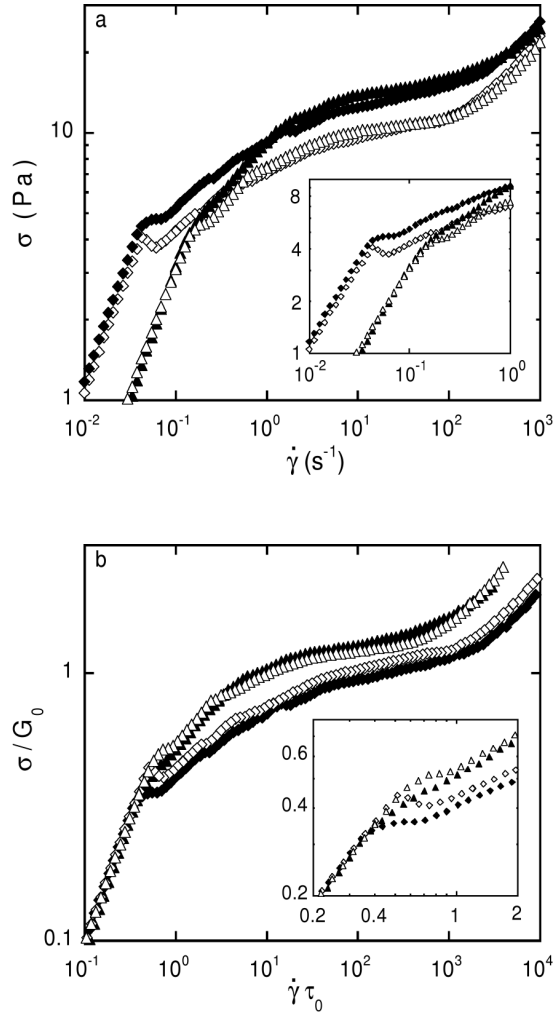


Figure 3.6: a: Flow curves of solutions with the same zero-shear viscosity, as obtained by either an increased temperature or the addition of chains stoppers. Pair I: 30 °C ( $\blacklozenge$ ) and  $x = 0.005$  ( $\diamond$ ); pair II: 40 °C ( $\blacktriangle$ ) and 0.015 ( $\triangle$ ). The inset shows a magnification of the area of the force curve where the maximum occurs. b: Same data, with the shear rate normalized by  $\tau_0$  and the shear stress by  $G_0$ .

## 3.5 Concluding remarks

In this paper, the rheology of solutions of a reversible supramolecular polymer is studied. This is done by comparing the effects of an increase in temperature and the addition of chain stoppers. Both methods decrease the average degree of polymerisation, but in different ways. The system under investigation were solutions in dodecane of hydrogen-bonded supramolecular polymer EHUT and chain stopper DBUT.

The linear rheology can be described by the Maxwell model. The dependence of the zero-shear viscosity and the terminal relaxation time on temperature is exponential. From Arrhenius plots, the activation energy for viscous flow was calculated to be  $2 \cdot 10^{-19}$  J.

The effect of chain stoppers on rheology is relatively small at low stopper fractions. Above a critical stopper fraction, the viscosity and relaxation time decrease strongly, following power law behavior with a scaling exponent  $-3.0$  for the zero-shear viscosity and  $-2.3$  for the terminal relaxation time. The results can be explained by a simple model describing the effect of the addition of chain stoppers on the average degree of polymerisation, and are consistent with previous experimental results.

The flow curve of EHUT solutions is very complex, it has a maximum and shows extreme shear thinning. Flow curves at various temperatures and stopper fractions were measured. Both show the same trends: decreasing viscosity, diminishing and disappearance of the maximum and overlap of flow curves at high shear rates. However, a direct comparison revealed considerable differences between pairs of flow curves with the same zero-shear viscosity (one curve obtained by increasing temperature, the other by adding chain stoppers). Reduced flow curves show that the differences are mostly associated with by differences in the terminal relaxation time. The results are consistent with a mechanism of shear-induced alignment and subsequent elongation of chains.

The results presented in this paper demonstrate that the use of chain stoppers can be a valuable tool to increase our understanding of the dynamics of supramolecular polymers. Without being the final answer, they provide new insight in the microscopic mechanisms underlying the complex rheological behavior of supramolecular polymer solutions.

## References

- [1] B. Jeong and A. Gutowska. *Trends in Biotechnology*, 20: 305–311, 2002.
- [2] R. Yerushalmi, A. Scherz, M. E. van der Boom, and H. B. Kraatz. *J. Mater. Chem.*, 15: 4480–4487, 2005.

- 
- [3] R. V. Ulijn. *J. Mater. Chem.*, 16: 2217–2225, 2006.
- [4] C. de las Heras Alarcón, S. Pennadam, and C. Alexander. *Chem. Soc. Rev.*, 34: 276–285, 2005.
- [5] N. M. Sangeetha and U. Maitra. *Chem. Soc. Rev.*, 34: 821–836, 2005.
- [6] J-M. Lehn. *Supramolecular chemistry: concepts and perspectives*. VCH, Weinheim, 1995.
- [7] A. Ciferri, editor. *Supramolecular polymers*. CRC Press, Boca Raton, 2 edition, 2005.
- [8] S. Kiyonaka, K. Sugayisu, S. Shinkai, and I. Hamachi. *J. Am. Chem. Soc.*, 124:10954–10955, 2002.
- [9] S. J. Rowan and J. B. Beck. *Faraday Discuss.*, 128:43–53, 2005.
- [10] S-L. Zhou, S. Matsumoto, H-D. Tian, H. Yamane, A. Ojida, S. Kiyonaka, and I. Hamachi. *Chem. Eur. J.*, 11:1130–1136, 2005.
- [11] J. M. J. Paulusse and R. P. Sijbesma. *Angew. Chem. Int. Ed.*, 45: 2334–2337, 2006.
- [12] M.E. Cates and S.J. Candau. *J. Phys.: Condens. Matter*, 2: 6869–6892, 1990.
- [13] J. Yang. *Curr. Opin. Colloid Interface Sci.*, 7: 276–281, 2002.
- [14] L. Brunsveld, B.J.B. Folmer, E.W. Meijer, and R.P. Sijbesma. *Chem. Rev.*, 101: 4071–4097, 2001.
- [15] J. van der Gucht, N.A.M Besseling, and M.A. Cohen Stuart. *J. Am. Chem. Soc.*, 124: 6202–6205, 2002.
- [16] J. van der Gucht, N.A.M Besseling, and G.J. Fleer. *J. Chem. Phys.*, 119: 8175–8188, 2003.
- [17] C.D Eisenbach and U.S. Schubert. *Macromolecules*, 26: 7372–7374, 1993.
- [18] T. Vermonden, J. van der Gucht, P. de Waard, A.T.M. Marcelis, N.A.M. Besseling, E.J.R. Sudhölter, G.J. Fleer, and M.A. Cohen Stuart. *Macromolecules*, 36: 7035–7044, 2003.
- [19] A. Arnaud, J. Belleney, F. Boue, L. Bouteiller, G. Carrot, and W. Wintgens. *Angew. Chem. Int. Ed.*, 43: 1718–1721, 2004.
- [20] E. A. Fogleman, W. C. Yount, J. Xu, and S. L. Craig. *Angew. Chem. Int. Ed.*, 41: 4026–4028, 2002.
-

## References

---

- [21] Y. Liu, Z. Fan, H-Y. Zhang, Y-W. YAng, F. Ding, S-X. Liu, X. Wu, T. Wada, and Y. Inoue. *J. Org. Chem.*, 68: 8345–8352, 2003.
- [22] H.W. Gibson, N. Yamguchi, and J.W. Jones. *J. Am. Chem. Soc.*, 125: 3522–3533, 2003.
- [23] R.P. Sijbesma, F.H. Beijer, L. Brunsveld, B.J.B. Folmer, J.H.K.K. Hirschberg, R.F. M. Lange, J.K.L. Lowe, and E.W. Meijer. *Science*, 278:1601–1604, 1997.
- [24] D. C. Sherrington and K. A. Taskinen. *Chem. Soc. Rev.*, 30: 83–93, 2001.
- [25] S. Boileau, L. Bouteiller, F. Lauprêtre, and F. Lortie. *New J. Chem.*, 24: 845–848, 2000.
- [26] F. Lortie, S. Boileau, L. Bouteiller, C. Chassenieux, B. Deme, G. Ducouret, M. Jalabert, F. Lauprêtre, and P. Terech. *Langmuir*, 18: 7218–7222, 2002.
- [27] J. van der Gucht, M. Lemmers, W. Knoben, N.A.M. Besseling, and M.P. Lettinga. *Phys. Rev. Lett.*, 97:108301, 2006.
- [28] F. Lortie, S. B. Boileau, L. Bouteiller, C. Chassenieux, and F. Lauprêtre. *Macromolecules*, 38: 5283–5287, 2005.
- [29] W. Knoben, N.A.M. Besseling, and M.A. Cohen Stuart. *Macromolecules*, 39: 2643–2653, 2006.
- [30] W. Knoben, N. A. M. Besseling, L. Bouteiller, and A. C. Stuart. *Phys. Chem. Chem. Phys.*, 7: 2390–2398, 2005.
- [31] P.J. Flory. *J. Am. Chem. Soc.*, 58: 1877–1885, 1936.
- [32] P.J. Flory. *Principles of polymer chemistry*. Cornell University press, Ithaca, New York, 1953.
- [33] H.J.A. Zweistra, N.A.M. Besseling, and M.A. Cohen Stuart. *J. Phys. Chem. B*, 110: 18269–18634, 2006.
- [34] M.E. Cates. *Macromolecules*, 20: 2289–2296, 1987.
- [35] P.G. de Gennes. *Scaling concepts in polymer physics*. Cornell University press, Ithaca, London, 1979.
- [36] M. Doi and S.F. Edwards. *The theory of polymer dynamics*. Clarendon, Oxford, 1986.
- [37] F. Kern, F. Lequeux, R. Zana, and S. J. Candau. *Langmuir*, 10: 1714–1723, 1994.

- [38] R.B. Bird and W.E. Stuart. *Transport phenomena*. John Wiley, New York, 1960.
- [39] R. Regina Alcantara, A.F. de Moura, and E.G. Fernandes jr. *Liq. Cryst.*, 29: 191–197, 2002.
- [40] A. Durand and E. Dellacherie. *Biomacromolecules*, 7: 958–964, 2006.
- [41] R.G. Larson. *The structure and rheology of complex fluids*. Oxford University Press, 1999.
- [42] T. Vermonden, M.J. van Steenberg, N.A.M. Besseling, A.T.M. Marcelis, W.E. Hennink, E.J.R. Sudhölter, and M.A. Cohen Stuart. *J. Am. Chem. Soc.*, 126: 15802–15808, 2004.
- [43] I. Couillet, T. Hughes, G. Maitland, F. Candau, and S.J. Candau. *Langmuir*, 20: 9541–9550, 2004.
- [44] V. Schmitt, F. Lequeux, A. Pousse, and D. Roux. *Langmuir*, 10: 955–961, 1994.
- [45] V. Schmitt, C.M. Marques, and F. Lequeux. *Phys. Rev. E*, 52: 4009–4015, 1995.



# 4

## Chain stoppers in reversible supramolecular polymer solutions, studied by static and dynamic light scattering and osmometry

### Abstract

The effect of the addition of chain stoppers to solutions of hydrogen bonded reversible supramolecular polymers was studied by vapor pressure osmometry and static and dynamic light scattering. Vapor pressure osmometry showed that within the range of concentrations studied, the average degree of polymerisation is independent of the overall monomer concentration and roughly inversely proportional to the mole fraction of chain stoppers, in agreement with theoretical predictions. The correlation length as measured by static light scattering has a maximum at the overlap concentration in solutions without chain stoppers. In the presence of a fixed fraction of chain stoppers, the results coincide with those without chain stoppers at low and high concentrations, but there is a plateau in the correlation length at intermediate concentrations. From the data, information about the association constant and the persistence length of the chains is obtained. The effectiveness of the chain stopper is discussed, and the results from osmometry and static light scattering are compared. Dynamic light scattering was used to measure the time autocorrelation function. From the characteristic decay time, the hydrodynamic correlation length was calculated. For solutions above the overlap concentration, the distribution of decay times showed a second peak at longer times. It is not yet fully understood what the mechanism behind this slow mode is.

### 4.1 Introduction

Supramolecular polymers are chains of monomers, held together by non-covalent, reversible interactions such as metal-ligand complexation or hydrogen bonding [1–6]. There is a dynamic equilibrium between bonded and free monomers and the breaking and reformation of the supramolecular bonds often occurs on experimental time scales, in which case the term *reversible* supramolecular polymers is appropriate. As a consequence of this equilibrium, the (average) length of the supramolecular polymer chains depends on the monomer concentration, and also on parameters such as temperature and the choice of solvent. These parameters can thus be used to adjust the chain length *in situ*, and therewith also the solution or material properties. For example, the rheological properties of supramolecular polymer systems can be varied easily and reversibly over a very wide range compared to classical covalent polymers [7–9]. This may be useful in industrial processes where high chain lengths and crosslink densities are often required to obtain the desired material properties, but the resulting high viscosities hamper processing. The strong concentration dependence of the viscosity may also be useful in other processes, such as polymerisation-induced phase separation [10]. Another potential application is the synthesis of ‘smart’ or self-healing materials which respond to changes in environmental conditions such as temperature or pH [11, 12].

It was shown that the incorporation of two complementary hydrogen bonding motifs in a single monomer is a successful method for the formation of supramolecular polymers. Especially arrays of multiple hydrogen bonding sites in apolar organic solvents display high association constants [13–16]. These bifunctional monomers can associate with each other into linear supramolecular chains. If the monomers contain more than two binding groups, branched chains and crosslinked networks can be formed. During synthesis and purification, one of the essential tasks is to avoid the presence of monofunctional monomers (monomers which have only one binding group), which are often called ‘chain stoppers’. If a monofunctional monomer binds to a supramolecular polymer, it adds a non-functional or ‘dead’ end to the chain, and the chain cannot grow further, hence the term ‘chain stoppers’. The presence of chain stoppers thus decreases the average chain length. Even very small amounts of chain stoppers can have a large effect on solution and material properties [13, 16]. However, chain stoppers can also be added deliberately in order to control the length of the chains and the properties of the system [17], see also chapters 3, 5, 6 and 7. One of the advantages of using chain stoppers to adjust the chain length is that the average chain length may be varied independently of other parameters such as the (overall) monomer concentration and temperature, which is otherwise impossible for supramolecular polymers. On the other hand, the chains retain the possibility to break and

recombine, which leads to unique properties, especially in the dynamics of supramolecular polymer solutions.

In some respects, supramolecular polymers are similar to wormlike micelles, which are also long, non-covalent aggregates of small molecules with a concentration and temperature dependent length [18–21]. Therefore, many of the theories and experimental techniques used for wormlike micelles can also be applied to supramolecular polymers. However, there are also important differences between the two. For example, the concept of monofunctional chain stoppers is only applicable to self-assembling systems based on very specific interactions. The formation of wormlike micelles is governed by less specific interactions between the surfactants and the solvent molecules. Therefore, in spite of the massive amount of literature on wormlike micelles, there are not much experimental data on chain stoppers and their effect on supramolecular polymer solutions.

It was shown previously that the bifunctional monomer *2,4-bis*(2-ethylhexylureido)toluene (EHUT, figure 4.1) forms long, rigid supramolecular chains in apolar organic solvents by the cooperative formation of four hydrogen bonds per monomer [22]. This was studied by IR spectroscopy, small angle neutron scattering, light scattering and viscosity measurements [23, 24], as well as isothermal titration calorimetry [25]. The linear rheology of EHUT solutions was studied by rheometry and dynamic light scattering of probe particles [26]. From the linear density of the chains, obtained from the neutron scattering data, the effective monomer length was calculated to be 0.18 nm, which suggests the presence of two or three monomers per axial repetition unit. Additional experiments led to the conclusion that EHUT can form both thin and thick fibers, depending on the experimental conditions [27].

An alkylated derivative of EHUT, *2,4-bis*(dibutylureido)toluene (DBUT), which could be used as a chain stopper for EHUT, was designed and synthesized [17]. Conveniently, EHUT and DBUT have the same molar mass (432 g/mol). As can be seen from figure 4.1, DBUT is strictly speaking not a monofunctional chain stopper, since it may still form two hydrogen bonds with EHUT with its secondary amine groups. However, DBUT was shown to be the most effective of a number of chain stoppers in reducing the viscosity of EHUT solutions, and was therefore selected for further experiments. The cooperativity in the simultaneous formation of four hydrogen bonds between two EHUT molecules probably strongly disfavors the formation of only two with DBUT, which explains the high effectiveness of DBUT as a chain stopper. The use of chain stoppers as a tool to tune the chain length is illustrated in chapter 5, in which the linear viscoelasticity of EHUT solutions is studied. By using chain stoppers, the effects of chain length and monomer concentration could be separated, which was previously impossible. It was also shown that experiments with chain stoppers can be used to obtain more information about

## 4.2. Theoretical background

---

the system without chain stoppers [17].

In the present paper, the effect of the addition of chain stopper DBUT on static and dynamic properties of EHUT solutions is investigated in more detail. The average degree of polymerisation at high stopper fractions is measured by vapor pressure osmometry (VPO), which gives new insight in the action of the chain stoppers. This technique has previously been used to study supramolecular polymers [28, 29], but we are not aware of any reports in which it is used to study the effect of chain stoppers on supramolecular polymer solutions. Static light scattering (SLS) is used to study the dependence of the correlation length on the amount of stoppers in dilute and semi-dilute solutions. Osmometry and SLS both yield information about the average chain length and the effectiveness of the stopper, and the results of both techniques are compared. The hydrodynamic correlation length is measured by dynamic light scattering (DLS), and the concentration dependence of the static and hydrodynamic correlation length are compared. Furthermore, a slow relaxation mode is observed in the DLS data of semidilute solutions. To our knowledge, this is the first time that a combined light scattering study of this kind was done on a supramolecular polymer system.

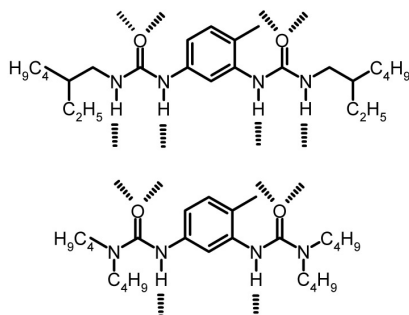
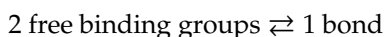


Figure 4.1: Bifunctional monomer EHUT (top) and monofunctional chain stopper DBUT (bottom). Possible hydrogen bonds are represented by dashed lines.

## 4.2 Theoretical background

### 4.2.1 Average chain length

In supramolecular polymer solutions, formation and breaking of bonds between monomers occurs simultaneously and continuously:



A chain of  $N$  monomers has  $N - 1$  bonds and 2 free binding groups at its ends. Consider a solution with monomer concentration  $c$  and number average degree of polymerisation  $\langle N \rangle$ . The average concentration of bonds in this solution is equal to  $(c/\langle N \rangle)(\langle N \rangle - 1)$ , the average concentration of end groups is  $2c/\langle N \rangle$ . The association constant  $K$  is assumed to be equal for all monomers, e.g. independent of the degree of polymerisation of the chain to which a monomer belongs.  $K$  can be written as

$$K = \frac{[\text{bonds}]}{[\text{free binding groups}]^2} = \frac{\langle N \rangle (\langle N \rangle - 1)}{4c} \quad (4.1)$$

which can be rewritten to give an expression for  $\langle N \rangle$ :

$$\langle N \rangle = \frac{1 + \sqrt{1 + 16Kc}}{2} \approx 2\sqrt{Kc} \quad (4.2)$$

where the approximation is justified if  $Kc \gg 1$ .

The formation of a supramolecular polymer by reversible association of bifunctional monomers is in some respects analogous to the formation of a covalent polymer by condensation polymerisation. The monomers of a (linear) condensation polymer are also bifunctional, and bonds between monomers are reversible, as they can be hydrolyzed by the liberated condensation product (often water). A theoretical treatment of condensation polymerisation was already given in the 1930s [30, 31]. The basic assumption is that there is a probability  $p$  that a binding group is part of a bond, which is again independent of the degree of polymerisation of the chain to which the bond belongs. This leads to an exponential chain length distribution with a number average degree of polymerisation given by

$$\langle N \rangle = \frac{1}{1-p} \quad (4.3)$$

and a degree of polydispersity of  $1+p$ . The concentration of bonds in a solution is  $pc$  and the concentration of free binding groups equals  $2c(1-p)$ . Substituting these relations in the first equality in equation 4.1 leads to

$$K = \frac{p}{4c(1-p)^2} \Rightarrow p \approx 1 - \frac{1}{\sqrt{4Kc}} \quad (4.4)$$

where the approximate equality applies for  $p$  close to unity. Substituting this in equation 4.3 leads to the expression for  $\langle N \rangle$  derived in equation 4.2. Thus, using the probability  $p$  to analyze the association process is equivalent to describing it in terms of  $K$  and  $c$ .

When a bifunctional monomer binds to an existing chain, a new functional end group is formed. In contrast, when a monofunctional monomer binds

## 4.2. Theoretical background

---

to a chain, the new chain end cannot bind another monomer and is therefore 'dead'. In other words, monofunctional monomers act as chain stoppers. Note that the concept of chain stoppers also applies to condensation polymerisation, where monofunctional monomers also decrease the average chain length (and therefore increase the number of chains at a given monomer concentration) by forming non-functional chain ends. In a simple approach, the addition of every  $n$  chain stoppers to a solution leads to the formation of one new chain. When a concentration  $k$  of chain stoppers is added to a solution, which makes up a fraction  $x = k/(c + k)$  of all monomers, the concentration of chains is increased by  $k/n = cx/n(1 - x)$ . The number average degree of polymerisation in the presence of a fraction  $x$  of chain stoppers is decreased and is given by:

$$\langle N(x) \rangle = \frac{n\langle N(0) \rangle}{n(1 - x) + x\langle N(0) \rangle} \approx n/x \quad (4.5)$$

where  $\langle N(0) \rangle$  is the number average number of monomers per chain without any chain stoppers as given by equation 4.2. The approximation of  $\langle N(x) \rangle$  to  $n/x$  is justified for sufficiently high values of  $\langle N(0) \rangle$  and  $x$ , when the term  $n(1 - x)$  in the denominator can be neglected. This condition applies if the number of 'dead' chain ends is much larger than the number of functional ones. Then, only the stopper fraction determines the average length of the chains, independent of monomer concentration and association constant (which determine  $\langle N(0) \rangle$ ).

In figure 4.2, the effect of the addition of chain stoppers as calculated with equation 4.5 is shown. Figure 4.2a shows that at low values for  $x/n$ , the effect of the stoppers is negligible. Only a small minority of the chains contain chain stoppers, the number of dead chain ends is small compared to the number of functional ones and  $\langle N \rangle \approx \langle N(0) \rangle$ . When the number of dead chain ends becomes of the same order of magnitude as the number of functional ones ( $x/n$  of the order of  $1/\langle N(0) \rangle$ ),  $\langle N \rangle$  starts to decrease significantly. At even higher stopper fractions, the number of dead chain ends is much larger than the number of functional ones, and  $\langle N \rangle$  no longer depends on  $\langle N(0) \rangle$ , but is fully determined by  $x$  and proportional to  $1/x$ , as indicated by the line with slope  $-1$  next to the curves. This is the regime where the approximation in equation 4.5 is justified. Figure 4.2b shows that at low monomer concentrations, the average chain length is not determined by the amount of stoppers.  $\langle N \rangle$  is proportional to  $c^{0.5}$  as indicated with the solid line with slope 0.5, the same dependence as without chain stoppers (equation 4.2). In this concentration range,  $\langle N(0) \rangle$  is still small compared to  $n/x$ , and most chains do not contain chain stoppers. When the monomer concentration is increased, the slope starts to level off, and eventually  $\langle N \rangle$  reaches a plateau at a value  $n/x$ , when virtually all chain ends are occupied by chain stoppers. In this range of concentrations, the average chain length is again independent of the monomer concentration,

and only determined by the stopper fraction.

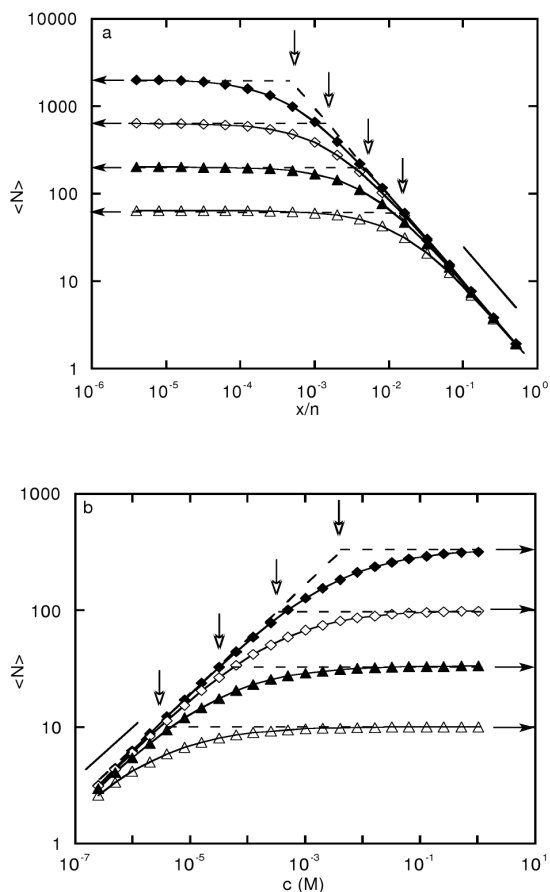


Figure 4.2:  $\langle N \rangle$ , calculated with equation 4.5 with  $K = 10^7 \text{ M}^{-1}$ . a:  $\langle N \rangle$  as a function of the normalized stopper fraction  $x/n$  for  $10^{-1}$  ( $\blacklozenge$ ),  $10^{-2}$  ( $\diamond$ ),  $10^{-3}$  ( $\blacktriangle$ ) and  $10^{-4}$  ( $\triangle$ ) M solutions. The line next to the curves indicates  $\langle N \rangle \sim 1/x$ . Open arrows indicate  $(x/n)'$ , solid arrows indicate  $\langle N(0) \rangle$ . b:  $\langle N \rangle$  as a function of the concentration of bifunctional monomers at normalized stopper fractions  $x/n$  of 0.003 ( $\blacklozenge$ ), 0.01 ( $\diamond$ ), 0.03 ( $\blacktriangle$ ) and 0.1 ( $\triangle$ ). The line next to the curves indicates  $\langle N \rangle \sim c^{0.5}$ . Open arrows indicate  $c'$ , solid arrows indicate  $n/x$ .

A critical concentration  $c'$  beyond which  $\langle N \rangle$  becomes independent of  $c$  at a given stopper fraction  $x/n$  can be estimated by calculating the concentration where the plateau value  $n/x$  and the line  $2\sqrt{Kc}$  describing the chain growth

## 4.2. Theoretical background

---

without chain stoppers intersect (represented by the open arrows in figure 4.2b):

$$2\sqrt{Kc'} = \frac{n}{x} \Rightarrow c' = \frac{1}{4K} \left(\frac{n}{x}\right)^2 \quad (4.6)$$

The same equation can be used to calculate a critical stopper fraction  $(x/n)'$  for a given monomer concentration (represented by the open arrows in figure 4.2a). From these figures, it can be seen that in order to be able to vary  $c$  and  $\langle N \rangle$  independently in a controlled way, both  $c$  and  $x$  have to exceed their critical value, which are mutually dependent. This criterium can be written as

$$(x\sqrt{c})' \gg \frac{n}{2\sqrt{K}} \quad (4.7)$$

When this condition is satisfied, the addition of chain stoppers thus offers the possibility to study the chain length and concentration dependence of supramolecular polymer solutions independently, which is otherwise impossible for supramolecular polymers without changing other parameters like temperature or solvent.

For a given supramolecular polymer system, equations may be derived which take into account more details and specific features of the monomers and chain stoppers. For example, for supramolecular polymers based on the well known ureidopyrimidinone-unit, it is known that the chain stoppers can bind to both ends of the chain, and can also bind to each other to form stopper dimers. An expression for  $\langle N(x) \rangle$  which takes into account these elements was derived [13]. For sufficiently high stopper fractions, the result of this expression is equal to that of equation 4.5 with  $n = 2$ . For EHUT, it is known that the association process is cooperative [22]. The formation of dimers has a lower association constant ( $K_2$ ) than the formation of higher oligomers or polymers ( $K_n$ ) [24, 25]. However, under conditions where the number of free monomers is small ( $\langle N(0) \rangle \gg 1$ ), dimer formation can be neglected. In that case, a single effective association constant  $K = K_n^2/K_2$  describes the association accurately and this  $K$  can be used for further calculations. In conclusion, for a specific system expressions for  $\langle N(x) \rangle$  may be derived which take into account more details than equation 4.5. Nevertheless, equation 4.5 is a very general equation describing the effect of adding chain stoppers to a supramolecular polymer solution which is useful under the appropriate conditions.

### 4.2.2 Static light scattering

With static light scattering (SLS), the time-averaged scattered intensity is measured at a number of scattering angles, corresponding to different magnitudes of the scattering vector  $q$ , given by  $(4\pi n_0/\lambda) \sin(\theta/2)$  where  $\lambda$  is the wavelength of the incident light,  $n_0$  is the solvent refractive index and  $\theta$  is the scattering

angle. From the  $q$ -dependence of the intensity, information about the characteristic length scales in the sample can be derived. The segment density correlation length in the solution can be found using the Ornstein-Zernike equation for the structure factor [32]:

$$I(q) \sim \frac{1}{1 + q^2 \xi^2} \quad (4.8)$$

In dilute solutions, the polymer chains do not interact, and the correlation length gives information about the (average) size of the individual molecules. The  $q$ -dependence of the scattered intensity is given by

$$I(q) \sim \frac{1}{1 + \frac{1}{3} q^2 \langle R_g^2 \rangle_z} \quad (4.9)$$

Where  $\langle R_g^2 \rangle_z$  denotes the  $z$ -average of the squared radius of gyration. Thus, for dilute solutions the segment density correlation length  $\xi$  from equation 4.8 can be identified as  $\sqrt{\langle R_g^2 \rangle_z / 3}$ .

For a mixture of rigid supramolecular rods with an exponential chain length distribution it can be derived that  $\langle R_g^2 \rangle_z = \langle L \rangle_w^2 / 4$ , where  $\langle L \rangle_w$  denotes the weight average length of the rods [33]. If the association constant is high ( $p \approx 1$ ), the polydispersity index  $M_w / M_n = 2$  (see section 4.2.1). For rods, the contour length is proportional to the molecular weight (or the degree of polymerisation), so the ratio of 2 also holds for the contour lengths:  $\langle L \rangle_w = 2 \langle L \rangle$ , with  $\langle L \rangle$  the number average contour length. Thus, it follows that in dilute solutions of supramolecular rods,  $\xi$  can be identified as  $\langle L \rangle / \sqrt{3}$ . If the effective monomer length (the chain length per monomer, denoted as  $l_m$ ) is known, the degree of polymerisation  $\langle N \rangle$  can be calculated from the relation  $\langle L \rangle = l_m \langle N \rangle$ .

For a flexible chain in a theta solvent, the radius of gyration of a chain scales with the degree of polymerisation as  $R_g \sim \langle N \rangle^{0.5}$ , whereas in a good solvent the exponent is 0.6 [34]. For a rodlike chain,  $R_g \sim \langle N \rangle$ , independent of solvent quality. For supramolecular polymers,  $\langle N \rangle \sim c^{0.5}$  (equation 4.2). In dilute solutions, it is therefore predicted that  $\xi$  increases with  $c$  according to a power law with an exponent between 0.25 (ideal flexible chains) and 0.5 (rodlike chains). If the solution is more concentrated and chains start to overlap (beyond the overlap concentration  $c^*$ ), the polymers form a transient network and the correlation length no longer contains information about the size of the individual chains, but it reflects the mesh size  $\xi_m$  of the network. The mesh size decreases with increasing polymer concentration, and it only depends on the total volume fraction of polymer in the system and not on  $\langle N \rangle$ . For flexible chains in the semidilute concentration regime, scaling theory predicts  $\xi \sim c^{-0.75}$  [34]. At even higher concentrations (marginal regime) and

## 4.2. Theoretical background

---

in solutions of less flexible chains, where excluded volume interactions are weaker, an exponent  $-0.5$  is predicted.

Summarizing, theory predicts for supramolecular polymer solutions that  $\xi$  increases with  $c$  at low concentrations due to the increasing degree of polymerisation, passes a maximum at  $c^*$  and decreases again in the semidilute and more concentrated regimes due to the decreasing mesh size. The scaling exponents contain information about the flexibility of the chains, solvent quality and concentration regime.

### crossover region

A cross-over between a length scale  $\xi_0$  in dilute solution and  $\xi_m$  in the semidilute regime can generally be described by an expression of the form  $\xi^{-\nu} = \xi_0^{-\nu} + \xi_m^{-\nu}$ . An equation of this form was previously derived in calculations of the depletion layer thickness in monodisperse solutions of covalent flexible polymers in a mean-field approach [35]. In this case, the dilute length scale  $\xi_0$  equals the radius of gyration of the polymers. Later, a very similar expression was derived in self-consistent field calculations for flexible supramolecular polymers in a mean-field approximation [36]. In this analysis, polydispersity was taken into account and  $\xi_0$  was found to be equal to the radius of gyration of a chain of number average length  $\langle N \rangle$ . The value of the exponent  $\nu$  determines the width of the cross-over region. In both cases, the exponent  $\nu$  was found to be 2, but for other systems different values of  $\nu$  may apply. As mentioned above, the length scale as measured by SLS for rigid rods with an exponential chain length distribution below the overlap concentration is  $\langle L \rangle / \sqrt{3}$ , and this may be substituted for  $\xi_0$ , leading to the following expression for  $\xi$ :

$$\frac{1}{\xi^\nu} = \frac{3^{\nu/2}}{\langle L \rangle^\nu} + \frac{1}{\xi_m^\nu} \quad (4.10)$$

### 4.2.3 Dynamic light scattering

Dynamic light scattering (DLS) measures temporal fluctuations of the scattered intensity arising from motion of the scatterers [32]. From the scattered intensity as a function of time, the intensity correlation function  $g^{(2)}(\tau)$  is calculated for a number of time intervals  $\tau$ :

$$g^{(2)}(\tau) = \frac{\langle I(t)I(t+\tau) \rangle}{\langle I(t) \rangle^2} \quad (4.11)$$

The intensity correlation function is related to the normalized field correlation function  $g^{(1)}(\tau)$  by the Siegert equation [32]

$$g^{(2)}(\tau) = 1 + A \left[ g^{(1)}(\tau) \right]^2 \quad (4.12)$$

where  $A$  is a constant of order unity depending on the geometry of the experimental set-up.

De Gennes developed a scaling theory for semidilute polymer solutions using a transient gel model [34]. According to this theory,  $g^{(1)}(\tau)$  is an exponentially decreasing function with a single decay rate constant  $\Gamma$ , which is determined by the scattering vector  $q$  and the so-called gel diffusion coefficient  $D_g$ , according to

$$g^{(1)}(\tau) = e^{-\Gamma\tau} = e^{-q^2 D_g \tau} \quad (4.13)$$

$D_g$  is given by

$$D_g = D_c \frac{M_g + M_o}{M_o} \quad (4.14)$$

where  $M_g$  is the gel modulus (the elastic or Young's modulus of the transient gel),  $M_o$  the osmotic modulus, defined as  $c(d\Pi/dc)$ , and  $D_c$  the collective diffusion coefficient, which is in turn related to the hydrodynamic correlation length  $\xi_H$  by the Stokes-Einstein equation [32]

$$D_c = \frac{k_B T}{6\pi\eta_0 \xi_H} \quad (4.15)$$

where  $\eta_0$  is the solvent viscosity. For polymers in a good solvent,  $M_o \gg M_g$  and  $D_c$  is effectively equal to  $D_g$ . Experimentally, a distribution of decay rate constants  $\Gamma$  is generally measured, each with its own weight  $w$ , so  $g^{(1)}(\tau)$  is given by

$$g^{(1)}(\tau) = \int_0^\infty w(\Gamma) e^{-\Gamma\tau} d\Gamma \quad (4.16)$$

Mostly, the value of  $\Gamma$  at the peak of the distribution is taken as 'the' decay rate constant and used for further calculations.

In dilute solutions, when the polymers do not interact, the collective diffusion coefficient reflects the motion of a single chain, and  $\xi_H$  corresponds to the (average) hydrodynamic radius of the polymer. In the semidilute and more concentrated regimes, the hydrodynamic correlation length corresponds to the hydrodynamic mesh size of the transient network, the average distance between entanglement points. With SLS, the average mesh size of the transient polymer network is measured, whereas DLS measures the average diffusion coefficient of the meshes. From this diffusion coefficient and the viscosity of the solvent, the size of the mesh can be calculated with equation 4.15. The hydrodynamic correlation length  $\xi_H$  measured by DLS is thus not equal to the static correlation length  $\xi$ , but it is of the same order of magnitude and it scales in the same way with concentration.

In addition to the decay rate constant associated with the collective diffusion coefficient a second, slower decay time is often present in viscoelastic

## 4.3. Experimental

---

polymer solutions in the semidilute concentration regime. The two modes will from now on be denoted as the fast and the slow mode, respectively. A slow relaxation mode can be found in many different systems, and it can have several physical origins [37, 38]. In order to determine which mechanism is relevant for a given system, it is useful to investigate the  $q$ -dependence of the slow mode. For example, if the slow mode is caused by diffusion of large aggregates or domains, this would lead to a decay rate constant proportional to  $q^2$ , as for any diffusive mode (equation 4.13). Alternatively, it was proposed that concentration fluctuations in the polymer network are coupled to viscoelastic stress [39–41], and this would lead to a slow mode with a  $q$ -independent decay rate.

## 4.3 Experimental

### 4.3.1 Materials

Cyclohexane (>99%) was obtained from Aldrich and used as received, unless stated otherwise. The syntheses of the self-associating monomer (EHUT) [22] and monofunctional chain stopper (DBUT) [17] are described elsewhere. The molar mass of both EHUT and DBUT is 432 g/mol. Solutions in cyclohexane were prepared by stirring at a slightly elevated temperature.

### 4.3.2 Osmometry

A Knauer vapor pressure osmometer was used to measure the osmotic pressure of solutions ranging in EHUT concentration from 4 to 17 g/l and in stopper fraction from 0.3 to 1 in cyclohexane at 30 °C. Solutions of naphthalene in cyclohexane were used as a calibration reference. The measured signal of EHUT solutions was converted to the number concentration of chains by comparison with this reference. No extrapolation to zero concentration was performed, and thus ideality (second virial coefficient  $B_2 = 0$ ) was assumed. It was checked that this assumption was valid (see section 4.4.1). Note that extrapolating to zero concentration, a widely used procedure in polymer science, is generally useless for supramolecular polymers, because of the concentration dependence of the average chain length.

### 4.3.3 Light scattering

For light scattering measurements, cyclohexane (refractive index  $n_0 = 1.426$ ) was filtered through a teflon filter (pore size 0.45  $\mu\text{m}$ ) before preparing solutions. Measurements were done at room temperature using an Argon ion laser with a wavelength of 514.5 nm. A pinhole detector was used with size

600  $\mu\text{m}$  for SLS and 200  $\mu\text{m}$  for DLS experiments. Solutions in cyclohexane were prepared with EHUT concentrations between 0.02 and 5 g/l and stopper fractions of 0 and 0.015.

### Static Light Scattering

The scattered intensity of samples ( $I_{\text{sample}}(q)$ ) was measured at  $5^\circ$  intervals at scattering angles between  $25$  and  $90^\circ$  (corresponding to values of  $q$  between  $7.5 \cdot 10^6$  and  $2.5 \cdot 10^7 \text{ m}^{-1}$ ). The scattered intensity of the pure solvent ( $I_{\text{solvent}}(q)$ ) was also measured. The reduced scattered intensity, denoted as  $i(q)$ , was used for further calculations:

$$i(q) = \frac{I_{\text{sample}}(q) - I_{\text{solvent}}(q)}{I_{\text{solvent}}(q)} \quad (4.17)$$

By using  $i(q)$  instead of the absolute scattered intensity, both scattering from the solvent and the angular dependence of the scattering volume are taken into account and corrected for. From linear fits to plots of  $1/i(q)$  as a function of  $q^2$ ,  $\xi$  was calculated with equation 4.8.

### Dynamic Light Scattering

The scattered intensity was measured at scattering angles of  $60$ ,  $90$  and  $120^\circ$ . In order to obtain correlation functions of sufficient quality, measuring times of 15 minutes per angle were used. The spectrum of decay rate constants was calculated from the correlation function using the CONTIN algorithm [42].

## 4.4 Results and discussion

Vapor pressure osmometry (section 4.4.1) can be used to obtain information about supramolecular polymer solutions within a certain range of monomer concentrations and stopper fractions, since it requires a minimum concentration of chains in order to have a measurable osmotic pressure. In practice, the method is therefore limited to high stopper fractions. Light scattering provides complementary information, since it requires a minimum concentration of objects with a certain minimum size. It can therefore be used to study conditions in which the chains are long (high concentrations, low stopper fractions). Thus, by using both techniques, a large range of monomer concentrations and stopper fractions can be covered. Static light scattering (section 4.4.2) provides information about the static correlation length in solutions. In section 4.4.3, the effectiveness of the chain stopper is discussed and the results from both techniques are compared. Dynamic light scattering experiments are described in section 4.4.4.

### 4.4.1 Vapor pressure osmometry

Osmometry experiments were limited to relatively high stopper fractions due to the detection limit of the apparatus ( $\gtrsim 1$  mM). Figure 4.3 shows the reciprocal normalized osmotic pressure ( $RTc/\Pi$ ) of EHUT solutions with constant stopper fraction ( $x = 0.30$ ) at various monomer concentrations. Assuming ideality (see below), this quantity equals  $\langle N \rangle$ . If there would be no chain stoppers present,  $\langle N \rangle$  should increase by approximately a factor 2 within the concentration range used (assuming  $\langle N \rangle \sim c^{0.5}$ ). The plot shows that  $\langle N \rangle$  is constant within the experimental error. Therefore, we are in the regime where  $\langle N \rangle$  is independent of  $c$  and only determined by  $x$ , and the approximation in equation 4.5 can be applied. The constancy of  $\langle N \rangle$  also shows that non-ideality of the solution can be neglected (if present, it is small compared to the experimental error), and that our method for determining the number concentration of chains from the osmotic pressure without extrapolating to zero concentration is valid. For a series of solutions with a constant EHUT concentration of

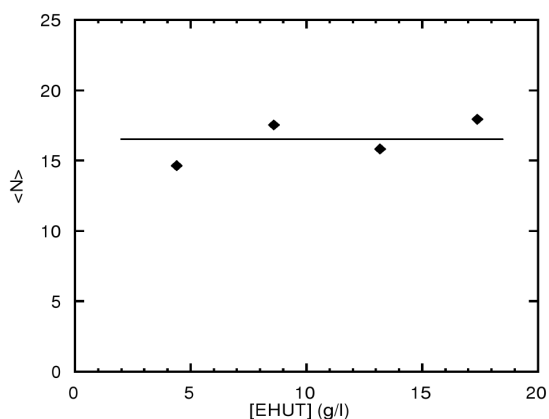


Figure 4.3:  $\langle N \rangle$  as a function of EHUT concentration at a constant stopper fraction ( $x = 0.30$ ). The horizontal line at  $\langle N \rangle = 16.6$  indicates the average value for the measured solutions.

4.4 g/l varying in stopper fraction from 0.3 to 0.7, the osmotic pressure was also measured and converted to  $\langle N \rangle$ . The results are shown by the solid symbols in figure 4.4. The decrease of  $\langle N \rangle$  with increasing  $x$  is described reasonably well by a power law with a slope of  $-1$ , indicated by the line which corresponds to  $\langle N \rangle = 4/x$ . Note that this is not a power law fit to the data, the line only serves to show that the data are broadly consistent with a power law with exponent  $-1$ . The approximate inverse proportionality with the stopper fraction

shows that the conditions for applying the approximation in equation 4.5 are met. The proportionality constant indicates that on average approximately 4 stoppers have to be added to the solution to create one new chain ( $n = 4$  in equation 4.5). This value for  $n$  means that DBUT is not a very efficient chain stopper. This is discussed in more detail in section 4.4.3.

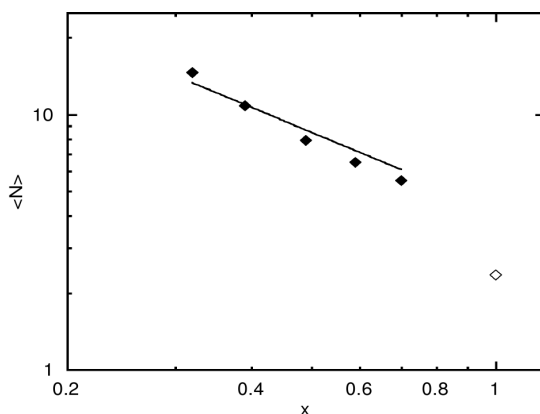


Figure 4.4: Number average degree of polymerisation  $\langle N \rangle$  as a function of stopper fraction  $x$  for EHUT solutions of 4.4 g/l in cyclohexane (◆). The line corresponds to  $\langle N \rangle = 4/x$ . The open symbol shows  $\langle N \rangle$  for a solution with only chain stoppers ( $x = 1$ ).

The osmotic pressure of two solutions of only chain stoppers ( $[\text{DBUT}] = 1$  and  $2 \text{ g/l}$ ,  $x = 1$ ) was also measured, and the osmotic pressure of both solutions was lower than expected based on their concentrations, approximately by a factor 2 (the open symbol in figure 4.4). This strongly suggests that DBUT is capable of forming dimers or small oligomers, leading to a decreased osmotic pressure compared to a purely monomeric solution. In DBUT, two of the hydrogen bond donating NH-groups which are present in EHUT are alkylated (see figure 4.1). However, the two remaining secondary amines in DBUT may still form hydrogen bonds with the carbonyl oxygens of other DBUT molecules. Recently, isothermal titration calorimetry experiments confirmed that DBUT is indeed capable of self-association [43].

#### 4.4.2 Static light scattering

Results of the static light scattering experiments are shown in figure 4.5. From a linear fit to the experimental data, the correlation length was calculated using equation 4.8. The linearity of the plots confirms that equation 4.8 applies to

our system for all concentrations used, both below and above the overlap concentration. Figure 4.6 shows the correlation length  $\xi$  for solutions of EHUT

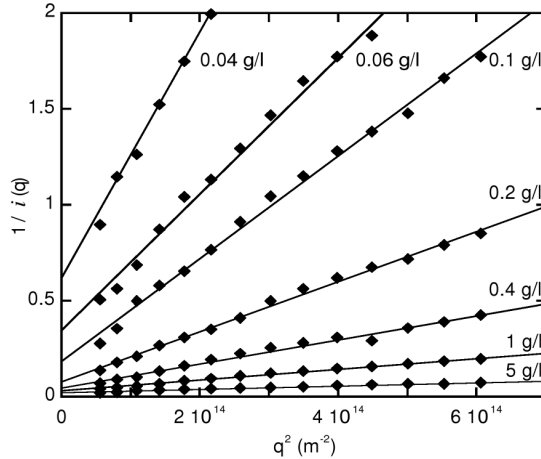


Figure 4.5: Reciprocal reduced scattered intensity as a function of  $q^2$  for EHUT solutions of various concentrations, all with  $x = 0.015$ . The lines are linear fits to the data.

in cyclohexane both with and without chain stoppers.

### Solutions without chain stoppers

At low concentrations, the correlation length is found to increase with increasing monomer concentration. Since in dilute solutions  $\xi$  reflects the size of the individual chains, the increase can be attributed to the growth of the chains. As mentioned in section 4.2.2,  $\xi$  can be identified as  $\langle L \rangle / \sqrt{3}$ . The data can be described reasonably well with the power law  $\xi = 600c^{0.5}$  (see figure 4.6), where  $c$  is given in g/l and  $\xi$  in nm. The exponent 0.5 indicates the presence of rodlike chains (see section 4.2.2). The proportionality constant 600 contains information about the association constant. Using an effective monomer length  $l_m$  of 0.18 nm [23],  $\langle N \rangle$  can be calculated from  $\xi$  and the relation becomes  $\langle N \rangle = 5.8 \cdot 10^3 c^{0.5}$ , again with  $c$  in g/l. According to equation 4.2, the proportionality constant is now equal to  $2\sqrt{K}$ , and  $K$  can be calculated to be  $8 \cdot 10^6$  l/g or  $4 \cdot 10^9$  M<sup>-1</sup>, using the molar mass of EHUT. Values for the association constant of EHUT in toluene and chloroform were measured previously by isothermal titration calorimetry, where  $K$  was found to be  $2 \cdot 10^6$  M<sup>-1</sup> in toluene at 40°C and  $1 \cdot 10^5$  M<sup>-1</sup> in chloroform at room temperature [25]. The present results

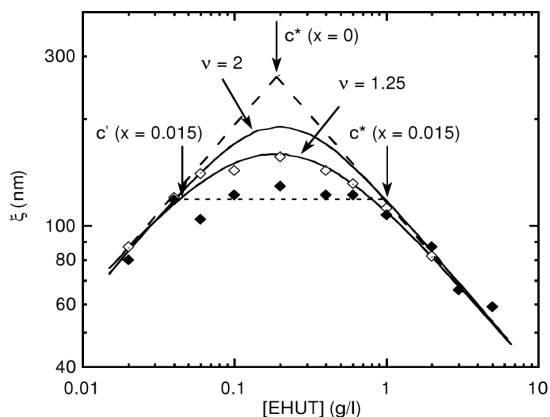


Figure 4.6: Static correlation length in EHUT solutions in cyclohexane without chain stoppers ( $\diamond$ ) and with a stopper fraction  $x = 0.015$  ( $\blacklozenge$ ). Arrows indicate the overlap concentrations with and without chain stoppers ( $c^*(x)$  and  $c^*(0)$ , respectively) and the critical concentration  $c'(x)$ . The dashed lines below and above  $c^*(0)$  indicate  $\xi = 600c^{0.5}$  and  $\xi = 120c^{-0.5}$ , respectively. The solid lines represent a fit of the experimental data to equation 4.10 with  $\nu = 2$  and  $\nu = 1.25$ , respectively. The dotted line indicates the plateau at 120 nm.

are in line with these findings, since both an increase in temperature and in solvent polarity will result in a decrease of the association constant. A number of assumptions and estimations have been made in the foregoing derivation, so the value of  $K$  is not very accurate. However, the analysis yields the order of magnitude of the association constant of EHUT in cyclohexane at room temperature. The association constant can also be estimated from the overlap concentration  $c^*$ , which was determined from viscosity measurements to be approximately 0.1 g/l without chain stoppers [26]. It is assumed that the chains are rigid rods with an average contour length  $\langle L \rangle = l_m \langle N \rangle$  where  $\langle N \rangle$  is given by equation 4.2, and that the chains occupy a volume equal to a sphere with a diameter equal to the rod contour length. As an estimate for the overlap concentration, the concentration at which these spheres fill the total volume of the system can be used. If  $c^*$  is known,  $K$  can be calculated:

$$K = \frac{3}{2\pi N_{av} l_m^3 (c^*)^2} \quad (4.18)$$

with  $N_{av}$  Avogadro's number. Using this expression and an overlap concentration of 0.1 g/l,  $K$  is calculated to be  $6 \cdot 10^6$  l/g ( $3 \cdot 10^9$  M $^{-1}$ ), in good agreement with the present result from light scattering. This agreement confirms that the

#### 4.4. Results and discussion

---

chains can be considered rodlike, at least up to their (average) length at the overlap concentration.

From concentrations above 0.06 g/l, deviations from the power law behavior are observed. This may be caused by the fact that the chains reach a length where they become longer than their persistence length and are no longer rigid rods. We may therefore estimate a lower limit for the persistence length of EHUT chains in cyclohexane from the onset of deviation from rodlike scaling. This occurs at a correlation length of approximately 150 nm, corresponding to a contour length of 250 nm (again using  $\xi = \langle L \rangle / \sqrt{3}$ ). The latter value is a lower limit for the persistence length, since the deviation from the theoretical concentration dependence for dilute rods can also be caused by the cross-over to the semidilute regime, in which case the chains can still be rigid at longer length scales. The correlation length reaches a maximum at approximately 0.2 g/l, which can be identified as the overlap concentration without chain stoppers. This is indicated as  $c^*(0)$  in figure 4.6, and can be calculated more precisely from the intersection of the linear extrapolations below and above the overlap concentration, which indeed occurs at 0.2 g/l. This result is in reasonable agreement with the value of 0.1 g/l from viscosimetry, especially since relatively few data points were measured close to  $c^*$  in the viscosity measurements [26]. When the concentration is increased further, the correlation length decreases, reflecting the decreasing mesh size in the polymer network. The concentration dependence of  $\xi$  is again consistent with a power law, this time with exponent  $-0.5$  (see figure 4.6). This scaling exponent was also found previously for the same system [26]. This exponent is expected for chains for which the persistence length is equal or longer than the mesh size, so the chains are rigid rods on the length scale  $\xi_m$ . This power law scaling is a good description for concentrations higher than approximately 0.8 g/l, where  $\xi \approx 150$  nm, which again leads to a lower limit for the persistence length of approximately 250 nm.

The correlation length is consistent with power laws at concentrations far below and above  $c^*$ . Equation 4.10 can be used to describe the cross-over between these regimes. With the scaling relations for rigid rods ( $\langle L \rangle \sim c^{0.5}$  and  $\xi_m \sim c^{-0.5}$ ) and the exponent  $\nu = 2$  (which was found in theoretical work for other systems [35, 36]), the equation fits the experimental data far away from  $c^*(0)$  but at concentrations around  $c^*(0)$ , the experimental  $\xi$  is systematically lower than the calculated value (see figure 4.6). This may be explained by the possibility mentioned above that the chains may be semiflexible around  $c^*$ , while they are rodlike at lower concentrations and rigid at the length scale of the mesh size at higher concentrations. This would affect the shape of the curve around  $c^*$ , but it is not taken into account in equation 4.10, in which the scaling exponents for rodlike chains are used for the whole concentration range. As an alternative explanation, the exponent  $\nu = 2$  was derived for flexible chains

in a mean-field approximation, whereas EHUT chains are certainly not fully flexible. It is possible that for semiflexible chains, a different value of  $\nu$  applies. Therefore,  $\nu$  was used as a fitting parameter, and the best results were obtained with  $\nu = 1.25$ , in which case the data are described well over the whole concentration range measured (see figure 4.6). A lower value of  $\nu$  corresponds to a wider crossover region. It is reasonable that the cross-over is less sharp for polydisperse rigid chains compared to flexible ones. When the longest chains in a polydisperse solution start to overlap, the short ones are still in the dilute regime. The difference in size between long and short chains is larger for rods ( $\langle R_g \rangle \sim \langle N \rangle$ ) than for coils ( $\langle R_g \rangle \sim \langle N \rangle^{0.5}$ ), which could explain the wider cross-over region. Furthermore, excluded volume interactions are stronger for coils than for rods, which may also lead to a more gradual cross-over between dilute and semidilute regime for rods. It is therefore reasonable that the value of  $\nu$  obtained from the present experiments is lower than 2.

### Solutions with chain stoppers

In these experiments, the stopper fraction  $x$  was kept constant at a value of 0.015, while the EHUT concentration varied between 0.02 and 5 g/l. At the lowest concentrations measured, the correlation lengths of the solutions with and without chain stoppers are approximately equal. The chain stoppers have a negligible effect on  $\langle N \rangle$ , which means that the number of functional chain ends is much larger than the number of dead ones. In other words, the chains are short and their number is so high that most of them are not terminated by chain stoppers.

Since the chain length increases with the square root of the monomer concentration, the number of chains also scales as  $c^{0.5}$ . The concentration of chain stoppers increases linearly with the total monomer concentration, so the number of chain stoppers increases relative to the number of chain ends if the overall EHUT concentration is increased at constant  $x$ . As a result, more chain ends will be formed by chain stoppers and the chain length is significantly decreased. At concentrations above approximately 0.04 g/l, the chain length becomes independent of  $c$ , leading to a plateau in  $\xi$  at approximately 120 nm, (see figure 4.6), similar to the plateaus in the theoretical figure 4.2b. The fact that  $\xi$  is determined by  $x$  indicates that the number of dead chain ends is much larger than the number of functional ones, according to equation 4.5. The onset of the plateau at  $c = 0.04$  g/l for  $x = 0.015$  corresponds to the critical condition of equation 4.7. By substituting these values for  $c$  and  $x$  and assuming  $K = 8 \cdot 10^6$  l/g (see section 4.4.2), the value of  $n$  can be calculated to be 17. The plateau region of the curve will be discussed in more detail below. Since the chains are shorter at a given monomer concentration in the presence of chain stoppers, the number of chains is higher (it is proportional to  $\langle N \rangle^{-1}$ ).

#### 4.4. Results and discussion

---

If we again assume that a chain occupies a volume equal to a sphere with a diameter equal to its contour length, the volume occupied by a single chain scales as  $\langle N \rangle^3$ . By combining these two scaling relations, it can be easily seen that the total volume occupied by the chains scales as  $\langle N \rangle^2$ , thus chains with chain stoppers occupy less volume than chains without chain stoppers at a given monomer concentration. As a result, more chains (a higher monomer concentration) is needed to fill the whole volume with chains, and the overlap concentration in the presence of chain stoppers is increased. The correlation length above the overlap concentration is independent of chain length, so solutions with and without chain stoppers should give the same value for  $\xi$ . The overlap concentration  $c^*(x)$  at a given stopper fraction can therefore be obtained by calculating the concentration at which the plateau level of  $\xi$  (120 nm for  $x = 0.015$ ) in the dilute regime and the semidilute correlation length  $\xi_m$  ( $120c^{-0.5}$ ) intersect (see figure 4.6). From this, it follows that the overlap concentration at a stopper fraction of 0.015 equals 1 g/l. Figure 4.6 shows that indeed at higher concentrations than this, the correlation lengths with and without stoppers are equal. The value of 1 g/l may thus be considered a reasonable estimate for  $c^*(x = 0.015)$ .

Using the present results, the overlap concentration at other stopper fractions can be estimated. The plateau in  $\xi$  is a result of the fact that  $\langle N \rangle$  becomes independent of  $c$  and is proportional to  $1/x$  (see figure 4.2b). Under these conditions, we can write for dilute rodlike chains  $\xi_{\text{plateau}} = A/x$  (using that  $\xi \sim \langle L \rangle \sim \langle N \rangle \sim 1/x$ ). The proportionality constant  $B$  can be calculated by substituting the present data ( $x = 0.015$ ,  $\xi_{\text{plateau}} = 120$  nm), leading to  $B = 1.8$  nm. As explained above, the overlap concentration can be found by calculating the intersection of the plateau with the semidilute correlation length. Above the overlap concentration, the correlation length is independent of  $\langle N \rangle$ , and therefore also of stopper fraction, and was found to be equal to  $120c^{-0.5}$  nm (if  $c$  is expressed in g/l). Equating this to  $1.8/x$  leads to the expression  $c^*(x) = (67x)^2$  (again in g/l). Note that this equation is based on experimental data, and it is affected by errors in the determination of the level of the plateau and the semidilute correlation length. It can therefore not be expected to give a very accurate prediction of  $c^*(x)$ , but it should give a reasonable estimate.

If equations 4.8 and 4.9 apply and the chains are rigid rods, the plateau correlation length of 120 nm would correspond to a number average contour length of approximately 200 nm. Equation 4.9 is valid for small values of  $q$ , that is if the probed length scale  $2\pi/q$  is larger than  $\xi$ . With values of  $q$  and  $\xi$  from our experiments this assumption is reasonable. As was mentioned in the discussion of the overlap concentration, the persistence length is estimated to be at least 250 nm. The plateau in  $\xi$  occurs at 120 nm, so it is reasonable to assume that chains with the corresponding contour length of 200 nm are indeed rigid. The assumption that  $p \approx 1$  is also reasonable, as can be seen when

the estimated value of  $K$  of  $4 \cdot 10^9 \text{ M}^{-1}$  is substituted in equation 4.4. Even at the lowest monomer concentrations,  $p$  is still very close to unity. In conclusion, equations 4.8 and 4.9 should apply reasonably well to our experimental system under the experimental conditions used in the present paper.

### 4.4.3 Effectiveness of chain stoppers

A chain stopper with the highest possible effectiveness has an infinitely high association constant with the supramolecular polymer chains, and can only associate to one side of the chain. Furthermore, the addition of a single chain stopper to a chain completely stops the chain from growing. In that case, the value of  $n$  (as defined in equation 4.5) equals 1. Generally, the effectiveness of a chain stopper can be reduced because of properties of the chains and properties of the chain stoppers.

The properties of the chains reduce the effectiveness for example if the stopper can bind to both sides of the chain (as is the case for the ureidopyrimidinone-based supramolecular polymers [13]). In that case the (minimum) value of  $n$  is 2. Thus, more stoppers have to be added to reach a given value of  $\langle N \rangle$ , and the chain stopper is less effective. For branched chains, the minimum value of  $n$  can even be much higher. The chain architecture also plays a role. If the chains have one monomer per axial repetition unit (the cross-section of the chain consists of a single monomer), the addition of one stopper to a chain end completely stops the chain from growing at that end. However, if the cross-section of the chain consists of more than one monomer (as was proposed for EHUT chains [23, 27]), a higher number of chain stoppers may have to bind to the chain at the same position to completely stop it from growing. If the number of associated chain stoppers at a certain position in the chain is less than this number, the chain may still grow further, and the chain stoppers may only form a 'defect' in the chain instead of stopping it. By this mechanism, chain stoppers can be incorporated in the chain, and this also reduces the effectiveness of the stopper. The stoppers themselves can also cause a decreased effectiveness. This is the case if they do not associate very strongly to the chains (in which case there will be free chain stoppers in solution) or if they form aggregates such as the proposed DBUT dimers mentioned in section 4.4.1. The combination of all these factors leads to an overall stopper effectiveness, which can be defined as  $1/n$  and which can range from 1 ( $n = 1$ , ideal stopper) to 0 ( $n = \infty$ , no stopper effect).

A chain of 200 nm (the contour length corresponding to the plateau value of  $\xi$  of 120 nm) consists of approximately 1100 monomers (using  $l_m = 0.18 \text{ nm}$ ). In our experiments, a stopper fraction of 0.015 was used. In order to get chains of 1100 monomers at a stopper fraction of 0.015, the value of  $n$  should be 17. The same value was also obtained from the critical concentration of

#### 4.4. Results and discussion

---

0.04 g/l at  $x = 0.015$  (see section 4.4.2). It is not surprising that the effectiveness derived from light scattering ( $n = 17; 1/n = 0.06$ ) is higher than that derived from osmometry ( $n = 4; 1/n = 0.25$ ). As mentioned in section 4.4.1, DBUT is probably capable of forming dimers or small oligomers. These aggregates are very small, and do not contribute significantly to the scattered intensity in SLS experiments, but they do contribute to the osmotic pressure. Thus, light scattering only gives information about chains above a certain size, whereas osmometry also measures the shortest chains and DBUT oligomers. The chain length as measured by osmometry will therefore be smaller than with light scattering and as a result, the calculated value of  $n$  will also be smaller. Since only a part of the chain length distribution is measured with light scattering, whereas osmometry measures all chains, the effectiveness as derived from osmometry (0.25) is probably a more reliable value for the overall effectiveness of DBUT.

In principle, the association constants in the EHUT/DBUT system (EHUT-EHUT, DBUT-DBUT and DBUT-EHUT) can be calculated from experimental data ( $\langle N \rangle$ ) as a function of  $c$  and  $x$  if the chain structure and architecture is also known. Unfortunately, this information is presently not available for the EHUT/DBUT system. EHUT certainly forms long, semiflexible linear structures with a very high association constant. However, the exact structure of EHUT chains is still ambiguous, especially since there is evidence which shows that the chains can change their structure depending on the conditions [27]. It is possible that the association of DBUT to a chain also affects the chain structure. It remains to be studied how DBUT associates to the different chain structures. There are independent estimates for the EHUT-EHUT association constant [25] (see also section 4.4.2), but not yet for the DBUT-DBUT and EHUT-DBUT association. So far, only preliminary experiments have been carried out in which the formation of these bonds has been studied qualitatively [43]. From the foregoing, it is clear that much work has to be done before a complete picture of the association of EHUT/DBUT can be constructed.

#### 4.4.4 Dynamic light scattering

At low concentrations, the distribution of decay rate constants obtained from a CONTIN analysis of the correlation function has a single peak which is related to the collective diffusion coefficient and the hydrodynamic correlation length, as explained in section 4.2.3. Above a certain concentration, a second peak, corresponding to a slow relaxation mode, appears at longer decay times. Typical correlation functions  $g^{(1)}(\tau)$  at different scattering angles and the corresponding spectra of relaxation times can be found in the supporting information.

Without chain stoppers, the slow mode is present at all concentrations mea-

sured, except for the lowest one (0.2 g/l). In the solutions with chain stoppers, the second peak only appears at concentrations above 1 g/l. Both observations indicate that the slow mode is only present above the overlap concentration as measured by SLS (0.2 g/l and 0.8 g/l without and with chain stoppers, respectively). The fact that the slow mode only appears above the overlap concentration suggests that it might have something to do with the formation of the transient polymer network. A typical result for the  $q^2$ -dependence of both modes is shown in figure 4.7. Both modes will be discussed in more detail below.

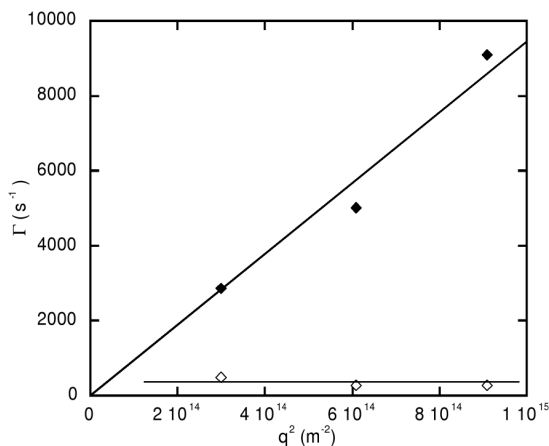


Figure 4.7:  $q^2$ -dependence of  $\Gamma_{fast}$  (◆) and  $\Gamma_{slow}$  (◇) for a 3 g/l EHUT solution with  $x = 0.015$ .  $\Gamma_{fast}$  is proportional to  $q^2$ , as indicated by the linear fit, which corresponds to  $\Gamma_{fast} = 9.45 \cdot 10^{-12} q^2$ . The horizontal line at  $\Gamma_{slow} = 335 \text{ s}^{-1}$  shows that the slow mode does not depend significantly on  $q$ .

### Fast mode

The peak value of  $\Gamma$  in the ‘fast’ peak ( $\Gamma_{fast}$ ), is taken as the decay rate constant which is related to the collective diffusion coefficient. When the values of  $\Gamma_{fast}$  at different scattering angles are plotted as a function of  $q^2$  (see figure 4.7), it can be seen that  $\Gamma_{fast}$  is proportional to  $q^2$ , which shows that the fast mode is indeed diffusive. The slope of the fitted line corresponds to the gel diffusion coefficient  $D_g$  of equation 4.13 and 4.14. Since cyclohexane is a good solvent for EHUT,  $M_o \gg M_g$  and  $D_g$  equals the collective diffusion coefficient  $D_c$  (equation 4.14). Using this, the hydrodynamic correlation length  $\xi_H$  can be calculated with equation 4.15. The results of this procedure are

#### 4.4. Results and discussion

shown in figure 4.8, where the hydrodynamic correlation length is plotted as a function of EHUT concentration for solutions with and without chain stoppers. For comparison, the static correlation length  $\xi_m$  as measured with SLS is also shown. It can be seen that the quality of the data obtained from DLS is less good than the SLS data. This is probably mainly caused by the limited quality of the correlation functions due to the low scattered intensity and the limited number of decay rates used in the CONTIN analysis. Therefore, only qualitative conclusions will be drawn based on the DLS results. Since there are no data

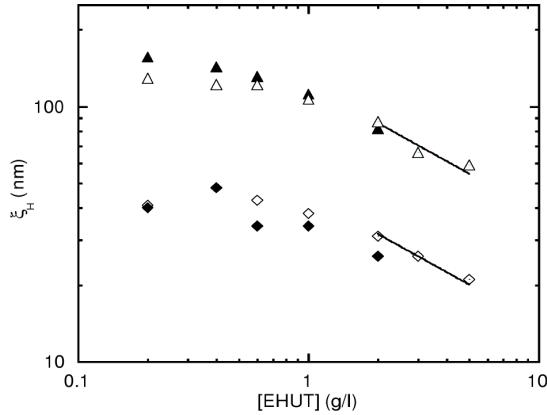


Figure 4.8: Hydrodynamic correlation length as a function of EHUT concentration for solutions without chain stoppers ( $\blacklozenge$ ) and for solutions with  $x = 0.015$  ( $\diamond$ ). The static correlation lengths for solutions without chain stoppers ( $\blacktriangle$ ) and with  $x = 0.015$  ( $\triangle$ ) are replotted from figure 4.6. The solid lines both have a slope  $-0.5$  and indicate  $\xi \sim c^{-0.5}$ .

below  $c^*$  for the solutions without chain stoppers (due to the low intensity of the scattered light), it is not possible to calculate the overlap concentration from the maximum in the correlation length as was done with SLS. However, it can be seen that as the concentration is decreased towards  $c^*$ ,  $\xi_H$  levels off. At concentrations  $> c^*$ ,  $\xi_H$  decreases and the results can be fitted with a power law with exponent  $-0.5$ . This is the same scaling exponent as found with SLS. It can be seen from figure 4.8 that the curves from SLS and DLS are more or less parallel over the whole range of concentrations measured. This shows that the hydrodynamic correlation length indeed depends on concentration in the same way as the static correlation length, but they are not equal. The difference between the values is approximately a factor of 3. Roughly the same factor was found for the ratio between the static and hydrodynamic radius of gyration for dilute solutions of monodisperse stiff chains [44].

### Slow mode

As can be seen from figure 4.7, the decay rate constant associated with the slow mode does not depend significantly on the scattering angle. Therefore it can be concluded that the slow mode is not caused by the diffusive motion of large aggregates or domains, as this would lead to a relaxation time proportional to  $q^2$ . The average of the measured values at different  $q$  is taken as  $\Gamma_{slow}$ , and the reciprocal of this equals  $\tau_{slow}$ . The concentration dependence of  $\tau_{slow}$  is shown in figure 4.9 for solutions with and without chain stoppers.

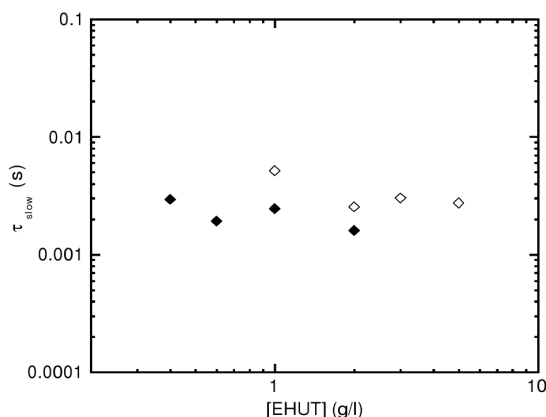


Figure 4.9: Decay time  $\tau_{slow}$  of the slow mode as a function of EHUT concentration for solutions without chain stoppers ( $\blacklozenge$ ) and for solutions with  $x = 0.015$  ( $\diamond$ ).

The fact that the slow mode only appears above the overlap concentration, and that there is no significant  $q$ -dependence suggest that it might be related to the viscoelastic relaxation time of the solutions, as mentioned in section 4.2.3. However, there is a large difference between the relaxation times obtained from the DLS measurements and from rheometry. The viscoelastic relaxation time  $\tau_0$  (from rheometry) has a value of a few seconds (see chapter 5), whereas  $\tau_{slow}$  (from DLS) of the same solution is only a few milliseconds (figure 4.9). In experiments with other polymers and also with wormlike micelles, a much closer agreement between these values was reported [45–48].

The large difference found in the present experiments could be related to the rigidity of the chains, or to the fact that for EHUT, several stress relaxation mechanisms (e.g. reptation and breaking of chains) occur on the same time scale (see chapter 5). But it is perhaps more realistic to assume that the slow decay time is not the result of coupling of concentration fluctuations

to viscoelastic relaxation and is therefore not (directly) related to  $\tau_0$ . More experiments are needed in order to find a conclusive answer.

## 4.5 Concluding remarks

In supramolecular polymer solutions, the number average degree of polymerisation  $\langle N \rangle$  is a function of the concentration  $c$  of bifunctional monomers:  $\langle N \rangle \sim c^{0.5}$ . The addition of a mole fraction  $x$  of monofunctional chain stoppers to the solution causes a decrease in  $\langle N \rangle$ . Within a certain range of concentrations and stopper fractions,  $\langle N \rangle$  is expected to be proportional to  $1/x$  and independent of  $c$ . For the system of bifunctional monomer EHUT and chain stopper DBUT in cyclohexane, vapor pressure osmometry and static and dynamic light scattering were performed on solutions with and without chain stoppers.

From osmotic pressure measurements,  $\langle N \rangle$  is indeed found to be independent of monomer concentration and proportional to  $1/x$  for the studied range of concentrations and stopper fractions. Results also indicate that DBUT forms small aggregates, thereby decreasing its effectiveness as a chain stopper.

The static correlation length in EHUT solutions without chain stoppers as measured with SLS has a maximum at the overlap concentration. From the overlap concentration and the scaling of the correlation length in dilute solutions, the association constant of EHUT in cyclohexane was estimated to be of the order of  $10^9 \text{ M}^{-1}$ , in agreement with results from previous experiments. The concentration dependence of the correlation length indicates that the persistence length of the chains is at least 250 nm. In the presence of a fixed fraction  $x$  of chain stoppers, there is a plateau in the correlation length above a certain monomer concentration, showing that the chain length is only determined by  $x$  and independent of monomer concentration under these conditions. Furthermore, the overlap concentration in the presence of chain stoppers is increased, due to the decreased chain length.

Dynamic light scattering is used to measure the hydrodynamic correlation length. It scales in the same way as the static correlation length and is of the same order of magnitude, in agreement with theoretical predictions. For solutions above the overlap concentration, the distribution of decay times shows a second, slow mode. The behavior of the slow decay time shows qualitative agreement with the terminal viscoelastic relaxation time measured previously with rheometry, but the latter is substantially longer. It is unclear if the slow mode is related to viscoelasticity, or which other physical process causes it.

## Appendix: CONTIN spectra

In this appendix, correlation functions as measured by DLS are shown for solutions below and above the overlap concentration. The corresponding spectra of relaxation times are also shown.

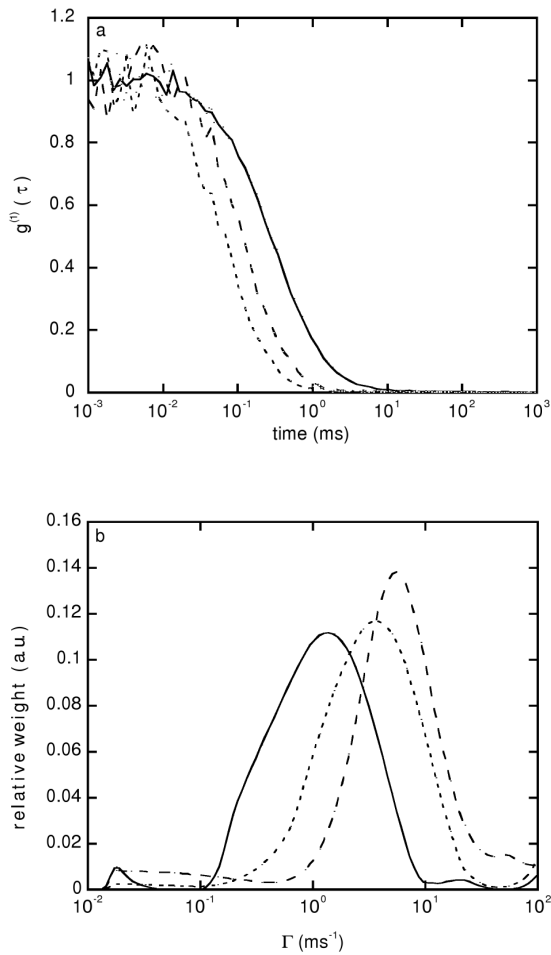


Figure 4.10: a: Normalized field autocorrelation function  $g^{(1)}(\tau)$  for a 0.4 g/l EHUT solution with  $x = 0.015$ , at scattering angles of  $60^\circ$  (solid line),  $90^\circ$  (dashed line) and  $120^\circ$  (dotted line). b: distribution of decay rate constants, obtained from a CONTIN analysis of  $g^{(1)}(\tau)$ .

#### 4.5. Concluding remarks

---

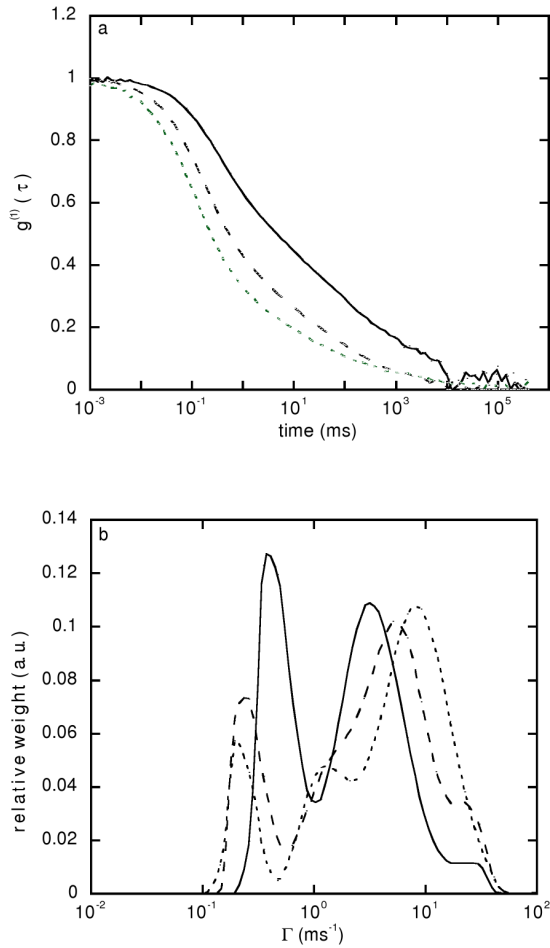


Figure 4.11: a: Normalized field autocorrelation function  $g^{(1)}(\tau)$  for a 3 g/l EHUT solution with  $x = 0.015$ , at scattering angles of  $60^\circ$  (solid line),  $90^\circ$  (dashed line) and  $120^\circ$  (dotted line). b: distribution of decay rate constants, obtained from a CONTIN analysis of  $g^{(1)}(\tau)$ .

For EHUT solutions with a stopper fraction of 0.015, the overlap concentration was estimated from the SLS results to be approximately 0.8 g/l. In figure 4.10, the results for an EHUT concentration of 0.4 g/l with  $x = 0.015$  (below the overlap concentration) is shown. From figure 4.10a, it can be seen that the correlation function decays from 1 to 0 over a relatively small range of decay times. With increasing scattering angle (increasing  $q$ ), the curves shift to shorter decay times, and thus to higher values of the decay rate constant  $\Gamma$ . Figure 4.10b shows that the spectrum of correlation times contains a single peak, which indeed shifts to higher values of  $\Gamma$  with increasing  $q$ .

Figure 4.11a shows the results for 3 g/l EHUT ( $x = 0.015$ ), which is well above the overlap concentration. The decay of the correlation function is much more gradual than below the overlap concentration. It is clear that the spectrum of relaxation times is much broader, and it may have more than one peak. Similar to the results at low concentrations, the correlation function shifts to faster decay times, and thus to higher values of  $\Gamma$  when the scattering angle increases from 60 to 120°. The corresponding CONTIN spectra are shown in figure 4.11b. The spectra indeed have two peaks. The 'fast' peak (at the highest value of  $\Gamma$ ) shows a clear angular dependence, it shifts to higher values of  $\Gamma$  with increasing  $q$ . In the example shown, the 'slow' peak seems to shift to somewhat lower values of  $\Gamma$ . However, the angular dependence of the slow mode is not systematic. When all the experimental data are taken into account, the position of the slow peak does not change significantly with scattering angle.

## References

- [1] J-M. Lehn. *Supramolecular chemistry: concepts and perspectives*. VCH, Weinheim, 1995.
- [2] N. Zimmerman, J.S. Moore, and S.C. Zimmerman. *Chem. Ind.*, 15: 604–610, 1998.
- [3] J.S. Moore. *Curr. Opin. Colloid Interface Sci.*, 4: 108–116, 1999.
- [4] A. Ciferri, editor. *Supramolecular polymers*. Marcel Dekker, New York, 2000.
- [5] L. Brunsveld, B.J.B. Folmer, E.W. Meijer, and R.P. Sijbesma. *Chem. Rev.*, 101: 4071–4097, 2001.
- [6] A.W. Bosman, L. Brunsveld, B.J.B. Folmer, R.P. Sijbesma, and E.W. Meijer. *Macromol. Symp.*, 201: 143–154, 2003.

## References

---

- [7] Lange R.F.M., M. van Gorp, and E.W. Meijer. *J. Polym. Sci. Pol. Chem.*, 37: 3657–3670, 1999.
- [8] A.T. ten Cate and R.P. Sijbesma. *Macromol. Rapid Commun.*, 23: 1094–1112, 2002.
- [9] O. Colombani, C. Barioz, L. Bouteiller, C. Chanéac, L. Fompérie, F. Lortie, and H. Montès. *Macromolecules*, 38: 1752–1759, 2005.
- [10] H.M. Keizer, R.P. Sijbesma, J.F.G.A. Jansen, G. Pasternack, and E.W. Meijer. *Macromolecules*, 36: 5602–5606, 2003.
- [11] S. Kiyonaka, K. Sugiyasu, S. Shinkai, and I. Hamachi. *J. Am. Chem. Soc.*, 124: 10954–10955, 2002.
- [12] S-L. Zhou, S. Matsumoto, H-D. Tian, H. Yamane, A. Ojida, S. Kiyonaka, and I. Hamachi. *Chem. Eur. J.*, 11: 1130–1136, 2005.
- [13] R.P. Sijbesma, F.H. Beijer, L. Brunsveld, B.J.B. Folmer, J.H.K.K. Hirschberg, R.F.M. Lange, J.K.L. Lowe, and E.W. Meijer. *Science*, 278: 1601–1604, 1997.
- [14] D.C. Sherrington and K.A. Taskinen. *Chem. Soc. Rev.*, 30: 83–93, 2001.
- [15] R.P. Sijbesma and E.W. Meijer. *Chem. Commun.*, pages 5–16, 2003.
- [16] G. Armstrong and M. Buggy. *J. Mater. Sci.*, 40: 547–559, 2005.
- [17] F. Lortie, S. Boileau, L. Bouteiller, C. Chassenieux, and F. Lauprêtre. *Macromolecules*, 38: 5283–5287, 2005.
- [18] M.E. Cates and S.J. Candau. *J. Phys. Condens. Matter*, 2: 6869–6892, 1990.
- [19] F. Lequeux. *Curr. Opin. Colloid Interface Sci.*, 1: 341–344, 1996.
- [20] L.M. Walker. *Curr. Opin. Colloid Interface Sci.*, 6: 451–456, 2001.
- [21] P.A. Hassan, J. Narayanan, and C. Manohar. *Curr. Sci. India*, 80: 980–989, 2001.
- [22] S. Boileau, L. Bouteiller, Lauprêtre F., and F. Lortie. *New J. Chem.*, 24: 845–848, 2000.
- [23] F. Lortie, S. Boileau, L. Bouteiller, C. Chassenieux, B. Demé, G. Ducouret, M. Jalabert, F. Lauprêtre, and P. Terech. *Langmuir*, 18: 7218–7222, 2002.
- [24] V. Simic, L. Bouteiller, and M. Jalabert. *J. Am. Chem. Soc.*, 125: 13148–13154, 2003.
- [25] A. Arnaud and L. Bouteiller. *Langmuir*, 20: 6858–6863, 2004.

- 
- [26] J. van der Gucht, N.A.M. Besseling, W. Knoben, L. Bouteiller, and M.A. Cohen Stuart. *Phys. Rev. E*, 67: 051106 1–10, 2003.
- [27] L. Bouteiller, O. Colombani, F. Lortie, and P. Terech. *J. Am. Chem. Soc.*, 127: 8893–8898, 2005.
- [28] M. Miyauchi, Y. Takashima, H. Yamaguchi, and A. Harada. *J. Am. Chem. Soc.*, 127:2984–2989, 2005.
- [29] Y. Hasegawa, M. Miyauchi, Y. Takashima, H. Yamaguchi, and A. Harada. *Macromolecules*, 38:3724–3730, 2005.
- [30] P.J. Flory. *J. Am. Chem. Soc.*, 78: 1877–1885, 1936.
- [31] P.J. Flory. *Principles of polymer chemistry*. Cornell University press, Ithaca, New York, 1964.
- [32] W. Brown, editor. *Light Scattering: Principled and Development*. Cornell University Press, Oxford, 1996.
- [33] R. C. Oberthur. *Makromol. Chem.*, 179(11):2693–2706, 1978.
- [34] P.G. de Gennes. *Scaling concepts in polymer physics*. Cornell University press, Ithaca, New York, 1979.
- [35] G. J. Fleer, A. M. Skvortsov, and R. Tuinier. *Macromolecules*, 36:7857–7872, 2003.
- [36] J. van der Gucht, N.A.M. Besseling, and G.J. Fleer. *Macromolecules*, 37: 3026–3036, 2004.
- [37] W. Brown and T. Nicolai. *Colloid Polym. Sci.*, 268:977–990, 1990.
- [38] E. Buhler and M. Rinaudo. *Macromolecules*, 33: 2098–2106, 2000.
- [39] F. Brochard and P.G. de Gennes. *Macromolecules*, 10: 1157–1161, 1977.
- [40] A.N. Semenov. *Physica A*, 166: 263–287, 1990.
- [41] M. Doi and A. Onuki. *J. Phys. II France*, 2: 1631–1656, 1992.
- [42] S.W. Provencher. *Makromol. Chem.*, 180: 201–209, 1980.
- [43] L. Bouteiller. *personal communication*.
- [44] W. Burchard. *Makromol. Chem., Macromol. Symp.*, 18:1–35, 1988.
- [45] M. Adam and M. Delsanti. *Macromolecules*, 18: 1760–1770, 1985.
-

## References

---

- [46] N. Nemoto, M. Kuwahara, M-L. Yao, and K. Osaki. *Langmuir*, 11: 30–36, 1995.
- [47] A. Koike, T. Yamamura, and N. Nemoto. *Coll. Polym. Sci.*, 272: 955–961, 1994.
- [48] E. Buhler, J.P. Munch, and S.J. Candau. *J. Phys. II France*, pages 765–787, 1995.

# 5

## **Dynamics of reversible supramolecular polymers: independent determination of the dependence of linear viscoelasticity on concentration and chain length by using chain stoppers**

### **Abstract**

The linear viscoelasticity of solutions of a hydrogen bonded reversible supramolecular polymer in the presence of a chain stopper was studied by rheometry and by dynamic light scattering using probe particles. The use of chain stoppers enabled the independent variation of the degree of polymerisation and the monomer concentration, and the effect of both parameters on rheology was investigated. Scaling exponents were obtained for the chain length and concentration dependence of the zero-shear viscosity and the terminal relaxation time and these were compared to theoretical values. The results indicate that the reversible supramolecular polymer is semiflexible, and that both breaking and reptation of chains contribute to the stress relaxation. The parameters from macroscopic rheometry were compared to microscopic values obtained from probe particle diffusion. The particles probe the macroscopic viscoelastic parameters if their size is large compared to the correlation length in the system and to the (persistence) length of the polymer chains.

## 5.1 Introduction

The dynamics of polymers and polymer solutions is one of the most studied topics in rheology. It is of great interest for industrial processes, but also from an academic point of view. During the past 15 years, a new class of polymers with unique rheological properties is receiving increasing interest. In these so-called *supramolecular* polymers, the monomers are not linked covalently, but by secondary interactions such as metal-ligand complexation or hydrogen bonding [1, 2]. A definition of the term ‘supramolecular polymer’ was given by Brunsveld *et al.* [3]. In many supramolecular polymers, the bonds break and reform on experimental time scales, which leads to a dynamic equilibrium and a continuous exchange between bonded and free binding groups. These systems are therefore sometimes named *reversible* supramolecular polymers. One of the major consequences of this reversibility is that the average number of monomers in a chain is a function of parameters such as the overall monomer concentration and temperature. Since the chain length can be adjusted *in situ* by varying these parameters, the rheology of these systems is also tunable. The continuous breaking and recombination of chains also has a marked effect on the rheology, since it contributes to the relaxation of stress [4, 5]. Upon applying a deformation, reversible supramolecular polymers will re-equilibrate faster than covalent ones because of this additional relaxation mechanism. In some respects, reversible supramolecular polymers are similar to wormlike micelles, which are also long reversible non-covalent aggregates, though the interactions which cause the formation of wormlike micelles are generally less specific. Nevertheless, many of the concepts and techniques developed for studying wormlike micelles can be applied to supramolecular polymers.

The use of multiple hydrogen bonds in the formation of supramolecular polymers has been one of the most successful approaches so far. Hydrogen bonded supramolecular polymers are based on the presence of two complementary hydrogen bonding motifs in one monomer [6–10]. These bifunctional monomers can associate with each other into linear supramolecular chains. If more than two binding groups are present, branched chains and cross-linked networks can be formed. One of these multiple hydrogen bonding monomers is 2,4-*bis*(2-ethylhexylureido)toluene, or EHUT (figure 5.1). This compound forms rigid linear chains of monomers in various apolar organic solvents by the cooperative formation of four hydrogen bonds per monomer, as was found by IR spectroscopy, small angle neutron scattering, static light scattering and capillary viscosimetry [11–14]. The linear density of the supramolecular chains suggests that two or three monomers are present per axial repetition unit, and a corresponding molecular structure was proposed [12]. The linear rheology of this system was investigated by rheometry and dynamic light scattering using probe particles [14].

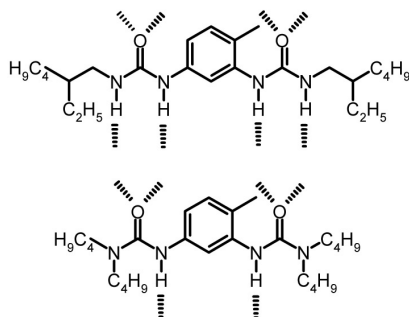


Figure 5.1: Bifunctional monomer EHUT (top) and chain stopper DBUT (bottom). Dashed lines represent the possible hydrogen bonds.

In general, the rheology of polymer solutions depends on the length (distribution) of the chains and on the concentration of polymer in the system [15, 16]. Supramolecular polymers are expected to show behavior which is different from covalent ones owing to the continuous breaking and formation of bonds. Furthermore, the chain length and polymer concentration are not independent, since the average degree of polymerisation is a function of monomer concentration. This complicates the determination of the separate effects of chain length and polymer concentration on rheological parameters. A method was reported by which under certain conditions the average chain length can be extracted from rheological data [17]. In principle, this would enable investigation of the chain length and concentration dependence by using solutions of equal concentration but with different mean chain lengths and vice versa. However, in order to change the chain length without changing concentration, other parameters such as temperature or solvent composition have to be changed. It is certainly useful to be able to measure the average chain length, but this method is not generally very useful for a systematic variation of chain lengths and concentrations. It would therefore be worthwhile to have a more elegant method to actively and independently control concentration and chain length. In the present paper, we achieve this by the addition of monofunctional monomers ('chain stoppers') to the solution. Addition of a bifunctional monomer to a chain leads to a functional chain end which can bind another monomer. Chain stoppers decrease the average chain length by adding a 'dead' end to the chain. The use of chain stoppers is possible due to the fact that supramolecular polymers are formed by linear association of bifunctional monomers, making this approach unique for supramolecular polymers. For example, wormlike micellar systems do not consist of bifunctional monomers, so the concept of monofunctional chain stoppers does not

apply.

As a chain stopper for EHUT, 2,4-bis(dibutylureido)toluene or DBUT (figure 5.1) was designed and synthesized [18, 19]. DBUT is not a perfect chain stopper for EHUT, since the remaining two amines in DBUT may still act as hydrogen bond donors. Nevertheless, DBUT was found to be the most effective of a number of chain stoppers in reducing the viscosity of EHUT solutions and was therefore selected for further experiments. The reason for the high effectiveness of DBUT is probably the strong cooperativity in the simultaneous formation of four hydrogen bonds in EHUT [11, 13], which disfavors the formation of only two hydrogen bonds with the amines in DBUT. In the present paper, the effect of the addition of DBUT on the viscoelastic properties of EHUT solutions is described in more detail. This was investigated by rheometry and by studying the motion of colloidal particles to probe the viscoelastic parameters on a microscopic length scale. The results are compared to similar experiments without chain stoppers [14] and to the model of Cates [4, 5], in which scaling relations for the concentration and chain length dependence of the zero-shear viscosity and the relaxation time are derived. To our knowledge, this is the first time that a systematic study of this kind was done.

## 5.2 Theoretical background

### 5.2.1 Chain stoppers

In a reversible supramolecular polymer solution, free binding groups are in equilibrium with bonded ones: two free groups can associate reversibly to form a bond. In the simplest model, the association constant  $K$  is independent of chain length (isodesmic association). From this equilibrium, the following expression for the average degree of polymerization  $\langle N \rangle$  as a function of the overall monomer concentration  $c$  and  $K$  can be derived:

$$\langle N \rangle = \frac{1 + \sqrt{1 + 16Kc}}{2} \approx 2\sqrt{Kc} \quad (5.1)$$

where the approximate equality applies if  $Kc \gg 1$ . When a fraction  $x$  of the monomers consists of monofunctional chain stoppers,  $\langle N \rangle$  will decrease. If it is assumed that one new chain is formed (one chain scission occurs) for every  $n$  chain stoppers added to the solution,  $\langle N \rangle$  is given by:

$$\langle N(x) \rangle = \frac{n\langle N(0) \rangle}{n(1-x) + x\langle N(0) \rangle} \approx \frac{n}{x} \quad (5.2)$$

Where  $\langle N(0) \rangle$  is the average degree of polymerisation without any stoppers, as given by equation 5.1. In equation 5.2,  $n$  is assumed to be a constant, but

in reality also the association of a stopper molecule is an equilibrium process so  $n$  will be a function of  $c$  and  $x$ . However, for sufficiently high values of  $K$ , the assumption of a constant  $n$  is reasonable. Note the analogy of these equations with the theory of condensation polymerisation [20, 21]. This is also an equilibrium process during the polymerisation step, and the presence of monofunctional monomers reduces the average chain length in the same way as for supramolecular polymers.

The approximation of  $\langle N(x) \rangle$  to  $n/x$  in equation 5.2 is justified if the number of functional chain ends is negligible compared to the number of dead ends. This is the case if both  $x$  and  $\langle N(0) \rangle$  are sufficiently large.  $K$  and  $n$  are constants for a given monomer/solvent system at a given temperature, so only  $c$  and  $x$  can be varied to satisfy this condition. In the range of values for  $c$  and  $x$  where the approximation holds,  $\langle N \rangle$  is independent of  $c$ , and this offers the possibility to vary the chain length and overall monomer concentration independently. By varying  $x$  at constant  $c$ , the average chain length is varied without changing the overall monomer concentration. Alternatively, the overall monomer concentration can be varied at constant chain length by keeping  $x$  constant and varying  $c$ .

### 5.2.2 Viscoelasticity of supramolecular polymers

The rheology of reversible supramolecular polymers is often considered within the framework of the theoretical model developed by Cates and co-workers [4, 5]. This model, originally developed for wormlike micelles, is based on the theory of reptation [15, 16], which was extended with the possibility for the chains to break and recombine. If the characteristic time for breaking is much faster than that for reptation, the polydispersity of the chains is not important and the model predicts exponential stress relaxation with a single relaxation time (Maxwell behavior) for all frequencies. If breaking is much slower than reptation, polydispersity makes the stress relaxation strongly non-exponential, and the Maxwell model does not apply. Thus, the frequency range over which the Maxwell model fits the experimental data is an indication of the predominant relaxation mechanism. There is a method to analyze this quantitatively by looking at deviations from exponential stress relaxation in a Cole-Cole plot ( $G''$  (the loss modulus) as a function of  $G'$  (the storage modulus)) [22]. This method is based on the fact that for purely exponential stress relaxation, a Cole-Cole plot has a semicircular shape. A semicircle is fitted to the experimental data at low frequency, and the diameter of this semicircle is compared to the high-frequency intercept with the  $G'$ -axis (the plateau modulus). For purely exponential stress decay, the ratio of the intercept and semicircle diameter equals unity, and it decreases for increasingly non-exponential stress relaxation. This parameter is related to the ratio between the breaking time

## 5.2. Theoretical background

---

and the terminal relaxation time. Even for systems which are considered to be fast-breaking, deviations from the Maxwell model occur at high frequencies, which is attributed to other relaxation mechanisms such as breathing and Rouse modes which are important at short times. The Cates model predicts scaling exponents for the the concentration and chain length dependence of the zero-shear viscosity  $\eta_0$  and the longest or terminal relaxation time  $\tau_0$ . At longer times (lower frequencies) than  $\tau_0$ , the loss modulus dominates the viscoelastic response and the solution displays viscous behavior. At shorter times (higher frequencies), the storage modulus dominates and the solution behaves elastic.

For polymers in general,  $\eta_0$  and  $\tau_0$  are predicted to depend on  $\langle N \rangle$  and  $c$  according to power laws:

$$\eta_0 \sim \langle N \rangle^\alpha c^\beta \sim c^{(\alpha/2)+\beta} \quad (5.3)$$

$$\tau_0 \sim \langle N \rangle^\gamma c^\delta \sim c^{(\gamma/2)+\delta} \quad (5.4)$$

From a mean-field approach, it follows that  $\langle N \rangle \sim c^{0.5}$  (equation 5.1). Substitution of this relation allows for the concentration and chain length dependence exponents to be combined into a single concentration dependence as was done in the right hand side of equations 5.3 and 5.4. For supramolecular polymers, the fact that  $\langle N \rangle$  is a function of  $c$  implies that without taking special measures, the exponents  $\alpha$  and  $\beta$  and  $\gamma$  and  $\delta$  cannot be measured separately and only the overall exponents are experimentally accessible.

Under conditions where the mean-field assumption is not valid, slightly different exponents are predicted [5]. If Maxwell behavior occurs, the elastic plateau modulus  $G_0$  can be obtained from the simple relation

$$\eta_0 = G_0 \tau_0 \quad (5.5)$$

$G_0$  is the plateau in  $G'(\omega)$  at high frequency that would occur if breaking of chains is the predominant relaxation mechanism at all time scales. If the Maxwell model does not apply at high frequencies, the values for  $G_0$  and  $\eta_0$  obtained from a fit to the experimental data at lower frequencies by using equation 5.5 do generally not correspond to a true plateau of  $G'(\omega)$  at high frequency or a true zero-shear viscosity. In this case the values for  $G_0$  and  $\eta_0$  are those that would occur if the low-frequency Maxwell behavior would extend over all frequencies. In other words, by using equation 5.5 it is assumed that the high frequency part of the spectrum has no significant contribution to these parameters.

The exponents  $\alpha$  to  $\delta$  depend on the characteristic times for breaking of a chain ( $\tau_b$ ) and of a second relaxation mechanism which depends on chain flexibility and for which the symbol  $\tau_r$  will be used [23, 24]. For flexible chains, reptation is the principal stress relaxation mechanism, so the characteristic

times for breaking and *reptation* determine the viscoelastic behavior. The predicted values for the viscosity are  $\alpha = 1, \beta = 3$  for fast-breaking chains ( $\tau_r \gg \tau_b$ ) and  $\alpha = 3, \beta = 15/4$  for slow-breaking chains ( $\tau_r \ll \tau_b$ ). For rigid rods, the characteristic times for breaking and *rotation* (angular reorientation) of a chain are the relevant parameters. For fast-breaking rods, the scaling exponents are  $\alpha = 2/7, \beta = 11/7$ . In the case of slow-breaking chains, the result is  $\alpha = 6, \beta = 3$ . The scaling exponents for the relaxation time are  $\gamma = 1, \delta = 3/4$  for flexible fast-breaking chains and  $\gamma = 3, \delta = 3/2$  for slow-breaking ones. Finally, for fast-breaking rodlike chains the exponents are  $\gamma = 9/7, \delta = 4/7$  and the values  $\gamma = 7, \delta = 2$  are derived for slow-breaking rods. All these scaling exponents are summarized in table 5.1.

Table 5.1: Scaling exponents ( $\alpha, \beta, \gamma, \delta$ ) for the chain length and concentration dependence of the zero-shear viscosity and the terminal relaxation time.

|                | slow-breaking                     | fast-breaking   |
|----------------|-----------------------------------|---|
| flexible chain | $3, \frac{15}{4}, 3, \frac{3}{2}$ | $1, 3, 1, \frac{3}{4}$                                |
| rodlike chain  | $6, 3, 7, 2$                      | $\frac{2}{7}, \frac{11}{7}, \frac{9}{7}, \frac{4}{7}$ |

The predictions from the Cates model have been tested experimentally for many wormlike micellar systems [25–28]. In micellar systems, there are no bifunctional monomers and therefore no monofunctional chain stoppers. When  $\eta_0$  or  $G_0$  is measured as a function of monomer concentration without added chain stoppers, both  $c$  and  $\langle N \rangle$  change, and the scaling exponents found experimentally are the overall exponents  $(\alpha/2) + \beta$  and  $(\gamma/2) + \delta$  of equations 5.3 and 5.4. The same is true for reversible supramolecular polymers without chain stoppers [14, 29]. In experiments with added chain stoppers,  $c$  and  $\langle N \rangle$  can be varied independently and the individual exponents  $\alpha$  to  $\delta$  can be found.

### 5.2.3 Probe particle diffusion

From the mean square displacement of a microscopic particle in a solution, information about the viscoelastic properties of the solution on a small length scale can be obtained [30–32]. With dynamic light scattering, the mean square displacement  $\langle \Delta r^2(t) \rangle$  of probe particles immersed in polymer solutions can be measured [33]. The mean square displacement of a particle of radius  $R$  in a viscoelastic solution of entangled polymer chains with a mesh size  $\xi \ll R$  is determined by the viscous drag due to the solvent and by the viscoelastic forces due to the polymer matrix [14]. At very short times, the elastic force due to the polymer chains is negligible, the particle effectively only

## 5.2. Theoretical background

---

experiences the friction due to the solvent. This leads to diffusive behavior:  $\langle \Delta r^2(t) \rangle = 6D_s t$ , where  $D_s$  is the diffusion coefficient associated with the particle moving through the pure solvent, according to the Stokes-Einstein relation:

$$D_s = \frac{k_B T}{6\pi R \eta_{\text{solvent}}} \quad (5.6)$$

In principle, hydrodynamic interactions between the particles and polymer chains decrease the short-time particle diffusion coefficient compared to its value in pure solvent, but this effect appears to be very small for our system [14]. As the particle diffuses further, it is slowed down by the elastic forces from the entangled polymer. The elastic force is proportional with particle displacement (assuming a harmonic elastic potential). When the elastic energy becomes of the order of the kinetic energy of the particle ( $k_B T$ ), the particle is effectively trapped in an elastic cage. If the polymer matrix behaves Maxwellian, this entrapment leads to a plateau in  $\langle \Delta r^2(t) \rangle$ , which is denoted as  $6\Delta r_p^2$  and is related to  $R$  and the elastic plateau modulus  $G_0$  of the medium:

$$\Delta r_p^2 = \frac{k_B T}{6\pi R G_0} \quad (5.7)$$

At even longer times, the polymer network itself also fluctuates due to reptation of the chains, and in the case of reversible supramolecular polymers also due to breaking and recombination of bonds. At these timescales, the motion of the particle is coupled to that of the polymer network, and there is a second diffusive regime, given by:

$$\langle \Delta r^2(t) \rangle = 6(\Delta r_p^2 + D_l t) \quad (5.8)$$

where  $D_l$  is the diffusion coefficient associated with the particle in the polymer solution with its macroscopic viscosity:

$$D_l = \frac{k_B T}{6\pi R \eta_{\text{solution}}} \quad (5.9)$$

Note that equation 5.8 can be used to obtain both the long-time diffusion coefficient (from the slope) and the plateau displacement (from the intercept). If equation 5.7 is subsequently used to calculate  $G_0$ , the microscopic plateau modulus is thus obtained from an extrapolation to  $t = 0$  of the experimental data at long times. This procedure is consistent with the use of equation 5.5 to calculate  $G_0$  from the macroscopic values of  $\eta_0$  and  $\tau_0$ , which also involves an extrapolation from long times (low frequencies) to short ones (high frequencies), as explained in section 5.2.2.

Equation 5.8 was derived from an analysis of particle motion in a Maxwellian viscoelastic fluid which ignored the solvent friction, and tested experimentally

[34]. An expression for  $\langle \Delta r^2(t) \rangle$ , valid for the whole time range was derived by including the solvent friction in the equation [14]:

$$\langle \Delta r^2(t) \rangle = 6\Delta r_p^2 \left[ 1 - \exp\left(-\frac{D_s t}{\Delta r_p^2}\right) \right] + 6D_1 t \quad (5.10)$$

It was demonstrated that not only  $\eta_0$  and  $G_0$  can be derived from the motion of probe particles through a viscoelastic medium, but the whole rheological spectrum can be found [33, 35]. However, the goal of the probe particle diffusion experiments in the present work is to compare the results with those previously obtained without chain stoppers [14] and with the Cates model. For those purposes, an analysis of the full spectrum would not lead to improved results, since only parameters are used which are accessible from the behavior at frequencies for which the Maxwell model still applies. Therefore we use equations 5.6-5.10, based on the Maxwell model, in our analysis.

It is often relevant to know how particles experience their microscopic environment, as well as to know the macroscopic solution properties. The viscoelastic parameters obtained by probing the motion of microscopic particles are not always equal to the macroscopic properties as measured by rheometry. In order for the particle to experience the macroscopic rheological properties of the sample, the mesh size  $\xi$  of the polymer network must be much smaller than the particle radius  $R$  so the solution can be regarded as a continuum. If this is not the case, the particle can slip through the meshes, leading to larger displacements and a lower microscopic viscosity compared to the macroscopic value. It has indeed been observed that the difference between microscopic and macroscopic viscosity of EHUT solutions decrease upon increasing the particle size or decreasing the mesh size (by increasing the concentration) [14]. For the elastic plateau modulus, it was found that the difference decreases with increasing particle size, but *increases* with increasing EHUT concentration. It was proposed that for the microscopic elastic modulus to equal the macroscopic value not only  $R \gg \xi$  should hold, but also  $R \gg L$ , where  $L$  is the length of the polymer (for more flexible chains,  $R \gg l_p$  is the appropriate condition, where  $l_p$  is the persistence length of the chain) [14, 36]. Note that with chain stoppers,  $L$  can be varied independent of  $c$  and  $\xi$ , so this hypothesis may be tested systematically by using supramolecular polymer solutions with chain stoppers. For actin filaments, it was indeed found experimentally that shorter chains give smaller differences [37].

## 5.3 Experimental

### 5.3.1 Materials

The synthesis of bifunctional monomer EHUT [11] and chain stopper DBUT [19] are published elsewhere. Cyclohexane (>99%) was obtained from Aldrich and used as received. Solutions were prepared by stirring at a slightly elevated temperature.

### 5.3.2 Dynamic light scattering by probe particles

Dynamic light scattering measurements were performed with an argon ion laser ( $\lambda = 514.5$  nm) and an optical fiber detector at  $90^\circ$  scattering angle, so the scattering vector  $q$  equals  $2.5 \cdot 10^7 \text{ m}^{-1}$ . In previous experiments, it was checked that varying the detection angle did not change the results [14]. The intensity correlation function was calculated using an ALV5000 digital correlator.

Monodisperse silica spheres with a radius of 250 nm (Monospher 250, Merck) were used as probe particles. The particles were stearylated by the method of Van Helden [38]. In cyclohexane, these particles exhibit hard-sphere interactions and the polymers do not adsorb to the surface. For the particle size and scattering vector used ( $qR = 6.2$ ), the form factor  $P(qR)$  of the silica particles is far from its minima, which occur at  $qR \approx 4.5$  and  $qR \approx 7.7$ .

EHUT solutions in cyclohexane with concentrations between 1 and 10 g/l were prepared, with stopper fractions  $x$  between 0 and 0.052. Approximately 10  $\mu\text{l}$  of a concentrated suspension of probe particles in cyclohexane was added to 2.5 ml samples. It was checked that changing the particle concentration in the sample did not affect the results and that scattering by the supramolecular polymers themselves was negligible compared to the contribution from the probe particles.

After measuring the intensity autocorrelation function  $g_2(\tau)$  for a sufficiently long time (up to one hour for the highest concentrations),  $g_2(\tau)$  was converted into the field autocorrelation function  $g_1(\tau)$  and subsequently  $\langle \Delta r^2(t) \rangle$  was calculated from  $g_1(\tau)$  by applying the relations

$$g_2(\tau) = 1 + A [g_1(\tau)]^2 \quad (5.11)$$

$$g_1(\tau) = \exp\left(-\frac{q^2}{6} \langle \Delta r^2(t) \rangle\right) \quad (5.12)$$

where  $A$  is an instrument parameter of order unity.

The parameters  $D_l$  and  $\Delta r_p^2$  were determined by fitting of  $\langle \Delta r^2(t) \rangle$  to equation 5.8, using a linear plot of the experimental data. A straight line was

obtained with slope  $6D_l$  and ordinate intercept  $6\Delta r_p^2$ . The microscopic viscosity and elastic plateau modulus were subsequently calculated using equation 5.7 and 5.9.

### 5.3.3 Rheometry

A Paar Physica MCR300 rheometer, equipped with a 75 mm cone-plate geometry was used to perform dynamic shear measurements on the same solutions as used for dynamic light scattering. To minimize evaporation of cyclohexane during the measurement, a solvent trap was used. At a constant strain amplitude of 10% and at 25 °C, the angular frequency  $\omega$  was varied from 0.01 to 50 rad/s and the storage modulus  $G'$  and loss modulus  $G''$  of the solutions were measured. By fitting of the curves of  $G'(\omega)$  and  $G''(\omega)$  in the low-frequency range to the Maxwell model with  $\eta_0$  and  $\tau_0$  as the adjustable parameters, values for these parameters were obtained. The zero-shear viscosity was also determined independently by measuring the shear stress at a number of shear rates between 0.01 and 0.1 s<sup>-1</sup> in a rotational shear experiment. There is a plateau in the viscosity at low shear rates, which equals the zero-shear viscosity.

## 5.4 Results and discussion

For the system of bifunctional monomer EHUT and chain stopper DBUT in cyclohexane, it is reasonable to assume that 2 stoppers are needed to break a chain ( $n = 2$ , see equation 5.2), based on the proposed chain structure with a cross section consisting of two monomers [12]. The association constant is estimated to be of order 10<sup>9</sup> M<sup>-1</sup>. This value was estimated from the overlap concentration as measured by viscosimetry [14] and the effective monomer length derived from SANS measurements [12]. It was shown previously that the association of EHUT is in fact not isodesmic, but cooperative [13, 39]. Experimental results from IR spectroscopy and isothermal titration calorimetry are described very well by a model which includes one association constant for the formation of dimers ( $K_2$ ) and a second one for the formation of longer oligomers and polymers ( $K_n$ ). However, if the average chain length is high and the number of monomers is relatively small, the association can be described by a single effective association constant  $K = K_n^2/K_2$ . Under the conditions used in the present paper, the average chain length is always  $\gg 1$ , so the use of the effective isodesmic association constant  $K$  is justified. Using the estimated value of  $K$ ,  $Kc \gg 1$  for all concentrations used and the approximation in equation 5.1 may be applied. For the lowest EHUT concentration used in this paper (1 g/l = 2.3 mM),  $\langle N(0) \rangle \approx 3000$  (equation 5.1), and the lowest stopper fraction used is 0.006. Therefore we may also apply the approximation in

equation 5.2 and assume that for all concentrations and stopper fractions used,  $\langle N \rangle \sim 1/x$ .

In section 5.4.1, the results from the macroscopic rheometry experiments are addressed. The zero-shear viscosity scaling results will be discussed in section 5.4.2. For a discussion of the scaling behavior of the relaxation time see section 5.4.3. Section 5.5 contains a discussion about the difference between the macroscopic results obtained from rheometry and the microscopic parameters obtained from probe particle diffusion.

### 5.4.1 Macroscopic viscoelasticity

In figure 5.2, a typical result for the frequency dependence of  $G'$  and  $G''$  is shown. At low frequencies, the loss modulus dominates, and the system displays viscous behavior. At higher frequencies, the storage modulus becomes more important, and eventually it dominates. At low frequencies, the agreement of the experimental data with the Maxwell model is good, but they start to deviate around the frequency where  $G'$  equals  $G''$ . This frequency is the inverse of the terminal relaxation time  $\tau_0$ . Since the Maxwell model describes the data well until this frequency,  $\tau_0$  can be determined accurately from the fit. The fitted values of  $\eta_0$  were found to be in perfect agreement with the values obtained from the independent stress-strain measurements. This confirms the assumption that the zero-shear viscosity is not significantly affected by contributions from the high frequency part of the spectrum (equation 5.5).

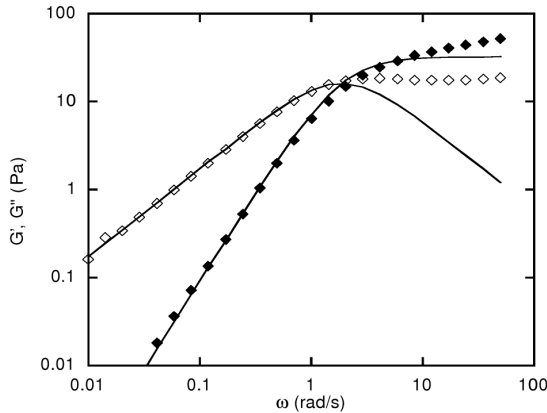


Figure 5.2: Storage modulus  $G'$  ( $\blacklozenge$ ) and loss modulus  $G''$  ( $\diamond$ ) of a 10 g/l EHUT solution with  $x = 0.015$  as a function of the angular frequency  $\omega$ . Lines correspond to the Maxwell model with  $\eta_0 = 17$  Pa s and  $\tau_0 = 0.5$  s.

The deviation from Maxwellian dynamics occurs at relatively low frequency compared to several fast-breaking wormlike micellar systems, which often remain Maxwellian at frequencies well beyond  $1/\tau_0$  [5, 24, 27]. This indicates that  $\tau_b$  is not much smaller than  $\tau_r$ , and that the system can therefore not be considered to be in the fast-breaking limit. After passing a weak maximum around  $\omega = 1/\tau_0$ , the experimental data show an equally weak minimum in  $G''$  which is often attributed to the onset of Rouse modes and other short-time relaxation mechanisms.

In order to try and obtain some information about the characteristic breaking time of the EHUT chains, the data were also plotted in a Cole-Cole representation (figure 5.3), following the method described in section 5.2.2 [22]. At low frequencies, the semicircle nicely fits the experimental data, but even before the top of the semicircle, deviations start to become significant. The experimental data display a minimum in  $G''$ , after which the curve bends upwards again, usually a sign that relaxation at high frequencies is dominated by Rouse modes. A clear minimum was not always present, but in none of the samples a strong decrease in  $G''$  at high frequencies was observed, making it impossible to extrapolate the experimental data to the  $G'$ -axis. Thus, this method cannot be applied here and we can only conclude qualitatively that the system is not fast-breaking, and that the characteristic breaking and reptation times are of the same order of magnitude. Looking at figures 5.2 and 5.3, it is clear that the deviations from Maxwell behavior are mainly due to the loss modulus, which deviates strongly both qualitatively and quantitatively at frequencies beyond  $1/\tau_0$ . The Maxwellian storage modulus, on the other hand, fits the experimental data until higher frequencies, and it deviates much less strongly. The value of  $G_0$  from the Maxwell fit can be regarded as a lower limit for the true plateau modulus.

It is probably possible to fit the experimental data over the whole frequency range by using a more complex relaxation function. However, the aim of the present paper is to obtain the parameters  $\eta_0$  and  $\tau_0$ , to determine their scaling behavior with  $\langle N \rangle$  and  $c$  and to compare the results with theoretical values predicted by the Cates model. These parameters are obtained accurately from the frequency range which is fitted well by the Maxwell model. Therefore, we do not attempt to fit the whole rheological spectrum, since this would not lead to different results.

### 5.4.2 Scaling of the zero-shear viscosity

In experiments with EHUT in cyclohexane without chain stoppers, it was found that  $\eta_0 \sim c^{3.3}$  [14]. The exponent 3.3 is the combined exponent  $(\alpha/2) + \beta$  from equation 5.3. The solid symbols in figure 5.4 show the zero-shear viscosity of solutions of equal overall monomer concentration with varying amounts of

## 5.4. Results and discussion

---

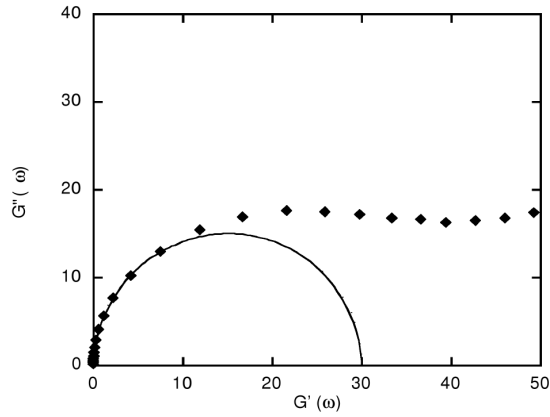


Figure 5.3: Cole-Cole plot of a 10 g/l EHUT solution with  $x = 0.015$ . The semicircle corresponds to the Maxwell model with  $\eta_0 = 17$  Pa s and  $\tau_0 = 0.5$  s.

chain stoppers. On the horizontal axis,  $1/x$  is plotted, which is proportional to  $\langle N \rangle$  (equation 5.2). The results can be fitted with a power law with exponent 2.7, which equals the chain length dependence exponent  $\alpha$ .

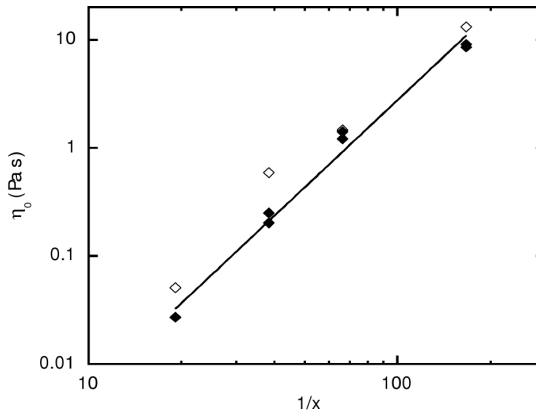


Figure 5.4: Zero-shear viscosity of 3 g/l EHUT solutions in cyclohexane as a function of the reciprocal stopper fraction. The line corresponds to  $\eta_0 = 1.2 \cdot 10^{-5}(1/x)^{2.7}$ . Results for macroscopic rheometry ( $\blacklozenge$ ) and probe particle diffusion measurements ( $\diamond$ ) are plotted.

The concentration dependence exponent  $\beta$  can be found by varying  $c$  and keeping  $x$  constant. The solution volumes were small because of the limited amount of material at our disposal, and the stoppers were added to each EHUT solution independently. The results are shown in figure 5.5 (solid symbols). The data in figure 5.5 are more scattered than in figure 5.4, which is probably due to limited precision of  $x$  resulting from the small amounts of stoppers which were added. It is hard to quantitatively predict the error in the viscosity arising from an error in the amount of stopper, but an estimate can be given. The maximum error in  $1/x$  is of the order of 10-15%, and given the  $\langle N \rangle^{2.7}$  scaling of the viscosity shown in figure 5.4, this could lead to an error in the viscosity of up to approximately 50%. The uncertainty in  $x$  can therefore be considered to be the major source for the scatter in figure 5.5. The data were fitted with a power law, this time with exponent 1.8, which equals  $\beta$ .

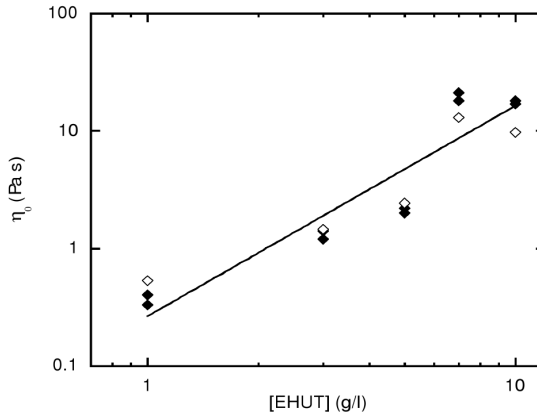


Figure 5.5: Zero-shear viscosity as a function of EHUT concentration for solutions with  $x = 0.015$  in cyclohexane. The line corresponds to  $\eta_0 = 0.26c^{1.8}$ . Results for macroscopic rheometry (◆) and probe particle diffusion measurements (◇) are plotted.

From the power law fits in figures 5.4 and 5.5, it follows that

$$\eta_0 = A \left( \frac{1}{x} \right)^{2.7} c^{1.8}, \quad A = 2.5 \cdot 10^{-6} \text{ Pa s (l/g)}^{1.8} \quad (5.13)$$

The proportionality constant  $A$  can be calculated from both fits by substitution in the left-hand side of equation 5.13 of the (fixed) values of  $c$  (3 g/l) and  $x$  (0.015), respectively. For the fit of the  $1/x$ -dependence,  $A$  is calculated to be  $1.2 \cdot 10^{-5} / 3^{1.8} = 2 \cdot 10^{-6} \text{ Pa s (l/g)}^{1.8}$ . In a similar way, the fit of the  $c$ -dependence

## 5.4. Results and discussion

---

gives  $A = 3 \cdot 10^{-6} \text{ Pa s (l/g)}^{1.8}$ . Both values agree within the experimental error. The average value of  $A$  is given in the right-hand side of equation 5.13. This relation is useful for future experiments, since it can be used to prepare solutions with a predetermined viscosity.

In order to compare our results with the predictions from the Cates model, the relation  $\langle N \rangle \approx n/x \sim 1/x$  (equation 5.2) is substituted in equation 5.13:

$$\eta_0 \sim \langle N \rangle^{2.7} c^{1.8} \quad (5.14)$$

The proportionality constant can no longer be calculated, since this requires the value of  $n$ , which is not known. For these experimental exponents, the overall concentration dependence exponent  $(\alpha/2) + \beta$ , which was derived in equation 5.3 assuming a mean-field dependence between  $\langle N \rangle$  and  $c$ , equals 3.2 and agrees within the experimental error with the value of 3.3 obtained previously without chain stoppers. This confirms the validity of the assumption of mean field scaling for the concentration dependence of the average degree of polymerisation ( $\langle N \rangle \sim c^{0.5}$ , equation 5.1). Values of the overall exponent around 3.5 are commonly found for flexible wormlike micellar systems [5, 26]. For EHUT, the exponent 3.3 was also interpreted as being close to the behavior of flexible chains in the fast-breaking limit ( $\alpha = 1$ ,  $\beta = 3$ , see table 5.1), the difference resulting from semiflexibility of the chains [14]. From the present results, a somewhat different interpretation arises. The exponents  $\alpha = 2.7$  and  $\beta = 1.8$  may be compared to the limiting cases of chain flexibility and breaking time shown in table 5.1. The experimental exponents are between the limits for flexible chains and rigid rods, and also between the limits for fast and slow breaking. This indicates that the chains are semiflexible and that the breaking and reptation times are of the same order of magnitude. The semiflexibility of the chains was confirmed by neutron [12] and light scattering [14], from which the persistence length was estimated to be at least 100 nm. The scaling exponents also confirm the suggestion, based on the relatively early departure from Maxwellian dynamics in the frequency dependence of the stress relaxation (figure 5.2), that the chains are not fast-breaking.

### 5.4.3 Scaling of the terminal relaxation time

Without chain stoppers, the zero-shear viscosity of EHUT solutions in cyclohexane was found to be proportional to  $c^{3.3}$ , and for the elastic plateau modulus, obtained from a fit to the Maxwell model in the low-frequency range, a scaling exponent of 1.8 was found [14]. Using equation 5.5, the scaling exponent for concentration dependence of the terminal relaxation time without chain stoppers equals  $3.3 - 1.8 = 1.5$ . Again, this exponent combines the chain length and concentration dependence and thus equals  $(\gamma/2) + \delta$  from equation 5.4. The results of rheometry experiments where  $1/x$  was varied at a constant  $c$

in order to find the chain length scaling exponent  $\gamma$  are shown in figure 5.6. The data are fit by a power law with exponent  $\gamma = 2.3$ . This value is consistent with EHUT chains which are semiflexible and for which breaking and reptation/reorientation occur on the same time scale, see table 5.1.

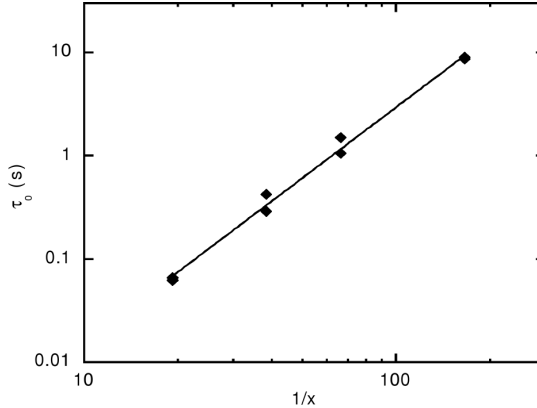


Figure 5.6: Terminal relaxation time  $\tau_0$  of 3 g/l EHUT solutions in cyclohexane as a function the reciprocal stopper fraction. The line corresponds to  $\tau_0 = 8 \cdot 10^{-5}(1/x)^{2.3}$ .

When the EHUT concentration was varied at a constant value of  $x$ , the results shown in figure 5.7 were obtained. Surprisingly, there seems to be no systematic change of the relaxation time with concentration, or at least it is undetectable due to the scatter in the data. As discussed in section 5.4.2, the scatter probably originates from variations in  $x$ . This behavior is very unexpected, since for all limiting cases for which the theoretical scaling exponents are given in table 5.1, a positive value of  $\delta$  is predicted, ranging from  $4/7$  for fast-breaking rods to 2 for slow-breaking rods, with the values for flexible chains lying between these limits. This result is discussed in more detail below.

Summarizing, the dependence of the terminal relaxation time on concentration and stopper fraction is found to be

$$\tau_0 = B \left( \frac{1}{x} \right)^{2.3} c^0, \quad B = 9 \cdot 10^{-5} \text{ s} \quad (5.15)$$

where the proportionality constant  $B$  was again calculated from substitution of the fixed values of  $c$  and  $x$ , as described in section 5.4.2 and the value of  $9 \cdot 10^{-5}$  is the average of the results obtained from the fits in figures 5.6 and

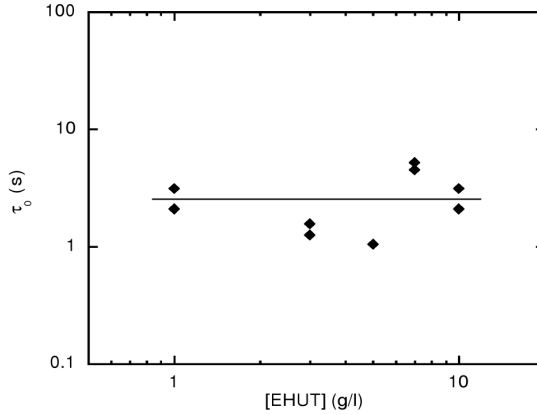


Figure 5.7: Terminal relaxation time as a function of EHUT concentration for solutions with  $x = 0.015$ . The line corresponds to  $\tau_0 = 2.5c^0$ .

5.7. Also in this case, the separate values agree within the experimental error. When the scaling of  $\langle N \rangle$  with  $x$  (equation 5.2) is substituted in equation 5.15, the following result is obtained:

$$\tau_0 \sim \langle N \rangle^{2.3} c^0 \quad (5.16)$$

When the experimentally determined exponents  $\gamma = 2.3$  and  $\delta = 0$  are combined into an overall concentration dependence exponent (see equation 5.4), a value of  $\gamma/2 + \delta = 1.2$  is found. This should be compared to the value of 1.5 as obtained for the concentration dependence without chain stoppers. The fact that two experimentally determined quantities are used to obtain the exponent makes the value of 1.5 somewhat less accurate. As with the zero-shear viscosity, we therefore conclude that both values are in reasonable agreement. Furthermore, it can be concluded that in the concentration range studied, the relaxation time is only determined by the chain length, and that the monomer concentration has a negligible effect.

From the foregoing, it is clear that the dependence of the terminal relaxation time on concentration cannot be explained straightforwardly and that more experiments are needed to gain a better understanding of the underlying mechanisms. The presence of chain stoppers may not only reduce the average chain length, but also have an additional influence. It is reasonable to assume that multiple stopper molecules are needed to create a full chain scission due to the assumed bimolecular cross-section of the EHUT chains, so the association of a lower number of stoppers may cause a defect in a chain, but may not completely stop it from growing further. Furthermore, DBUT is not strictly

a monofunctional monomer, since it still has two hydrogen bond donors in the protons of the secondary amines (see figure 5.1). Therefore, chains may grow further even after the association of the theoretical maximum number of stoppers, also causing a chain defect. These defects may somehow cause the unexpected behavior, for example by affecting the chain flexibility. The possible effect of chain defects on viscoelastic behavior was also proposed in the interpretation of experimental data for a different supramolecular polymer system [29]. Another possible explanation is that the chain stoppers induce the formation of crosslinks, which would affect the rheology.

## 5.5 Microscopic versus macroscopic viscoelasticity

A typical result from the probe particle diffusion experiments is shown in figure 5.8a. In pure cyclohexane,  $\langle \Delta r^2 \rangle$  is proportional to  $t$  for the whole time range, indicating purely diffusive behavior with a diffusion coefficient  $D_s$ . This short-time diffusion coefficient corresponds within the experimental error to the value calculated from the known solvent viscosity and the particle radius with equation 5.6. For viscoelastic EHUT solutions, there are indeed two diffusive regimes, one at short times, corresponding to a low (solvent) viscosity and another at long times, corresponding to a high (solution) viscosity. Between these diffusive regimes, the slope of the curve is smaller, but there is no true plateau in the mean square displacement. The linear representation shown in figure 5.8b is used to fit a straight line to the experimental data at long correlation times. The slope of the fitted line is  $6D_l$ , and the ordinate intercept is equal to  $6\Delta r_p^2$ , according to equation 5.8. The result of equation 5.10 with the parameters obtained in this way is also shown in figure 5.8b (solid line). These values were used to calculate the microscopic viscoelastic parameters  $\eta_0$  and  $G_0$  with equations 5.7 and 5.9, respectively.

The dashed line in figure 5.8a is the result of equation 5.10 with  $\Delta r_p^2$  and  $D_l$  calculated from the macroscopic viscoelastic parameters with equations 5.7 and 5.9, respectively. Both lines agree with the experimental data in the diffusive regimes, but fail at intermediate times, where they both show a true plateau in  $\langle \Delta r^2(t) \rangle$ . The lack of a plateau in the experimental data was also observed in previous experiments with EHUT [14] and is not surprising, since also the macroscopic storage modulus does not have a high-frequency plateau, as shown in figure 5.2. In the derivation of equation 5.10, it is assumed that the polymer network is Maxwellian at all time scales. This assumption is not valid at short times (high frequencies), as can be seen from figures 5.2 and 5.3. The time range in which the plateau is predicted corresponds to frequencies where the Maxwell model is no longer valid and other relaxation mechanisms such as Rouse or breathing modes become important. This non-Maxwellian stress

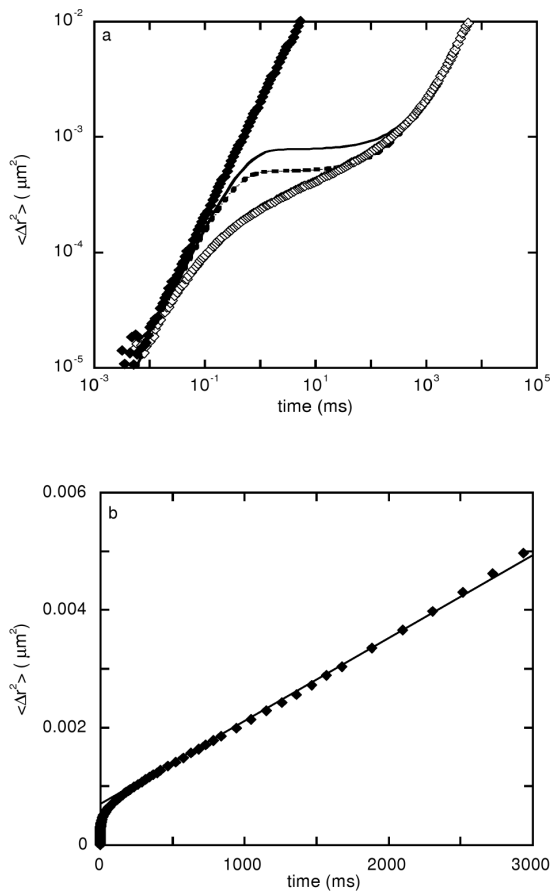


Figure 5.8: a: Mean square displacement of a 250 nm radius probe particle in a 5 g/l EHUT solution in cyclohexane with  $x = 0.015$  ( $\diamond$ ) and in pure cyclohexane ( $\blacklozenge$ ). The solid line is a fit to equation 5.10, the dotted line is calculated using the macroscopic viscoelastic parameters. b: EHUT solution data on a linear scale.

relaxation affects the particle motion, and equation 5.10 no longer accurately describes the particle motion. The value of  $G_0$  found in this way may be compared to the value from the Maxwell fit to the macroscopic rheological data, since both values are obtained from an extrapolation of the experimental data at long times (low frequencies), as explained in sections 5.2.2 and 5.2.3.

As expected for the EHUT concentrations and particle size used, the microscopic viscosities calculated from the probe particle motion (shown in figures 5.4 and 5.5 by the open symbols) are approximately equal to the macroscopic viscosities both at constant  $c$  and constant  $\langle N \rangle$ . Agreement between the microscopic and macroscopic viscosity for 250 nm particles was also found in EHUT solutions without chain stoppers for  $c \gtrsim 1$  g/l, which was supported by light scattering experiments, from which it was found that the mesh size for a 1 g/l EHUT solution (the lowest concentration used for rheometry, corresponding to the largest mesh size) is approximately 100 nm, which is indeed still smaller than the particle radius (250 nm), albeit not very much [14]. The present results are further evidence that the ratio of mesh size and particle size determines the friction experienced by a probe particle and therefore also its thermal motion, and that the chain length itself is not relevant.

In the experiments without chain stoppers, the values of  $G_0$  derived from probe particle diffusion experiments were systematically much lower than those obtained from macroscopic rheometry [14]. Even at high concentrations (small correlation lengths), where the microscopic and macroscopic viscosity were the same, the difference in  $G_0$  did not decrease. On the contrary, both values were approximately equal at low concentrations and the difference only increased with increasing concentration. Furthermore, smaller particles gave larger differences. It was suggested [14, 36] and observed experimentally [37] that it is not only the ratio between  $\xi$  and  $R$  which determines the difference between the microscopic and macroscopic elastic plateau modulus. Additionally, the ratio of the length of the chains (or in the case of more flexible chains the persistence length) and the particle radius also determines the microscopic viscoelastic behavior. This would explain the increasing difference with increasing concentration observed without chain stoppers and the effect of particle size. Our present results are further evidence that indeed both the conditions  $R \ll \xi$  and  $R \ll \langle L \rangle$  determine the difference between the macroscopic and microscopic viscoelasticity. In the experiments with shortened chains (figure 5.9a), it is indeed observed that the difference between microscopic and macroscopic values of  $G_0$  is smaller than in experiments without chain stoppers (figure 5.9b).

The microscopic values are in most cases still somewhat lower than the macroscopic ones. Furthermore, the difference between the microscopic and macroscopic values still seems to increase slightly with increasing concentration, although the data are not conclusive due to the small number of points

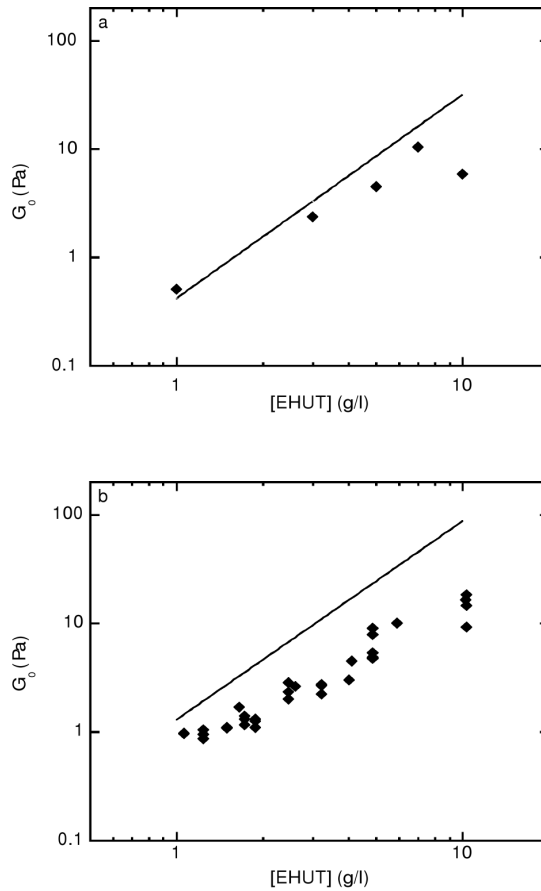


Figure 5.9: a: Microscopic elastic plateau modulus  $G_0$  as a function of EHUT concentration for solutions in cyclohexane with  $x = 0.015$ . The line corresponds to the power law fit to the macroscopic data. b: Same for solutions without chain stoppers. Data were taken from [14], with permission.

and the small concentration range. The presence of chain stoppers reduces the chain length, but it is very well possible that even in the presence of stoppers the average chain length is not much smaller than the particle radius, especially since it is not known exactly how many chain stoppers have to be associated to create a totally non-functional ('dead') chain end. From the proposed chain structure, it is reasonable to assume that at least 2 stopper molecules are needed, so at a stopper fraction of 0.015, there would be at least  $2/0.015 \approx 135$  monomers in a chain (equation 5.2), resulting in a lower limit for the average chain length of 24 nm, using the effective monomer length of 0.18 nm from SANS measurements [12], one order of magnitude smaller than the particle radius of 250 nm. However, given the results presented in this paper, it is likely that the addition of DBUT to EHUT solutions causes more effects than just shortening of the chains, and the average chain length is therefore probably larger than this lower limit and this may result in the observed differences between microscopic and macroscopic viscoelastic parameters.

## 5.6 Concluding remarks

The rheology of reversible supramolecular polymer solutions depends strongly on the average degree of polymerisation and the overall monomer concentration. By using chain stoppers, the chain length and overall monomer concentration could be varied independently and the effect of both parameters on rheology was studied using bifunctional monomer EHUT and chain stopper DBUT as a model system.

The linear viscoelasticity at low frequencies was analyzed in terms of the Maxwell model and characterized by the zero-shear viscosity and the terminal relaxation time. The dependence of the zero-shear viscosity on monomer concentration ( $\eta_0 \sim c^{1.8}$ ) and chain length ( $\eta_0 \sim \langle N \rangle^{2.7}$ ) were in agreement with experiments without chain stoppers, and offered a more accurate interpretation of the data. The scaling exponents indicate that the chains are semiflexible, and that the time scales on which the chains break and reptate/reorient are of the same order of magnitude. The terminal relaxation time depends strongly on chain length ( $\tau_0 \sim \langle N \rangle^{2.3}$ ), but there is no significant concentration dependence, which is not predicted by theory and remains to be explained. The results are consistent with those obtained without chain stoppers.

The motion of probe particles through networks of reversible supramolecular polymers was studied by dynamic light scattering. From this, information about the viscoelasticity of the solutions on a microscopic level was obtained. In agreement with previous results, the microscopic viscosity is equal to its macroscopic value if the mesh size of the polymer network is much smaller than the particle radius. For the elastic plateau modulus, the difference be-

tween microscopic and macroscopic values is not only determined by the mesh size and the particle radius, but also by the length of the polymer chains. Shorter chains show better agreement between microscopic and macroscopic values.

## References

- [1] J.-M. Lehn. *Supramolecular Chemistry: Concepts and Perspectives*. VCH, Weinheim.
- [2] A. Ciferri, editor. *Supramolecular Polymers*. Marcel Dekker, New York.
- [3] L. Brunsveld, B.J.B. Folmer, Meijer E.W., and R.P. Sijbesma. *Chem. Rev.*, 101: 4071, 2001.
- [4] M.E. Cates. *Macromolecules*, 20: 2289, 1987.
- [5] M.E. Cates and S.J. Candau. *J. Phys.: Condens. Matter*, 2: 6869, 1990.
- [6] D.C. Sherrington and K.A. Taskinen. *Chem. Soc. Rev.*, 30: 83, 2001.
- [7] R.P. Sijbesma, F.H. Beijer, L. Brunsveld, B.J.B. Folmer, J.H.K.K. Hirschberg, R.F.M. Lange, J.K.L. Lowe, and E.W. Meijer. *Science*, 278: 1601, 1997.
- [8] R.P. Sijbesma and E.W. Meijer. *Chem. Comm.*, 2003: 5.
- [9] V. Berl, M. Schmutz, M.J. Krische, G. Khoury, and J.-M. Lehn. *Chem. Eur. J.*, 8: 1227, 2002.
- [10] F. Lortie, S. Boileau, and L. Bouteiller. *Chem. Eur. J.*, 9: 3008, 2003.
- [11] S. Boileau, L. Bouteiller, F. Lauprêtre, and F. Lortie. *New J. Chem.*, 24: 845, 2000.
- [12] F. Lortie, S. Boileau, C. Chassenieux, B. Demé, G. Ducouret, M. Jalabert, F. Lauprêtre, and P. Terech. *Langmuir*, 18: 7218, 2002.
- [13] V. Simic, L. Bouteiller, and M. Jalabert. *J. Am. Chem. Soc.*, 125: 13148, 2003.
- [14] J. van der Gucht, N.A.M. Besseling, W. Knoben, L. Bouteiller, and M.A. Cohen Stuart. *Phys. Rev. E*, 67: 051106, 2003.
- [15] M. Doi and S.F. Edwards. *The Theory of Polymer Dynamics*. Clarendon Press, Oxford.
- [16] P.G. de Gennes. *Scaling Concepts in Polymer Physics*. Cornell University Press, Ithaca, New York.

- [17] R. Granek and M.E. Cates. *J. Chem. Phys.*, 96: 4758, 1992.
- [18] F. Lortie. *PhD Thesis, Université Paris Val de Marne, France*, 2001.
- [19] F. Lortie, S. Boileau, C. Chassenieux, and F. Lauprêtre. *Macromolecules*, 38: 5283–5287, 2005.
- [20] P.J. Flory. *J. Am. Chem. Soc.*, 78: 1877, 1936.
- [21] P.J. Flory. *Principles of Polymer Chemistry*. Cornell University Press, Ithaca, New York.
- [22] M.S. Turner and M.E. Cates. *Langmuir*, 7: 1590, 1991.
- [23] M.E. Cates, C.M. Marques, and J.-P. Bouchaud. *J. Chem. Phys.*, 94: 8529, 1991.
- [24] F. Kern, F. Lequeux, R. Zana, and S.J. Candau. *Langmuir*, 10: 1714, 1994.
- [25] F. Lequeux. *Curr. Opin. Coll. In.*, 1: 341, 1996.
- [26] L.J. Magid. *J. Phys. Chem. B*, 102: 4064, 1998.
- [27] S.J. Candau and R. Oda. *Colloids Surf., A*, 183: 5, 2001.
- [28] L.M. Walker. *Curr. Opin. Coll. In.*, 6: 451, 2001.
- [29] T. Shikata, D. Ogata, and K. Hanabusa. *J. Phys. Chem. B*, 108: 508, 2004.
- [30] T. Gisler and D.A. Weitz. *Curr. Opin. Coll. In.*, 3: 586, 1998.
- [31] F.C. Mackintosh and C.F. Schmidt. *Curr. Opin. Coll. In.*, 4: 300, 1999.
- [32] A. Mukhopadhyay and S. Granick. *Curr. Opin. Coll. In.*, 6: 423, 2001.
- [33] T.G. Mason and D.A. Weitz. *Phys. Rev. Lett.*, 74: 1250, 1995.
- [34] J.H. Van Zanten and K.P. Rufener. *Phys. Rev. E*, 62: 5389, 2000.
- [35] F. Gittes, B. Schnurr, P.D. Olmsted, F.C. Mackintosh, and C.F. Schmidt. *Phys. Rev. Lett.*, 79: 3286, 1997.
- [36] A.C. Maggs. *Phys. Rev. E*, 57: 2091, 1998.
- [37] F.G. Schmidt, B. Hinner, and E. Sackmann. *Phys. Rev. E*, 61: 5646, 2000.
- [38] A.K. van Helden, J.W. Jansen, and A. Vrij. *J. Colloid Interface Sci.*, 81: 354, 1981.
- [39] A. Arnaud and L. Bouteiller. *Langmuir*, 20: 6858, 2004.



# 6

## Direct measurement of depletion and hydrodynamic forces in solutions of a reversible supramolecular polymer

### Abstract

In this paper, the investigation of surface forces in semi-dilute solutions of a non-adsorbing hydrogen-bonded reversible supramolecular polymer is described. Colloidal Probe Atomic Force Microscopy was used for direct measurement of depletion forces. Hydrodynamic drag on the AFM cantilever with the colloidal probe was measured both far away from and close to the planar substrate surface. The results indicate that the presence of the depletion layer causes slip at the surfaces with a large apparent slip length. Our analysis explains how the presence of slip enables the measurement of (relatively weak) depletion forces in solutions with a high viscosity by significantly reducing the hydrodynamic forces. The range and magnitude of the measured depletion forces are qualitatively in agreement with previous experiments and theoretical predictions. Due to the relatively large experimental error, no quantitative conclusions can be drawn. Depletion-induced phase separation of suspensions of stearylated silica particles was also observed. Phase separation becomes more pronounced with increasing polymer concentration.

## 6.1 Introduction

The presence of non-adsorbing polymers in a dispersion of colloidal particles causes an attractive interaction between the particles, which may lead to flocculation or phase separation of the dispersion [1, 2]. This so-called depletion interaction is of practical importance in many systems such as dairy products [3], ink and paint formulations [4] and sickle hemoglobin fibers [5].

In this paper, we focus on depletion forces induced by *supramolecular polymers*. These are chains of monomers, held together by non-covalent interactions such as hydrogen bonding or metal-ligand complexation [6–8]. Often, the bonds between the monomers break and recombine on experimental time scales, and for these systems the term *reversible* supramolecular polymers is used. In many respects, supramolecular polymers are similar to classical covalent polymers. For example, at sufficiently high concentrations they form viscous solutions or gels due to entanglement of chains, and it has been shown that their material properties can be comparable to those of ‘normal’ covalent polymers [9]. However, the fact that the bonds between monomers are non-covalent also gives supramolecular polymers special and exciting properties compared to their covalent counterparts. For example, the chain length (distribution) is not fixed, but depends on monomer concentration, temperature and other parameters. Furthermore, due to the continuous breaking and recombination of reversible supramolecular polymer chains, these systems reach thermodynamic equilibrium more easily than covalent polymers [9, 10].

In addition to their bulk and solution properties, supramolecular polymers are also expected to display some special features differing from those of their covalent counterparts in their interfacial behavior [11–13]. The interfacial properties of supramolecular polymers are highly dynamic, and can be tuned by the same parameters (monomer concentration, temperature, etc.) which determine the solution behavior. Surface forces in solutions of non-adsorbing supramolecular polymers were treated theoretically by Van der Gucht *et al.* [14, 15]. They predict that attractive depletion forces occur, and that the range of these interactions has a *maximum* at the overlap concentration. Currently, surface forces, even when they are as weak as the depletion force, can be directly measured by several experimental techniques, such as the Surface Force Apparatus, Atomic Force Microscopy (AFM) and Total Internal Reflection Microscopy. Using these techniques, direct measurement of depletion forces in aqueous and non-aqueous solutions of charged and neutral covalent polymers has been reported, as reviewed by Jenkins [1] and Tuinier [2]. Depletion forces induced by the presence of wormlike micelles were also measured [16]. In many respects, the latter are similar to supramolecular polymers, since they are also long, non-covalent aggregates of small molecules.

When measuring interactions in liquids with AFM, one has to consider

non-equilibrium effects which may affect the measured force [17]. When a colloidal probe approaches the planar substrate, it is subject to hydrodynamic drag. For the measurement of thermodynamic equilibrium forces, it is therefore important to ensure that the motion is sufficiently slow, so the hydrodynamic forces are small compared to the force which is to be measured. Furthermore, the presence of a surface generally perturbs the structure of liquids. These structural changes may lead to a different viscosity close to the surface compared to the bulk value. Since the viscosity in the gap between the colloidal probe and the substrate determines the hydrodynamic drag (at small separations), hydrodynamic forces may be different than expected from the bulk viscosity. When two surfaces approach each other, very high shear rates can occur in the gap, which can also affect the local structure of the liquid, and its viscosity. These effects are especially important when measuring surface forces in complex fluids, like semidilute or more concentrated polymer solutions, since these often have a high viscosity and non-Newtonian rheology (a shear rate-dependent viscosity).

The bifunctional monomer *2,4-bis(2-ethylhexylureido)toluene* (EHUT) forms linear supramolecular chains in various apolar solvents by the cooperative formation of four hydrogen bonds between two consecutive monomers [18]. EHUT solutions were studied by spectroscopic techniques, light and neutron scattering, calorimetry and rheometry [14, 19, 20]. These experiments showed that EHUT has a very high association constant and is capable of forming long, semiflexible supramolecular chains. The effect of the addition of monofunctional monomer *2,4-bis(dibutylureido)toluene* (DBUT) was also studied [21]. This monomer has only one binding group and if it binds to a chain, it prevents further growth of the chain. Monofunctional monomers decrease the average degree of polymerisation and thereby cause, for example, a decrease in solution viscosity. Because of these effects, they are also known as *chain stoppers*. It was demonstrated that DBUT can be used to vary the average degree of polymerisation in EHUT solutions in a controlled way, independent of the overall monomer concentration [22–24].

Recently, we reported the first experimental investigation of depletion forces in supramolecular polymer solutions [24]. In this study, depletion forces between stearylated silica surfaces immersed in EHUT/DBUT solutions in cyclohexane were measured directly by means of Colloidal Probe Atomic Force Microscopy (CP-AFM). Moreover, it was demonstrated that the interaction can easily be tuned *in situ* by the addition of chain stoppers, an effect which can never occur with covalent polymers, since these have a fixed chain length. In the present paper, we investigate the depletion forces in the EHUT/DBUT system in more detail. Furthermore, hydrodynamic and other non-equilibrium effects are considered.

## 6.2 Theoretical background

### 6.2.1 Depletion interaction

The origin of the depletion interaction lies in the loss of entropy a polymer suffers when it is in close proximity to a surface [1, 2]. If this entropy loss is not compensated by an attractive adsorption enthalpy, the polymer will tend to stay away from the surface. This leads to a layer close to the surface with a lower polymer concentration than in the bulk solution, called the depletion layer. When two particles in a solution of non-adsorbing polymer approach each other to such a distance that their depletion layers overlap, the osmotic pressure in the gap between the particles is lower than in the surrounding solution. As a result of this imbalance in osmotic pressure, the particles are pushed together. In other words, there is an attractive force between the particles.

This phenomenon was analyzed quantitatively for the first time by Asakura and Oosawa [25, 26], who started by modelling polymers as hard spheres between parallel surfaces. They assumed that the polymer concentration profile is a step function. If the depletion layers of the two surfaces overlap by a volume  $\Delta V$ , and the surfaces are pushed together by the osmotic pressure of the bulk solution  $\Pi_{bulk}$ , the depletion free energy  $G_{dep}$  is given by the product

$$G_{dep} = -\Delta V \Pi_{bulk} \quad (6.1)$$

The Derjaguin approximation [27, 28] relates the interaction *free energy* per unit area  $G(h)/A$  between two planar surfaces of area  $A$  at a separation distance  $h$  to the interaction *force*  $F(h)$  between spherical particles with radii  $r_1$  and  $r_2$ . This approximation may be used if the separation distance between the surfaces is much smaller than the radii of the particles. For the case of one spherical particle with radius  $r_1 = R$  and a planar surface ( $r_2 = \infty$ ), this leads to

$$F(h) = 2\pi R \frac{G(h)}{A} \quad (6.2)$$

This relationship is convenient for CP-AFM experiments, in which the interaction force between a spherical particle and a planar surface is measured. The measured force (which depends on the area of interaction, and thus on the size of the particle) can directly be converted to the interaction free energy per unit area between two planar surfaces by dividing it by  $2\pi R$ .

The depletion force between a spherical particle and a planar surface is given by [29]:

$$F_{dep}(h) = \begin{cases} -\pi(2R + h)(2\delta - h)\Pi_{bulk} & \text{if } 0 < h \leq 2\delta \\ \approx -2\pi R(2\delta - h)\Pi_{bulk} & \text{if } h \ll R \\ 0 & \text{if } h > 2\delta \end{cases} \quad (6.3)$$

where  $2\delta$  is the separation distance where the surfaces start to interact (the interaction distance). In reality, there is of course no sharp kink in the force profile at  $h = 2\delta$  as predicted by equation 6.3, but a continuous transition. Nevertheless, the linear force profile is a reasonable approximation for separations smaller than approximately  $1.7\delta$  [30].

In the Asakura-Oosawa (AO) model, the characteristic length scale of the polymer solution is assumed to be much smaller than the radius of curvature of the surface. This is also the case in our CP-AFM experiments. Significant deviations from the AO model can occur in the depletion force and the phase behavior of suspensions when the particles are not much larger than the characteristic length scale of the polymer solution [31–34].

The use of equation 6.3 is not limited to dilute solutions or to spherical polymers. It can be applied to a much wider range of conditions as long as  $\delta$  and  $\Pi_{bulk}$  are correctly identified and the correct concentration dependencies are used.

### 6.2.2 Concentration dependence of $\delta$

In the AO model, the interaction distance  $2\delta$  occurring in equation 6.3 is exactly twice the depletion layer thickness. In the general case this is not strictly true, as the depletion attraction tends to begin at slightly larger separations [30, 35]. However, the difference is small and beyond our experimental accuracy. Moreover, the depletion layer thickness and the interaction distance scale in the same way with concentration. Therefore, we will hereafter not discriminate between the two, we use  $\delta$  to denote the thickness of the depletion layer and take  $2\delta$  as the interaction distance.

In dilute polymer solutions, interactions between polymer chains may be neglected, and  $\delta$  is approximately equal to the (average) radius of gyration  $R_g$  of a single polymer [25, 26]. For covalent polymers,  $R_g$  is fixed so at low concentrations, the depletion layer thickness is constant and only the osmotic pressure term in equation 6.3 depends on the polymer concentration. Supramolecular polymers, on the other hand, have a concentration dependent degree of polymerisation. For a supramolecular polymer with an association constant  $K$  for the formation of a bond between two monomers (which is assumed to be independent of the length of the chain to which a monomer binds), the average degree of polymerisation  $\langle N \rangle$  at an overall monomer concentration  $c$  is given by [23, 36]:

$$\langle N \rangle \sim \sqrt{Kc} \quad (6.4)$$

This equation is valid for (on average) long chains, that is if  $Kc \gg 1$ . Because of this concentration dependence of  $\langle N \rangle$ ,  $R_g$  and  $\delta$  increase with increasing monomer concentration.

## 6.2. Theoretical background

---

Above the overlap concentration ( $c^*$ ) the chains form a transient network with a characteristic mesh size  $\xi$ , which is the correlation length. In this regime, the depletion layer thickness is no longer determined by the size of the individual polymers, but it is approximately equal to  $\xi$ . The number of entanglement points increases with increasing concentration, and hence the average mesh size decreases. Therefore,  $\delta$  also decreases with increasing concentration. Furthermore,  $\xi$  is independent of the chain length and only determined by the overall polymer concentration. Therefore, the fact that supramolecular polymers have a concentration-dependent degree of polymerisation does no longer play a role, and the concentration dependence of  $\delta$  is the same as for covalent polymers [37]:

$$\delta \approx \xi \sim c^{-\alpha} \quad (6.5)$$

where  $\alpha = 0.75$  for flexible chains (that is, if  $\xi$  is much larger than the persistence length), and  $\alpha = 0.5$  for rods ( $\xi$  smaller than the persistence length).

In theoretical work on depletion interactions in ideal, flexible supramolecular polymers, it was shown that the depletion layer thickness indeed increases at low polymer concentrations due to the growth of the polymer chains [14, 15]. At the overlap concentration,  $\delta$  passes a maximum and in the semidilute regime it decreases again due to the decreasing mesh size of the polymer network. This behavior is qualitatively different from that of covalent polymers, for which  $\delta$  is constant at low concentrations and there is no maximum in the depletion layer thickness.

### 6.2.3 Concentration dependence of $\Pi_{bulk}$

For dilute solutions, the bulk osmotic pressure of an ideal polymer solution is simply given by Van 't Hoff's law:  $\Pi_{bulk} = \rho kT$ , where  $\rho$  is the concentration of *polymers*. For supramolecular polymers, it has to be taken into account that an increase in the overall *monomer* concentration results in an increase in the number of chains, but the average degree of polymerisation is also increased. Since  $\langle N \rangle \sim c^{0.5}$  (equation 6.4), the concentration of polymer chains must also scale as  $c^{0.5}$  (the sum of both exponents is unity):

$$\Pi_{bulk} \sim \rho \sim c^{0.5} \quad (6.6)$$

This result is independent of the flexibility of the chains.

In the semidilute regime, the osmotic pressure is not determined by the number of chains, but by the number of meshes, which is related to the average mesh size ( $\Pi_{bulk} \sim \xi^{-3}$ ) and is again independent of the length of the chains [37]. Using the scaling relations for  $\xi$  as a function of  $c$  from equation 6.5, the osmotic pressure for supramolecular polymers in the semidilute regime is given by

$$\Pi_{bulk} \sim c^\beta \quad (6.7)$$

with  $\beta = 9/4$  for flexible chains and  $\beta = 3/2$  for rod-like chains.

## 6.2.4 Non-equilibrium forces in Colloidal Probe Atomic Force Microscopy

In CP-AFM, a micron-sized particle is attached to an AFM cantilever [38]. The cantilever with the colloidal probe is then placed above a planar surface (the substrate) and this surface is moved up and down by a piezoelectric crystal, thereby varying the distance between the colloidal probe and the substrate. From the deflection of the cantilever during this motion, the force which the colloidal particle experiences can be calculated if the spring constant of the cantilever is known. From these data, a force-distance curve can be constructed. A comprehensive review on force measurements by AFM was recently given by Butt *et al.* [17]. Several non-equilibrium contributions to the force curve should be considered when measuring surface forces in complex fluids. Below, hydrodynamic forces, shear effects and entrapment of polymer in the gap are discussed.

### Hydrodynamic forces

Consider an isolated spherical particle of radius  $R$  which moves with a velocity  $v$  through a medium with viscosity  $\eta$ . The particle experiences a hydrodynamic drag force  $F_h$ , which is proportional to the particle velocity. The friction coefficient  $\zeta_\infty^{sphere}$ , defined as  $F_h/v$ , is given by [39]

$$\zeta_\infty^{sphere} = -6\pi\eta R \left( \frac{R + 2b}{R + 3b} \right) \quad (6.8)$$

The parameter  $b$  is the (apparent) slip length. If there is no boundary slip (that is, the liquid at the surface of the particle has the same velocity as the particle itself)  $b$  equals zero and the friction coefficient is the well-known Stokes friction  $-6\pi\eta R$ . Under perfect slip conditions ( $b = \infty$ , meaning that the tangential velocity of the liquid at the surface is zero), the friction coefficient is reduced to  $-4\pi\eta R$ . For intermediate values of the liquid velocity at the particle surface (partial slip), the slip length has a finite non-zero value. It can be seen from equation 6.8 that the effect of slip on an isolated particle is always relatively small, and it only has to be considered if  $b$  is of the same order of magnitude as or larger than the particle size.

If the particle is close to a planar surface, the flow of the fluid around the particle is hindered, and the hydrodynamic friction is increased. An exact expression for the friction force of a spherical particle near a planar surface moving perpendicular to this surface was derived by Brenner [40]. When

## 6.2. Theoretical background

---

the surface separation  $h$  between the particle and the planar surface is much smaller than the radius of the particle ( $h \ll R$ ), the friction coefficient can be approximated by the expression

$$\zeta^{\text{sphere}}(h) = -\frac{6\pi\eta R^2}{h} f^*(h) \quad (6.9)$$

where  $f^*(h)$  is a correction factor which equals unity for no-slip conditions. If slip occurs, the correction factor  $f^*(h)$  in equation 6.9 is given by [41]

$$f^*(h) = \frac{h}{3b} \left[ \left( 1 + \frac{h}{6b} \right) \ln \left( 1 + \frac{6b}{h} \right) - 1 \right] \quad (6.10)$$

where the slip length is assumed to be equal for both surfaces. In contrast to the case of an isolated particle (equation 6.8), slip can have a large influence on the friction coefficient when the particle is close to a solid surface. Slip can occur as a result of molecular properties of the solvent and the surface, or it may be due to roughness of the surface. It can also be the result of a layer with a reduced viscosity near the surface [42, 43], such as a depletion layer [44]. If there is a depletion layer of thickness  $\delta$  and the viscosity is approximated by a step function with a value  $\eta_s$  at distances  $< \delta$  from the surface, and the bulk value  $\eta$  at distances  $\geq \delta$ , the apparent slip length is given by [41, 44]

$$b = \delta \left( \frac{\eta}{\eta_s} - 1 \right) \quad (6.11)$$

Here, essentially the same assumption was made as previously used in equation 6.3, where the polymer concentration was assumed to be a step function which goes from zero to the bulk value at a distance  $\delta$  from the surface. Therefore, in this approximation the viscosity  $\eta_s$  within the depletion layer can be identified as the viscosity of the pure solvent.

A more detailed analysis of depletion-induced slip, based on a more realistic polymer concentration profile, was presented by Tuinier [44]. However, only ideal (very dilute) solutions of flexible chains in a mean-field approximation were considered. Under these conditions, there is a simple relation between the (local) polymer concentration and the viscosity, which allows accurate calculation of the apparent slip length. We cannot apply the same analysis to our experimental system, because it does not consist of dilute flexible chains, but rather of semidilute semiflexible ones, for which the relation between local concentration and viscosity is much more complicated. When the polymer concentration profile near the surface in the equations of Tuinier is replaced by a step function, the result reduces to equation 6.11.

### Shear effects

Another non-equilibrium effect which may be important in CP-AFM experiments is the non-Newtonian behavior of many fluids under shear. When the colloidal probe and the sphere are pushed together, liquid is forced out of the gap, during which high shear rates can occur. This can lead to both an increase of the viscosity in the gap (when the liquid is shear thickening), or a decreased viscosity (for shear thinning liquids). The viscosity in the gap determines the hydrodynamic drag on the cantilever and the particle (vide infra), and the effective hydrodynamic drag may therefore be different from that expected for the (zero-shear) bulk viscosity. Solutions of semiflexible polymers often show shear thinning due to shear-induced alignment of the chains, which facilitates the flow and reduces the viscosity. The shear profile between a sphere and a flat substrate is non-uniform, with maximum shear rates occurring at a certain distance from the symmetry axis, and it also depends on the presence of slip. For Newtonian liquids between surfaces with a slip length  $b$  (which is assumed to be independent of the shear rate  $\dot{\gamma}$ ) which are approaching each other with a velocity  $v$ , the maximum shear rate at separation  $h$  can be calculated by [45]:

$$\dot{\gamma}_{max} = 9v \sqrt{\frac{2R}{3h^3}} \times \frac{\sqrt{g^* - 1 - 3b/h}}{(2 - 3b/h + g^*)(2 + 15b/h + g^*)} \quad (6.12)$$

where  $g^* = \sqrt{4 + 24b/h + 9(b/h)^2}$ . From this equation, it can be seen that the presence of slip reduces the maximum shear rate. This is due to the fact that the shear is 'concentrated' in the slip layer of thickness  $b$ . This layer has a low viscosity, which leads to high shear rates at a given shear stress. As a consequence, the maximum shear rate outside the slip layer, which is calculated with equation 6.2.4, is reduced. Under perfect slip conditions ( $b = \infty$ ), all the shear takes place at the surfaces, and the shear rate in the gap is zero.

### Restricted equilibrium of the polymer solution

Consider a spherical particle moving towards a planar surface through a polymer solution. The system is in equilibrium if the chemical potential in the gap between the surfaces equals that in the bulk solution. If the particle approaches the surface sufficiently slowly, the polymers have time to move out of the gap, thereby keeping the chemical potential in the gap constant. However, if the outflow of polymer is slow compared to the velocity with which the particle and the surface approach each other, polymers become 'trapped' in the gap. In a theoretical work on depletion forces in supramolecular polymer solutions, it was demonstrated that the increase of polymer concentration in the gap leads to a repulsive contribution to the interaction force [15]. Depending on the

## 6.3. Experimental

---

conditions, this repulsion can be much stronger than the attractive depletion force, leading to a net repulsive interaction between the surfaces.

Each of the non-equilibrium effects discussed above introduces a considerable complication which is difficult to analyse experimentally. On one hand, the chemical potential of the solution in the gap may be different from the bulk value due to entrapment of polymer chains. This will generally affect the local viscosity, also when the solution is fully Newtonian. On the other hand, the viscosity of a non-Newtonian liquid in the gap may be different from the bulk value due to the occurrence of high shear rates, also when the approach is sufficiently slow to prevent entrapment of chains. When both effects occur simultaneously, the behavior becomes very complex. The viscosity in the gap (which determines the hydrodynamic drag at a given approach velocity) is a function of the shear rate and of the local chemical potential. In turn, both the shear rate and the chemical potential in the gap are a function of the velocity with which the surfaces approach each other. This complex interplay makes the quantitative analysis of these phenomena very difficult.

From the foregoing, it is clear that the measurement of surface forces by CP-AFM can be complicated by many factors. Independent measurement of the rheological properties of the liquid under investigation may help to estimate which effects should be considered, and which may be neglected. If independent data on the equilibrium surface forces are also available, this can also facilitate the analysis. For example, if it is known that depletion forces occur, the presence of a depletion layer with a lower viscosity than the bulk solution may be assumed, and this can explain the reduced hydrodynamic drag, as described above.

## 6.3 Experimental

### 6.3.1 Solutions

Samples of bifunctional monomer EHUT and monofunctional chain stopper DBUT were a kind gift from L. Bouteiller, Université Pierre et Marie Curie, Paris, France. Cyclohexane (Aldrich, >99%) was used as received. Solutions were prepared by stirring overnight at approximately 40 °C. They were left to cool down to room temperature and equilibrate for at least one day. A constant mole fraction  $x$  of DBUT (defined as  $x = \frac{[DBUT]}{([EHUT]+[DBUT])}$ ) of 0.10 was used in all experiments.

## 6.3.2 Materials

### Preparation of stearyl-coated silica surfaces

A piece of silicon wafer (WaferNet, Eching, Germany) was oxidized and coated with stearyl alcohol (Aldrich) by the method described by Wijting *et al* [30]. The static contact angle of a water droplet on a well-coated surface was typically between 100 and 110 °. Pieces with dimensions of approximately 1 × 1 cm were cut from the coated wafer and used for CP-AFM measurements.

Monodisperse silica spheres with a radius of 14 nm (Ludox HS40, Aldrich) were used for phase separation experiments. For CP-AFM force measurements, silica spheres with a radius of 3 μm (Philips laboratories, Eindhoven, the Netherlands) were used. Both types of spheres were coated with stearyl alcohol by the method described by Van Helden *et al.* [46]. The Van der Waals interaction between stearylated silica surfaces in cyclohexane is negligibly small due to the very similar refractive indices of the materials. Therefore, only steeply repulsive interactions are present between these surfaces.

### Preparation of AFM cantilevers

For CP-AFM experiments, the large stearylated silica spheres ( $R = 3 \mu\text{m}$ ) were attached to long (200 μm), thin-legged silicon nitride AFM cantilevers (Veeco Instruments). These cantilevers have a nominal spring constant of 0.06 N/m, but the real value can differ from the nominal value by as much as a factor of 2 due to variations in cantilever geometry. The colloidal probes were attached to the cantilevers using the setup designed by Giesbers *et al* [47]. In this method, an etched tungsten wire, which can be moved using a three-way translation stage, is used to handle the glue (Epikote 1004F epoxy resin, Shell Amsterdam, the Netherlands) and the spherical particles. The procedure by which a stearyl-coated particle was glued to an AFM tip was described previously by Wijting *et al.* [30].

## 6.3.3 Colloidal probe AFM

All force measurements were done at ambient temperature using a Nanoscope IIIa SPM controller with a PicoForce scanner (Veeco Instruments). A glass liquid cell was used in combination with a Kalrez ® 4001 O-ring (Dupont Dow) with an inner diameter of 6.0 mm, and a width of 2.6 mm, corresponding to standard dimensions AS-568-108. A schematic representation of the setup is shown in figure 6.1. Liquids were introduced in the liquid cell by means of a glass syringe and teflon tubing.

After placing the stearylated silica surface on the piezo scanner and inserting the cantilever with the colloidal probe in the liquid cell, the O-ring was

### 6.3. Experimental

---

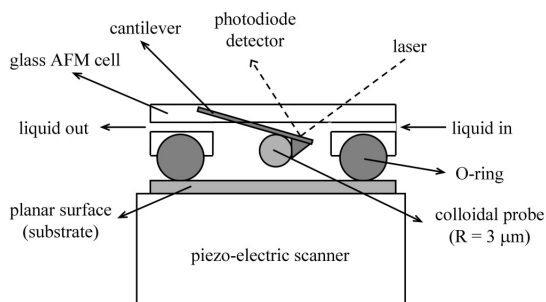


Figure 6.1: Schematic representation (not to scale) of the experimental setup of the AFM liquid cell. See text for characteristic dimensions.

installed and the cell was filled with pure cyclohexane and left to equilibrate for at least 30 minutes. The spring constant of the cantilever was then determined by the thermal noise method, which involves measuring the thermal vibrations of the cantilever at a large distance from the surface [48]. From a fit of a simple harmonic oscillator model to the power spectrum of the vibrations, the spring constant was calculated using the Nanoscope software (version 6.12r1, Veeco Instruments). For all colloidal probe cantilevers used (from different wafers), the spring constant was found to be between 0.03 and 0.09 N/m, within the expected margin compared to the nominal value of 0.06 N/m of the bare cantilever. A deflection away from the surface (due to a repulsive force between the probe and the substrate) is defined as ‘positive’, whereas attractive forces are ‘negative’.

#### Depletion force

The pure cyclohexane was replaced by EHUT/DBUT solutions by carefully flushing the cell with approximately 2 ml of solution. Force curves were measured after another equilibration period of 30 minutes, using scan ranges between 50 and 150 nm and scan velocities between 5 and 50 nm/s.

#### Hydrodynamic force

Hydrodynamics were studied using a 70 g/l EHUT solution, also containing chain stopper DBUT ( $x=0.10$ ). For this solution, force curves were collected

while the scan velocity was varied from 4 to 1000 nm/s at a fixed scan range of 100 nm. This was done at both large and small separation between the colloidal probe and the substrate surface (maximum separation approximately  $5\ \mu\text{m}$  and 50 nm, respectively).

### 6.3.4 Phase separation

To study depletion-induced phase separation, a concentrated suspension of the small stearylated silica spheres ( $R = 14\ \text{nm}$ ) was prepared. The particle concentration was determined by weighing 1 ml of suspension, evaporating the solvent and weighing the remaining solid particles. This yielded a particle concentration of  $2 \times 10^2\ \text{g/l}$ .

In glass tubes with screw caps, 0.5 ml of EHUT/DBUT solution was added to 0.5 ml of particle suspension. The suspensions were placed in an oven at a temperature of  $50\ ^\circ\text{C}$  and homogenized by shaking. Subsequently, the solutions were allowed to cool down to room temperature overnight, and it was visually checked whether the system had phase separated. Photographs of the tubes were taken.

## 6.4 Results

It was checked that EHUT does not adsorb onto the stearylated silica surface. This was done by preparing a suspension of stearylated silica particles in a 1 g/l EHUT solution. Before the particles were added, the EHUT concentration was determined by measuring the absorbance at 222 nm (the extinction coefficient of EHUT in cyclohexane was determined to be  $\epsilon_{222} = 2.6 \times 10^4\ \text{M}^{-1}\text{cm}^{-1}$ ). The suspension was homogenized by sonicating for 1 hour and shaken overnight for equilibration. The particles were removed by centrifugation, and the EHUT concentration in the supernatant was measured. No significant decrease in EHUT concentration was observed. A control experiment with uncoated silica did yield a significant decrease in EHUT concentration, showing that EHUT does adsorb to bare silica, but not to the stearylated particles.

Previously, the motion of stearylated silica particles through EHUT solutions with and without chain stoppers has been studied by Dynamic light scattering [14, 22]. These experiments also showed no indication of adsorption of EHUT onto the particles.

### 6.4.1 Depletion force measurements

Even though the Van der Waals forces between stearylated silica surfaces in cyclohexane are very small, perfect hard-wall interactions between a colloidal

## 6.4. Results

---

probe and a planar substrate are usually not found in CP-AFM experiments [29, 30]. This is generally explained by the roughness of both surfaces, which is typically of the order of a few nm for (stearyl)ated silica. This roughness causes the surfaces to touch with their extremities a few nm before they are completely in contact, which leads to a steric repulsion. After filling the liquid cell with cyclohexane, the interaction curve between the stearylated colloidal probe and the planar surface was measured. Thus, if both the probe particle and the substrate are well-coated with stearyl alcohol, it is expected that there is only a short-range steric repulsion between the surfaces. Therefore, only combinations of probe and substrate for which there was no measurable interaction at separations larger than a few nm were used for further experiments. A typical force curve in cyclohexane is shown in figure 6.2a. A force curve for a 100 g/l EHUT concentrations (with a stopper fraction  $x$  of 0.10) is shown in figure 6.2b. At least five force curves, all measured during approach of the surfaces, are plotted together in one figure.

The overlap concentration for EHUT chains without chain stoppers in cyclohexane is approximately 0.1 g/l [14, 23]. At higher concentrations, the solutions become viscoelastic and the zero-shear viscosity increases steeply with concentration. Without chain stoppers, EHUT solutions of the concentrations used in the current experiments would have an extremely high viscosity, and effectively be gels. It is in practice impossible to bring such a solution into the AFM liquid cell and perform CP-AFM experiments. To solve this problem, chain stoppers were added to decrease the average chain length, and thus the viscosity, to such an extent that the solutions could be injected into the AFM liquid cell. At the stopper fraction used in our experiments (0.10), the solutions are still highly viscous: the zero-shear viscosity of the lowest concentration used (70 g/l,  $x = 0.10$ ) is 2 Pa s, over 2000 times the solvent viscosity. The viscosities of the solutions with EHUT concentrations of 100 and 140 g/l are 5 and 10 Pa s, respectively. A rough estimate of the overlap concentration can be found by extrapolating the concentration dependence of the viscosity to the solvent viscosity [14] ( $\approx 10^{-3}$  Pa s). This leads to a value of the overlap concentration at  $x = 0.10$  of approximately 3 g/l. Furthermore, it was found that at a fixed EHUT concentration of 100 g/l, the solution passes from semidilute to dilute at a stopper fraction of approximately 0.20 [24], confirming that the solutions used here ( $x = 0.10$ ) are above the overlap concentration.

From the foregoing, it is clear that the solutions used in the CP-AFM experiments are well above the overlap concentration. In that case, the depletion layer thickness and the bulk osmotic pressure are only determined by the mesh size of the transient polymer network, and not by the size of the individual chains. Hence, the addition of chain stoppers will not affect the equilibrium depletion interaction, which is measured in the experiments.

Measurements at EHUT concentrations lower than 70 g/l did not yield a

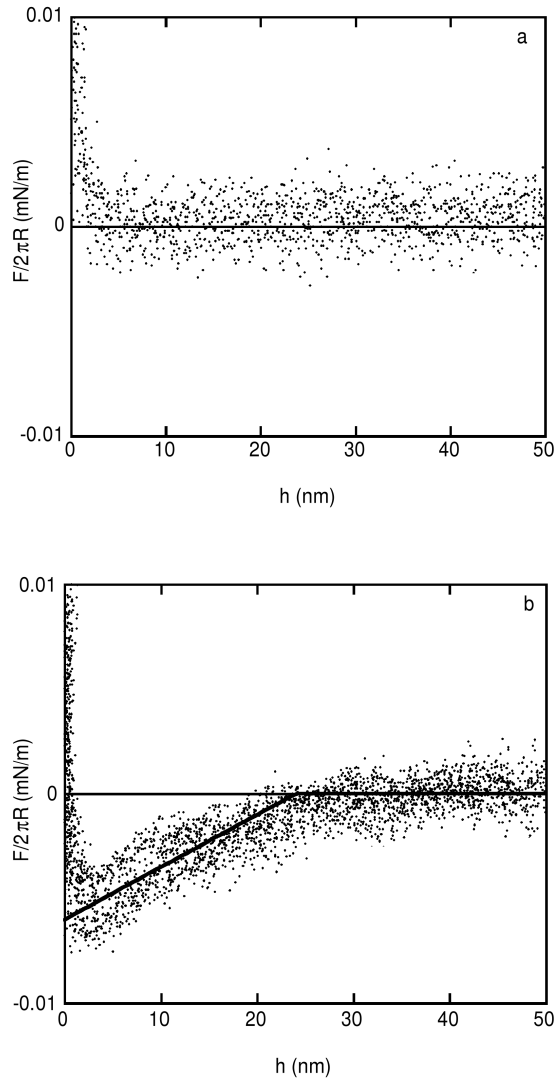


Figure 6.2: Normalized interaction force between stearylated silica surfaces. a: cyclohexane; b: 100 g/l EHUT,  $x = 0.10$ . The solid line is a fit to equation 6.3. Values of  $\delta$  and  $\Pi_{bulk}$  were obtained from the fit.

measurable attraction, and the force curve at these concentrations is essentially the same as in pure cyclohexane. At an EHUT concentration of 100 g/l (figure 6.2b), there is a well-detectable attraction. No experiments could be done at higher concentrations than 140 g/l. Even with chain stoppers, the solution viscosity is then so high that it becomes very hard to bring the solution into the liquid cell. Furthermore, very slow scan rates have to be used, otherwise the weak depletion attraction is overwhelmed by hydrodynamic repulsion (see section 6.4.2). With our instrument, scan velocities lower than 5 nm/s did not yield useful results, because of slow drift of the piezo position. This also limits the range of concentration which can be used.

According to equation 6.3, the force curve should be a straight line with a slope equal to the bulk osmotic pressure  $\Pi_{bulk}$  at separations smaller than  $2\delta$ , and coincide with the abscissa at larger separations. The line in figure 6.2b is a fit to this equation of the data between 5 and 20 nm. At shorter separations, the steric repulsion dominates and at separations larger than approximately  $1.5\delta$ , deviations from linearity are expected [30]. The depletion layer thickness  $\delta$  and the bulk osmotic pressure  $\Pi_{bulk}$  were determined from these fits to equation 6.3. From the scatter in the experimental data, an estimate for the error interval was made.

### Depletion layer thickness

The concentration dependence of  $\delta$  is shown in figure 6.3. For all concentrations used, the attraction starts at a separation of approximately 20 nm, indicating that the depletion layer thickness (half of this value) is approximately 10 nm. From previous experiments, it was found that the persistence length of EHUT chains in cyclohexane is  $\geq 200$  nm [23]. On the length scale of the depletion layer thickness, the chains can therefore be assumed to be rigid rods. For a semidilute solution of rods, the depletion layer thickness is expected to decrease with increasing concentration according to a power law  $\delta \sim c^{-0.5}$  (section 6.2.1). In previous light scattering experiments, the scaling law  $\xi = 120c^{-0.5}$  [23] was found (when  $\xi$  is expressed in nm and  $c$  in g/l). If we assume that  $\delta = \xi$ , the depletion layer thickness in the present experiments would range from 14 nm (70 g/l) to 10 nm (140 g/l), as shown by the solid line in figure 6.3. We therefore conclude that the measured depletion layer thickness of approximately 10 nm is in agreement with the light scattering results. However, the CP-AFM measurements do not show a clear decrease of  $\delta$  with increasing concentration, whereas such a decrease is predicted by theory and observed in the light scattering results. On the other hand, due to the relatively large experimental error and the weak concentration dependence, the results do not refute the predicted scaling behavior. A scaling law with the theoretical exponent  $-0.5$  and a somewhat smaller prefactor describes the

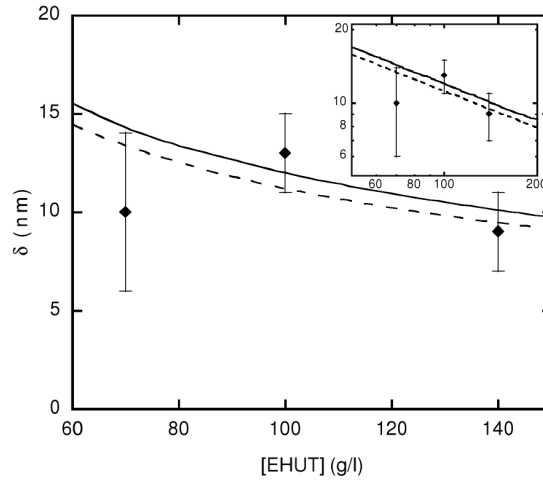


Figure 6.3: Depletion layer thickness  $\delta$  as a function of EHUT concentration. The solid line corresponds to  $\delta = 120c^{-0.5}$ , the dashed line corresponds to  $\delta = 112c^{-0.5}$ . Bars indicate the estimated error interval. Inset: same data on a double logarithmic scale.

data within the experimental error. The dashed line in figure 6.3 shows this scaling law:  $\delta = 112c^{-0.5}$ .

### Osmotic pressure

$\Pi_{bulk}$  for the three EHUT concentrations used is shown in figure 6.4. The expected concentration dependence of the osmotic pressure for semidilute rodlike chains is  $\Pi_{bulk} \sim c^{1.5}$  (section 6.2.1). The fitted curves indeed show an increase in slope with increasing concentration. However, the increase is smaller than expected based on a power law scaling with exponent 1.5. In that case,  $\Pi_{bulk}$  should increase with almost a factor of 3 when the concentration is increased from 70 to 140 g/l. Figure 6.4 shows only an approximately twofold increase in the osmotic pressure over this concentration range. If a power law fit is made to our data, the resulting exponent is 1.0 (see the solid line in figure 6.4), meaning that the increase in the experimental data is linear. The best fit with the theoretical scaling exponent 1.5 is also shown in the figure (dashed line). Even though this fit describes the data less satisfactorily, it is still within the error interval. Again, the limited concentration range of the experimental data do not allow a quantitative analysis of any power law scaling in the concentration dependence. In section 6.4.4, some possible explanations for the

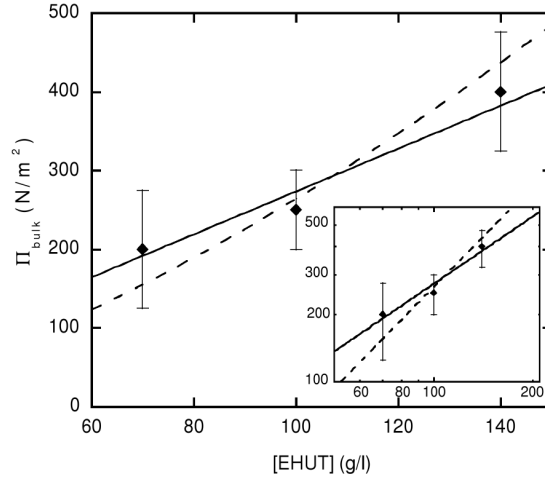


Figure 6.4: Bulk osmotic pressure (as derived from a fit of the measured force curves to equation 6.3) as a function of EHUT concentration. The solid line corresponds to  $\Pi_{bulk} = 2.9c^{1.0}$ . The dashed line corresponds to  $\Pi_{bulk} = 0.26c^{1.5}$ . Bars indicate the estimated error interval. Inset: same data on a double logarithmic scale.

weak concentration dependence will be discussed.

## 6.4.2 Hydrodynamic forces

To study the hydrodynamic forces which are caused by the motion of the AFM cantilever with the colloidal probe through viscous EHUT solutions, a 70 g/l EHUT solution containing DBUT ( $x = 0.10$ ) was used. The viscosity of this solution was independently determined by rheometry to be 2 Pa s.

### Hydrodynamics at large separations

The hydrodynamic drag on the cantilever with the attached probe was measured at a large surface separation (10  $\mu\text{m}$ ) from the substrate surface, where there is no interaction between the colloidal probe and the surface. By moving the cantilever, we therefore only measure hydrodynamic drag forces. A typical result is shown in figure 6.5a (for a scan velocity of 200 nm/s). If the cantilever is not moving, there is no net force acting on it, and this equilibrium position is defined as the zero of force. As the cantilever starts to move downwards, it is deflected upwards by hydrodynamic drag, as indicated by a positive force

(solid symbols). The force soon reaches a plateau at approximately 100 pN and is not a function of the separation between the particle and the surface, in line with the expectation for an isolated object (equation 6.8). After moving over a distance of 100 nm, the cantilever is stopped for 10 seconds. There is no hydrodynamic drag anymore, and the cantilever relaxes to its equilibrium position. After this delay time, the cantilever is moved in the other direction, away from the surface. It now experiences the same hydrodynamic force as during the approach, but in the opposite direction (open symbols). The average of the absolute values of the force plateaus is taken as the hydrodynamic drag force on the cantilever at this particular scan velocity. In this way, the hydrodynamic drag force was determined for various scan velocities. The results are presented in figure 6.5b. This figure shows that the hydrodynamic drag force increases linearly with scan velocity, again in agreement with the prediction for an isolated object (equation 6.8). The slope of the curve, which equals 0.45 g/s, equals the effective drag coefficient  $\zeta_\infty$  of the cantilever with the particle attached to it.

For our final purpose, measurement of depletion forces, it is relevant to compare the result obtained at large separations between the sphere and the surface ( $\zeta_\infty$ ) with the hydrodynamic force  $\zeta(h)$  at small separations. To do this,  $\zeta_\infty$  may be split into a contribution from the spherical colloidal probe and a contribution which takes into account the presence of the cantilever:

$$\zeta_\infty = \zeta_\infty^{sphere} + \Delta\zeta_\infty^{cant} \quad (6.13)$$

From the known viscosity of the solution (2 Pa s), the hydrodynamic drag on the isolated probe particle can be calculated. As a first assumption, we may use the expression for the drag coefficient of an isolated sphere with non-slip boundary conditions:  $-6\pi\eta R$  (equation 6.8). Under this assumption, which will be justified later,  $\zeta_\infty^{sphere}$  can be calculated to be 0.11 g/s. The remainder of the total drag coefficient (0.34 g/s) can be attributed to the drag on the cantilever itself and to the fact that the sphere is in fact not isolated but attached to the cantilever.

### Hydrodynamics at small separations

The effect of the presence of the substrate surface was studied by bringing the cantilever very close to the surface (maximum separation approximately 50 nm), and again moving the cantilever back and forth over a distance of 100 nm with various scan velocities. This means that for a part of the force curve, the colloidal probe is in contact with the substrate. A typical force curve, measured when the surface was approached with a scan velocity of 200 nm/s, is shown in figure 6.6a. When the cantilever moves towards the surface, it is deflected upwards, as a consequence of a drag force away from the

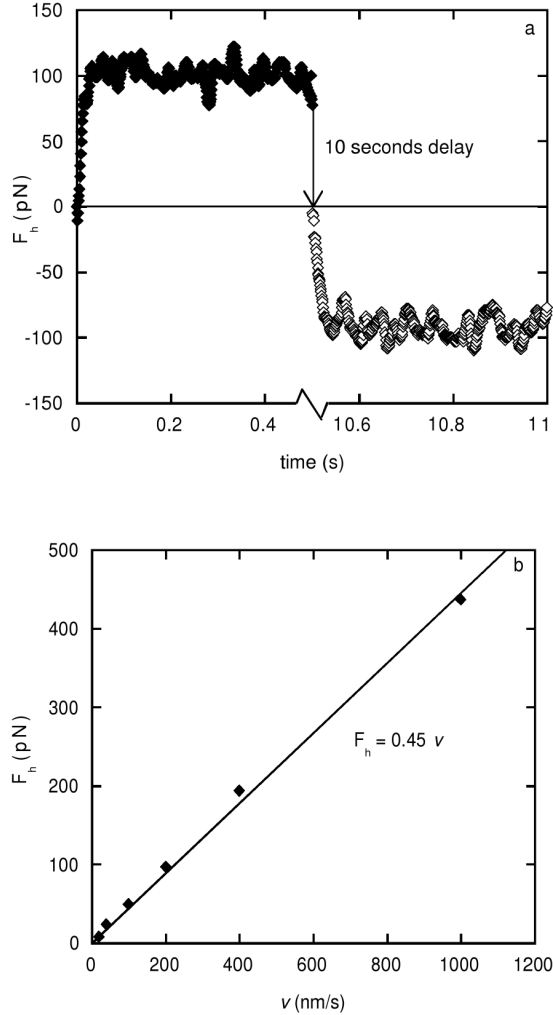


Figure 6.5: Hydrodynamic drag force  $F_h$  on a cantilever with a colloidal probe particle ( $R = 3\mu\text{m}$ ) in a 70 g/l EHUT solution containing DBUT ( $x = 0.10$ ) far away from the surface. a: As a function of time at a scan velocity of 200 nm/s. Approach ( $\blacklozenge$ ) and retract ( $\diamond$ ) data are plotted. A delay time of 10 s was used between successive approach and retract curves; b: As a function of scan velocity  $v$ . The line is a linear fit to the experimental data. The slope of the line represents the effective friction coefficient  $\zeta_\infty$

surface. The total hydrodynamic force may again be split into a contribution due to the sphere and a contribution due to the presence of the cantilever:  $\zeta(h) = \zeta^{sphere}(h) + \Delta\zeta^{cant}(h)$ . Even when the colloidal probe and the planar surface are in close contact, the cantilever is still microns away from the surface. The hydrodynamic drag on the cantilever will therefore not or hardly be affected by the presence of the surface, and remains at its original value:  $\Delta\zeta^{cant}(h) = \Delta\zeta_{\infty}^{cant} = 0.34$  g/s. The probe particle, on the other hand, will experience a different hydrodynamic force  $\zeta^{sphere}(h)$  compared to its value  $\zeta_{\infty}^{sphere}$  at large separations. The total hydrodynamic force is thus given by

$$\zeta(h) = \zeta^{sphere}(h) + \Delta\zeta_{\infty}^{cant} \quad (6.14)$$

Equations 6.9-6.11 can be used to calculate  $\zeta^{sphere}(h)$  for a given apparent slip length  $b$ . The value of 0.11 g/s as obtained from the hydrodynamic drag at large separation was used for  $\zeta_{\infty}^{sphere}$  in these equations, and a constant contribution from the cantilever  $\Delta\zeta_{\infty}^{cant} = 0.34$  g/s was assumed. The resulting hydrodynamic force  $v\zeta(h)$  (with  $\zeta(h)$  calculated with equation 6.14) for different values of the apparent slip length is shown in figure 6.6a.

If there would be no slip at the surface, the hydrodynamic drag could be described by equation 6.9 with  $f^*(h)$  set to unity. With a particle radius of 3  $\mu\text{m}$  and a maximum separation of 50 nm this would lead to a hydrodynamic drag force of tens of thousands of pN. Clearly, such forces are not found experimentally. The measured drag force is only a few 100 pN, which indicates that there is slip, very likely caused by the presence of the depletion layer with a reduced viscosity. If the apparent slip length is calculated with equation 6.11 using  $\eta = 2$  Pa s (bulk viscosity),  $\eta_s = 1 \times 10^{-3}$  Pa s (solvent viscosity) and  $\delta = 10$  nm (a reasonable value for the depletion layer thickness, see section 6.4.1), it equals  $2 \cdot 10^4$  nm. As a first approximation, this value of  $b$  was used for calculating the hydrodynamic drag force with equations 6.10 and 6.9. It can be seen from figure 6.6 that this calculation leads to a large underestimation of the drag force. This is not surprising, as the value of  $2 \times 10^4$  nm is based on the assumption that within a layer of 10 nm from the surface, there is no polymer present at all, and the fluid in this layer has the viscosity of the pure solvent. In reality, there will be some polymer present in the depletion layer, and the viscosity in the depletion layer gradually increases from that of the pure solvent to the bulk value.

The experimental data at large separations are best described by assuming an effective slip length of 220 nm (the thick solid line in figure 6.6a). With a depletion layer thickness of 10 nm, this indicates that the average viscosity in the depletion layer is 23 times lower than the bulk value. Note that the assumption of a particle with non-slip boundary conditions (made in the beginning of the analysis, see section 6.4.2) is reasonable, since the slip length is much smaller than the particle radius, and the slip correction in equation 6.8

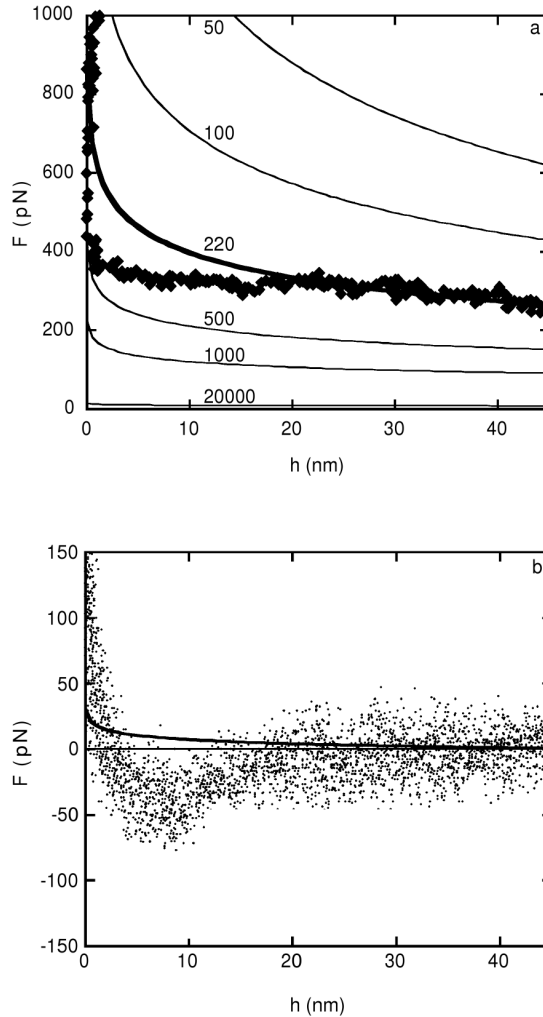


Figure 6.6: a: Interaction force  $F$  between a colloidal probe particle ( $R = 3\mu\text{m}$ ) and the substrate in a 70 g/l EHUT solution with chain stoppers ( $x = 0.10$ ) close to the surface at a scan velocity of 200 nm/s. Symbols denote experimental data, lines are calculated with equations 6.9-6.11 and 6.14. The numbers next to the lines are the values of the apparent slip length used for the calculation. b: Interaction force as in figure a, at a scan rate of 10 nm/s. The base line is chosen such that  $F = 0$  at a separation distance of 50 nm. Symbols denote experimental data, the line is the result of equations 6.9-6.11 and 6.14 with  $b = 220$  nm.

is therefore small. The calculated drag force with  $b = 220$  nm fits the experimental data well at separations larger than 20 nm. At smaller separations, the measured repulsive force is smaller than the predicted hydrodynamic repulsion. The difference between the two curves can be identified as the depletion force. Thus, the depletion force can in principle be calculated by subtracting the calculated curve (accounting for the contribution of hydrodynamics to the interaction force) from the experimental data. However, the depletion force is more accurately determined when a lower scan velocity is used. When a scan velocity of 20 nm/s or lower is used, the hydrodynamic drag (calculated with equation 6.10 and 6.9 using  $b = 220$  nm) remains at a virtually constant value until very small separations. This means that the contribution of hydrodynamics to the interaction force is effectively constant. In this case, subtraction of the hydrodynamic force from the experimental data is effectively the same as a baseline shift of the force curve such that the interaction force is zero at large separations. The presence of a depletion force now shows up as an attractive well (negative force) in the force curve at small separations. The solid line in figure 6.6b shows that the normalized hydrodynamic force (shifted along the force-axis such that it equals zero at  $h = 50$  nm) is indeed almost independent of separation distance until very small separations. Thus, by choosing the base line such that  $F = 0$  at large separations, the depletion force can be measured directly without having to subtract the hydrodynamic force from the experimental data. This method was used for the depletion force measurements described in section 6.4.1, and also in reference [24].

From previous experiments, it is known that EHUT solutions have a very complex rheological behavior [49]. For example, the solutions are strongly shear thinning above a certain shear rate. This shear thinning behavior may also occur in the gap between the particle and the substrate. This would also lead to a decreased viscosity in the gap (just as the presence of a depletion layer), and may therefore (partly) explain the reduced hydrodynamic drag on the probe particle and the cantilever, as explained in section 6.2.4. However, since the force curves clearly show a depletion force (which is supported by the phase separation experiments discussed in section 6.4.3), we may assume that the effect of the depletion layer dominates. Furthermore, since the polymer concentration in the depletion layer is much lower than in the bulk solution, the rheological behavior of the depletion layer may not be the same as that of the bulk solution. It is therefore not certain that at a shear rate where the bulk solution is shear thinning, this is also the case in the depletion layer. Finally, due to the relatively large effective slip length compared to the typical separation distance at which the interaction occurs ( $b = 220$  nm,  $h \leq 50$  nm), the shear rates in the gap are significantly reduced compared to the no-slip case (equation 6.2.4). However, as explained in section 6.2.4, the shear rates in

the depletion layer itself will be higher, due to the low local viscosity. Thus, the highest shear rates occur in the region with the lowest polymer concentration (and the shortest chains). This may prevent the solution from shear thinning, since shorter chains start shear thinning (aligning) at higher shear rates than long ones. Summarizing, there is a reduced polymer concentration in the gap, which leads to a large apparent slip length. Due to the slip, the shear rates in the gap (outside the depletion layer) are reduced, while the shear rates in the depletion layer are increased. These effects reduce the hydrodynamic forces. It is uncertain what the rheological behavior of the solution is at the local concentration and shear rate in the gap. This is a demonstration of the highly complex interplay between the local concentration, viscosity and shear rate mentioned in section 6.2.4. At this point, we can therefore not conclude with great certainty that the reduction of the hydrodynamic drag, which is experimentally observed, can be completely attributed to the effect of the depletion layer, since other mechanisms (such as shear thinning) may also occur. It is questionable if it is at all possible to distinguish the hydrodynamic effect of a reduced viscosity caused by the presence of a depletion layer from that caused by shear thinning. However, the effect of the depletion layer is the only effect of which we are certain that it should occur, and we can describe our experimental data reasonably well using this contribution only. Moreover, it has been found in previous CP-AFM experiments that the measured forces are in good agreement with the predictions for the depletion force [24]. This is another indication that depletion is the dominant contribution.

### 6.4.3 Macroscopic phase separation

Due to the refractive index matching, suspensions of stearylated silica particles in cyclohexane scatter very little light. Up to high particle concentrations, the suspensions are (to the naked eye) clear with a yellowish color. However, some turbidity can be observed if the samples are illuminated from below by a beam of white light against a black background in a darkened room. A suspension of particles ( $R = 14$  nm) in pure cyclohexane is shown in figure 6.7a. As can be seen, the suspension consists of a single phase and scatters homogeneously. The bright spot at the bottom of the tube is the reflection of the light source.

Figures 6.7b, c and d show suspensions with the same particle concentration with different EHUT concentrations and with a fixed fraction of chain stopper DBUT ( $x = 0.10$ ). The images clearly demonstrate that EHUT is capable of inducing phase separation in these suspensions. A suspension in a solution with an EHUT concentration of 10 g/l forms two phases (figure 6.7b), separated by a mirror-like interface. The bottom phase is more turbid, which indicates that this is the particle-rich phase. The phase separation is not very pronounced, as the top phase is also quite turbid, which indicates that

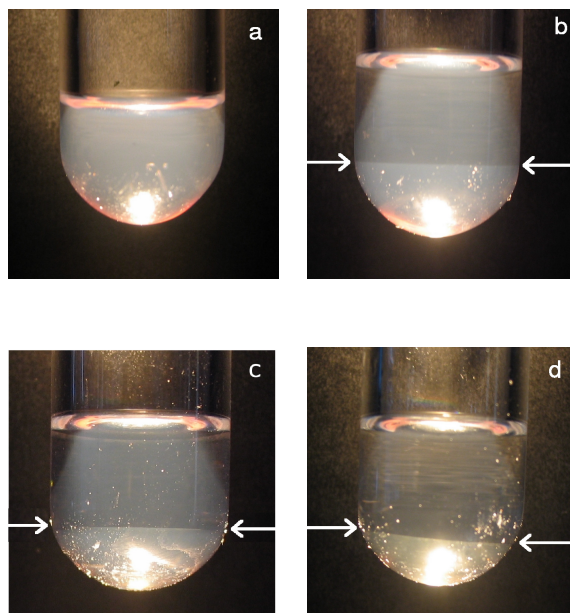


Figure 6.7: Tubes containing suspensions of stearyl silica spheres ( $R = 14$  nm) in EHUT/DBUT solutions ( $x = 0.10$ ) of different concentrations in cyclohexane. EHUT concentrations are indicated. a: 0 g/l (pure cyclohexane); b: 10 g/l; c: 50 g/l; d: 140 g/l. Arrows indicate the position of the mirror-like interface between the particle-rich bottom phase and the polymer-rich top phase.

it still contains a significant concentration of particles. With increasing EHUT concentration, the concentration difference between the two phases becomes more pronounced, as can be observed from the increased difference in turbidity between the phases. At concentrations of 50 g/l (figure 6.7c) and higher, the difference in refractive index between the phases is sufficiently large to observe a mirror-like interface between the phases without special lighting or other measures. At the highest concentration used (140 g/l, figure 6.7d) a concentrated particle-rich phase is present at the bottom of the tube, and the EHUT-rich phase on top hardly scatters any light, indicating that it contains few particles.

In the phase separation experiments described above, the particle size is much smaller than in the CP-AFM experiments. Indeed, the particle size and the polymer mesh size are of the same order of magnitude. Thus, the condi-

tion  $R \gg \xi$  is not satisfied, and deviations from the simple AO model are to be expected [31–34]. Furthermore, our experimental system consists of four components: particles, solvent, bifunctional monomers and chain stoppers. All components have their own distribution over the phases. The phase behavior can therefore not be described or studied by the usual methods such as that of Bodnár *et al.* [50], which are derived for three-component systems (particles, solvent and polymer). Detailed quantitative treatment of the phase behavior and construction of a phase diagram are beyond the scope of this paper. Nevertheless, the experiments presented here demonstrate that the depletion forces are sufficiently strong to induce phase separation in a colloidal suspension. The increase of the difference in turbidity between the phases indicates that the depletion force becomes stronger with increasing polymer concentration.

### 6.4.4 Discussion

#### Colloidal probe AFM

The results presented in section 6.4.1 for the depletion layer thickness and the osmotic pressure are qualitatively in line with previous experiments and theoretical predictions, although in both cases the concentration dependence seems weaker than expected. Since the range of concentrations that could be used is small, perfect agreement with theory can hardly be expected. Therefore we will not present an extensive quantitative discussion on the possible sources of the deviations. However, some brief remarks can be made.

In section 6.2.1, scaling exponents for the concentration dependence of  $\delta$  and  $\Pi_{bulk}$  were derived. The only difference with the exponents for covalent polymers is the introduction of a concentration dependence of the average chain length. Polydispersity, which is inevitably present in supramolecular polymers, was not taken into account. Short chains can come closer to the surface without losing entropy than long ones. This decreases the depletion layer thickness, since in section 6.2.2 the radius of gyration of a chain of average length was used, while the surface area will be predominantly occupied by the short chains. It was shown theoretically that when two surfaces are pushed together, the long chains are the first to be excluded from the gap, leading to a decreased average chain length in the gap [15]. This effect could even be stronger for supramolecular polymers than for covalent ones. If a long supramolecular chain comes so close to the surface that it starts to lose entropy, it could overcome this unfavorable situation by breaking up into smaller chains which are still unhindered by the presence of the surface. This mechanism could enhance the chain length segregation at the surface. However, it is not so much the value of  $\delta$  and  $\Pi_{bulk}$  which deviates from the prediction, but the concentration dependence. Since polydispersity does not depend on concen-

tration, it is not expected that it would affect the concentration dependence of the depletion interaction. Furthermore, in theoretical work where polydispersity was taken into account, it was found that flexible supramolecular polymers obey the same scaling laws as derived in section 6.2.1, both below and above the overlap concentration [15, 51].

The supramolecular chains are assumed to be rigid rods on the length scale of the depletion layer thickness. This seems to be a valid approximation, given the estimated persistence length of the chains ( $\geq 200$  nm) [23] and the values of  $\delta$  obtained from the CP-AFM experiments ( $\approx 10$  nm) and light scattering [14]. Furthermore, the theoretical concentration dependence of both  $\delta$  and  $\Pi_{bulk}$  for flexible chains is stronger than that of rigid rods (see section 6.2.1). Therefore, the weak concentration dependence found experimentally cannot be explained by assuming some degree of flexibility of the chains.

Measurements of the depletion force were all done at low scan velocities ( $< 20$  nm/s), to ensure that hydrodynamic drag on the cantilever was kept at a constant value until very small separations (see section 6.4.2). The very fact that a weak force such as the depletion attraction can be measured already shows that there is little hydrodynamic repulsion. Nevertheless, it is possible that the measured attraction is decreased due to a repulsive contribution from the hydrodynamics, especially at small separations. This effect would be stronger at higher EHUT concentrations, and this might explain the weak concentration dependence found experimentally.

Since the EHUT solutions used are highly viscous and the polymers are strongly entangled, movement of the polymer chains will be slow. This is true even though supramolecular polymers generally reach equilibrium faster than covalent ones, due to their ability to break and reform. When the colloidal probe and the planar surface approach each other, some polymer chains may be trapped between them, thereby increasing the polymer concentration in the gap. This would cause a repulsive contribution to the interaction force, as mentioned in section 6.2.4. At higher EHUT concentrations, the viscosity is higher, motion of the chains becomes even slower, and more chains could be trapped, which could affect the concentration dependence. Again, the fact that a net attractive force is measured indicates that the repulsive contribution originating from non-equilibrium effects is small, but it may not be negligible.

Finally, it is also possible that EHUT has a (very low) affinity for the stearylated silica surfaces, which would lead to a decreased depletion force. It was previously demonstrated that the depletion attraction between stearylated silica surfaces in solutions of poly(dimethylsiloxane) in cyclohexane (a well known model system for studying depletion interaction) as measured by CP-AFM was systematically lower than expected [30]. The experimental data were quantitatively explained by assuming a small attractive interaction between the polymer segments and the surface.

### Macroscopic phase separation

The lowest EHUT concentration where a depletion force could be measured with CP-AFM was 70 g/l. On the other hand, phase separation was observed in solutions with EHUT concentrations as low as 10 g/l. Recently, phase separation in solutions of supramolecular polymers containing chain stoppers (without particles) was investigated theoretically [52]. It was found that fractionation of chain stoppers occurs: the stopper fraction in the concentrated phase is lower than in the dilute phase. It was proposed that phase separation may be used as a method to remove chain stoppers from supramolecular polymer solutions. In the present case, phase separation occurs between a phase with a high particle concentration (and a low concentration of supramolecular polymer) and a phase with a high polymer concentration (and a low concentration of particles). It is expected that fractionation in the present particle-containing system is even more pronounced, because the longest chains are most strongly excluded from the particle surface. Thus, the particle-rich phase contains a higher stopper fraction and thus a relatively high number of relatively short chains compared to the polymer-rich phase. This fractionation of chain stoppers between the two phases could lead to an enhanced depletion attraction. This could also (partly) explain the observation that phase separation already occurs at concentrations where the depletion force could not be measured with CP-AFM.

## 6.5 Concluding remarks

Depletion interactions in solutions of a hydrogen-bonded reversible supramolecular polymer were studied experimentally by direct measurement by means of the Colloidal Probe AFM technique and by studying depletion-induced phase separation. Solutions in cyclohexane of bifunctional monomer EHUT were used, to which a fixed fraction of monofunctional chain stopper DBUT was added to reduce the viscosity.

When measuring surface forces in viscous solutions with AFM, the effect of hydrodynamic drag on the cantilever has to be taken into account. The hydrodynamic forces on the cantilever were measured both at large and small separations between the colloidal probe and the substrate surface. The presence of a depletion layer with a decreased viscosity causes slip at the surfaces, thereby dramatically decreasing the hydrodynamic forces. The experimental results can be described by assuming an apparent slip length, which is determined by the thickness of the depletion layer and the average viscosity in that layer with respect to the bulk viscosity. At sufficiently low scan velocities, the hydrodynamic drag upon approach of the surfaces effectively has a constant value until very small separations. This facilitates the direct measurement of

depletion forces.

Depletion forces were measured in EHUT solutions far above the overlap concentration, where the thickness of the depletion layer is expected to be approximately equal to the correlation length in the solution. The depletion layer thickness at these concentrations is approximately 10 nm, which is in agreement with previous measurements of the correlation length. The concentration dependence of the depletion layer thickness and the bulk osmotic pressure seems to be weaker than predicted by theory. This may be explained by the presence of a repulsive contribution to the measured force curve, caused by non-equilibrium effects such as hydrodynamic drag or entrapment of chains in the gap.

A suspension of stearylated silica spheres in these solutions phase separates at sufficiently high polymer concentrations. Phase separation becomes stronger with increasing EHUT concentration.

## References

- [1] P. Jenkins and M. Snowden. *Adv. Colloid Interface Sci.*, 68: 57–96, 1996.
- [2] R. Tuinier, R. Rieger, and C. G de Kruif. *Adv. Colloid Interface Sci.*, 103: 1–31, 2003.
- [3] E. Ten Grotenhuis, R. Tuinier, and C. G. de Kruif. *J. Dairy Sci.*, 86: 764–769, 2003.
- [4] D. F. K. Hughes, I. D. Robb, and P. J. Dowding. *Langmuir*, 15: 5227–5231, 1999.
- [5] C. W. Jones, J. C. Wang, F. A. Ferrone, R. W. Briehl, and M. S. Turner. *Faraday Discuss.*, 123: 221–236, 2003.
- [6] J-M. Lehn. *Supramolecular chemistry: concepts and perspectives*. VCH, Weinheim, 1995.
- [7] A. Ciferri, editor. *Supramolecular polymers*. Marcel Dekker, New York, 2000.
- [8] L. Brunsveld, B. J. B. Folmer, E. W. Meijer, and R. P. Sijbesma. *Chem. Rev.*, 101: 4071–4097, 2001.
- [9] R. F. M. Lange, M. Van Gorp, and E. W. Meijer. *J. Polym. Sci. A.*, 37: 3657–3670, 1999.
- [10] A. W. Bosman, L. Brunsveld, B. J. B. Folmer, R. P. Sijbesma, and E. W. Meijer. *Macromolec. Symp.*, 201: 143–154, 2003.

## References

---

- [11] J. van der Gucht, N. A. M. Besseling, and M. A. C. Stuart. *J. Am. Chem. Soc.*, 124: 6202–6205, 2002.
- [12] J. van der Gucht, N. A. M. Besseling, and G. J. Fleer. *J. Chem. Phys.*, 119: 8175–8188, 2003.
- [13] H. J. A. Zweistra and N. A. M. Besseling. *Phys. Rev. Lett.*, 96:078301, 2006.
- [14] J. van der Gucht, N. A. M. Besseling, W. Knoben, L. Bouteiller, and M. A. Cohen Stuart. *Phys. Rev. E*, 67:051106, 2003.
- [15] J. van der Gucht and N. A. M. Besseling. *J. Phys. Condens. Matter*, 15: 6627–6645, 2003.
- [16] P. Kekicheff, F. Nallet, and P. Richetti. *J. Physique II*, 4: 735–741, 1994.
- [17] H. J. Butt, B. Cappella, and M. Kappl. *Surf. Sci. Rep.*, 59: 1–152, 2005.
- [18] S. Boileau, L. Bouteiller, F. Lauprêtre, and F. Lortie. *New J. Chem.*, 24: 845–848, 2000.
- [19] F. Lortie, S. Boileau, L. Bouteiller, C. Chassenieux, B. Demé, G. Ducouret, M. Jalabert, F. Lauprêtre, and P. Terech. *Langmuir*, 18: 7218–7222, 2003.
- [20] A. Arnaud and L. Bouteiller. *Langmuir*, 20: 6858–6863, 2004.
- [21] F. Lortie, S. B. Boileau, L. Bouteiller, C. Chassenieux, and F. Lauprêtre. *Macromolecules*, 38: 5283–5287, 2005.
- [22] W. Knoben, N. A. M. Besseling, L. Bouteiller, and M. A. Cohen Stuart. *Phys. Chem. Chem. Phys.*, 7: 2390–2398, 2005.
- [23] W. Knoben, N. A. M. Besseling, and M. A. Cohen Stuart. *Macromolecules*, 39: 2643–2653, 2006.
- [24] W. Knoben, N. A. M. Besseling, and M. A. Cohen Stuart. *Phys. Rev. Lett.*, 97: 068301, 2006.
- [25] S. Asakura and F. Oosawa. *J. Chem. Phys.*, 22: 1255–1256, 1954.
- [26] S. Asakura and F. Oosawa. *J. Polym. Sci.*, 33: 183–192, 1958.
- [27] B. V. Derjaguin. *Kolloid Z.*, 69: 155–164, 1934.
- [28] J. Israelachvili. *Intermolecular and Surface Forces*. Academic Press, London, 2nd edn., 1991.
- [29] A. Milling and S. Biggs. *J. Colloid Interface Sci.*, 170: 604–606, 1995.

- 
- [30] W. K. Wijting, W. Knoben, N. A. M. Besseling, F. A. M. Leermakers, and M. A. Cohen Stuart. *Phys. Chem. Chem. Phys.*, 6: 4432–4439, 2004.
- [31] M. Fuchs and K. S. Schweizer. *Europhys. Lett.*, 51: 621–627, 2000.
- [32] M. Fuchs and K. S. Schweizer. *J. Phys.: Condens. Matter*, 14: R239–R269, 2002.
- [33] K-H. Lin, J. C. Crocker, A. C. Zeri, and A. G. Yodh. *Phys. Rev. Lett.*, 87: 088301, 2001.
- [34] Y.-L. Chen and K. S. Schweizer. *J. Phys. Chem. B*, 108: 6687–6696, 2004.
- [35] J. Lyklema. *Fundamentals of Interface and Colloid Science, volume V: Soft Colloids*. Elsevier Academic press, Amsterdam, 2005.
- [36] M. E. Cates and S. J. Candau. *J. Phys. Condens. Matter*, 2: 6869–6892, 1990.
- [37] P. G. de Gennes. *Scaling concepts in polymer physics*. Cornell University press, Ithaca, New York, 1979.
- [38] W. A. Ducker, T. J. Senden, and R. M. Pashley. *Nature*, 353: 239–241, 1991.
- [39] H. J. Keh and S. H. Chen. *Chem. Eng. Sci.*, 52: 1789–1805, 1997.
- [40] H. Brenner. *Chem. Eng. Sci.*, 16: 242–251, 1961.
- [41] O. I. Vinogradova. *Langmuir*, 11: 2213–2220, 1995.
- [42] N. V. Churaev, V. D. Sobolev, and A. N. Somov. *J. Colloid Interface Sci.*, 97: 574–581, 1984.
- [43] B. V. Derjaguin and N. V. Churaev. *Langmuir*, 3: 607–612, 1987.
- [44] R. Tuinier and T. Taniguchi. *J. Phys. Condens. Matter*, 17: L9–L14, 2005.
- [45] R. G. Horn, O. I. Vinogradova, M. E. Mackay, and N. Phan-Thien. *J. Chem. Phys.*, 112: 6424–6433, 2000.
- [46] A. K. van Helden, J. W. Jansen, and A. Vrij. *J. Colloid Interface Sci.*, 81: 354–368, 1981.
- [47] M. Giesbers. *PhD Thesis*. Wageningen University, the Netherlands, 2001.
- [48] J. L. Hutter and J. Bechhoefer. *Rev. Sci. Instrum.*, 64: 1868–1873, 1993.
- [49] J. van der Gucht, M. Lemmers, W. Knoben, N. A. M. Besseling, and M. P. Lettinga. *Phys. Rev. Lett.*, 97:108301, 2006.
-

## References

---

- [50] I. Bodnár and W. D. Oosterbaan. *J. Chem. Phys.*, 106: 7777–7780, 1997.
- [51] J. van der Gucht and N. A. M. Besseling. *Phys. Rev. E*, 65: 051801, 2002.
- [52] H. J. A. Zweistra, N. A. M. Besseling, and M. A. Cohen Stuart. *J. Phys. Chem. B*, 110: 18269–18634, 2006.

# 7

## Long range depletion forces induced by associating small molecules

### Abstract

In this paper, we report experimental observations of depletion interactions in solutions of a (hydrogen-bonded) reversible supramolecular polymer. Depletion forces were measured directly by Colloidal Probe Atomic Force Microscopy. The range of the depletion force is consistent with existing independent experimental data. The interaction can be tuned by adding monofunctional chain stoppers to the solution, a possibility which is unique to supramolecular polymers. The depletion force is shown to be strong enough to induce phase separation in a colloidal suspension.

## 7.1 Introduction

The presence of an interface generally perturbs the structure of liquids [1]. It may affect the density or the orientation of the molecules near the interface, and in the case of solutions also the local concentration. The perturbation extends into the liquid over a characteristic distance, which is usually determined by the size of the molecules. Free energy is stored in the perturbed zone, and when two interfaces approach each other to such a distance that their perturbation zones overlap, this gives rise to a force between the interfaces. These forces are known as 'structural forces' [2]. An example is the solvation (hydration) force between smooth surfaces in a pure liquid, which occurs as a result of the layering of molecules. Solvation forces are often oscillatory with a period given by the molecular diameter, and they decay over a few periods. In solutions, structural forces may also occur due to the solute. A well-known example is the depletion force in non-adsorbing polymer solutions [3, 4]. Depletion forces are of practical importance in many systems such as paints and food emulsions. They also play an important role in biological systems, where they have been studied in the context of for example bacterial aggregation and DNA compaction. The range of the depletion interaction does usually not exceed the size of the polymer chains. In this Letter, we focus on depletion forces in solutions of a special class of (small) molecules, namely those capable of associating to *reversible supramolecular polymers*. In contrast with the cases mentioned above, the forces in these solutions extend over many times the molecular size.

Reversible supramolecular polymers are chains of small molecules, held together by non-covalent interactions such as hydrogen bonding or metal-ligand complexation [5]. The reversibility of the bonds gives these polymers exceptional properties compared to their covalent counterparts. For example, the chain length distribution is not fixed, but depends on monomer concentration, temperature and other parameters and can thus easily be adjusted. Furthermore, reversible supramolecular polymers have faster dynamics than covalent ones owing to the continuous breaking and reformation of bonds [6–8], see also chapter 5.

A variety of applications in which the unique properties of supramolecular polymers are used are currently being developed [9]. Supramolecular polymers hold promise as 'intelligent' materials which respond to environmental conditions such as temperature, light or other stimuli [10]. In some respects, supramolecular polymers are similar to wormlike micelles [7], which are also long, non-covalent aggregates of small molecules. Applications of supramolecular polymers can therefore be expected in the same areas where wormlike micelles are used, such as the oil industry and cosmetics [11]. However, the bonds between the monomers in supramolecular polymers are much more

specific than those in wormlike micelles, and this offers additional possibilities to control their properties. Interesting examples are the use of specific ‘chain stoppers’ [8] (vide infra) which is also discussed in chapters 3 to 6, and the regulation of colloidal stability by supramolecular brushes [12], see also chapter 8.

To form linear chains, the monomers of a supramolecular polymer must be bifunctional: a monomer contains two binding groups. If we assume that there is a single association constant  $K$  (independent of the length of the chain to which a monomer binds) which determines the equilibrium between breaking and formation of bonds, the number average degree of polymerisation  $\langle N \rangle$  at an overall concentration  $c$  of bifunctional monomers is  $\langle N \rangle \approx 2\sqrt{Kc}$ . This equation holds if the chains are long, that is if  $Kc \gg 1$  (see chapter 4). The presence of more than two binding groups per monomer leads to the formation of branched chains and networks. Monomers with only one binding group can bind to a chain, but the chain cannot grow any further. These monofunctional monomers are known as ‘chain stoppers’, and they decrease the average chain length. If a fraction  $x$  of chain stoppers is present (defined as  $x = k/(c + k)$ , where  $k$  is the concentration of chain stoppers),  $\langle N \rangle$  is given by:

$$\langle N(x) \rangle \approx \frac{\langle N(0) \rangle}{(1 - x) + x\langle N(0) \rangle} \quad (7.1)$$

where  $\langle N(0) \rangle$  is the average degree of polymerisation without chain stoppers. At sufficiently high  $x$  and  $\langle N(0) \rangle$ ,  $\langle N(x) \rangle$  is proportional to  $1/x$  and independent of the overall monomer concentration.

Arrays of multiple hydrogen bonds display high association constants in apolar solvents and are useful building blocks for supramolecular polymerisation [13, 14]. Bis-urea 2,4-*bis*(2-ethylhexylureido)toluene (EHUT) forms long semiflexible supramolecular chains in apolar solvents by the cooperative formation of four hydrogen bonds between two consecutive monomers [15]. Monofunctional monomer 2,4-*bis*(dibutylureido)toluene (DBUT) can be used as a chain stopper for EHUT [8], see also chapters 3 to 6.

Despite the considerable interest in supramolecular polymers in recent years [5], few reports address the behavior of supramolecular polymers at interfaces. This is particularly true for depletion forces, which have only been treated theoretically [16, 17] (and references therein). Depletion forces can be observed experimentally by studying depletion interaction-induced phase separation of colloidal suspensions, but they can also be measured directly [4]. There are reports of the experimental observation of depletion forces induced by covalent polymers, but also by spherical [18] and wormlike [19] micelles. In this Letter, we report the first experimental observations of depletion forces in reversible supramolecular polymer solutions, both by direct measurement by means of Colloidal Probe Atomic Force Microscopy (CP-AFM) and by

depletion interaction-induced phase separation.

## 7.2 Theoretical background

Depletion forces were analyzed quantitatively for the first time by Oosawa and Asakura [20]. They argued that the polymer concentration near a non-adsorbing wall is lower than in the bulk solution, due to the loss of entropy a polymer suffers when it is close to the surface. The layer with a reduced polymer concentration is called the depletion layer. When two particles approach each other to such a distance that their depletion layers overlap, there is an osmotic pressure difference between the bulk solution and the gap separating the surfaces, which pushes the surfaces together. Let us assume that the polymer concentration is zero within a distance  $\delta$  (the depletion layer thickness) from the surface, and equal to the bulk value at distances  $\geq \delta$ . In that case, the osmotic pressure difference  $\Delta\Pi$  between the depletion layer and the bulk solution simply equals the bulk osmotic pressure ( $\Pi_{bulk}$ ). If there is a gap of width  $h$  between the surfaces, the depletion layers overlap if  $h < 2\delta$ . The overlap volume  $\Delta V$  depends on  $h$  and is determined by the geometry of the surfaces. The depletion free energy  $G_{dep}$  is given by  $G_{dep} = -\Delta V \Delta\Pi$ . Differentiating  $G_{dep}$  with respect to  $h$  gives the depletion force  $F_{dep}$ . For a spherical particle with radius  $R$  and a planar surface at separations  $h \ll R$ , the typical geometry in CP-AFM experiments, a good approximation of the depletion force at small separations ( $h \lesssim 1.5\delta$ ) is given by [19]:

$$F_{dep}(h) = \begin{cases} -2\pi R(2\delta - h)\Pi_{bulk} & \text{if } 0 < h \leq 2\delta \\ 0 & \text{if } h > 2\delta \end{cases} \quad (7.2)$$

Using the Derjaguin approximation [2], the force can be converted into the interaction free energy per unit area between two planar surfaces of area  $A$ :  $F_{dep}/2\pi R = G_{dep}/A$ . In dilute solutions, the depletion layer thickness is approximately equal to the radius of gyration  $R_g$  of the polymer, and the osmotic pressure is given by Van 't Hoff's law. Note that for supramolecular polymers (without chain stoppers), the average degree of polymerisation increases with the overall monomer concentration. This implies that the concentration of chains is not proportional to the overall monomer concentration, as is the case for covalent polymers, but to  $c^{0.5}$ . In semidilute solutions (above the overlap concentration), the polymers form a transient network with an average mesh size  $\xi$ , the correlation length. This length only depends on the overall concentration, and not on the length of the individual chains. Hence, when considering supramolecular polymers,  $\xi$  is not affected by the concentration dependence of  $\langle N \rangle$ . In this regime,  $\delta \approx \xi$ , and also the osmotic pressure is determined by  $\xi$ :  $\Pi_{bulk} \sim \xi^{-3}$  [17, 19].

## 7.3 Experimental

In CP-AFM experiments, a colloidal sphere is firmly attached to an AFM cantilever [21]. The cantilever with the probe is placed above a planar surface (substrate), and the distance between the probe particle and the substrate is varied. By measuring the deflection of the cantilever, the interaction force between the colloidal probe and the substrate as a function of the separation distance can be calculated. In our experiments silica surfaces were used, coated with stearyl alcohol ( $\text{SiO}_2\text{-C}_{18}$ ) [22, 23], with cyclohexane as the solvent. The Van der Waals interaction in this system is negligibly small due to the matched refractive indices of the materials. Therefore, only hard-wall interactions are present between the surfaces in the pure solvent. The experimental procedure was previously described in detail by Wijting *et al.* [23]. The spring constant of the cantilever was determined by the thermal noise method [24] to be  $0.075 \pm 0.05$  N/m. Force curves were measured using small scan ranges (50–150 nm) and low scan velocities (10–50 nm/s). Note that for all separations used in our experiments,  $h \ll R$  and we may therefore use equation 7.2 to fit our experimental data at separations  $\lesssim 1.5\delta$ .

## 7.4 Results and discussion

First, it was checked that EHUT does not adsorb to the  $\text{SiO}_2\text{-C}_{18}$  surfaces. There was no measurable decrease in EHUT concentration (measured by UV absorption) upon the addition of  $\text{SiO}_2\text{-C}_{18}$  particles to an EHUT solution, which indicates that EHUT does indeed not adsorb to the particles. Also previous experiments showed no indication of any adsorption [25]. A typical force curve in pure cyclohexane is shown in figure 7.1 (inset). Even though the Van der Waals forces between  $\text{SiO}_2\text{-C}_{18}$  surfaces in cyclohexane are very small, perfect hard-wall interactions between a colloidal probe and a planar substrate are usually not found in CP-AFM experiments. This is generally explained by roughness of the surfaces. For (stearylated) silica, this roughness is typically a few nm. The force curve for an EHUT/DBUT solution (100 g/l EHUT,  $x=0.10$ ) is also shown in figure 7.1. The chain stopper was added to decrease the viscosity of the solution to such an extent that it could be injected into the AFM liquid cell. At the EHUT concentration and stopper fraction used in this experiment, the solution is still highly viscous (5 Pa s, over 5000 times the solvent viscosity). This indicates that the solution is far above the overlap concentration. Hence, the depletion layer thickness and the osmotic pressure are determined by the mesh size of the transient polymer network. An attractive interaction is clearly visible in the force curve. A fit to equation 7.2 using the data at separations between 3 and 20 nm is shown in figure 7.1 as the solid line. From the slope of

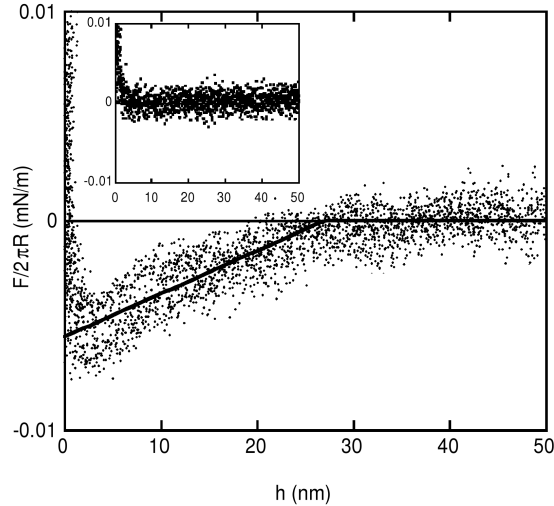


Figure 7.1: Normalized interaction force between  $\text{SiO}_2\text{-C}_{18}$  surfaces in a 100 g/l EHUT solution containing DBUT ( $x = 0.10$ ) in cyclohexane. Eight force curves are plotted. The line is a fit to equation 7.2. Inset: interaction in pure cyclohexane.

the fitted line and the intersection with the abscissa, values of  $\Pi_{bulk}$  and  $\delta$  were obtained.

The attraction starts at a separation of  $26 \pm 2$  nm, indicating that the depletion layer thickness is  $13 \pm 2$  nm. Previous light scattering experiments showed that the correlation length in the semidilute regime follows the scaling law  $\xi = 120c^{-0.5}$ , see chapter 4. If we apply this relation and assume that  $\delta = \xi$ , the depletion layer thickness in the present experiment ( $[\text{EHUT}] = 100$  g/l) should be 12 nm. We conclude that the measured depletion layer thickness is in good agreement with the light scattering results. The fitted line in figure 7.1 has a slope of  $230 \pm 70$  N/m<sup>2</sup>. Unfortunately, we have no independent measure of the osmotic pressure to confirm this value.

Figure 7.2 shows  $\delta$  for a number of stopper fractions, ranging from 0.10 to 0.40. By increasing the amount of chain stoppers, the average degree of polymerisation  $\langle N \rangle$  is decreased, as is the solution viscosity. As long as the solution remains semidilute, this will not affect  $\xi$ , and therefore also the range of the depletion interaction is expected to be constant. On the other hand, if  $x$  is sufficiently high, the chains become so short that they do not overlap anymore and the solution passes from the semidilute to the dilute regime. In that case,  $\delta$  is determined by the (average) size of the chains, which is a function

of  $x$  (equation 7.1). The ‘overlap stopper fraction’ where this crossover occurs is denoted by  $x^*$ . The depletion interaction can thus be tuned by adding monofunctional monomers to the solution. This is only possible owing to the reversibility and specificity of the interactions between the monomers, and this effect can therefore never occur in covalent polymers, nor in wormlike micellar systems. Figure 7.2 shows that  $\delta$  can indeed be changed by the addition of

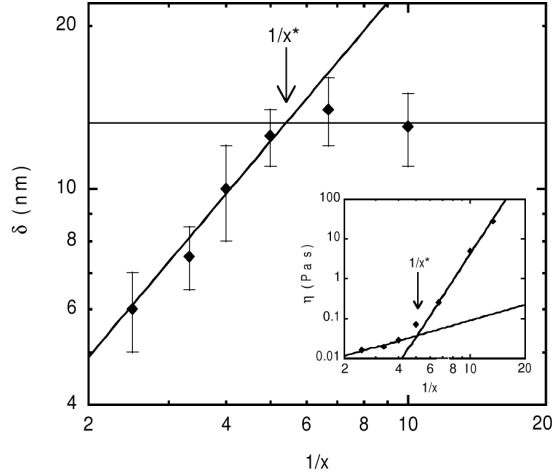


Figure 7.2: Depletion layer thickness  $\delta$  as a function of the inverse stopper fraction  $1/x$ . The inverse overlap fraction  $1/x^*$  is denoted in the figure. Inset: viscosity of the same solutions.

chain stoppers. Data are plotted as a function of  $1/x$ , since  $\langle N \rangle$  is predicted to be proportional to this quantity at sufficiently high  $x$  (equation 7.1). At stopper fractions lower than approximately 0.20 ( $1/x > 5$ ),  $\delta$  is constant within the experimental error, as denoted by the horizontal line at  $\delta = 13$  nm. When  $x$  is increased further ( $1/x \leq 5$ ), a clear decrease in  $\delta$  is observed, indicating a crossover to the dilute regime. The line corresponds to  $\delta = 2.4/x$ . EHUT chains are semiflexible, with a persistence length  $\geq 200$  nm, see chapter 4. On the length scale of  $\delta$ , the chains can therefore be regarded as rigid rods, for which  $\delta \approx R_g \sim \langle N \rangle$  (in the dilute regime). The proportionality of  $\delta$  with  $1/x$  indicates that  $\langle N \rangle \sim 1/x$ , which is indeed expected for high stopper fractions (equation 7.1). From the intersection of the lines, the overlap stopper fraction can be found:  $x^* \approx 0.18$ .

Beside the transition of  $\delta$  at  $x^*$ , also the solution viscosity is expected to show a crossover from a relatively weak (power law) dependence on  $x$  in dilute solutions to a much stronger dependence in the semidilute regime.

## 7.5. Concluding remarks

---

Therefore, the viscosity of the solutions was also measured, as shown in figure 7.2 (inset). The viscosity indeed starts to increase steeply at  $x \approx 0.20$ , whereas the dependence at higher stopper fractions is much weaker. This observation also leads to an estimate of  $x^*$  of approximately 0.20, in agreement with the value obtained from the measured depletion layer thickness.

It is interesting to investigate if the depletion forces caused by EHUT are strong enough to induce phase separation in a colloidal suspension. To study this, equal volumes of an EHUT/DBUT solution and a suspension of  $\text{SiO}_2\text{-C}_{18}$  particles ( $R = 14$  nm, 200 g/l) in cyclohexane were mixed in glass tubes. After homogenization, the suspensions were allowed to equilibrate. A suspension of particles in pure cyclohexane is shown in figure 7.3a. It consists of a single phase and scatters homogeneously. Figure 7.3b shows a suspension with the

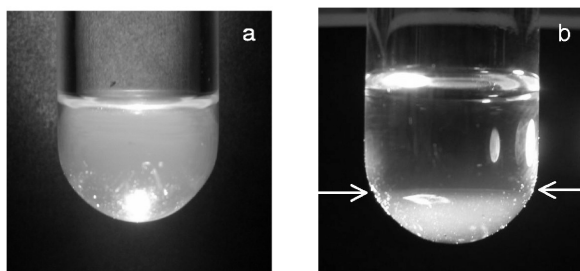


Figure 7.3: Tubes containing suspensions of  $\text{SiO}_2\text{-C}_{18}$  spheres ( $R = 14$  nm) in a: pure cyclohexane; b: 100 g/l EHUT,  $x = 0.10$ . Arrows indicate the position of the interface between the two phases.

same particle concentration in a solution of 100 g/l EHUT with added DBUT ( $x = 0.10$ ). The suspension has separated into a particle-rich bottom phase (which has the highest turbidity) and a polymer-rich top phase. The phases are separated by a mirror-like interface (not visible on the photographs). This result demonstrates that the depletion forces are strong enough to induce phase separation.

## 7.5 Concluding remarks

In summary, depletion interactions in solutions of a hydrogen-bonded reversible supramolecular polymer (bifunctional monomer EHUT and monofunctional chain stopper DBUT) were studied experimentally for the first time. This was done by directly measuring the depletion force by means of CP-AFM. The thickness of the depletion layer was analysed, and the results are consis-

tent with previous light scattering measurements of the correlation length. It is demonstrated that the depletion interaction can be tuned by the addition of chain stoppers. This effect is unique for reversible supramolecular polymers. It is also shown that the depletion forces induced by supramolecular polymers can give rise to phase separation in a colloidal suspension.

## References

- [1] J. Lyklema. *Fundamentals of interface and colloid science Vol. II: Solid-liquid interfaces*. Academic press, London, 1995.
- [2] J. N. Israelachvili. *Intermolecular and surface forces*. Academic press, London, 2nd edition, 1991.
- [3] P. Jenkins and M. Snowden. *Adv. Colloid Interface Sci.*, 68, 1996.
- [4] R. Tuinier, J. Rieger, and C. G. de Kruif. *Adv. Colloid Interface Sci.*, 103:1–31, 2003.
- [5] A. Ciferri, editor. *Supramolecular polymers*. Marcel Dekker, New York, 2nd edition, 2005.
- [6] R. F. M. Lange, M. Van Gorp, and E. W. Meijer. *J. Polym. Sci. A: Polym. Chem.*, 37:3657–3670, 1999.
- [7] M.E. Cates and S.J. Candau. *J. Phys.: Condens. Matter*, 2:6869–6892, 1990.
- [8] F. Lortie, S. B. Boileau, L. Bouteiller, C. Chassenieux, and F. Lauprêtre. *Macromolecules*, 38:5283–5287, 2005.
- [9] A. W. Bosman, R. P. Sijbesma, and E. W. Meijer. *Materials Today*, 7:34–39, 2004.
- [10] S. J. Rowan and J. B. Beck. *Faraday Discuss.*, 128:43–53, 2005.
- [11] J. Yang. *Curr. Opin. Colloid Interface Sci.*, 7:276–281, 2002.
- [12] J. van der Gucht, N. A. M. Besseling, and M. A. C. Stuart. *J. Am. Chem. Soc.*, 124:6202–6205, 2002.
- [13] R. P. Sijbesma, F. H. Beijer, L. Brunsveld, B. J. B. Folmer, J. H. K. K. Hirschberg, R. F. M. Lange, J. K. L. Lowe, and E. W. Meijer. *Science*, 278:1601–1604, 1997.
- [14] D. C. Sherrington and K. A. Taskinen. *Chem. Soc. Rev.*, 30:83–93, 2001.

## References

---

- [15] F. Lortie, S. Boileau, L. Bouteiller, C. Chassenieux, B. Demé, G. Ducouret, M. Jalabert, F. Lauprêtre, and P. Terech. *Langmuir*, 18:7218–7222, 2003.
- [16] J. van der Gucht, N. A. M. Besseling, and G. J. Fleer. *J. Chem. Phys.*, 119:8175–8188, 2003.
- [17] J. van der Gucht and N. A. M. Besseling. *J. Phys. Condens. Matter*, 15:6627–6645, 2003.
- [18] P. Richetti and P. Kékicheff. *Phys. Rev. Lett.*, 68:1951–1954, 1992.
- [19] P. Kékicheff, F. Nallet, and P. Richetti. *J. Phys. II France*, 4:735–741, 1994.
- [20] S. Asakura and F. Oosawa. *J. Chem. Phys.*, 22:1255–1256, 1954.
- [21] W. A. Ducker, T. J. Senden, and R. M. Pashley. *Nature*, 353:239–241, 1991.
- [22] A. K. van Helden, J. W. Jansen, and A. Vrij. *J. Colloid Interface Sci.*, 81:354–368, 1981.
- [23] W. K. Wijting, W. Knoben, N. A. M. Besseling, F. A. M. Leermakers, and M. A. Cohen Stuart. *Phys. Chem. Chem. Phys.*, 6:4432–4439, 2004.
- [24] J. L. Hutter and J. Bechhoefer. *Rev. Sci. Instrum.*, 64:1868–1873, 1993.
- [25] J. van der Gucht, N. A. M. Besseling, W. Knoben, L. Bouteiller, and M. A. C. Stuart. *Phys. Rev. E*, 67:051106, 2003.

# 8

## Functionalisation of silica surfaces with 2,7-diamido-1,8-naphthyridines

### Abstract

The behavior of supramolecular polymers at surfaces, and especially that of end-attached supramolecular 'brushes', is a very interesting subject with potential applications. Supramolecular polymers based on the UPy- and Napy-units would be a good experimental model system. In this paper, functionalisation of silica surfaces with 2,7-diamido-1,8-naphthyridines (Napys) is reported. A trimethoxysilyl-terminated Napy is synthesized and used for functionalisation of strips of an oxidized silica wafer. Characterization of the surface by contact angle measurement, ellipsometry and fluorescence spectroscopy demonstrate that Napy is indeed bound to the surface. Furthermore, the functionalised surface is capable of reversible and specific binding of ureido-pyrimidinones (UPys). Unfortunately, the trimethoxysilyl-Napy is susceptible to degradation. Preliminary experiments towards a more stable Napy-derivative are reported.

### 8.1 Introduction

Silica (silicon dioxide,  $\text{SiO}_2$ ) is one of the most abundant chemical compounds on earth. Beside its natural occurrence, silica particles can also be manufactured in a wide variety of types [1]. Depending on the preparation method and conditions, particles with a virtually unlimited diversity in shape, size, porosity can be made. It is therefore not surprising that silica is used in countless applications. To name just a few, silica particles are used as stationary phase in various types of chromatography, as adsorbents, absorbents (desiccants), reinforcing agents, flow enhancers and viscosity modifiers. The range of applications can be increased even further by attaching a functional molecule to the silica surface [2, 3]. The structural and mechanical properties of the silica can then be combined with the specific chemical or physical properties of the bound molecules. In principle, any molecule can be bound to the surface if it can be connected to a suitable coupling agent. The most widely used coupling agents are organosilanes, *via* which many different types of molecules have been attached to silica surfaces.

Not only small molecules can be attached to silica surfaces, polymers can also be used for functionalisation [4, 5]. If the grafting density (the number of attached chains per unit area) is sufficiently high, the chains are forced to stretch normal to the surface. An array of such stretched polymer chains is called a polymer 'brush'. Polymer brushes were originally designed to enhance colloidal stability. When two brush-covered colloids approach each other to such a distance that their brush layers overlap, the increased osmotic pressure in the gap between the particles gives rise to a repulsive force which prevents the particles from coagulating. Later, polymer brushes were also found to control or prevent the adsorption of undesired material (e.g. proteins), and to change the wetting or adhesion properties of surfaces.

A relatively recent development in polymer science is the emergence of so-called *reversible supramolecular* polymers [6–8]. In contrast to 'normal' polymers, the monomers of supramolecular polymers are not connected by covalent bonds. Instead, supramolecular polymers are chains of individual (small) molecules, held together by reversible secondary interactions such as metal-ligand complexation or hydrogen bonding. The reversibility of the bonds allows for the chains to break and recombine, and for a continuous exchange of free and bound monomers.

As a result of this equilibrium, reversible supramolecular polymers are highly dynamic materials. The (average) degree of polydispersity is not fixed, but depends on the overall monomer concentration, temperature and other parameters. Reversible supramolecular polymers also have faster dynamics than covalent polymers, because the breaking and recombination of chains provides an additional mechanism for stress relaxation [9], see also chapters

3 and 5. Because of these properties, supramolecular polymers hold great promise as easily processable [10] and ‘intelligent’ or ‘self-healing’ materials which respond to external stimuli [11–13]. The rheological properties and fast dynamics may also be of use in applications such as paints or inkjet printing, which require the flow properties of liquids to change rapidly [14].

Beside the different bulk and solution properties, supramolecular polymers at surfaces are also expected to display some special features compared to their covalent counterparts. For example, it was recently demonstrated that the range and strength of the depletion interaction, induced by non-adsorbing supramolecular polymers, can be adjusted *in situ* by varying the length of the supramolecular chains, as described in chapters 6 and 7. This effect can never occur in covalent polymers, since these have a fixed chain length. This result demonstrates that also the interfacial properties of supramolecular polymers are highly dynamic, and can be easily adjusted. Theoretical studies show that also adsorbing supramolecular polymers have interesting properties, which set them apart from covalent ones [15, 16]. The formation of supramolecular brushes has also been the subject of theoretical work [15, 17], and of some experimental efforts as well [18–24]. It is predicted that the interaction between surfaces, both covered by a supramolecular brush, depends on the symmetry of the monomers [17]. Symmetric monomers (BB-type, where B is a self-complementary binding group) give rise to attractive forces, whereas asymmetric acceptor-donor monomers (AD-type) introduce directionality in the chains, which leads to a repulsive interaction.

Perhaps the most widely used supramolecular polymers are those based on the 2-ureido-4-[1H]-pyrimidinone (UPy) moiety (figure 8.1a) [25]. This unit has a high dimerisation constant in apolar solvents, owing to the simultaneous formation of four hydrogen bonds in a self-complementary donor-donor-acceptor-acceptor (*ddaa*) array. By attaching two UPy groups to a spacer, bifunctional BB-type monomers are formed which can associate to supramolecular polymer chains. The UPy unit can also exist in a different tautomeric form, in which the hydrogen bonding groups form an *adda* array. In this tautomeric form, it can selectively form heterodimers with the complementary *daad* hydrogen bonding array of 2,7-diamido-1,8-naphthyridines (Napy, figure 8.1b) [26]. Mixtures of bifunctional monomers containing two UPys and monomers containing two Napy can thus form alternating block copolymers [27]. Recently, the synthesis of AD-type monomers, containing one UPy group and one Napy group, was also reported [28]. The association of these monomers introduces directionality in the supramolecular chains. The different types of supramolecular polymers based on combination of UPy- and Napy-units are schematically depicted in figure 8.1c.

The UPy–Napy system is well-suited to test the theoretical predictions about the surface behavior of (non)-directional supramolecular chains exper-

## 8.1. Introduction

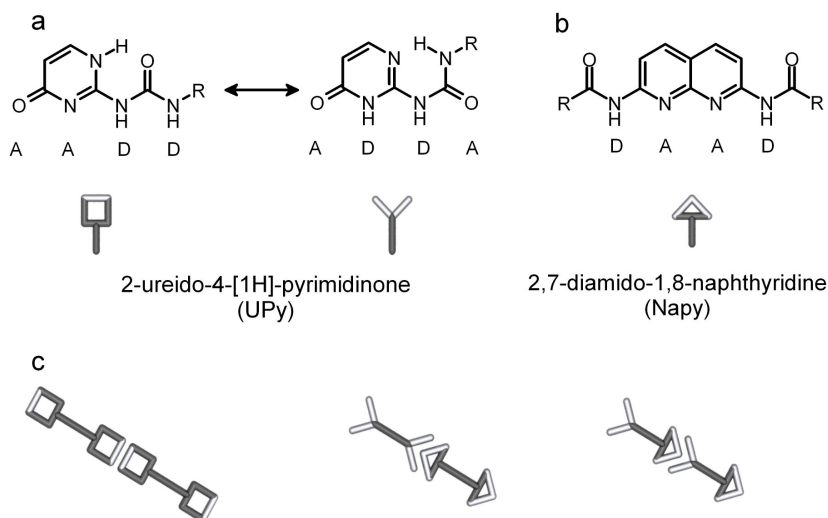


Figure 8.1: Supramolecular polymers from UPy and Napy units. a: tautomeric forms of UPy with an *aadd* and *adda* hydrogen bonding array; b: *daad* hydrogen bonding array of Napy; c: possible supramolecular polymerisations with UPy and Napy groups: homopolymer from self-complementary (BB type) bis-UPy monomers (left), alternating block copolymer from bis-UPy and bis-Napy monomers (middle), directional homopolymer from AD-type UPy-Napy monomers.

imentally since both symmetric, non-directional UPy-UPy and Napy-Napy monomers as well as asymmetric, directional UPy-Napy monomers can be synthesized. To enable the growth of a supramolecular brush from a surface, the surface has to be functionalised with either a UPy or a Napy group (see figure 8.2). Functionalisation of gold [18–20] and silica [29] surfaces with UPy molecules has been reported. However, an end-attached supramolecular polymer chain consisting of UPy-UPy or UPy-Napy monomers, starting from a UPy-functionalised surface (figures 8.2a and b), will always have a UPy as the terminal group. Due to the self-complementarity of the UPy unit, these chains will have a strong tendency to form loops at the surface, instead of extending into the solution and forming a true brush. The Napy unit is more suitable for surface functionalisation. A chain of UPy-UPy monomers, starting from a Napy-functionalised surface (figure 8.2c) is always terminated by a UPy group and will therefore tend to form loops. On the other hand, an end-attached chain of UPy-Napy monomers growing from a Napy-covered surface is terminated

by Napy groups, which do not have a high affinity for the Napy groups on the surface and a supramolecular brush can be formed (figure 8.2d). Thus, by using a Napy-functionalised surface, supramolecular polymers consisting of both directional UPy–Napy and non-directional UPy–UPy monomers can be end-attached to the surface. This enables the experimental investigation of the theoretically predicted differences in surface forces, induced by these supramolecular chains [17].

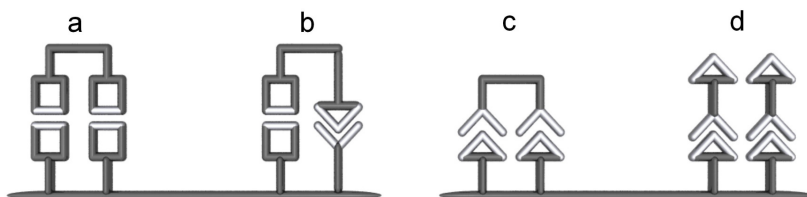


Figure 8.2: Supramolecular polymers at UPy- and Napy-functionalised surfaces. a: UPy–UPy polymer at a UPy-surface; b: UPy–Napy polymer at a UPy-surface; c: UPy–UPy polymer at a Napy-surface; d: UPy–Napy polymer at a Napy-surface.

Beside serving as a starting point for the formation of a supramolecular brush, Napy-functionalised surfaces could also be used as a highly selective adsorbent, which specifically binds molecules containing a UPy-group. Such selective materials may for example be used in chromatographic applications [30].

In this paper, we report on the synthesis of Napy derivatives, designed to be used for the functionalisation of silica surfaces. The most promising molecules were used for the functionalisation of strips of oxidized silicon wafer. The results of the surface modification and some preliminary characterisation of the functionalised surface are presented.

## 8.2 Experimental

### 8.2.1 Synthesis

#### General methods

$^1\text{H}$ - and  $^{13}\text{C}$ -NMR spectra were recorded on a Varian Gemini 300 spectrometer. Chemical shifts are reported in ppm relative to a tetramethylsilane standard. Peak multiplicities are denoted as *s* (singlet), *d* (doublet), *t* (triplet), *q* (quadruplet), *m* (multiplet) or *br* (broadened peak). MALDI-TOF-MS spectra were

## 8.2. Experimental

---

recorded on a PerSeptive Biosystems Voyager-DE-PRO instrument using an  $\alpha$ -cyano-4-hydroxycinnamic acid matrix. A Perkin Elmer Spectrum One FT-IR instrument equipped with a Universal ATR sampling Accessory was used for recording infrared spectra. Commercial reagents and solvents were used as received.

### 5-[7-(2-Ethyl-hexanoylamino)-[1,8]naphthyridin-2-ylcarbamoyl]-pentanoic acid methyl ester (1)

Starting compound 2-Ethyl-hexanoic acid (7-chloro-[1,8]naphthyridin-2-yl)-amide (2) was synthesized according to literature procedure [31]. To 155 mg (0.5 mmol) of 2 were added 96 mg (0.6 mmol) of 5-Carbamoyl-pentanoic acid methyl ester, 98 mg (0.7 mmol) of  $K_2CO_3$ , 1.7 mg (1.5 mol%) of  $Pd(OAc)_2$  and 10.6 mg (3.6 mol%) of Xantphos. The reaction mixture was dissolved in 2 ml of dry 1,4-dioxane. After stirring under  $N_2$  atmosphere at 100 °C under reflux for 20 h, the mixture was cooled, filtered over diatomaceous and evaporated in vacuo. The product was purified by column chromatography (silica gel, methanol/chloroform 1:50 v/v). After evaporation of the solvent, 114 mg (53%) of 1 was obtained.  $^1H$ -NMR ( $CDCl_3$ ):  $\delta$ = 9.78 (br, 1H), 9.16 (br, 1H), 8.52 (d, 1H,  $J=9$  Hz), 8.41 (d, 1H,  $J=9$  Hz), 8.15 (d, 1H,  $J=9$  Hz), 8.12 (d, 1H,  $J=9$  Hz), 3.66 (s, 3H), 2.45 (t, 2H,  $J=7$  Hz), 2.29 (t, 2H,  $J=4$  Hz), 2.25 (m, 1H), 1.54-1.73 (m, 8H), 1.24-1.27 (m, 4H), 0.81-0.94 (m, 6H) ppm;  $^{13}C$ -NMR ( $CDCl_3$ ):  $\delta$ = 175.7, 173.7, 172.1, 154.28, 154.1, 153.4, 139.0, 138.9, 118.1, 113.8, 113.7, 51.4, 50.2, 36.8, 33.4, 32.1, 29.5, 29.1, 25.7, 24.1, 22.6, 13.7, 11.8 ppm; MALDI-TOF-MS: (m/z) calculated: 428.24; observed: 429.19 ( $M+H^+$ ), 451.17 ( $M+Na^+$ ); FT-IR (ATR):  $\nu$ = 3304, 2957, 2931, 2873, 1734, 1688, 1607, 1583, 1540, 1500, 1460, 1436, 1381, 1311, 1282, 1219, 1169, 1134, 910, 854, 802  $cm^{-1}$ .

### 5-[7-(2-Ethyl-hexanoylamino)-[1,8]naphthyridin-2-ylcarbamoyl]-pentanoic acid (3)

To 59 mg (0.14 mmol) of 1, was added exactly one equivalent of  $LiOH \cdot H_2O$  (5.88 mg). The mixture was dissolved in 3 ml methanol/ $H_2O$  (3:1 v/v) to which was added 2 ml of 1,4-dioxane, and stirred at room temperature for 5 h. The solution was neutralized by the addition of 1 M HCl, after which the solvent was evaporated under vacuo and 37 mg (65%) of product was obtained.  $^1H$ -NMR ( $CDCl_3$ ):  $\delta$ = 9.05-9.50 (br, 2H), 8.25-8.70 (m, 6H), 7.88-8.05 (m, 4H), 3.66 (s, 3H), 2.45 (t, 2H,  $J=7$  Hz), 2.29 (t, 2H,  $J=4$  Hz), 2.25 (m, 1H), 1.54-1.73 (m, 8H), 1.24-1.27 (m, 4H), 0.81-0.94 (m, 6H) ppm; MALDI-TOF-MS: (m/z) calculated: 414.23; observed: 287.32, 415.38 ( $M+H^+$ ), 429.40; FT-IR (ATR):  $\nu$ = 3600-3050, 2930, 2860, 1702, 1667, 1621, 1590, 1551, 1531, 1494, 1458, 1389, 1299, 1262, 1230, 1170, 1132, 946, 909, 853, 803  $cm^{-1}$ .

### 11-triethoxysilanyl-undecanoic acid amide (4)

93 mg (0.50 mmol) of Undec-10-enoic acid amide was dissolved in 2 ml chloroform, and 10 equivalents (838 mg) of triethoxysilane and 1 mol% (1 mg) of PtO<sub>2</sub> were added to the solution. The reaction mixture was stirred at reflux temperature (65 °C) for 40 h. The solvent and the excess amount of silane were evaporated under vacuo at 80 °C. <sup>1</sup>H-NMR (CDCl<sub>3</sub>): δ= 5.80 (br, 1H), 5.50 (br, 1H), 3.80-3.85 (m, 6H), 2.22 (t, 2H, J=3 Hz), 1.63 (t, 2H, J=3 Hz), 1.20-1.30 (m, 23H), 0.88 (t, 2H, J=7 Hz) ppm; <sup>13</sup>C-NMR (CDCl<sub>3</sub>): δ= 175.7, 77.1, 35.8, 31.7, 29.4, 29.3, 29.2 (2C), 29.1, 25.4, 22.5, 14.0 ppm; MALDI-TOF-MS: (m/z) calculated: 347.25; observed: 326.45, 480.59.

#### **11-(3-trimethoxysilylanyl-propylsulfanyl)-undecanoic acid [7-(2-ethyl-hexanoylamino)-[1,8]naphthyridin-2-yl]-amide (5)**

Starting compound Undec-10-enoic acid [7-(2-ethyl-hexanoylamino)-[1,8]naphthyridin-2-yl]-amide (**6**) was synthesized according to literature procedure [31]. 125 mg (0.28 mmol) of **6** was dissolved in 3 ml tetrachloromethane together with 275 mg (five equivalents) of 3-trimethoxysilylanyl-propane-1-thiol and 14 mg of AIBN. The reaction mixture was stirred at reflux temperature (80 °C) for 24 h. The product was repeatedly precipitated from cold pentane (4 °C) to remove the excess of thiol. The product was obtained in 67% yield (119 mg). <sup>1</sup>H-NMR (CDCl<sub>3</sub>): δ= 8.40-8.60 (m, 2H), 8.05-8.20 (m, 2H), 3.57 (s, 9H), 2.55 (m, 6H), 1.10-1.90 (m, 26H), 0.74-1.00 (m, 8H) ppm; <sup>13</sup>C-NMR (CDCl<sub>3</sub>): δ= 176.4, 173.7, 154.0, 139.7, 117.4, 113.8, 112.0, 77.133, 50.5, 50.2, 37.6, 35.9, 34.9, 32.0, 29.6, 29.2, 27.4, 25.7, 25.0, 22.6, 13.8, 11.8 ppm; MALDI-TOF-MS: (m/z) calculated: 648.99; observed: 649.17 (M<sup>+</sup>); FT-IR (ATR): ν= 3600-3100, 2926, 2854, 1688, 1608, 1535, 1500, 1459, 1386, 1311, 1285, 1172, 1134, 1081, 1020, 911, 854, 802 cm<sup>-1</sup>.

#### **11-(3-trimethoxysilylanyl-propylsulfanyl)-undecanoic acid (7-acetylamino-[1,8]naphthyridin-2-yl)-amide (7)**

The same procedure as in the synthesis of **5** was followed, starting from 265 mg (0.41 mmol) of Undec-10-enoic acid (7-acetylamino-[1,8]naphthyridin-2-yl)-amide (**8**) [31], 730 mg of 3-trimethoxysilylanyl-propane-1-thiol and 26 mg of AIBN. The reaction was done under Ar atmosphere. After completion of the reaction and evaporation of the solvent, the mixture was distilled in vacuo (Kugelrohr, < 0.1 mbar, 120 °C, 3 h) to remove the excess thiol. The product was subsequently precipitated from pentane in a yield of 202 mg (50%) and stored under Ar. <sup>1</sup>H-NMR (CDCl<sub>3</sub>): δ= 10.09 (br, 1H), 9.64 (br, 1H), 8.45 (q, 2H, J=9 Hz), 8.07 (d, 2H, J=8 Hz), 3.57 (s, 9H), 2.70 (m, 2H), 2.42-2.54 (m, 4H), 2.22 (s, 3H), 1.50-1.81 (m, 6H), 1.22 (m, 12H), 0.76 (t, 2H, J=8 Hz) ppm; <sup>13</sup>C-NMR (CDCl<sub>3</sub>): δ= 172.9, 170.0, 154.3 (2C), 153.0, 139.0, 117.8, 113.7, 113.6, 50.4, 37.5, 34.9, 31.8, 29.6, 29.3, 29.2, 29.1, 29.0, 28.9, 28.8, 25.0, 24.7, 22.9, 8.4 ppm.

## 8.2. Experimental

---

### 2-Ethyl-hexanoic acid (7-4-[3-(3-triethoxysilylanyl-propyl)-ureido]-phenyl-amino-[1,8]naphthyridin-2-yl)-amide (9)

Starting compound 2-Ethyl-hexanoic acid [7-(4-amino-phenylamino)-[1,8]naphthyridin-2-yl]-amide (10) was synthesized according to literature procedure [32]. 75 mg (0.20 mmol) of 10 and 75 mg (0.30 mmol) of 3-Isocyanato-triethoxypropyl-silane were dissolved in dry THF (1 ml) and stirred under reflux (70 °C) for 24 h. A small amount of DMAP was added to the reaction mixture. After evaporation of the solvent, the product was precipitated from hexane. After filtration, 59 mg (46%) of product was obtained. FT-IR (ATR):  $\nu = 3400\text{-}3000, 2968, 2929, 2875, 1657, 1604, 1548, 1497, 1441, 1406, 1387, 1319, 1282, 1229, 1167, 1141, 1101, 1075, 956, 919, 845, 801\text{ cm}^{-1}$ .

### 8.2.2 Functionalisation and characterisation of SiO<sub>2</sub> surfaces

Pieces of 1×2 cm were cut from a silicon wafer bearing a natural oxide layer. The strips were cleaned by immersing them in piranha solution (H<sub>2</sub>O<sub>2</sub>/H<sub>2</sub>SO<sub>4</sub> 1:2 v/v). 5 mg of trimethoxysilyl-Napy 7 was dissolved in 4 ml of 1,4-dioxane. A clean strip was placed in a Schlenk tube and immersed in the Napy-solution. The mixture was refluxed (103 °C) overnight under Ar atmosphere. After the strip was thoroughly washed with chloroform and pentane, it was placed overnight in pure hexamethyldisilazane (HMDS) at reflux temperature (127 °C) and under Ar atmosphere in order to replace any remaining silanol groups on the silica surface by a trimethylsilane (TMS) group [2]. The strip was again washed with chloroform and pentane and stored under Ar.

The static contact of a water droplet on silica strips was measured after piranha treatment (SiO<sub>2</sub>), after functionalisation with 7 (SiO<sub>2</sub>-Napy) and after capping with HMDS (SiO<sub>2</sub>-Napy/TMS). As a control experiment, strips treated only with HMDS (SiO<sub>2</sub>-TMS) were also prepared and analysed. A Sentech SE400 ellipsometer ( $\lambda = 632.8\text{ nm}$ , angle of incidence 70°) was used to measure the thickness of the bound layer. A three-layer model was used, consisting of (1) silicon (real refractive index  $n = 3.85$ , imaginary part  $k = -0.02$ ), (2) silica plus bound organic material ( $n = 1.46$ ) and (3) air ( $n = 1.00$ ). The organic layer is thus treated as an extension of the silica layer, since its refractive index is not exactly known but is expected to be around 1.5.

Fluorescence spectra of functionalised strips were recorded using a Edinburgh Instruments FS920 spectrophotometer. Napy excitation spectra were measured from 300-420 nm (emission wavelength 430 nm). To study the binding properties of the functionalised strips, the strips were immersed for 15 minutes in a 10<sup>-5</sup> M solution of UPy-perylenebisimide (denoted as UPy-perylene, see figure 8.3) in chloroform and fluorescence spectra of the UPy-perylene were measured. UPy-perylene excitation spectra were measured from 420-560 nm (emission wavelength 570 nm). A second spectrum was recorded after the

strips were washed with 1 ml of toluene to remove any non-specifically bound UPy-perylene. After treatment of the strips with methanol/THF (1:1 v/v, 15 minutes exposure), another spectrum was recorded. To check that the binding to the surface is caused by the interaction between the surface-bound Napy and the UPy, and not by the perylene, the same experiment was carried out with a perylene without a UPy attached to it.

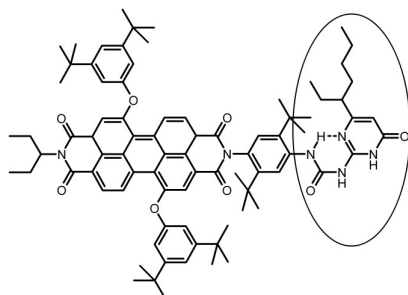


Figure 8.3: UPy-perylenebisimide (UPy-perylene) used for studying the UPy binding on Napy-functionalised surfaces. The UPy group is encircled. A perylenebisimide without a UPy attached to it (perylene) was used as a blank.

## 8.3 Results and discussion

### 8.3.1 Synthesis

#### Synthesis of a carboxyl-Napy *via* amidation and hydrolysis

In previous work, the Palladium (Pd) catalyzed amidation of 2-chloro- and 2,7-dichloro-1,8-naphthyridines was extensively studied [31]. The non-symmetric (7-chloro-[1, 8]naphthyridin-2-yl)-amide **2** is therefore a convenient starting point for our present investigation. The strategy chosen here involves the amidation of **2** by 5-Carbamoyl-pentanoic acid methyl ester to form methoxycarbonyl-Napy **1**, and subsequent hydrolysis of the methyl ester with LiOH to obtain the carboxylic-acid terminated Napy **3** (see figure 8.4). The carboxylic acid can be coupled to an amine-functionalised silica surface to yield Napy-functionalised silica.

The Pd-catalyzed amidation of **2** was done with Pd(OAc)<sub>2</sub> as the Pd-source, Xantphos as the ligand and K<sub>2</sub>CO<sub>3</sub> as the base in refluxing 1,4-dioxane. These conditions were previously found to give high conversions and good yields [31]. The desired product **1** was indeed obtained in a high purity, based on the

### 8.3. Results and discussion

$^1\text{H}$ - and  $^{13}\text{C}$ -NMR spectra, IR and mass spectroscopy. The yield (53%) was not very high. This is probably due to partial degradation of the product during column chromatography.

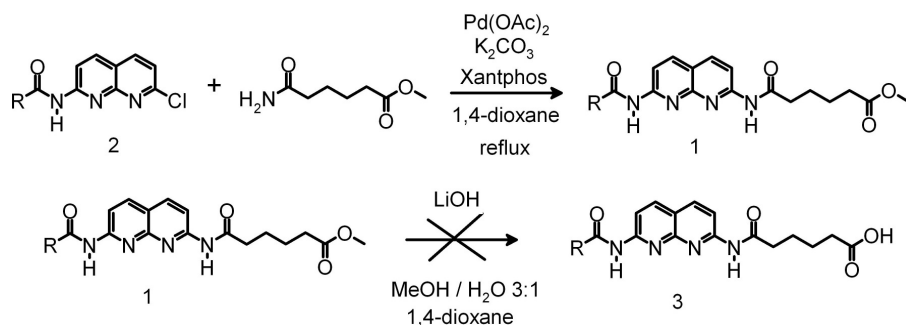


Figure 8.4: Pd-catalyzed amidation and hydrolysis of **2** (**R** = ethylhexyl-).

In the second step, exactly one equivalent of the mild hydrolyzing agent LiOH was added to purified **1** to hydrolyse the methyl ester to the corresponding carboxylic acid (figure 8.4). The stoichiometry is crucial in this reaction, since there are also amide bonds present which are susceptible to alkaline hydrolysis. The 2-ethylhexanoylamino substituent was chosen because of its relatively high stability towards hydrolysis, but it can nevertheless be hydrolyzed, as can the amide bond in the 5-methoxycarbonyl-hexanoylamino group. Generally, esters are more easily hydrolyzed than amides, so if care is taken with the stoichiometry and mild reaction conditions are chosen, it should be possible to selectively hydrolyze the ester bond, and leave the amide bonds intact.

In spite of the precautions, hydrolysis of the amide bonds still occurs. In the  $^1\text{H}$ -NMR spectrum, there are too many signals between 7.5 and 8.5 ppm, where the protons on the naphthyridine rings are located. This indicates an asymmetric substitution of the rings, and thus hydrolysis of either one or both of the amide bonds of **1**. The mass spectrum has a peak at  $m/z=415.38$ , corresponding to the desired product **3**. However, there is also a peak at  $m/z=429.40$ , corresponding to the starting compound **1**. The highest peak is at  $m/z=287.32$ , a mass which corresponds to the product which is formed by the hydrolysis of the amide bond in the 2-ethylhexanoylamino substituent of **3**. These results indicate that the desired reaction occurs, but there are significant side reactions due to hydrolysis of the amide bond(s). In an attempt to separate **3** from the hydrolysis products, the crude mixture was purified using column chromatography. After this purification step, the product peak at 415.38 has

disappeared from the mass spectrum mixture, whereas the other peaks are still present. Thus, instead of yielding the purified **3**, column chromatography has removed **3** from the reaction mixture.

#### Synthesis of a triethoxysilyl-Napy *via* hydrosilylation and amidation

As an alternative route, the Pt-catalyzed hydrosilylation of Undec-10-enoic acid amide with triethoxysilane to form 11-triethoxysilylanyl-undecanoic acid amide **4** was investigated (figure 8.5). In a second step, **4** could be coupled to **2** by the Pd-catalyzed amidation reaction described above. This would yield a triethoxysilane-terminated Napy, which could then be bound to a silica surface.

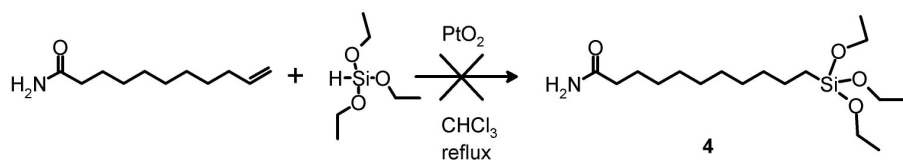


Figure 8.5: Pt-catalyzed hydrosilylation of Undec-10-enoic acid amide.

The reaction was done in refluxing chloroform with PtO<sub>2</sub> as the Pt-source [33] and with a tenfold excess of the silane. The reaction was stopped when the characteristic peaks in the <sup>1</sup>H-NMR spectrum corresponding to the protons in and next to the double bond (5.8, 5.0 and 2.0 ppm, respectively) were no longer present. After removal of the solvent and the excess silane, the <sup>13</sup>C-NMR spectrum shows no peaks above 100 ppm, except for the amide carbon at 175.7 ppm. This indicates that the double bond has indeed disappeared completely. If **4** is formed, the carbon next to the silicium atom should give a characteristic signal around 10 ppm. However, this signal is absent in the spectrum. The base peak of the mass spectrum is at m/z=326.45, which corresponds to the mass of the dimer of the silane. This indicates that instead of the desired hydrosilylation, probably *hydrogenation* occurs. The other product of this reaction, undecanoylamine, has a nominal molecular mass of 185, and cannot be seen in the mass spectrum. From these results, it was concluded that **4** has not been formed.

#### Synthesis of a trimethoxysilyl-Napy *via* addition of a thiol to a Napy-olefin

The third approach starts from Napy **6**, which has a terminal olefin, to which a thiol could be coupled in a radical reaction [34]. If this coupling is done with 3-trimethoxysilylanyl-propane-1-thiol, the result would be trimethoxysilyl-Napy

### 8.3. Results and discussion

---

**5**, with which a modification of a silica surface could be done (see figure 8.6). AIBN was used as the initiator, and the reaction was done in refluxing tetrachloromethane.

$^1\text{H-NMR}$  was used to check the conversion, based on the characteristic olefin peaks at 2.0, 5.0 and 5.8 ppm. The excess thiol was removed by repeated washing and precipitation from cold pentane until the methoxy signals in the  $^1\text{H-NMR}$  spectrum had the right intensity (corresponding to 9 protons). The mass spectrum has a peak at  $m/z=649.17$ , corresponding to the molar mass of **5**, and also the other spectral data confirm that **5** has indeed been formed. There is also a mass peak at  $m/z=287.07$ , which could correspond to a by-product formed by the hydrolysis of one of the amide bonds by the thiol. It was attempted to precipitate **5** from dry ether and methanol to remove any impurities, but no solid precipitate was formed. This may be due to the presence of the 2-ethylhexanoylamino group, which is very well soluble and thus makes crystallisation more difficult. NMR spectra of the oily precipitate yielded strange results (low resolution and wrong peak intensities), and also the mass spectrum still showed too many peaks. The results suggest that the synthesis is successful, but the product is not stable under the applied conditions.

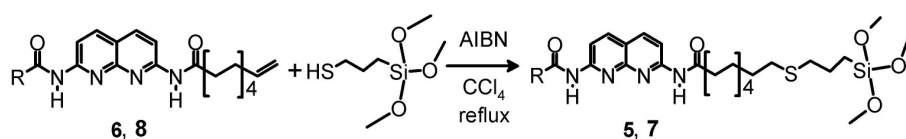


Figure 8.6: Coupling of 3-trimethoxysilylpropane-1-thiol to Napy-olefins **6** ( $\text{R}$  = ethylpentyl-) and **8** ( $\text{R}$  = methyl).

To improve the crystallisability, starting compound **6**, (bearing the 2-ethylhexanoylamino substituent) was replaced by **8** (which contains a less soluble acetylamino group), so product **7** should be obtained. To avoid contact with air, much care was taken to do the reaction and purification under dry conditions ( $\text{Ar}$  atmosphere). Instead of repeated washing and precipitation from pentane, vacuum distillation was used to remove the excess thiol. After distillation, the residu was precipitated from pentane, which yielded **7** as a yellowish solid. This compound was used for functionalisation of silica strips and colloidal particles.

### 8.3.2 Functionalisation of SiO<sub>2</sub> strips

#### Contact angle

After piranha treatment, the static contact angle  $\theta$  of a water droplet on a strip is  $< 10^\circ$ . After functionalisation with 7 and washing with chloroform and pentane,  $\theta$  increases to approximately  $75^\circ$ . After HMDS treatment, it increases further to  $80 - 85^\circ$ . A clean surface which is only treated with HMDS has an even higher contact angle:  $\theta \approx 95^\circ$ . This result indicates that Napy is bound to the surface, but there are some free silanol groups left, which are subsequently capped by the HMDS treatment. The results are summarized in table 8.1.

#### Ellipsometry

For all types of surfaces, two different strips were used and five different spots were measured on each strip. Measured values for  $\Psi$ ,  $\Delta$  and the calculated layer thickness  $d$  are given in table 8.1. For a clean silica strip, the thickness of the oxide layer is found to be  $3.1 \pm 0.2$  nm. This is a reasonable value for a naturally oxidized silicon surface. After functionalisation with Napy, the layer thickness is increased to  $6.2 \pm 0.4$  nm, which can be attributed to the binding of Napy to the surface. Here, it is assumed that the Napy layer is a homogeneous layer with a refractive index 1.46, equal to that of the oxide layer. Both are crude estimations and therefore no conclusions can be drawn about the actual layer thickness and the bound amount of Napy. The trimethylsilane (TMS) layer which is formed by the HMDS treatment is expected to be thinner than a Napy-layer. However, a SiO<sub>2</sub>-TMS surface has a layer thickness of  $7.9 \pm 0.4$  nm, so the layer seems thicker rather than thinner. This is probably also due to the adopted three-layer model and the uncertainty in the refractive index and composition of the layer. These results therefore support the contact angle measurements, but do not allow any quantitative conclusions to be drawn.

Table 8.1: Characterization of functionalised silica strips: static contact angle  $\theta$ , ellipsometry parameters  $\Psi$  and  $\Delta$  and the calculated layer thickness  $d$ .

| surface                    | $\theta$ ( $^\circ$ ) | $\Psi$ ( $^\circ$ ) | $\Delta$ ( $^\circ$ ) | $d$ (nm)      |
|----------------------------|-----------------------|---------------------|-----------------------|---------------|
| SiO <sub>2</sub>           | $< 10$                | $10.41 \pm 0.03$    | $170.1 \pm 0.6$       | $3.1 \pm 0.2$ |
| SiO <sub>2</sub> -Napy     | $70 - 75$             | $10.70 \pm 0.05$    | $161.5 \pm 0.8$       | $6.2 \pm 0.4$ |
| SiO <sub>2</sub> -Napy/TMS | $80 - 85$             | -                   | -                     | -             |
| SiO <sub>2</sub> -TMS      | $95$                  | $10.93 \pm 0.06$    | $157.1 \pm 0.9$       | $7.9 \pm 0.4$ |

#### Fluorescence

Figure 8.7a shows the Napy excitation spectrum ( $\lambda_{\text{emission}} = 430$  nm) of a SiO<sub>2</sub>-Napy/TMS strip. The spectrum has two absorption maxima, at 335 and 350 nm.

### 8.3. Results and discussion

---

For comparison, the spectra of a clean  $\text{SiO}_2$  strip and a  $\text{SiO}_2$ -TMS strip are also shown. As expected, these strips show no absorption at all. These results demonstrate that silica surfaces can be functionalised by trimethoxysilyl-Napy 7.

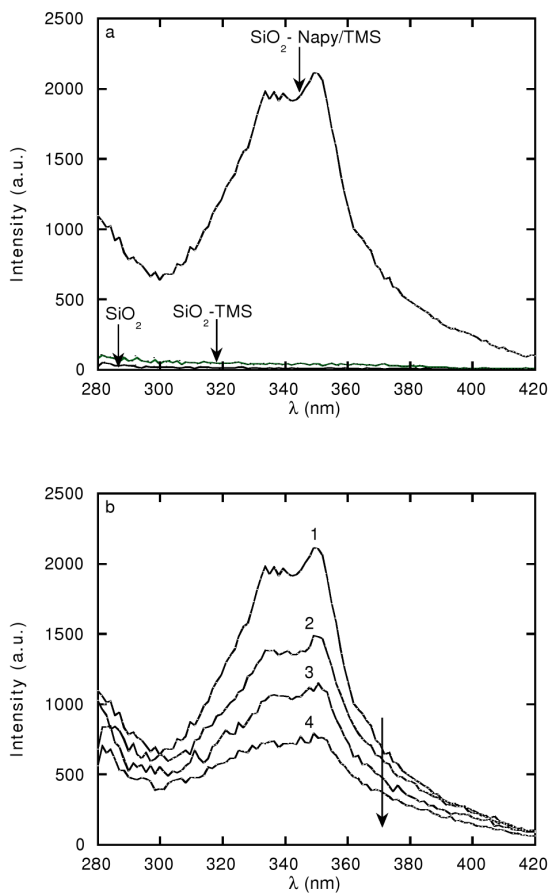


Figure 8.7: Napy excitation spectra at an emission wavelength of 430 nm. a: Spectra of  $\text{SiO}_2$ ,  $\text{SiO}_2$ -TMS and  $\text{SiO}_2$ -Napy/TMS; b: Degradation of the surface-bound Napy. Original Napy excitation spectrum (1), after one binding and washing cycle (2), after one week of storage (3), after a second binding and washing cycle (4).

To investigate the capability of the  $\text{SiO}_2$ -Napy/TMS surface to specifically bind UPys, the functionalised surface was exposed to a  $10^{-5}$  M solution of

a mono-UPy with a fluorescent perylene group (figure 8.3). The excitation spectra ( $\lambda_{\text{emission}} = 570 \text{ nm}$ ) of the strips are shown in figure 8.8a. As expected, the first spectrum (recorded before UPy-perylene treatment) shows no peaks (the 'bumps' in the spectrum between 460 and 480 nm are an artefact caused by the lamp). After exposure of the surface to the UPy-perylene, spectrum 2 was recorded, which has peaks at 515 and 555 nm. The spectrum is very similar to the solution spectrum of the UPy-perylene (shown in the inset), which shows that this molecule is indeed present at the surface. Surprisingly, the intensity of the spectrum is lower than that of the surface-bound Napy, even though the UPy-perylene is a much stronger fluorescent probe than the Napy. Furthermore, the fact that the artefact between 460 and 480 nm is clearly visible also indicates that the fluorescent intensity of the UPy-perylene is very low. This suggests that the number of bound UPy-perylenes is small, for example due to a low binding constant with the surface-bound Napy. On the other hand the fluorescence intensity may also be quenched by interactions between the bound UPy-perylene or by the presence of the surface. To remove weakly and unspecifically bound UPy-perylene, the surface was washed with a small amount of toluene, which is a good solvent for the UPy-perylene. This did not result in a decrease of the intensity (spectrum 3), which indicates that the UPy-perylene is indeed specifically bound by the Napy. The intensity even seems to increase slightly, but this is probably due to a local variation in the UPy-perylene concentration on the surface. To check the reversibility of the binding, the surface was washed with a mixture of methanol and THF. After this treatment, all UPy-perylene was indeed removed, and the original spectrum of the SiO<sub>2</sub>-Napy/TMS surface was recovered (spectrum 4).

These experiments demonstrate that a UPy-perylene is specifically and reversibly bound to a Napy-functionalised silica surface. However, they do not exclude the possibility that the binding is caused by the perylene group instead of the UPy. Therefore, the same experiments were also done with a  $10^{-5} \text{ M}$  solution of the perylene without the UPy group attached to it. The spectra are shown in figure 8.8b. Also in this case, the perylene binds to the surface (spectrum 2). However, when the surface is washed with a small amount of toluene, the perylene is nearly completely rinsed off (spectrum 3). This result demonstrates that binding of the perylene to the surface is weak and non-specific. Thus, it can be concluded from figures 8.8a and b that the surface-bound Napy 7 is capable of reversibly and specifically binding UPys. Silica surfaces, functionalised with 7 could thus be used for the preparation of supramolecular brushes consisting of bis-UPy (possibly in combination with bis-Napy) and UPy-Napy monomers.

After the functionalised strip had been treated with UPy-perylene solution and washed with methanol/THF, the Napy excitation spectrum was recorded again (figure 8.7b, spectrum 2). After one week, this procedure (recording

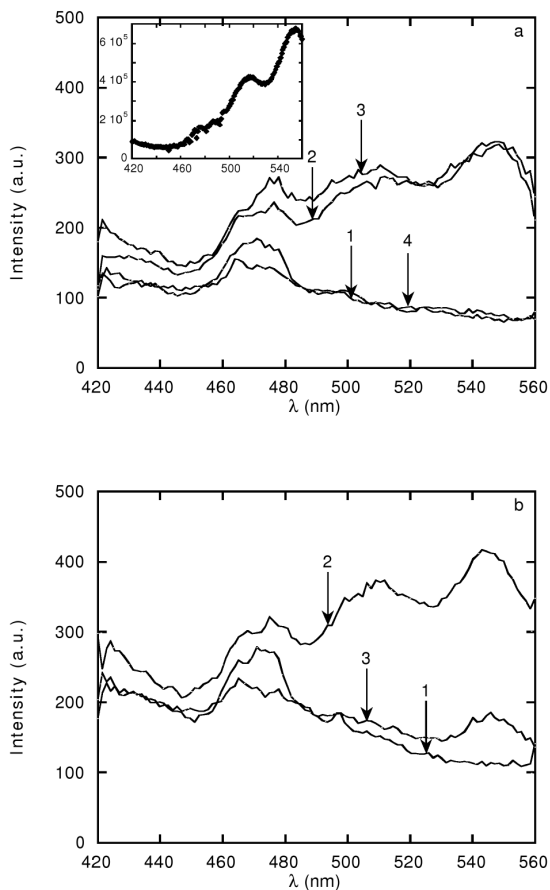


Figure 8.8: Perylene excitation spectra at an emission wavelength of 570 nm. a: Spectra of a SiO<sub>2</sub>-Napy/TMS surface (1), after exposure to UPy-perylenes (2), after rinsing with toluene (3), after washing with methanol/THF (4). The inset shows the solution spectrum of the UPy-perylenes in chloroform; b: Spectra of a SiO<sub>2</sub>-Napy/TMS surface (1), after exposure to perylene (2), after rinsing with toluene (3).

of the Napy spectrum (spectrum 3), treatment with UPy-perylene, washing with methanol/THF, recording of another Napy spectrum (spectrum 4)) was repeated. From these spectra, it is clear that the intensity of the spectrum decreases in time, indicating that Napy is removed from the surface. Perhaps some of the Napy molecules were not covalently bound to the surface, but only physically adsorbed. The washing step with methanol/THF, a competitive solvent for hydrogen bonding, may rinse these Napys off the surface. On the other hand, after one week in which the strip was not used, the intensity has decreased further. This suggests that the surface-bound Napy is subject to some kind of degradation process. The Napy may be hydrolyzed and thus be detached from the surface. Washing with the polar solvents methanol and THF could accelerate the hydrolysis. Furthermore, it was noticed that after a few weeks, Napy 7 did not dissolve in chloroform anymore. This is probably a different type of instability, caused by polymerisation and crosslinking of the triethoxysilyl-groups. This leads to the formation of an insoluble network. Compound 7 is thus not only labile when bound to the silica surface, but the bulk material also degrades.

### 8.3.3 Preliminary results

#### Functionalisation of SiO<sub>2</sub> particles

In addition to the functionalisation of silica strips, it was also attempted to prepare Napy-functionalised colloidal particles. Monodisperse silica particles with a diameter of 250 nm (Monospher 250, Merck) and 5.6  $\mu\text{m}$  (non-porous Microspheres, Bangs Labs) were functionalised with Napy and HMDS by the same procedure as used for the strips. 5 mg of trimethoxysilyl-Napy 7 was used to functionalise 100 mg of particles. The particles were collected after several centrifugation/resuspension cycles in pentane and chloroform. The particles had a yellowish color, which indicates that Napy has indeed been bound.

No extensive characterisation of the modified particles was performed, but some preliminary experiments were done. The stability of suspensions of functionalised particles in toluene was compared to that of bare silica particles. By visual inspection, the Napy- and Napy/TMS functionalised particles seem to be much more stable in toluene than bare SiO<sub>2</sub> particles, but less stable than SiO<sub>2</sub>-TMS particles. This observation can be explained by the difference in hydrophobicity of the surfaces, and is consistent with the contact angle measurements on functionalised strips (table 8.1). However, none of the suspensions yielded useful results in Dynamic Light Scattering experiments. Cumulant analysis of the correlation functions yielded unrealistic particle sizes and polydispersities. This could be the result of the aggregation of well-functionalised particles, but it may also be due to an improper functionalisation procedure. If

a part of the particle surface is left unfunctionalised (e.g. because the particle suspension is not stable and the particles already aggregate during the functionalisation reaction), the presence of these patches of bare silica could also lead to aggregation of the particles.

In another experiment, mono- and bis-UPys were added to suspensions of SiO<sub>2</sub>-Napy/TMS. It is expected that the binding of bis-UPys to the particles destabilizes the suspension and leads to bridging flocculation. Mono-UPys, on the other hand, cannot form bridges and could even have a sterically stabilizing effect. It was indeed observed that a suspension of SiO<sub>2</sub>-Napy/TMS to which bis-UPys were added flocculated, whereas a suspension with mono-UPys did not. As expected, the addition of either mono- or bis-UPys to suspensions of SiO<sub>2</sub>-TMS did not have any effect. However, the results were not very reproducible and seemed to depend on the preparation method of the suspensions. The lack of reproducibility may be related to the aforementioned degradation of the Napy.

#### **Synthesis of a 2-amino-7-amido-1,8-naphthyridine**

From the results presented above, it can be concluded that functionalisation of the silica surface with trimethoxysilyl-Napy 7 works, but is far from optimal. Especially the degradation of 7 hinders the characterisation of the functionalised surfaces. The synthesis of a Napy which is less susceptible to hydrolysis is desirable. A fruitful strategy in this respect has been the replacement of one or both of the hydrolyzable amide substituents on the naphthyridine rings by amines [32]. In a first attempt to synthesize such a 2-amino-7-amido-1,8-naphthyridine with a triethoxysilane-linker (9), the coupling of 3-Isocyanato-triethoxypropyl-silane to 2-Ethyl-hexanoic acid [7-(4-amino-phenylamino)-[1,8]naphthyridin-2-yl]-amide (10) was performed (see figure 8.9). The reaction was done with a 50% excess of the isocyanate by refluxing in dry THF for 24 h. A small amount of DMAP was added to the reaction mixture. After precipitation of the crude product from hexane, a brownish powder was obtained. The <sup>1</sup>H-NMR spectrum was not conclusive about the purity of the formed product, but the infrared spectrum showed that no isocyanate was left. Functionalisation of a silica strip was done by the method as described in section 8.2. Instead of capping the remaining silanol groups with HMDS, a 1:1 mixture of HMDS and trimethylsilylchloride (TM-SCl) was used to prevent the accumulation of acidic and alkaline species (HCl and NH<sub>3</sub> from reaction with TMSCl and HMDS, respectively [2]) which could catalyze hydrolysis of the Napy. Unfortunately, no bound Napy was detected on the functionalised strip by fluorescence spectroscopy.

Some other alternatives were briefly attempted, but did not yield very promising initial results. An isocyanate-terminated Napy was synthesized which could be coupled to aminopropylsilica, but it was hard to determine if

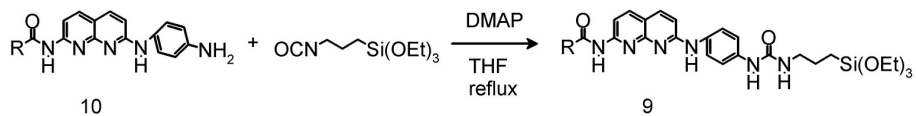


Figure 8.9: Coupling of 3-Isocyanato-triethoxypropyl-silane to 2-Ethyl-hexanoic acid [7-(4-amino-phenylamino)-[1,8]naphthyridin-2-yl]-amide **10** (**R** = ethylpentyl-).

the isocyanate was formed and to purify the product [35]. The synthesis of isocyanatopropyl-silica and subsequent reaction with a hydroxyl-terminated Napy was also attempted, but hardly any Napy was detected at the surface [35].

## 8.4 Concluding remarks

The preparation of a surface, functionalised with 2,7-diamido-1,8-naphthyridines (Napys) would open up new possibilities for experimental investigations in the interesting field of supramolecular polymers at surfaces. In this paper, functionalisation of silica surfaces with Napys is investigated. Several synthetic pathways towards a suitable Napy-derivative were attempted. Coupling of an olefin-terminated Napy to a trimethoxysilyl-thiol was the most promising alternative. Silica strips were functionalised with the resulting trimethoxysilyl-Napy (**7**). Remaining silanol groups were capped by reaction with HMDS.

The functionalised surfaces were characterized by contact angle measurements, ellipsometry and fluorescence spectroscopy. The results provide evidence that silica surfaces can be functionalised with **7** and that these surfaces are capable of specifically and reversibly binding UPys. However, the stability of **7** is low (both in bulk and at the surface), and this results in the loss of a significant part of the bound Napys in time, probably due to hydrolysis.

The synthesis of a Napy-derivative which can be coupled to silica and is less susceptible to hydrolysis is desirable. Some preliminary attempts were done, but these were not yet successful. A possible alternative to the use of silica could be the functionalisation of gold surfaces by Napy-thiols, although functionalisation of silica is probably more relevant in terms of applications.

## References

- [1] R.K. Iler. *The colloid chemistry of silica and silicates*. Cornell University Press, Ithaca, New York, 1955.
- [2] E.F. Vansant, P. Van der Voort, and K.C. Vrancken. *Characterization and chemical modification of the silica surface*. Elsevier Science B.V., Amsterdam, 1995.
- [3] A.P. Legrand, editor. *The surface properties of silicas*. John Wiley & Sons Ltd, Chichester (UK), 1998.
- [4] G.J. Fleer, M.A. Cohen Stuart, J.M.H.M. Scheutjens, T. Cosgrove, and B. Vincent. *Polymers at interfaces*. Chapman & Hall, London, 1993.
- [5] E.P.K. Currie, W. Norde, and M.A. Cohen Stuart. *Adv. Colloid Interface Sci.*, 100-102: 205–265, 2003.
- [6] J-M. Lehn. *Supramolecular chemistry: concepts and perspectives*. VCH, weinheim, 1995.
- [7] A. Ciferri, editor. *Supramolecular polymers*. 2nd ed., Marcel Dekker, New York, 2005.
- [8] L. Brunsveld, B.J.B. Folmer, E.W. Meijer, and R.P. Sijbesma. *Chem. Rev.*, 101: 4071–4097, 2001.
- [9] M.E. Cates and S.J. Candau. *J. Phys.: Condens. Matter*, 2: 6869–6892, 1990.
- [10] B.J.B Folmer, R.P. Sijbesma, Versteegen. R.M., J.A.J. van der Rijt, and E.W. Meijer. *Adv. Mater.*, 12: 874–878, 2000.
- [11] S. J. Rowan and J. B. Beck. *Faraday Discuss.*, 128:43–53, 2005.
- [12] S-L. Zhou, S. Matsumoto, H-D. Tian, H. Yamane, A. Ojida, S. Kiyonaka, and I. Hamachi. *Chem. Eur. J.*, 11:1130–1136, 2005.
- [13] S. Kiyonaka, K. Sugayisu, S. Shinkai, and I. Hamachi. *J. Am. Chem. Soc.*, 124:10954–10955, 2002.
- [14] A.W. Bosman, R.P. Sijbesma, and E.W. Meijer. *Mater. Today*, 7: 34–39, 2004.
- [15] J. van der Gucht, N.A.M. Besseling, and G.J. Fleer. *J. Chem. Phys.*, 119:8175–8188, 2003.
- [16] H.J.A. Zweistra and N.A.M. Besseling. *Phys. Rev. Lett.*, 96:078301, 2006.

- 
- [17] J. van der Gucht, N.A.M. Besseling, and M.A. Cohen Stuart. *J. Am. Chem. Soc.*, 124:6202–6205, 2002.
- [18] S. Zou, Z. Zhang, Försch, W. Knoll, H. Schönherr, and G.J. Vancso. *Langmuir*, 19:8618–8621, 2003.
- [19] S. Zou, H. Schönherr, and G.J. Vancso. *J. Am. Chem. Soc.*, 127:11230–11231, 2005.
- [20] S. Zou, H. Schönherr, and G.J. Vancso. *Angew. Chem. Int. Ed.*, 44:956–959, 2005.
- [21] F. Kersey, G. Lee, P. Marszalek, and L.S. Craig. *J. Am. Chem. Soc.*, 126:3038–3039, 2004.
- [22] J. Kim, Y. Liu, S.J. Ahn, S. Zauscher, J.M. Karty, Y. Yamanaka, and S.L. Craig. *Adv. Mater.*, 17:1749–1753, 2005.
- [23] H. Xu, T.B. Norsten, O. Uzunn, E. Jeoung, and V.M. Rotello. *Chem. Comm.*, :5157–5159, 2005.
- [24] K. Viswanathan, H. Ozhalici, C.L. Elkins, C. Heisey, T.C. Ward, and T.E. Long. *Langmuir*, 22:1099–1105, 2006.
- [25] R.P. Sijbesma, F.H. Beijer, L. Brunsveld, B.J.B. Folmer, J.H.K.K. Hirschberg, R.F. M. Lange, J.K.L. Lowe, and E.W. Meijer. *Science*, 278:1601–1604, 1997.
- [26] X-Z. Wang, X-Q. Li, X-B. Shao, X. Zhao, P. Deng, X-K. Jiang, Z-T. Li, and Y-Q. Chen. *Chem. Eur. J.*, 9:2904–2913, 2003.
- [27] G.B.W.L. Ligthart, H. Ohkawa, R.P. Sijbesma, and E.W. Meijer. *J. Am. Chem. Soc.*, 127:810–811, 2005.
- [28] O.A. Sherman, G.B.W.L. Ligthart, R.P. Sijbesma, and E.W. Meijer. *Angew. Chem. Int. Ed.*, 45:2072–2076, 2006.
- [29] W.A. Goedel *et al.* , unpublished data.
- [30] B.W.T. Gruijters, M.A.C. Broeren, F.L. van Delft, R.P. Sijbesma, P.H.H. Hermkens, and F.P.J.T. Rutjes. *Org. Lett.*, 8:3163–3166, 2006.
- [31] G.B.W.L. Ligthart, H. Ohkawa, R.P. Sijbesma, and E.W. Meijer. *J. Org. Chem.*, 71:375–378, 2006.
- [32] G.B.W.L. Ligthart, C.F. Cörvers, R.P. Sijbesma, and E.W. Meijer. *Eur. J. Org. Chem.*, in preparation, 2006.
-

## References

---

- [33] N. Sabourault, G. Mignani, A. Wagner, and C. Mioskowski. *Org. Lett.*, 4:2117–2119, 2002.
- [34] A. Iuliano, P. Salvadori, and G. Félix. *Tetrahedron: Asymmetry*, 10:3353–3364, 1999.
- [35] G.B.W.L. Ligthart. , personal communication.

# Summary

## Introduction

Ever since the pioneering work of Staudinger, Carothers and others in the 1920s, it is generally accepted that polymers are compounds with a high molecular weight, consisting of chains of covalently bound recurring structural units (monomers). During the last two decades, there has been an enormously increasing interest in self-assembly and supramolecular chemistry: the spontaneous formation of structures by molecular association by non-covalent interactions.

Among the many examples of supramolecular structures are *supramolecular polymers*. Like their covalent counterparts, these are chains of monomers. However, the monomers are not connected by covalent bonds but by weaker, reversible interactions such as hydrogen bonding or metal-ligand complexation. There is a continuous exchange between bound and free monomers, and chains can break and recombine reversibly. This gives supramolecular polymers some unique properties. For example, the average degree of polymerisation is not fixed, but depends on the overall monomer concentration, temperature and other parameters. Because of the reversibility of the bonds, supramolecular polymers hold promise for numerous applications where 'tunable' material properties are desirable, such as sensors, self-healing materials, colloidal stabilisation and rheology modifiers.

A linear supramolecular polymer consists of monomers with two binding groups (bifunctional monomers). Monomers with higher functionalities induce branching. Monomers with only one binding group can bind to a chain, but they prevent other monomers from binding to that chain end. These monofunctional monomers are therefore called *chain stoppers*. By blocking chain ends, chain stoppers decrease the average degree of polymerisation. Even a small amount of chain stoppers can already have a significant effect on the chain length, and therefore on the material properties. At sufficiently high stopper fractions, the average degree of polymerisation is even completely determined by the chain stoppers, and independent of the overall monomer concentration.

## Summary by chapter

The chain-stopping effect of monofunctional monomers was readily recognized when the first supramolecular polymers were synthesized, but has hardly been investigated quantitatively. In this thesis, the effect of chain stoppers on solutions of supramolecular polymers is studied in more detail.

In chapters 2–7, experiments with supramolecular polymer ‘EHUT’ and chain stopper ‘DBUT’ are described. Bisurea EHUT forms long supramolecular chains in apolar organic solvents by the formation of four hydrogen bonds between consecutive monomers. DBUT is an alkylated derivative of EHUT in which hydrogen bonding is partially blocked.

Because of the continuous breaking and reformation of bonds between monomers, supramolecular polymers have interesting rheological properties. In **chapter 2**, the rheology of EHUT solutions is described. At low shear rates, the system is Newtonian and behaves according to the Maxwell model. This surprisingly simple behavior is in agreement with the well-known theoretical model for the dynamics of wormlike micelles by Cates *et al.*. At higher shear rates, the solutions are strongly shear thinning. This is attributed to shear-induced alignment of polymer chains. Transient rheology shows metastable stress plateaus and very slow equilibration, which are indications that the solution separates into two phases with different shear rates (‘shear banding’). Heterodyne light scattering is used to measure velocity profiles in the gap of the Couette geometry. The profiles confirm the existence of shear bands. Moreover, *three* different shear banding regimes can be identified upon increasing the applied shear rate. The first shear banding transition (at the lowest shear rates) may be caused by a mechanical instability related to the alignment of chains. At higher shear rates, the shear banding may be related to the origination and subsequent disappearance of a flow-induced phase.

In **chapter 3**, the effects on rheology of EHUT solutions of the addition of chain stoppers and an increase of temperature are compared. Both decrease the average degree of polymerisation, but in different ways. Upon increasing temperature, both the zero-shear viscosity and the terminal relaxation time decrease exponentially over the whole temperature range studied. When a small amount of chain stoppers is added, the effect is relatively small. However, beyond a certain critical stopper fraction, the viscosity and the relaxation time decrease strongly, following power-laws. This behavior can be explained by a simple model which describes the effect of the addition of chain stoppers on the average degree of polymerisation. When comparing flow curves of solutions with the same zero-shear viscosity (one of which contains chain stoppers, and the other is at an elevated temperature), differences occur at shear rates

beyond the linear regime. The differences are largely explained by a difference in relaxation time between the solutions. The results are consistent with a mechanism of shear-induced alignment and subsequent elongation of chains.

The effect of chain stoppers on the average degree of polymerisation is investigated in more detail in **chapter 4**. Static and dynamic light scattering and vapor pressure osmometry are used. Osmometry at high stopper fractions show that the average degree of polymerisation is inversely proportional to the stopper fraction, and independent of the overall monomer concentration. Static light scattering is used to measure the correlation length in EHUT solutions with and without chain stoppers. Without chain stoppers, the correlation length as a function of the overall monomer concentration has a maximum at the overlap concentration. Results yield estimates for the association constant and the persistence length of EHUT chains. When a fixed fraction of chain stoppers is added, a plateau rather than a maximum in the correlation length is measured. The results of both osmometry and light scattering indicate that DBUT is not a very efficient chain stopper. CONTIN analysis of dynamic light scattering data yields the distribution of decay times, from which the hydrodynamic correlation length is calculated. The results are in line with those from static light scattering. Above the overlap concentration, a second 'slow' peak appears in the distribution. It is not clear what the origin of this 'slow' mode is.

**Chapter 5** deals with the linear rheology of EHUT/DBUT solutions. The stopper fractions used are sufficiently high to enable the independent variation of the overall monomer concentration and the average degree of polymerisation. Since the average degree of polymerisation normally depends on the overall monomer concentration, this information is not experimentally accessible without the use of chain stoppers. Thus, the dependence of the zero-shear viscosity and the terminal relaxation time on both parameters can be measured independently. Measured scaling exponents are in agreement with previous experiments without chain stoppers, but contain more information about the chains. Results indicate that the chains are semiflexible (in agreement with previous experiments), and that both breaking and reptation of chains contribute significantly to stress relaxation. The macroscopic rheometry data are compared to the microscopic results from probe particle diffusion measurements. Both results are in agreement when the particles are large compared to the correlation length in the system and to the (persistence) length of the chains.

The interfacial behavior of EHUT and DBUT is addressed in **chapter 6**. Colloidal Probe Atomic Force Microscopy experiments are described in which the interaction force between stearylated silica surfaces in EHUT/DBUT solutions are measured. Since EHUT does not adsorb to the surfaces, there is an attrac-

tive depletion interaction. The range of the interaction is in good agreement with previous measurements of the correlation length. The dependence of the depletion layer thickness and the slope of the interaction curve on the overall monomer concentration are qualitatively in agreement with theoretical predictions, but the concentration dependence seems to be weaker than expected. Since the EHUT/DBUT solutions used are highly viscous, hydrodynamic effects have to be considered. At small separations between the probe particle and the substrate, the hydrodynamic drag is much smaller than expected based on the solution viscosity. Results indicate that the decreased drag force is the result of surface slip, caused by the presence of the depletion layer. This layer has a much lower viscosity than the bulk solution. Therefore, the liquid is pushed out of the gap between the particle and the substrate more easily. In agreement with theoretical predictions, depletion-induced phase separation of a colloidal suspension becomes more pronounced with increasing polymer concentration. It is noticeable that phase separation already occurs at concentrations where the depletion force is too small to be measured directly. Some possible explanations are discussed.

Whereas chapter 6 describes AFM force measurements in solutions with varying overall monomer concentrations, in **chapter 7** the stopper fraction is varied. When the amount of chain stoppers is increased, the solution passes from the semidilute to the dilute regime. This results in a marked decrease of the depletion layer thickness and solution viscosity, in agreement with theoretical predictions. This 'tunability' of the depletion force is unique to supramolecular polymers. It is shown that the depletion forces are strong enough to induce phase separation in a colloidal suspension of stearylated silica particles.

**Chapter 8** does not deal with EHUT and DBUT, but with supramolecular polymers based on the heterocomplementary ureido-pyrimidinone ('UPy') and 2,7-diamido-1,8-naphthyridine ('Napy') units. Some Napy derivatives were synthesized, with the purpose of functionalising silica surfaces. A Napy-functionalised surface could be used for the fabrication of supramolecular polymer brushes, or as a highly specific and reversible adsorbent for UPys. Functionalised strips of silica wafer were studied by contact angle measurement, ellipsometry and fluorescence spectroscopy. Results indicate that Napy groups are indeed bound to the surface. Moreover, the surface-bound Napys are capable of specifically binding Upys. Unfortunately, the surface-bound Napy is not stable, and it disappears from the surface. This is probably caused by hydrolysis by water from the air. Some preliminary attempts to synthesize a more stable Napy derivative are reported.

## Concluding remarks

Supramolecular polymers are chains of monomers, connected by non-covalent interactions. Bifunctional monomers lead to the formation of linear chains, whereas monomers with only one binding group act as chain stoppers by blocking chain ends. This has been known for a long time, but the quantitative effects have not received much attention. In this thesis, the effect of chain stoppers on supramolecular polymer solutions is studied in more detail.

By adding chain stoppers to a supramolecular polymer solution, the average degree of polymerisation decreases. This effect can be described by a simple model. At sufficiently high stopper fractions, the average degree of polymerisation is completely determined by the chain stoppers, and independent of the overall monomer concentration. Results of osmometry, rheology and light scattering experiments are consistent with the model. By using chain stoppers, information about the supramolecular polymer chains can be obtained which is otherwise not experimentally accessible.

Beside the solution behavior, also the interfacial properties of supramolecular polymers are highly dynamic. The presence of polymers often affects the interaction between surfaces. Since the length of supramolecular polymers can easily and reversibly be adjusted, the range and strength of the interaction can also be tuned. This is demonstrated by measurement and controlled variation of the depletion interaction.

Chain stoppers are often regarded as a contamination of a supramolecular polymer which is hard to get rid of. The results in this thesis show that they can also be a valuable tool in supramolecular polymer research.



# Samenvatting voor dummies

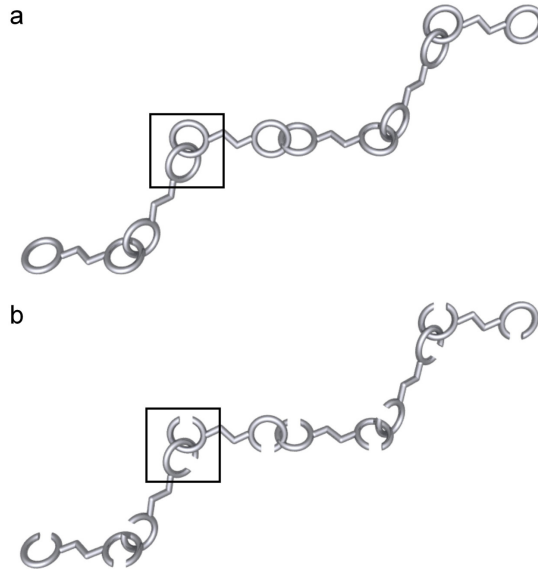
## Inleiding

### Polymeren

Al sinds de prehistorie gebruiken mensen de materialen die de natuur levert voor het maken van bijvoorbeeld gereedschappen, kleding en sieraden. Eerst had men alleen de beschikking over hout, steen, klei, huiden en botten, later ook over brons en ijzer. Ook natuurlijke vezels zoals wol, katoen en zijde werden al zeer vroeg toegepast. Hoewel er steeds betere technieken werden ontwikkeld om deze materialen in handen te krijgen en te bewerken, bleef men lang afhankelijk van dezelfde (natuurlijke) materialen. Het duurde tot de negentiende eeuw voor het eerste (semi-)synthetische materiaal ontwikkeld werd. Deze mijlpaal wordt vaak toegeschreven aan Charles Goodyear, die in 1839 ontdekte hoe natuurlijk rubber door een behandeling met zwavel (vulkanisatie) veel beter bruikbaar werd voor allerlei toepassingen. Het eerste volledig synthetische materiaal werd in 1907 uitgevonden door Leo Bakeland, die het naar zichzelf vernoemde: bakeliet.

De moleculen van sommige materialen, zoals cellulose (het belangrijkste bestanddeel van hout), zetmeel, DNA, wol en rubber, bevatten ongelooflijk veel atomen, en zijn dus erg zwaar. Vanwege hun grote gewicht worden deze materialen *polymeren* genoemd, ze bevatten veel ('poly') eenheden. Wetenschappers waren er lange tijd van overtuigd dat polymeren uit kleinere moleculen bestonden, die in een soort klontje aan elkaar zaten. De Duitse chemicus Hermann Staudinger was in 1920 de eerste die beweerde dat polymeren geen klontjes van kleine moleculen zijn, maar juist extreem grote moleculen, die hij *macromoleculen* noemde. Hoewel lang niet iedereen hem meteen gelijk gaf, verzamelde zich steeds meer experimenteel bewijs dat polymeren inderdaad macromoleculen zijn. Deze experimenten leidden onder andere tot de ontwikkeling van bekende polymeren zoals nylons en polyester. In de decennia die volgden werden er continu nieuwe polymeren uitgevonden met steeds meer verschillende en steeds betere eigenschappen. Tegenwoordig kom je ze werkelijk overal tegen: in kleding, computers, auto's en verpakkingsmaterialen, maar ook in verf, medicijnen en levensmiddelen.

## Supramoleculaire polymeren



Figuur 1: Schematische weergave van polymeerketens. a: covalent polymeer, de bindingen tussen de monomeren (kader) zijn niet reversibel; b: supramoleculair polymeer, met reversibele bindingen tussen de monomeren (kader).

Polymeren bestaan uit lange ketens van repeterende eenheden (monomeren), zoals een ketting is opgebouwd uit een aantal schakels. De monomeren zitten gewoonlijk stevig aan elkaar vast, met chemische oftewel covalente bindingen. Die zijn zo sterk, dat ze alleen met veel geweld (bijvoorbeeld zeer hoge temperatuur of sterk zuur) verbroken kunnen worden. De ketens van covalente polymeren hebben dus een vaste lengte. Een schematische weergave van een covalent polymeer is te zien in figuur 1a. In de laatste twee decennia is er steeds meer belangstelling voor het maken van structuren waarbij moleculen met zwakkere, niet-covalente bindingen aan elkaar zitten. Deze tak van de scheikunde heet *supramoleculaire* chemie. Inmiddels zijn er allerlei verschillende structuren ontworpen en gemaakt, waaronder *supramoleculaire polymeren*. Net als covalente polymeren zijn dit lange ketens van monomeren. De bindingen tussen de monomeren zijn nu echter veel zwakker, waardoor ze spontaan kunnen breken, maar zich ook weer zelf kunnen herstellen. De bindingen zijn dus *reversibel*: ze worden continu verbroken en gevormd. In feite is een supramoleculair polymeer dus geen macromolecuul, want het

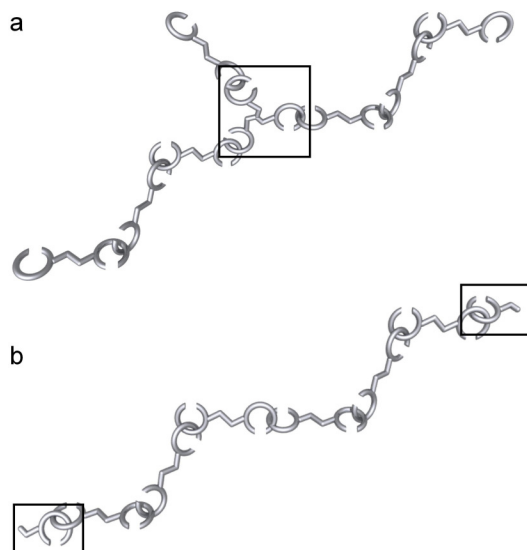
bestaat uit een groot aantal losse moleculen, die zichzelf aaneen rijgen tot een keten. Ironisch genoeg vertoont deze nieuwe klasse van polymeren meer overeenkomsten met het oude idee van polymeren als aggregaten van kleine moleculen!

Figuur 1b toont een schematische weergave van een supramoleculair polymeer. Het voordeel van een polymeer met reversibele bindingen is dat de lengte van de ketens gemakkelijk veranderd kan worden. De ketens worden bijvoorbeeld langer als er extra monomeren toegevoegd worden, die zich aan bestaande ketens kunnen binden. Een verhoging van de temperatuur zorgt er daarentegen voor dat de bindingen gemakkelijker los schieten, en de ketens juist korter worden. Doordat de ketenlengte van supramoleculaire polymeren kan variëren, reageren deze moleculen zeer sterk op hun omgeving. Ze zijn daarom interessant voor toepassingen in 'slimme' materialen die reageren op bijvoorbeeld temperatuur, of materialen die zichzelf na een beschadiging herstellen door ze simpelweg te verwarmen. Een totaal ander product waarbij supramoleculaire polymeren van pas kunnen komen, is inkt voor inkjet printers. Het voortdurend breken en vormen van bindingen zorgt ervoor dat de inkt vloeibaar is op het moment dat hij uit het apparaat komt, maar op het papier razendsnel vast wordt, zodat hij niet uitloopt.

## Ketenstoppers

De monomeren van de ketens in figuur 1 bevatten twee 'bindingsplaatsen' (de 'ogen' van de schakels). Dit soort monomeren rijgt zich aaneen tot lineaire ketens. Monomeren met drie of meer bindingsplaatsen kunnen ook voorkomen, zij zorgen voor vertakkingen van de ketens, zie figuur 2a. Deze 'vertakkers' worden verder buiten beschouwing gelaten. Monomeren met slechts één bindingsplaats kunnen ook aan een keten binden, maar aan dat monomeer kunnen geen nieuwe monomeren meer binden. De keten kan dus niet meer verder groeien (figuur 2b). Deze monomeren worden daarom ook wel 'ketenstoppers' genoemd.

Door het blokkeren van keteneindes zorgen ketenstoppers ervoor dat de ketens korter worden. Minieme hoeveelheden ketenstoppers kunnen al dramatische effecten hebben op de ketenlengte, en daarmee op de eigenschappen van het polymeer. Om de ketens zo lang mogelijk te maken (wat nodig is om een stevig materiaal te krijgen) is het daarom van groot belang dat er uitsluitend monomeren met twee bindingsplaatsen aanwezig zijn, en geen ketenstoppers. Ketenstoppers kunnen als 'foutje' ontstaan bij het maken van 'gewone' monomeren met twee bindingsplaatsen. Het is vaak erg moeilijk om de ketenstoppers van de gewone monomeren te scheiden, omdat ze erg veel op elkaar lijken. Ketenstoppers zijn dan dus een ongewenste vervuiling van het polymeer. Aan de andere kant kunnen ketenstoppers ook bewust toegevoegd



Figuur 2: Verschillende types monomeren. a: monomeren met drie bindingsplaatsen (kader) zorgen voor vertakkingen; b: monomeren met één bindingsplaats (ketenstoppers, kaders) blokkeren verdere groei van de keten.

worden om de lengte van de ketens te veranderen.

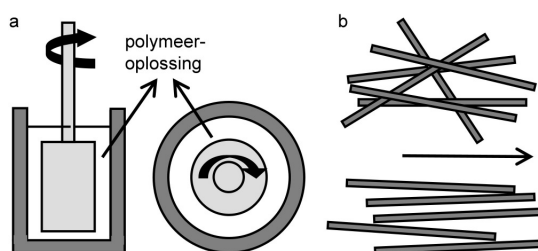
Tot nu toe werd het effect van ketenstoppers meestal kwalitatief bekeken. Men voegde bijvoorbeeld ketenstoppers toe aan een oplossing van ketens, en zag dan dat de oplossing minder visceus (stroperig) werd, doordat de kortere ketens gemakkelijker langs elkaar heen bewegen. Maar hoe groot dat effect nu precies is, en hoe dat afhangt van de hoeveelheid ketenstoppers, wordt meestal niet gemeten. In dit proefschrift wordt het effect van ketenstoppers op oplossingen van supramoleculaire polymeren uitgebreider onderzocht. Daarbij wordt er steeds vanuit gegaan dat de 'gewone' monomeren 100% zuiver zijn, en wordt bewust een bepaalde hoeveelheid ketenstoppers toegevoegd.

## Experimenten en resultaten

Voor de experimenten die worden beschreven in hoofdstukken 2 tot en met 7, is gebruikt gemaakt van het supramoleculaire polymeer 'EHUT', en ketenstopper 'DBUT'. Als dit supramoleculaire polymeer wordt opgelost, vormt het lange ketens die in elkaar verstrengeld raken. Daardoor bewegen ze moeilijk

langs elkaar heen en zijn de oplossingen meestal erg stroperig (ze hebben een hoge viscositeit).

In supramoleculaire polymeren worden er continu bindingen tussen monomeren verbroken en gevormd. Hierdoor kunnen supramoleculaire polymeren snel herstellen van een verstoring, zoals het roeren van een oplossing. Tijdens het roeren worden de ketens opgerekt en vervormd, en het duurt enige tijd voor ze zich aan de nieuwe situatie hebben aangepast. Supramoleculaire polymeren passen zich dus sneller aan dan covalente ketens. Figuur 3a toont een schematische weergave van een *rheometer*, een apparaat waarmee de effecten van stromingen bestudeerd worden. De cylinder in het midden wordt met een bepaalde snelheid rondgedraaid, waardoor de vloeistof rond gaat stromen. Vervolgens wordt zeer nauwkeurig gemeten hoeveel kracht daarvoor nodig is. Het kost natuurlijk meer kracht om met de cylinder te laten draaien in een pot stroop (hoge viscositeit) dan om diezelfde snelheid te bereiken in een glas water (lage viscositeit). Dit soort experimenten geeft dus informatie over het stromingsgedrag (de *rheologie*) van vloeistoffen.



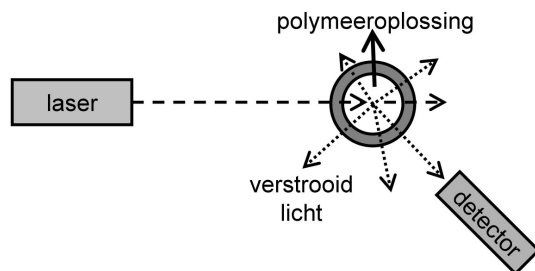
Figuur 3: Rheologie van supramoleculaire polymeren. a: schematische weergave van een rheometer. Links: zij-aanzicht (dwarsdoorsnede); rechts: bovenaanzicht; b: bij lage draaisnelheden (de pijl geeft de stromingsrichting aan) liggen de ketens kris-kras door elkaar (boven), bij hoge snelheden oriënteren ze zich in de stromingsrichting (onder).

Voor eenvoudige vloeistoffen is er een simpel lineair verband tussen de draaisnelheid en de benodigde kracht: voor een twee keer zo hoge draaisnelheid is twee keer zo veel kracht nodig. In **hoofdstuk 2** wordt beschreven dat oplossingen van EHUT hieraan alleen bij zeer lage draaisnelheden voldoen. Bij hogere snelheden blijkt dat er veel minder kracht nodig is dan verwacht volgens het lineaire verband. Dit wordt verklaard doordat de ketens boven een bepaalde draaisnelheid de neiging hebben om zich in de stromingsrichting te oriënteren (zie figuur 3b). Daardoor stromen ze gemakkelijker langs elkaar heen, en is er minder kracht nodig dan wanneer ze in alle richtingen door

elkaar heen zouden liggen. Dit effect kan er zelfs toe leiden dat de oplossing zich opsplijt in (simpel gezegd) een snelstromend en een langzaamstromend gebied. EHUT blijkt in maar liefst drie verschillende gebieden van draaisnelheden zo'n opsplitsing te vertonen.

In **hoofdstuk 3** worden twee manieren om de ketens te verkorten met elkaar vergeleken: het verhogen van de temperatuur en het toevoegen van ketenstoppers. Beide leiden tot een afname van de viscositeit, maar wel op een verschillende manier. Als er weinig ketenstoppers toegevoegd worden (minder dan ongeveer 1% van de totale hoeveelheid monomeren) is het effect niet zo groot. Bij hogere hoeveelheden neemt de viscositeit echter zeer snel af. Er is dus een soort omslagpunt in het effect van de ketenstoppers. Een eenvoudig model dat beschrijft hoe de ketenlengte verandert door het toevoegen van ketenstoppers, kan de resultaten verklaren. Bij verhoging van de temperatuur daalt de viscositeit volgens een exponentieel verband, in overeenstemming met andere polymeren en theoretische voorspellingen. Ook blijkt dat twee oplossingen van gelijke viscositeit (waarvan de ene ketenstoppers bevat en de andere verwarmd is) zich niet hetzelfde gedragen bij hogere draaisnelheden. Dit wordt grotendeels verklaard doordat de bindingen tussen de monomeren bij hogere temperatuur gemakkelijker breken, en zich ook weer sneller herstellen.

Het effect van ketenstoppers op de lengte van de ketens wordt nader bestudeerd in **hoofdstuk 4**. Hiervoor wordt onder andere gebruik gemaakt van lichtverstrooiing. Dit is een techniek waarbij met een laserbundel op de oplossing geschoten wordt, zie figuur 4. Als zich in de oplossing deeltjes boven een bepaalde grootte bevinden (bijvoorbeeld polymeerketens), verstrooien die het licht: ze zenden het naar alle kanten uit. Een detector meet het licht dat uitgezonden wordt. De gemeten intensiteit op verschillende plekken bevat informatie over de grootte en de vorm van de deeltjes. Uit de fluctuaties van het signaal in de tijd kan de bewegingssnelheid van de deeltjes worden afgeleid. Aangezien grote deeltjes langzamer bewegen dan kleine, kan ook hieruit de grootte van de deeltjes worden afgeleid. De resultaten laten zien dat de ketenstoppers er inderdaad voor zorgen dat de ketens korter worden. Bovendien blijkt het onder bepaalde omstandigheden zo te zijn, dat de lengte van de ketens volledig bepaald wordt door de hoeveelheid ketenstoppers. Daarnaast wordt er op basis van de resultaten een schatting gemaakt van de sterkte waarmee de EHUT monomeren aan elkaar binden. Ook blijkt dat de ketens langer zijn dan verwacht. Daaruit kan geconcludeerd worden dat DBUT geen erg efficiënte ketenstopper is. Waarschijnlijk kan de keten in sommige gevallen toch nog doorgroeien als er een ketenstopper aan gebonden zit. Dit heeft te maken met de precieze structuur van de EHUT ketens en van



Figuur 4: Schematische weergave van lichtverstrooiing. De invallende laserbundel wordt door de polymeerketens in alle richtingen verstrooid. De verplaatsbare detector registreert de gemiddelde intensiteit en de fluctuaties van de verstrooide bundel.

DBUT.

In **hoofdstuk 5** worden de afzonderlijke effecten van ketenlengte en het totaal aantal monomeren op het stromingsgedrag (rheologie) onderzocht. Dit is normaal gesproken niet mogelijk voor supramoleculaire polymeren, omdat als het aantal monomeren gevarieerd wordt, ook de ketenlengte verandert (zie de inleiding van deze samenvatting). Daardoor wordt er een soort gemiddeld effect gemeten. Door gebruik te maken van ketenstoppers kunnen de ketenlengte en de totale hoeveelheid monomeren echter wel onafhankelijk van elkaar worden gevarieerd. De resultaten geven nieuwe informatie over de flexibiliteit van de ketens, en over de snelheid waarmee bindingen tussen monomeren breken en vormen.

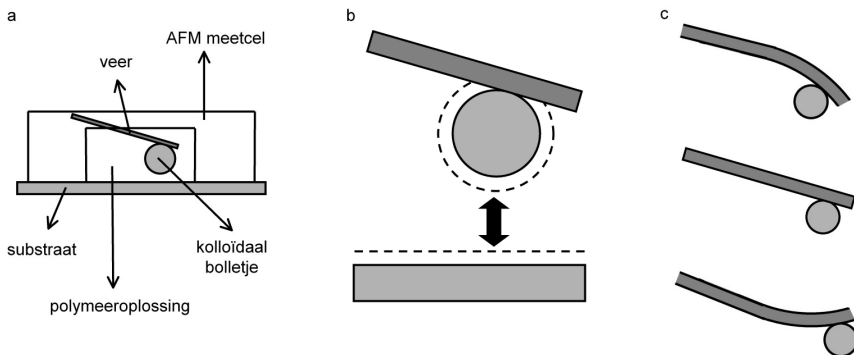
Daarnaast worden in dit hoofdstuk experimenten beschreven waarbij minuscule bolletjes (met een diameter van 0,00025 millimeter) aan oplossingen van EHUT en DBUT worden toegevoegd. Met behulp van lichtverstrooiing kan hun bewegingssnelheid gemeten worden. Net als experimenten met de rheometer geeft dit informatie over de rheologie van de oplossing (in een visceuze vloeistof bewegen de bolletjes langzamer), maar op een veel kleinere schaal. Uit deze experimenten wordt dan ook informatie verkregen over de microscopische structuur van de oplossingen, die vervolgens vergeleken wordt met de resultaten van de experimenten met de rheometer.

Veel producten en systemen bevatten *kolloïden*: deeltjes met een grootte tussen (ongeveer) een duizendste en een miljoenste millimeter ( $10^{-6}$  –  $10^{-9}$  meter). Deze deeltjes kunnen vast zijn (bijvoorbeeld pigmentdeeltjes in verf), maar ook vloeibaar (bijvoorbeeld vetbolletjes in melk) of gasvormig (bijvoorbeeld luchtbelletjes in de schuimkraag op een glas bier). Ook onze bloedcellen

zijn enkele duizendste millimeters groot, en bloed is dus ook een kolloïdaal systeem.

Over het algemeen is het wenselijk dat de kolloïdale deeltjes los van elkaar rond blijven zweven, en niet samenklonteren. Gebeurt dat wel, dan is het systeem instabiel en zakken de pigmentklonten naar de bodem van de verfpot, scheidt de melk, en zakt de schuimkraag in. Het zal niemand verbazen dat het samenklonteren van bloedcellen tot ernstige aandoeningen kan leiden. Om samenklonteren te voorkomen, moeten de deeltjes elkaar onderling afstoten.

In veel kolloïdale systemen (waaronder alle bovengenoemde voorbeelden) zijn ook polymeren aanwezig, die de stabiliteit kunnen beïnvloeden, zowel in positieve als in negatieve zin. Daarom wordt er veel onderzoek gedaan naar de krachten tussen deeltjes, en de invloed van polymeren hierop. Een manier om deze kolloïdale krachten direct te meten is Atomic Force Microscopy (AFM), oftewel atomaire krachtmicroscopie (zie figuur 5). Bij deze techniek wordt een kolloïdaal bolletje (met een diameter van een paar duizendste millimeter) aan een metalen staafje bevestigd, dat als 'veer' dient. Vervolgens wordt de veer met het bolletje zeer dicht boven een plat oppervlak ('substraat') gebracht, en op en neer bewogen. Als het bolletje en het substraat elkaar aantrekken, buigt de veer naar beneden door. Bij afstoting buigt de veer juist naar boven. Uit deze afbuiging kan de kracht tussen het bolletje en het substraat bereken worden.



Figuur 5: Krachtmeting met de Atomic Force Microscope. a: dwarsdoorsnede van de meetopstelling. De verschillende onderdelen zijn niet op schaal; b: beweging van de veer met het bolletje ten opzichte van het substraat. De polymeerloze laagjes zijn aangegeven met stippellijnen; c: buiging van de veer bij aantrekking (boven), geen kracht (midden) en afstoting (onder).

Hoofdstukken 6 en 7 beschrijven krachtmetingen met de AFM in oplos-

singen van EHUT en DBUT. Het bolletje en het substraat zijn zo gekozen, dat de polymeren er niet graag dicht in de buurt zitten. Vlak naast het oppervlak van zowel het bolletje als het substraat ontstaat daardoor een laagje vloeistof zonder polymeren (zie figuur 5b). Als het bolletje en het substraat zo dicht bij elkaar worden gebracht dat deze polymeerloze laagjes elkaar overlappen, treedt er een aantrekkende kracht op, die bekend staat als 'depletiekracht'. Deze kracht is van belang voor de stabiliteit van bijvoorbeeld zuivelproducten, verf en inkt. Ook zou de depletiekracht een rol spelen bij de ziekte sikkelcelanemie, waarbij rode bloedcellen niet goed functioneren en samenklonteren.

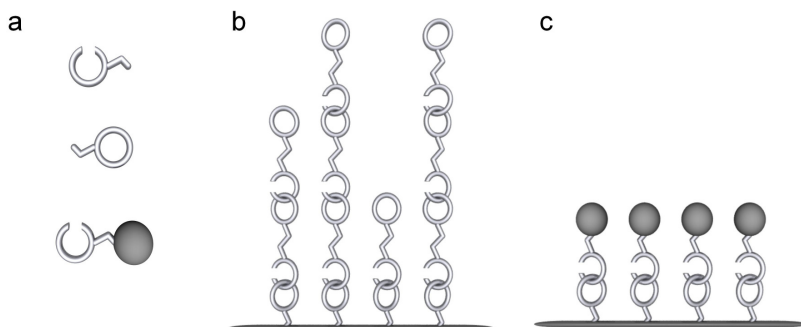
De sterkte van de depletiekracht en de afstand waarover hij optreedt worden bepaald door het aantal polymeerketens en hun grootte. Bij supramoleculaire polymeren kan de lengte van de ketens gemakkelijk veranderd worden, en dus zou ook de depletiekracht moeten veranderen.

In **hoofdstuk 6** wordt de totale hoeveelheid monomeren gevarieerd, en wordt gekeken hoe daarmee de reikwijdte en de sterkte van de depletiekracht veranderen. De resultaten zijn redelijk in overeenstemming met de verwachtingen. De gebruikte oplossingen hebben een zeer hoge viscositeit. Bij het op en neer bewegen van de veer moet daarom rekening worden gehouden met de weerstand van de vloeistof, de 'hydrodynamische kracht'. Vooral bij kleine afstanden tussen het bolletje en het substraat kan deze kracht sterk oplopen, omdat de vloeistof dan uit de dunne spleet tussen beide oppervlakken geperst moet worden. Uit de resultaten blijkt dat de hydrodynamische kracht veel kleiner is dan verwacht. Dit wordt verklaard door de aanwezigheid van de polymeerloze depletie laag aan het oppervlak. In deze laag is de viscositeit veel lager dan in de rest van de oplossing, en dit maakt het wegstromen van de vloeistof aanzienlijk gemakkelijker.

In **hoofdstuk 7** wordt niet de totale hoeveelheid monomeren gevarieerd, maar de hoeveelheid ketenstoppers. Uit de experimenten blijkt dat de depletiekracht verandert als er ketenstoppers aan de oplossing toegevoegd worden. De ketens worden korter, en dit leidt tot een kleinere reikwijdte van de kracht. Deze 'instelbaarheid' van de depletiekracht kan nooit optreden bij covalente polymeren, die immers een vaste lengte hebben.

**Hoofdstuk 8** gaat niet over EHUT en DBUT, maar over een supramoleculair polymeer op basis van de bindingsplaatsen 'UPy' en 'Napy', zie figuur 6a. In dit hoofdstuk wordt beschreven hoe een Napy vastgezet kan worden op een oppervlak. Supramoleculaire polymeren zouden vanaf zo'n gemodificeerd oppervlak de oplossing in kunnen groeien, en zo een laag van rechtop staande polymeren aan het oppervlak vormen, zie figuur 6b. Dergelijke lagen worden 'borstels' genoemd, en worden gebruikt om de stabiliteit van kolloïdale deeltjes te vergroten, of om het oppervlak te beschermen tegen vervuiling. Je kunt hierbij denken aan een scheepsromp, waaraan bijvoorbeeld algen niet

kunnen hechten, of contactlenzen waaraan eiwitten niet hechten, en die dus langer schoon blijven. De dikte van een borstel hangt af van de lengte van de polymeerketens. De dikte van een supramoleculaire borstel kan dus gemakkelijk veranderd worden door de lengte van de polymeerketens te variëren. In



Figuur 6: Supramoleculair polymeer aan een oppervlak. a: De bindingsplaatsen 'UPy' (boven), 'Napy' (midden) en een fluorescente UPy (onder); b: Supramoleculaire polymeerborstel met UPys en Napys. Een Napy-bindingsplaats wordt vastgezet op het oppervlak, de ketens groeien de oplossing in; c: Binding van fluorescente UPys aan het Napy-oppervlak.

hoofdstuk 8 wordt een Napy chemisch zodanig veranderd, dat hij geschikt is om aan een oppervlak vast te zetten. De oppervlakken met Napy-groepen worden bestudeerd door er een fluorescente UPy-groep aan te laten binden (figuur 6c). Door de intensiteit van de fluorescentie te meten, kan bepaald worden hoeveel UPys (en daardoor ook hoeveel Napys) er gebonden zijn aan het oppervlak. Uit de resultaten blijkt dat de Napy inderdaad vast zit aan het oppervlak, en dat hij nog steeds in staat is om bindingen te vormen met een UPy-groep. Het gemodificeerde oppervlak is echter niet stabiel: na verloop van tijd verdwijnt de Napy van het oppervlak, waarschijnlijk door reactie met water uit de lucht.

## Conclusies

Supramoleculaire polymeren zijn ketens van monomeren, die met niet-covalente bindingen aan elkaar zitten. Lineaire ketens worden gevormd door monomeren met twee bindingsplaatsen. Monomeren met één bindingsplaats werken als ketenstoppers. Hoewel dit effect al lang bekend is, is er tot nu toe weinig aandacht besteed aan de precieze effecten van ketenstoppers. In dit proefschrift

wordt het effect van ketenstoppers op supramoleculaire polymeeroplossingen nader onderzocht.

Door het toevoegen van ketenstoppers neemt de gemiddelde ketenlengte af. Boven een bepaalde hoeveelheid ketenstoppers wordt de ketenlengte zelfs volledig bepaald door de ketenstoppers. Deze effecten kunnen beschreven worden door een eenvoudig model. De resultaten van rheologie- en lichtverstrooiingsexperimenten zijn in overeenstemming met dit model. Door de toevoeging van ketenstoppers kan informatie worden verkregen over de eigenschappen van de ketens, die anders niet toegankelijk zou zijn.

De krachten tussen kolloïdale deeltjes worden vaak beïnvloed door de aanwezigheid van polymeerketens. Een voorbeeld hiervan is de depletiekracht, die bepaald wordt door het aantal polymeren en hun lengte. Doordat de lengte van supramoleculaire polymeren gemakkelijk veranderd kan worden, kan ook de depletiekracht als het gecontroleerd gevarieerd worden.

Supramoleculaire polymeren zijn een veelbelovende nieuwe soort materialen. Het voortdurend breken en herstellen van bindingen tussen monomeren zorgt voor unieke en zeer dynamische eigenschappen in vergelijking met covalente polymeerketens. Een van de gevolgen hiervan is dat de lengte van de ketens varieert met bijvoorbeeld de temperatuur. Voor sommige toepassingen kan het ongunstig zijn als de ketenlengte verandert, bijvoorbeeld omdat het materiaal dan te visceus wordt. In dit soort gevallen zouden ketenstoppers nuttig kunnen zijn. Door voldoende ketenstoppers toe te voegen kan de ketenlengte constant gehouden worden, terwijl de bindingen wel de mogelijkheid behouden om te breken en zich opnieuw te vormen, en het supramoleculaire karakter dus behouden blijft.

Ketenstoppers worden vaak beschouwd als een lastig te verwijderen verontreiniging van een supramoleculair polymeer. De resultaten in dit proefschrift tonen echter aan dat ze ook een nuttig instrument kunnen zijn voor zowel onderzoek naar als toepassingen van supramoleculaire polymeren.



# Dankwoord

Een promotie-onderzoek is een ontdekkingsreis. Op een zonnige dag vertrek je met een lekker briesje in de rug op zoek naar een proefschrift en een doctorstitel. De uiteindelijke bestemming wordt voor een groot deel bepaald door de navigatiekunsten van de bemanning. Gaan we linksom of rechtsom? Volgen we zo lang mogelijk de bekende route, of proberen we iets radicaal anders? Er zijn periodes van windstilte, waarin je stuurloos ronddobbert, afgewisseld met stormen die je in een mum van tijd vele kilometers verder brengen.

Na iets meer dan vier jaar is er nu een einde gekomen aan mijn promotiereis. Het is een avontuurlijke tocht geweest, waarin voorspoed en tegenslag elkaar op klassieke wijze aflossen. Gelukkig was ik niet alleen, en op deze plaats wil ik dan ook een aantal mensen bedanken die mij onderweg op koers hebben gehouden. Maar ook degenen die ‘slechts’ als aangenaam gezelschap hebben meegereisd, wil ik niet overslaan.

Degene die hier zonder meer als eerste genoemd moet worden is *Klaas Besseling*, mijn co-promotor. Klaas, het is ons nooit echt gelukt om vaste overlegmomenten te plannen. Uiteindelijk bleek dit ook helemaal niet nodig, want je maakte altijd uitgebreid tijd als ik in jouw kamer verscheen om iets te vragen of te bespreken. Ook mijn manuscripten kwamen stevast terug met zeer bruikbaar commentaar, waaruit bleek dat ze met aandacht gelezen waren. Kortom, ik vond onze samenwerking zeer vanzelfsprekend, prettig en vruchtbaar. Dat is iets waarop iedere promovendus jaloers kan zijn, en waarvoor ik je bij deze dan ook heel hartelijk wil bedanken.

Als een manuscript eenmaal door Klaas en mij goedgekeurd was, ging het voor een laatste ‘frisse blik’ naar mijn promotor, *Martien Cohen Stuart*. Martien, je hebt een groot aantal promovendi onder je hoede, en natuurlijk ook nog de gehele leerstoelgroep om je mee bezig te houden. Ik heb me er vaak over verbaasd hoe je na een kort verslag van de stand van zaken toch nuttige suggesties kon leveren. Mijn dank voor je belangstelling en je bijdrage aan dit proefschrift, in het bijzonder voor je hulp bij de perikelen rond het manuscript voor hoofdstuk 4.

*Laurent Bouteiller* also deserves a prominent place in this acknowledgement. The molecules synthesized in his laboratory, ‘EHUT’ and ‘DBUT’, are used in almost every chapter in this thesis. Laurent, needless to say that this research

could not have been done without your contribution. Thank you very much for your generosity in providing EHUT and DBUT samples whenever I asked for them.

Behalve fysische chemie wilde ik in mijn onderzoek ook graag ‘iets synthetisch’ doen. Daarom heb ik enkele maanden doorgebracht op het laboratorium voor Macromoleculaire en Organische chemie van de Technische Universiteit Eindhoven, in de groep van Bert Meijer. Het is aan de goede en intensieve begeleiding van *Ronald Ligthart* en *Rint Sijbesma* te danken dat ik hoofdstuk 8 van dit proefschrift heb kunnen schrijven. Ronald, bedankt voor de vele tijd en energie die je aan mij besteed hebt. Ik hoop dat ik je niet te veel in de weg heb gelopen bij mijn geklungel in het onvergetelijke SMO lab 3. Rint, bedankt voor je belangstelling voor mijn project, voor de goede tips en suggesties, en voor de gelegenheid om in jullie groep mee te mogen draaien.

Naast mijn reguliere onderwijstaak heb ik me als begeleider mogen bemoeien met het MSc-thesis onderzoek van *Marc Lemmers*. Marc, ik vond het erg leuk om met je samen te werken. Het resultaat was ook meer dan bevredigend. Het feit dat jouw naam nu als co-auteur boven een PRL prijkt, spreekt voor zich.

Een belangrijk deel van Marc's werk bestond uit het doen van metingen bij het Forschungs Zentrum Jülich, in de groep van Jan Dhont. De hulp en gastvrijheid en bovenal het enthousiasme van *Pavlik Lettinga* hebben ertoe bijgedragen dat de metingen na enkele vergeefse pogingen uiteindelijk toch geslaagd zijn. For the execution of the experiments, the technical assistance of *Hartmut Kriegs* was invaluable.

Tot zover de mensen die inhoudelijk hebben bijgedragen aan mijn proefschrift. Ook ‘de rest’ van mijn collega's verdient echter een woord van dank. Niet alleen voor alle borrels, fietstochten en labuitjes, maar vooral voor de geweldige sfeer op Fysko. De koffiepauzes alleen al maakten het, ongeacht de voortgang van het onderzoek, de moeite waard om de berg op te fietsen. Mijn kamergenoten *Stefan* en *Marat* wil ik bedanken voor het gezelschap.

De Student Conference in 2005, die ik samen met *Maykel Roelen*, *Bart Postmus* en *Henk Zweistra* heb mogen organiseren, was voor mij een van de hoogtepunten van de afgelopen vier jaar. De voorbereiding was al leuk, de week zelf overtrof al mijn verwachtingen. Maykel, Bart en Henk, bedankt voor de goede samenwerking en een meer dan geslaagde conferentie.

Buiten het laboratorium stond ik ook af en toe in een sporthal tegen een bal te slaan. Aan de ene kant loopt de hoeveelheid volleybal soms de spuigaten uit, aan de andere kant biedt *Scylla* een sociaal leven dat ik niet zou willen missen.

Mijn dank gaat met name uit naar mijn teamgenoten van de afgelopen jaren, met wie ik vaak en lang 'geboomd' heb, maar gelukkig niet te veel over mijn werk.

*Pap, mam*, er is natuurlijk geen beginnen aan om jullie bijdrage in de afgelopen bijna 28 jaar te beschrijven. Ik houd het dus hier maar bij het uitspreken van mijn enorme waardering voor jullie voortdurende belangstelling en steun op alle mogelijke gebieden.

Zelfs tijdens de allerlaatste momenten van de reis, de verdediging van mijn proefschrift, kan ik nog rekenen op de steun van mijn paranimfen *Joris Knobben* en *Jordi Elings*. Joris, ik vond het fijn een andere promovendus zo dichtbij te hebben, ook al staan onze onderwerpen mijlenver van elkaar. Ik ben je nog net voorgebleven, maar het scheelt niet veel. Jordi, bedankt voor de belangstelling die je altijd getoond hebt voor mijn onderzoek, en veel succes met het afronden van je eigen studie.

Zoals gebruikelijk zijn de laatste woorden voor de belangrijkste persoon. *Yolanda*, jij hebt de afgelopen jaren ongetwijfeld het meest van iedereen met mij meegeleefd. Jouw rust en relativiseringsvermogen (wat we voor elkaar wel altijd hebben, maar voor onszelf niet) hebben me enorm geholpen. Ik hoop dat we als twee ex-flutAIO's nog heel lang 'gewoon heel gelukkig' mogen zijn met elkaar.

## List of publications

- *Brownian particles in supramolecular polymer solutions*  
J. van der Gucht, N.A.M Besseling, W. Knoben, L. Bouteiller and M.A. Cohen Stuart. *Phys. Rev. E* 67, 051106, **2003**
- *Depletion interaction measured by colloidal probe atomic force microscopy*  
W.K. Wijting, W. Knoben, N.A.M. Besseling, F.A.M. Leermakers and M.A. Cohen Stuart. *Phys. Chem. Chem. Phys.* 6, 4432–4439, **2004**
- *Dynamics of reversible supramolecular polymers: Independent determination of the dependence of linear viscoelasticity on concentration and chain length by using chain stoppers*  
W. Knoben, N.A.M. Besseling, L. Bouteiller and M.A. Cohen Stuart. *Phys. Chem. Chem. Phys.* 7, 2390–2398, **2005**
- *Chain stoppers in reversible supramolecular polymer solutions studied by static and dynamic light scattering and osmometry*  
W. Knoben, N.A.M. Besseling and M.A. Cohen Stuart. *Macromolecules* 39, 2643–2653, **2006**
- *Long range depletion forces induced by associating small molecules*  
W. Knoben, N.A.M. Besseling and M.A. Cohen Stuart. *Phys. Rev. Lett.* 97, 068301, **2006**
- *Multiple shear-banding transitions in a supramolecular polymer solution*  
J. van der Gucht, M. Lemmers, W. Knoben, N.A.M. Besseling and M.P. Lettinga. *Phys. Rev. Lett.* 97, 108301, **2006**
- *Rheology of a reversible supramolecular polymer, studied by comparison of the effects of temperature and chain stoppers*  
W. Knoben, N.A.M. Besseling and M.A. Cohen Stuart *J. Chem. Phys.*, in press
- *Direct measurement of depletion and hydrodynamic forces in solutions of a reversible supramolecular polymer*  
W. Knoben, N.A.M. Besseling and M.A. Cohen Stuart *Langmuir*, submitted

# Levensloop

Op maandag 9 april 1979 maakte Wout Knoben in Arnhem kennis met de wereld. 18 jaar later, in 1997, nam hij aan het Lorentz College te Arnhem zijn Gymnasiumdiploma in ontvangst. In datzelfde jaar begon Wout met een studie Moleculaire wetenschappen aan Wageningen Universiteit (toen nog Landbouwniversiteit Wageningen geheten). Zijn eerste afstudeeronderzoek vond plaats bij het Laboratorium voor Organische chemie, en ging over de enzymatische scheiding van een racemisch lacton in zijn enantiomeren. Daarna deed Wout een afstudeervak bij het laboratorium voor Fysische Chemie en Kolloïdkunde. In dit project onderzocht hij een waterstofbruggebonden supramoleculair polymeer. Tenslotte liep Wout stage bij de Stichting Communicatie Centrum Chemie (C3) in Leidschendam. In juni 2002 studeerde hij af, met de kwalificatie 'met lof'. Vervolgens begon hij in september 2002 aan een promotie-onderzoek aan het laboratorium voor Fysische Chemie en Kolloïdkunde van Wageningen Universiteit. Hier hield hij zich wederom bezig met supramoleculaire polymeren, in het bijzonder met het onderzoeken van het effect van de aanwezigheid van zogenaamde 'ketenstoppers'. Dit onderzoek heeft geresulterd in het proefschrift dat nu voor u ligt.

# Education programme

## Discipline specific activities

- Molecular modelling, Wageningen, The Netherlands, 2002
- Winterschool, Han sur Lesse, Belgium, 2003
- RPK B: Polymer physics, Utrecht, The Netherlands, 2003
- World polymer congress, Paris, France, 2004
- Annual conference, Schiermonnikoog, The Netherlands, 2005
- Liquid matter conference, Utrecht, The Netherlands, 2005
- Student conference, Biezenmortel, The Netherlands, 2005
- Surface forces conference, Moscow, Russia, 2006
- Dutch polymer days, Lunteren, The Netherlands, 2003-2006
- Vloeistoffen en grensvlakken, Lunteren, The Netherlands, 2004, 2006

## General courses

- Science journalism, Wageningen, The Netherlands, 2005

## Optional courses and activities

- Preparation PhD research proposal, 2002
- Work group meetings, 2002-2006
- Colloquia, 2002-2006
- Excursion BASF, Ludwigshafen, Germany, 2005
- Excursion Henkel, Düsseldorf, Germany, 2005

